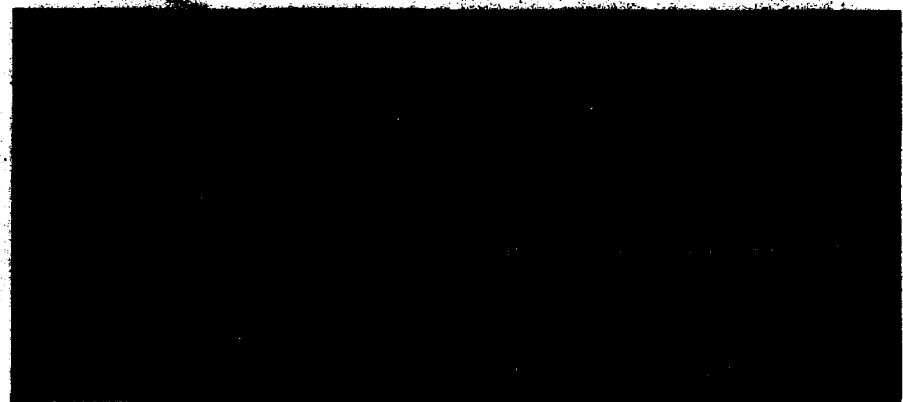


DTIC FILE COPY

(1)

AGARD-LS-167

AD-A21103 AGARD-LS-167



AGARD LECTURE SERIES No.167

**Blading Design
for
Axial Turbomachines**

DTIC
ELECTE
S AUG 01 1989 D
D8



DISTRIBUTION AND AVAILABILITY
ON BACK COVER

DISTRIBUTION STATEMENT A
Approved for public release
Distribution Unlimited

80 2 101 09

NORTH ATLANTIC TREATY ORGANIZATION
 ADVISORY GROUP FOR AEROSPACE RESEARCH AND DEVELOPMENT
 (ORGANISATION DU TRAITE DE L'ATLANTIQUE NORD)

AGARD Lecture Series No.167
BLADING DESIGN FOR AXIAL TURBOMACHINES

Accession For	
NTIS	<input checked="" type="checkbox"/>
DTIC	<input type="checkbox"/>
Unannounced	<input type="checkbox"/>
Justification	
By	
Distributed	
Accession Files	
Dist	Av
A-1	

This material in this publication was assembled to support a Lecture Series under the sponsorship of the Propulsion and Energetics Panel of AGARD and the Consultant and Exchange Programme of AGARD presented on 1-2 June 1989 in Toronto, Canada, on 15-16 June 1989 in Cologne, Germany and on 19-20 June 1989 in Ecully (near Lyon), France.

THE MISSION OF AGARD

According to its Charter, the mission of AGARD is to bring together the leading personalities of the NATO nations in the fields of science and technology relating to aerospace for the following purposes:

- Recommending effective ways for the member nations to use their research and development capabilities for the common benefit of the NATO community;
- Providing scientific and technical advice and assistance to the Military Committee in the field of aerospace research and development (with particular regard to its military application);
- *Continuously stimulating advances in the aerospace sciences relevant to strengthening the common defence posture;*
- Improving the co-operation among member nations in aerospace research and development;
- Exchange of scientific and technical information;
- Providing assistance to member nations for the purpose of increasing their scientific and technical potential;
- Rendering scientific and technical assistance, as requested, to other NATO bodies and to member nations in connection with research and development problems in the aerospace field.

The highest authority within AGARD is the National Delegates Board consisting of officially appointed senior representatives from each member nation. The mission of AGARD is carried out through the Panels which are composed of experts appointed by the National Delegates, the Consultant and Exchange Programme and the Aerospace Applications Studies Programme. The results of AGARD work are reported to the member nations and the NATO Authorities through the AGARD series of publications of which this is one.

Participation in AGARD activities is by invitation only and is normally limited to citizens of the NATO nations.

The content of this publication has been reproduced directly from material supplied by AGARD or the authors.

Published May 1989

Copyright © AGARD 1989
All Rights Reserved

ISBN 92-835-0512-3



Printed by *Specialised Printing Services Limited*
40 Chigwell Lane, Loughton, Essex IG10 3TZ

PREFACE

The efficiency and performance of the turbomachinery components of future aero engines can considerably be improved by applying recent advances in understanding the flow behaviour of axial compressor and turbine bladings. Thus, the optimal profile pressure distribution as input for new blading design methods has an important effect on losses and flow deflection. The boundary-layer behaviour has to be carefully taken into account with respect to laminar-turbulent transition, shock-boundary-layer interaction and separation effects. In addition to these aerodynamical questions, unsteady effects and the limitations from structural and vibrational conditions also have to be taken into account.

The Lecture Series deals with two main topics:

- design methods and their principles, limitations
- application to axial compressors and turbines, experience.

This Lecture Series, sponsored by the Propulsion and Energetics Panel of AGARD, has been implemented by the Consultant and Exchange Programme.

* * *

Le rendement et les performances des pièces des turbomachines destinées à être incorporées aux futurs systèmes de propulsion pourraient être sensiblement améliorés par la mise en oeuvre des progrès réalisés récemment en ce qui concerne la définition du comportement des écoulements dans des compresseurs axiaux et sur les aubes de turbine.

Il s'ensuit que la répartition optimale des pressions sur le profil, en tant qu'élément dans les nouvelles méthodes pour la conception d'aubes de turbine, a des conséquences importantes sur les pertes et sur la déflexion de l'écoulement. Le comportement de la couche limite en fonction de la transition laminaire/turbulent, des interactions choc/couche limite et des effets de décollement doit être systématiquement pris en compte.

En plus de ces questions d'ordre aérodynamique, il faut également tenir compte des effets instationnaires et des contraintes imposées par les conditions structurales et vibratoires.

Le Cycle de Conférences traite principalement des deux sujets suivants:

- les méthodes de conception, leurs principes et limitations
- les applications aux compresseurs et turbines axiaux, et l'expérience acquise.

Ce Cycle de Conférences est présenté dans le cadre du programme des consultants et des échanges, sous l'égide du Panel AGARD de Propulsion et d'Energétique.

LIST OF SPEAKERS

Lecture Series Director: Prof. Dr Ing. L. Fottner
Institut für Strahlantriebe
Universität der Bundeswehr München
Werner Heisenberg Weg 39
8014 Neubiberg
Germany

AUTHORS/SPEAKERS

Mr P. Bry
SNECMA—Centre de Villaroche
Service Développement Turbines
77550 Moissy-Cramayel
France

Prof. G.K. Serovy
Dept. of Mechanical Engineering
3038 ME/ESM
Iowa State University
Ames, Iowa 50011
USA

Dr-Ing. J. Hourmouziadis
Motoren und Turbinen Union München
Postfach 50 06 40
8000 München
Germany

Dr-Ing. H. Starken
Institut für Antriebstechnik
DLR
Postfach 90 60 58
5000 Köln 90
Germany

Dr G. Meauzé
Chef De Groupe de Recherches
ONERA
29, Avenue de la Div. Leclerc
92320 Châtillon sous Bagneux
France

Dr P. Stow
Chief of Theoretical Science
Rolls-Royce plc
P O Box 31
Derby DE2 8BJ
United Kingdom

Dr A.J. Wennerstrom
Air Force Wright Aeronautical Lab./POTX
Wright Patterson AFB
Ohio 45433-6563
USA

CONTENTS

	Page
PREFACE	iii
LIST OF SPEAKERS	iv
	Reference
REVIEW OF TURBOMACHINERY BLADING DESIGN PROBLEMS by L.Fottner	1
DESIGN CRITERIA FOR OPTIMAL BLADING DESIGN by H.Starken	2
OVERVIEW ON BLADING DESIGN METHODS by G.Meauzé	3
PERFORMANCE PREDICTION FOR AXIAL-FLOW COMPRESSOR AND TURBINE BLADING by G.K.Serovy	4
BLADING DESIGN FOR MULTI-STAGE HP COMPRESSORS by P.Stow	5
TRANSONIC AND SUPERSONIC COMPRESSOR BLADING DESIGN by A.J.Wennerstrom	6
BLADING DESIGN FOR COOLED HIGH-PRESSURE TURBINES by P.F.Bry	7
AERODYNAMIC DESIGN OF LOW PRESSURE TURBINES by J.Hourmouziadis	8

REVIEW ON TURBOMACHINERY BLADING DESIGN PROBLEMS

by

L. Fottner

Prof. Dr.-Ing., Universität der Bundeswehr München
 Institut für Strahlantriebe
 Werner Heisenberg Weg 39
 D-8014 Neubiberg, Germany

SUMMARY

This report is the introductory paper for the AGARD Lecture Series No 167 on "Blading Design for Axial Turbomachines". Based on the design objectives for the bladings of highly-loaded, high Mach number turbocomponents the main problem areas to be taken into account during the design process are derived. These refer to the flow field conditions with respect to the effect of Mach number on the profile contour shape, to the aerodynamic loading, especially of compressor bladings and to the boundary-layer behaviour. In addition, blading design has to account for secondary flow effects and to unsteady flow conditions. These problem areas are being treated in detail in the subsequent Lecture Series papers.

LIST OF SYMBOLS

C_p	pressure coefficient
D^+	Lieblein diffusion factor
k	roughness
l	blade chord
M	Mach number
r	radius
Re	Reynolds number
t	pitch
TET	turbine entry temperature
β	flow angle
ω	loss coefficient

1. INTRODUCTION

The efficiency of advanced turbojet aero engines is considerably affected by the aerodynamic characteristics of the turbocomponents. Using the latest knowledge regarding the flow deflection behaviour of the cascades and as a result of better understanding of the actual flow, the efficiency of these components has been considerably increased in the last years. Future development will have the following objectives:

- high or even higher efficiency
- large working range, also taking into account inlet distortions
- lower manufacturing effort and cost, which means a reduction in size, weight, and number of blades. This requirement can only be met by reducing the number of stages, which means increasing the aerodynamic stage loading.

At these conditions the aerodynamic quality of the blading is of great importance. The objective of the blading design is to realize a given design velocity triangle (result of a through-flow calculation) with minimal losses and to have a sufficient working range at off-design conditions. Up to now the blading is designed with the aid of empirical methods. Especially compressor bladings are mainly designed using profile families which have been developed years ago. Cascade test results are the basis for the empirical design of such cascades, consisting of NACA 65, NGTE or DCA profile shapes. The design of turbine cascades has to take into account additional conditions, such as blade cooling, so that profile families are not widely used for turbine bladings. Within the last years it has been shown that new concepts for the bladings of compressors and turbines will increase the efficiency. These methods are of the inverse or direct iterative type, i.e. they calculate the profile shape for a given pressure distribution on suction and pressure surface. Thus, the pressure distribution as an input for these methods has to be optimised with respect to some optimisation criteria. These criteria are oriented at the special application case. For compressor cascades mainly aerodynamic parameters, as losses and safe working range have to be considered. The design of turbine cascades is additionally affected by blade cooling and structural conditions.

Thus, blading design is highly influenced by the internal flow field, expressed by

- aerodynamic loading with respect to flow deflection,
- Mach number level
- Boundary-layer behaviour (Reynolds number and turbulence influence)

- and in case of cooled turbine bladings by blowing effects of coolant air.

In addition to these primary effects, blading design of turbomachines is also affected by the special feature of turbomachines like

- multi-stage components
- secondary flow effects
- unsteady flow conditions

This report as an overview paper does not include detailed reference informations, these being referred to the respective papers of this Lecture Series. The reference list at the end of this report contains monographies which have been valuable in preparing the programme of this Lecture Series.

2. INTERNAL FLOW FIELD

The internal flow fields encountered in current turbomachines are viscous, compressible and unsteady. The flow passage geometry provides a completely three-dimensional flow, and a significant fraction of the flow occurs in rotating passages. Some of the important phenomena influencing flow fields in modern axial-flow compressor blade rows are shown in Fig. 1. The flow is

- three-dimensional, the flow channel being given by the hub and casing contour and the profile contours on suction and pressure surface
- viscous, losses being generated by friction, mixing and shock/boundary-layer interaction
- compressible, with supersonic inlet (compressors) and exit (turbines) conditions
- unsteady due to the unsteady inlet conditions of rotating and stationary blade rows of stages and multi-stage machines.

These features have a significant effect on the overall flow field, but they are not the only influential factors. What Fig. 1 does not emphasize is that the phenomena shown take place in a strong through-flow or primary flow which is generally understandable in terms of the physical laws and corresponding equations of fluid dynamics. Many of the features of the flow field shown in Fig. 1 might therefore be called secondary flows or secondary effects. This suggests that such flows may be accounted for separately after determination of the primary flow field in a given case. Turbomachine flow fields occur in passages characterized by some unique geometric and kinematic features, which do not occur in other typical complex flows, either internal or external. These are shown in Fig. 2, which also introduces the idea of looking at the flow field in a representative meridional, hub-to-tip section of a turbomachine. An initial unique feature is the sequence of rotating and stationary internal flow passages. The effects of rotation on the flow within rotor blade rows should be considered. A second unique feature existing in turbomachine flow field is the transfer of energy in the flow process as work done on or by the fluid as it traverses the rotating elements.

2.1 Profile shapes

The profile shape is strongly influenced by the Mach number. As an example, Fig. 3 shows the radial Mach number distribution for some cascades of a 3-stage transonic compressor. The Mach number of the first rotor reaches 1.45 at the tip and remains supersonic over a large region of the blade height. The inlet velocities of the following cascades decrease to lower Mach number values. The stator cascades are subsonic, but the Mach number sometimes exceeds the critical value, thus producing local supersonic fields terminated by a compression shock.

The profile-type to be chosen for optimal flow deflection is directly dependent on the Mach number level. The areas of application of some profile-types are also indicated in Fig. 3. At Mach numbers larger than 1.2 special profile types (transonic profiles) should be used to reduce the shock losses at these supersonic inlet conditions. Double circular arc profiles have shown good results for the Mach number region between 0.8 and 1.1. For lower Mach number values NACA 65 profile blades are widely used. But, as has been already mentioned, for Mach numbers larger than the critical value local supersonic fields with a terminating compression shock are experienced with conventional blades. Thus, the compression shock should be minimised and it had been shown that it is possible to design cascades for supercritical inlet conditions without any compression shock (supercritical profiles).

Transonic compressor profiles

The flow conditions in a transonic cascade are mainly effected by the compression shock. This shock is composed of two parts. According to Schlieren pictures of cascade tests, there is a normal compression shock in the blade passage and an oblique shock in front of the cascade which is influenced by expansion waves emanating from the profile contour. Thus, the normal compression shock produces high losses (shock losses and shock/boundary-layer interaction losses), while the losses of the oblique shock can be

neglected. The objective of a blading design for transonic profiles is therefore to minimize the loss due to the normal compression shock. The consequent realisation of the above mentioned optimisation criteria for transonic profiles (lowest Mach number in front of the compression shock) leads to a straight suction surface from the leading edge to the shock position. This wadgetype profile (MTU 1, Fig. 4) is composed of a straight camber line in the supersonic region and a circular arc camber line in the subsonic region behind the compression shock. The profile shape is given by a superposition of this camber line and a thickness distribution consisting of the leading edge circle and wedge shape within the supersonic region and of a NACA 65 thickness distribution within the subsonic part behind the compression shock. The design of such transonic profiles has to take into account the following conditions:

- unique incidence condition at the leading edge
- transition point between supersonic and subsonic part is given by a shock model of a normal shock emanating from the leading edge of the adjacent blade and normal to the suction surface of the considered blade.
- deviation at the trailing edge according to empirical correlations for subsonic cascades consisting of NACA 65 blades.

In order to reduce the aerodynamic loading of the subsonic part of the cascade, the multiple circular arc (MCA) type of blades has a small amount of supersonic expansion from the leading edge to the shock position. The definition of this supersonic expansion has to be done with respect to avoiding separation of the boundary-layer at the shock position. The camber line of these MCA-type blades (MTU 3, Fig. 4) is composed of two circular arcs. The profile shape is given by a superposition of this camber line and the thickness distribution as explained for MTU 1 type blades.

Supercritical compressor profiles

The principle of supercritical profiles is successfully used for aircraft profiles and is now also being applied to compressor bladings. If the inlet Mach number is increased to a value larger than the critical Mach number (i.e. that Mach number at which at first locally sonic velocity is reached), a local region with supersonic velocity is established on the profile suction surface. This supersonic region is limited by the sonic line upstream and a compression shock downstream. This compression shock produces shock losses and via the interaction with the boundary-layer also additional losses. These shock and interaction losses are the reason for the strong increase of losses with increasing Mach number above the critical Mach number. If it were possible to design a profile with a continuous deceleration from supersonic to subsonic velocities (i.e. shockfree deceleration), this loss increase could be shifted to larger Mach numbers. In order to solve this problem it was necessary to have an inverse blading design method, i.e. to prescribe the desired velocity distribution and to calculate the resulting profile shape.

Since those methods to calculate transonic flow fields methods are now available, it is possible to design supercritical blades also for compressor cascades. It should be mentioned that this cascade is shockfree for the design condition and it has to be carefully checked if the off-design behaviour is also sufficient. Since these inverse design methods allow individual optimisation of a blade, taking into account only the connection between pressure distribution and profile shape, these methods should also be applicable to wholly subsonic flow fields, so that there is a wide field of application for these new blading concepts.

Profile shapes for turbines

As has been already mentioned the design of turbine cascades has to take into account not only aerodynamic optimisation criteria but some additional considerations like blade cooling. Therefore the use of profile families is very limited and the blading design takes place in an iterative manner by recalculation of a given profile shape and correcting this shape in order to produce a prescribed velocity distribution. Like for compressor cascades, the velocity distribution on suction and pressure surface is an important optimisation criterion because of its influence on boundary-layer development and thus on the losses. In turbine bladings, where blade cooling is necessary due to high temperatures, blading design has also to consider the effect of mixing cooling air with mainstream flow. When directly used for cooling, the air fraction derived from the compressor is blown through the shaft and discs to vent holes. It then undergoes pressure losses and entropy increments, so that mixing of the coolant with the external flow entails aerodynamic losses. There is a considerably negative effect on boundary-layer behaviour due to the crossflow between cooling air and main stream which leads in combination with mixing losses to a remarkable efficiency decrease with increasing turbine inlet temperature (Fig. 5).

Research into cooling procedures imply analytical and experimental work, in order to obtain heat transfer data providing the boundary conditions needed for structural predictions, namely thermal fatigue, creep progression and chemical deterioration. The problems associated with these procedures amount to finding devices which will maximize the heat transfer while minimizing coolant mass flow and the resulting losses. Flow passages inside the airfoils must offer a sufficient area for the local heat transfer requirements; their geometry is so complex that it is hardly possible to estimate even crudely

the heat transfer coefficients from straight forward computations. The designer must then start with a preliminary estimate of the profile geometry in order to compute a first approximation of the three-dimensional turbine flow field and heat transfer rate. The way in which the coolant discharge interferes with the mainstream must also be accounted for, in applying subsequent corrections to the first design.

2.2 Blade loading of compressor cascades

In future developments the manufacturing effort and the cost will have to be taken into account to a greater extent, which means a reduction in size, weight and number of blades with the aerodynamic quality being maintained at its present level at least. The requirements can only be met by reducing the number of stages, i.e. increasing the aerodynamic loading with sufficient working range. Highly-loaded compressor cascades are, however, considerably limited in their working range and losses will rise. An attempt must therefore be made to avoid separation of the boundary-layer by suitable measures. Apart from the frequently applied method of splitting the deflection to two airfoils (tandem cascades), which, however, does not result in a reduction of manufacturing efforts, there are possibilities of increasing the maximum lift which have been successfully used in aircraft aerodynamics:

- suction of the boundary-layer prone to separation
- blowing of high-energy air to the boundary-layer prone to separation.

For turbomachine application, boundary-layer control is in practice limited to blowing by means of slot or slit profiles. In the case of slot profiles, the air required to effect the boundary-layer is blown through slots from the pressure to the suction surface exploiting the pressure gradient between the pressure and suction surfaces, where as in the case of slit profiles a secondary air supply is needed to blow the air through slots in the suction surface (Fig. 6).

2.3 Profile boundary-layer behaviour

Blading design methods use the profile velocity distribution as a criterion for the aerodynamic quality of the design, i.e. they take into account the close connection between the profile losses (due to blade boundary-layer) and the blade surface velocity distribution. Thus, the velocity distribution being input for these methods has to be optimized with respect to low losses of the blading. With respect to the boundary-layer state of actual turbomachinery blades, it is essential to find velocity distributions with the laminar-turbulent transition point as far downstream as possible. In particular, two factors effect the transition behaviour, namely the pressure gradient on the blade surface and the free stream turbulence. Experience on several turbine cascades at design conditions shows a mixed laminar-turbulent boundary-layer on the suction surface and a mostly laminar boundary-layer on the pressure surface. It is therefore necessary to primarily optimize the velocity distribution on the suction surface with respect to low losses. The laminar boundary-layer should be maintained as far downstream as possible. Transition is required to take place without forming a laminar separation bubble. The extent of a rearward deceleration has to be carefully limited to avoid flow separation in this region (Fig. 7). Thus, determination of the transition region becomes very important prescribing the profile velocity distribution. We have to distinguish between natural transition and transition via a laminar separation bubble.

When the overall blade chord Reynolds number (R_c) gets low enough, the laminar boundary-layer reaches the separation point before transition is achieved. After the laminar boundary-layer separates, it forms a laminar free shear layer that eventually undergoes transition to turbulence. The turbulent free shear layer is able to do enough diffusion by entrainment of high energy free stream fluid to reattach to the surface as a turbulent boundary-layer. This short bubble is seen as a small perturbation on the pressure distribution; its effect on the flow outside of the bubble region is minimal. As R_c continues to decrease, the laminar free shear layer grows in length. This growth causes the turbulent free shear layer to do more diffusion to reattach at a pressure near the inviscid pressure value (see Fig. 8). Finally, R_c becomes so low and the laminar shear layer so long that the turbulent entrainment process can no longer support the diffusion required for reattachment with a value close to the inviscid pressure level. This is when the bubble starts to significantly affect the flow outside the bubble region. The velocity peak and circulation decrease, thereby reducing the pressure gradient over the bubble. This allows the turbulent shear flow to reattach as a long bubble, i.e. that is the short bubble as burst into a long bubble. As R_c is further lowered, the velocity peak and circulation is further decreased. Finally, the bubble is so long that reattachment on the blade surface is no longer possible. The flow is then completely separated, and there is little change to the flow field around the profile with continued decrease of Reynolds number.

To summarize, within the incidence operating range of the cascade, there are four flow regimes possible across a large Reynolds number range (disregarding turbulent separation due to off-design conditions):

- R_c sufficiently high for transition to occur before separation
- short bubble region (before bursting)

- long bubble region (after bursting)
- complete separation

The conditions necessary for the formation of a laminar separation bubble are an adverse pressure gradient of sufficient magnitude to cause laminar separation and flow conditions over the blade surface such that the boundary-layer will be laminar at the separation point. Inherent in the second condition is that the blade surface be smooth, that the free stream turbulence level shall be relatively low, and that the distance between the stagnation and separation points be moderate (or more precisely, that the boundary-layer Reynolds number at the laminar separation point be less than that required for transition).

Blade surface roughness effects blade profile loss when the surface roughness elements protrude from the laminar or viscous sublayer of the turbulent boundary-layer. As long as the roughness elements are submerged within the viscous sublayer no further reduction of friction losses is achievable below the so called "hydrodynamically smooth" value. Friction drag in that regime depends exclusively on Reynolds number. As soon as the roughness elements protrude from the viscous sublayer due to a thinner sublayer as the result of increased Reynolds number, the friction loss function turns toward independence of Reynolds number within a small Reynolds number interval. After that transition region friction drag is exclusively a function of the roughness height itself (Fig. 9). Analysis of limited experimental data reveals that critical roughness Reynolds number of compressor blades manufactured with typical present day methods as for-ging/etching and electrochemical machining are around 90 and therefore very close to sand type roughness if roughness height is based on the largest peaks. The steadily increasing pressure ratios and flow velocities in modern gas turbine compressors increase the Reynolds number over chord length ratio in the back end of the compression system to an extent that even with the best presently available manufacturing methods noticeable losses of potentially achievable efficiency gains must be accepted. The latter applies primarily to all missions with high inlet pressure, i.e. low kinematic viscosity. The roughness problem occurs primarily in the higher Reynolds number regime where turbulent attached flow predominates.

3. SECONDARY AND UNSTEADY FLOW EFFECTS

It is not the objective of this chapter to present a complete documentation of these very important problem fields. Secondary and unsteady flow effects have to be taken into account during the whole design process of a turbomachine.

Since secondary flow regions (Fig. 10) are always the origine of higher losses, the blading design in these regions has to consider these additional effects to get an optimal solution. The objective of optimal blading design is, to shape a blading from hub to tip in order to reduce also secondary losses. Blading design has to consider the following flow effects:

- Cascade passage vortex
- Corner vortex
- Tip clearance vortex
- Horseshoe vortex
- Annulus end wall boundary-layer

These terms do not refer to flow field occurrences which are independent mechanisms. As can be observed in experiments they overlap and interact.

The state of the art in axial turbomachinery has advanced to the point where further improvements will have to come also from a better understanding and eventual control of the unsteady flow phenomena which occur in turbomachines. These unsteady flows have a significant influence on efficiency, aerodynamic stability of the compression system, aeroelastic stability, forced response, and noise generation (see Fig. 11).

A comprehensive report on these topics has just been published as "AGARD Manual on Aeroelasticity in Axial-Flow Turbomachines" (AGARD-AG-298, Vol. 1 and 2) by Platzer and Carta. The first volume attempts to review the field of unsteady turbomachinery aerodynamics. The reader will notice that most methods are still limited to the two-dimensional (cascade) flow approximation, although great progress has been made in the inclusion of blade geometry and loading effects. The current status of the underlying aerodynamic theory and of the major results are described. The importance of three-dimensional flow effects is still insufficiently understood. Viscous flow effects are discussed in the chapter on stall flutter. Rigorous methods for the computation of unsteady boundary-layer effects are beginning to be developed. Great progress has been made in the field of computational fluid dynamics. Its application to the problem of unsteady transonic cascade flows is reviewed. A separate volume will have to be devoted in the near future to the numerical computation of unsteady flows in turbomachines because of the rapid advances in the field of computational fluid dynamics. The final four chapters present the status of the unsteady aerodynamic and aeroelastic measurement techniques and of the available experimental cascade and rotor results. Whenever possible a comparison between theory and experiment was attempted in the various chapters. The need for well-controlled test cases was recognized a few years ago. This effort is currently in progress. In the second volume the structural dynamics characteristics and analysis methods applicable to single blades and whole bladed assemblies are reviewed.

REFERENCES

- Hirsch, Ch., Denton, J.D. (Edts.)
Through Flow Calculations in Axial Turbomachines
AGARD-AR-175 (1981)
- Japikse, D. (Edt.)
International Seminar on Advanced Turbomachinery Performance
Concepts 85 Conf. Proc. (1985)
- Ucer, A.S., Stow, P., Hirsch, Chr. (Edts.)
Thermodynamics and Fluid Mechanics of Turbomachinery (Vol I and II)
Martinees Nijhoff Publishers, Dordrecht (1985)
- Fottner, L. (Edt.)
Test Cases for Computation of Internal Flows in Aero Engine Components
AGARD-AR-275 (1989)

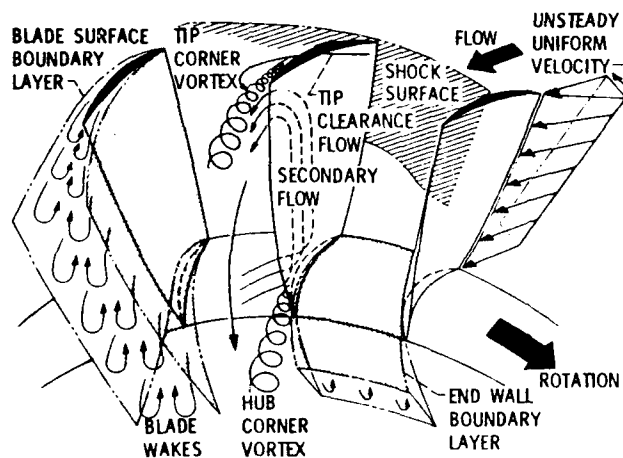


Fig. 1 Flow phenomena in axial-flow turbomachines

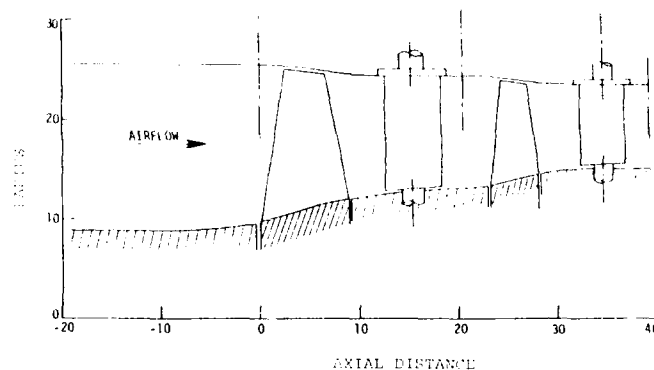


Fig. 2 Meridional section of a 2-stage axial compressor

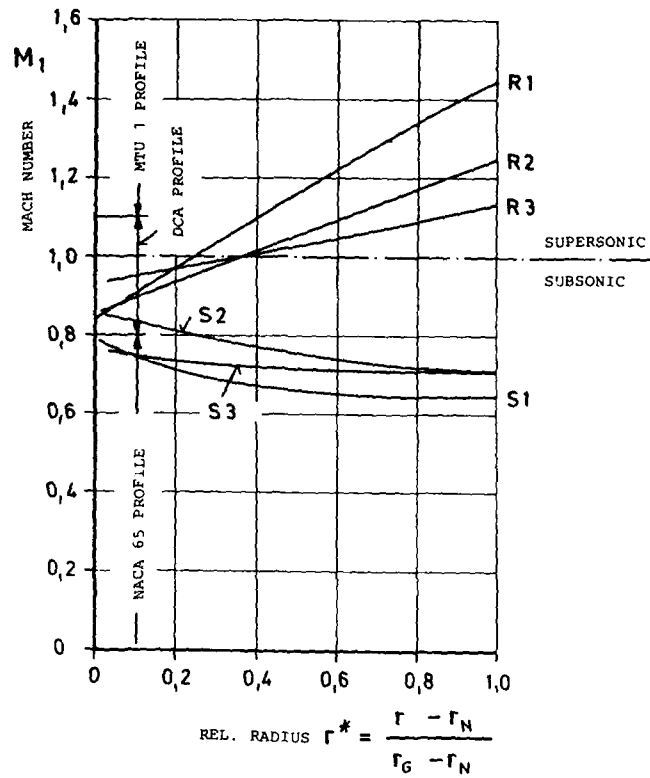


Fig. 3 Radial Mach number distribution of bladings of a 3-stage axial compressor

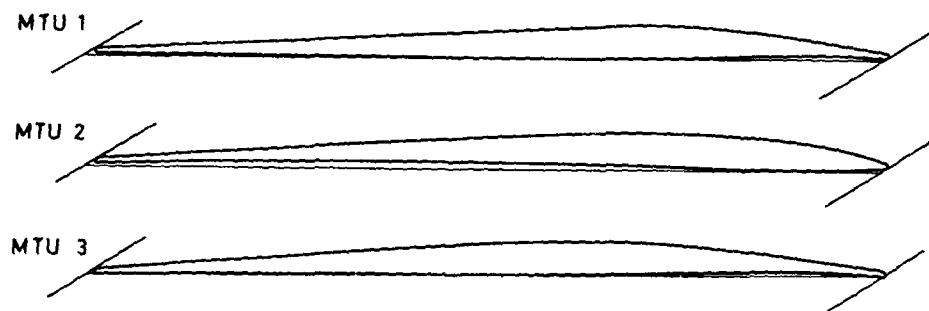


Fig. 4 Profile shapes for transonic compressor cascades

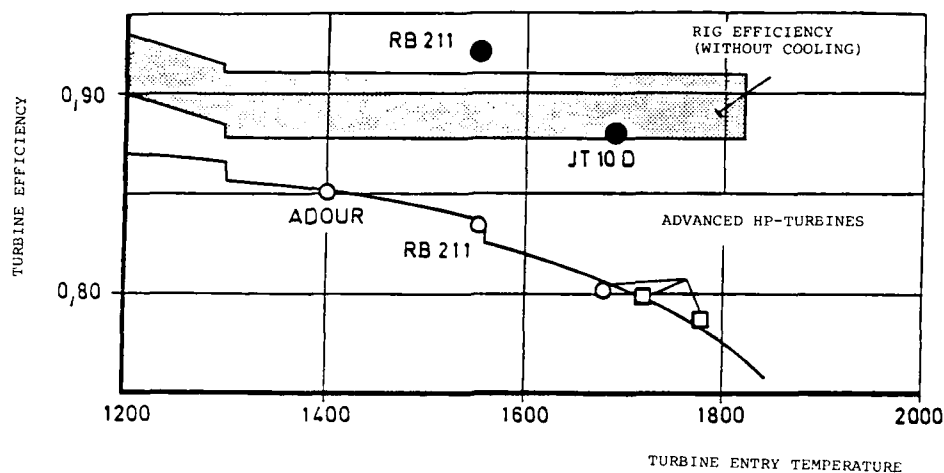


Fig. 5 Effect of blade cooling on turbine efficiency

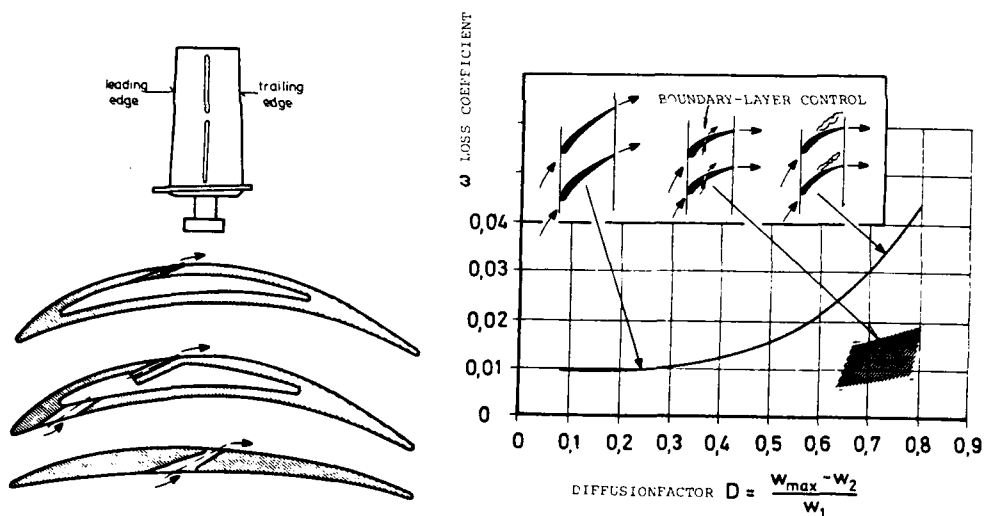


Fig. 6 Boundary-layer control for highly loaded compressor cascades

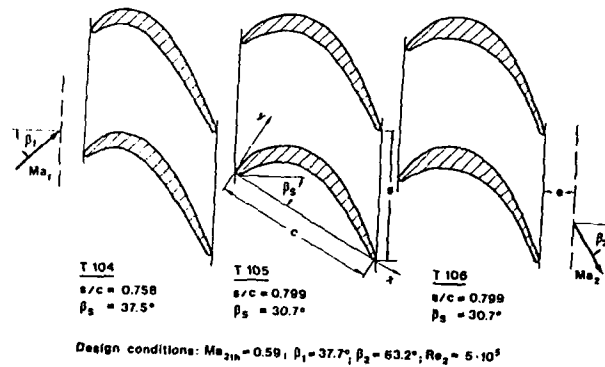
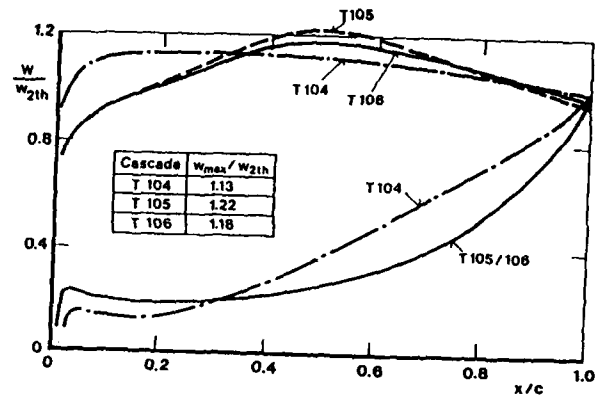


Fig. 7

Optimisation of a turbine cascade profile shape

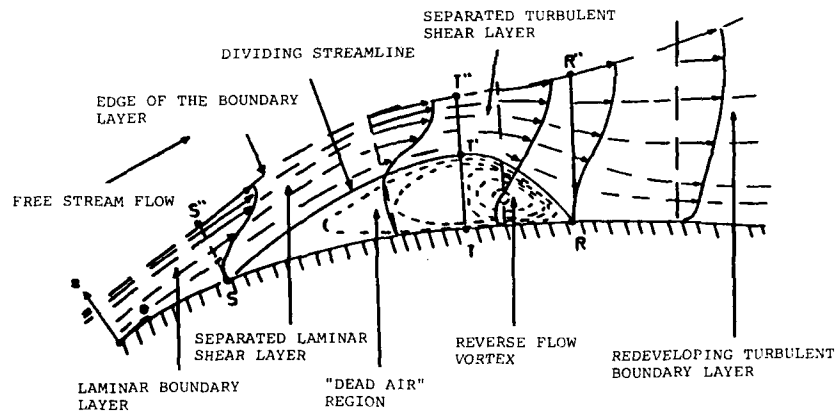
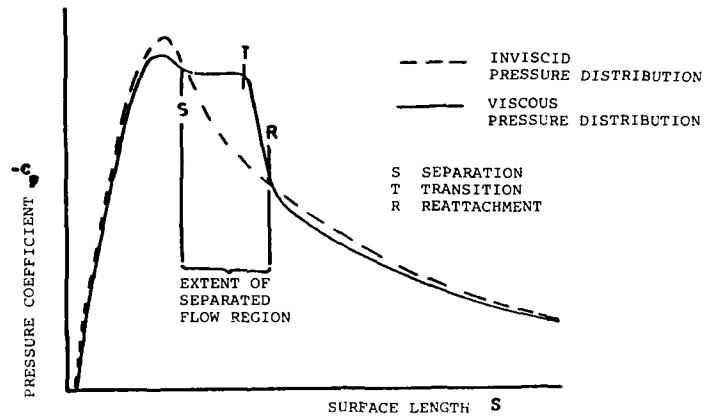


Fig. 8

Transition phenomena

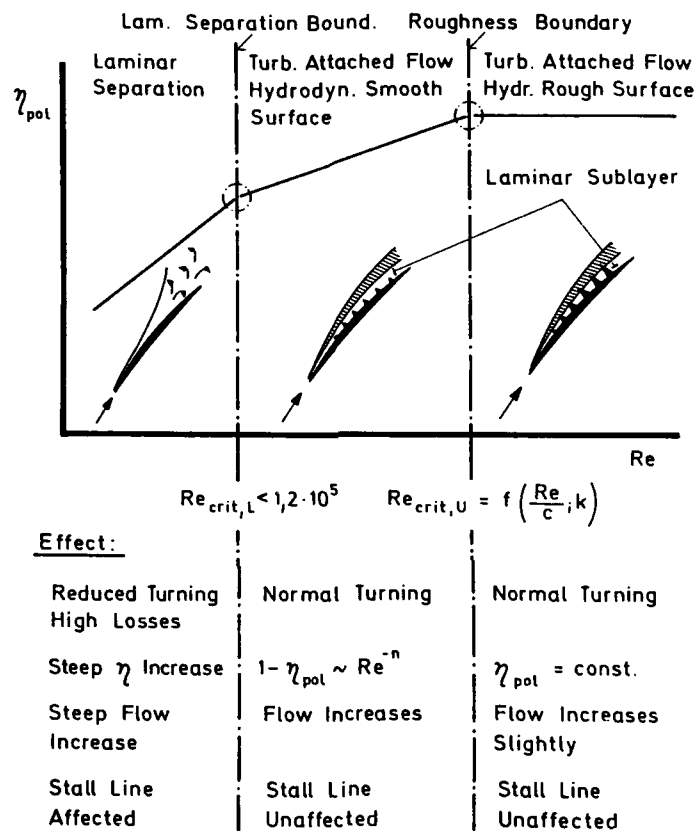


Fig. 9 Effect of blade roughness on boundary-layer behaviour

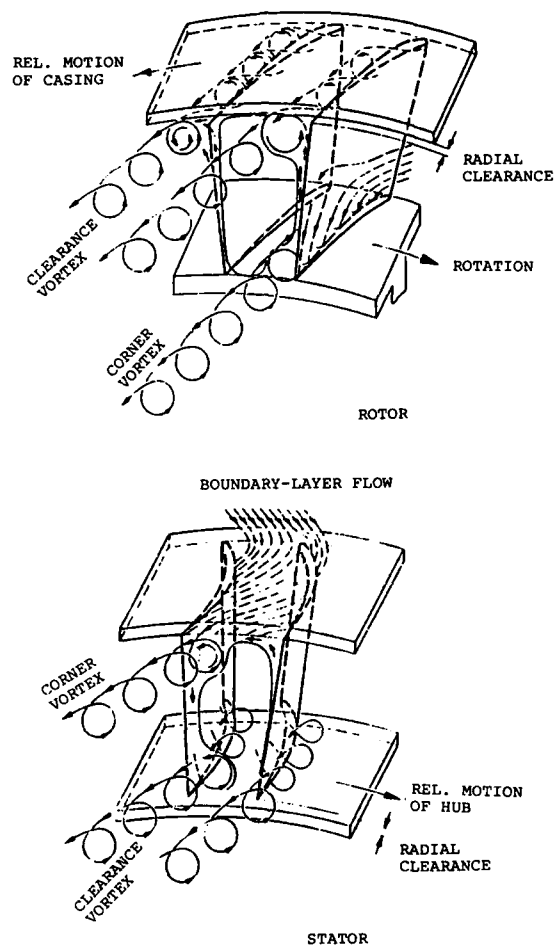


Fig. 10

Secondary flow regions in rotor and stator of an axial-flow compressor

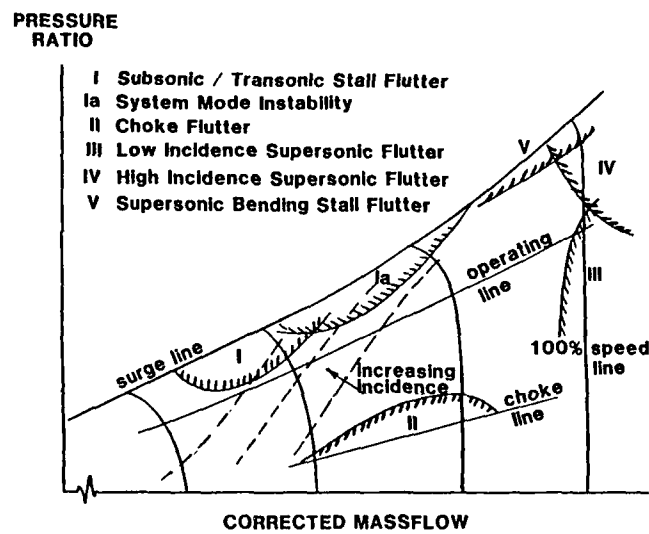


Fig. 11

Flutter limits in a compressor performance map

DESIGN CRITERIA FOR OPTIMAL BLADING DESIGN

by
Hans Starcken
Institut für Antriebstechnik
DLR
Linder Höhe
5000 Köln 90
W.-Germany

SUMMARY

Since about 1975 numerical methods are available to compute cascade blade shapes from prescribed surface velocity distributions in compressible flow ranges. Two-dimensional or quasi three-dimensional inverse or design methods enabled thereby the improvement of compressor and turbine cascades via an optimized blade pressure distribution. The theoretical and experimental development of such pressure distributions is described for the subsonic, supercritical, transonic and supersonic velocity range of compressor cascades. The equivalent problems in turbine cascades are indicated.

LIST OF SYMBOLS

a	sonic velocity	T	transition point
c	chord	T_u	turbulence intensity
d	blade thickness	v	velocity
H_{32}	boundary layer shape parameter = δ_2/δ_2^*	w	velocity
I	Tolmien-Schlichting instability point ²	x	coordinate along chord and axial chord
l	chord	β	flow angle
M	Mach number	δ_2	boundary layer momentum loss thickness
M_E	surface Mach number	Θ	flow turning - $\nu_1 - \nu_2$
M^*	intersection Mach number (Fig.34)	ρ	density
M_{is}	isentropic Mach number = $f(p/p_{tot1})$	ω	loss coefficient
M_{ss}	pre-shock Mach number	ω_s	$= p_{tot1} - p_{tot2} / p_{tot1} - p_1$ shock loss coefficient
p	static pressure	\dots	axial velocity density ratio (AVDR)
p_{tot}	total pressure		$= \rho_2 \cdot v_2 \cdot \sin \beta_2 / \rho_1 \cdot v_1 \cdot \sin \beta_1$
Re	Reynolds number		
R_N	leading edge radius		
s	spacing		
t	spacing		

SUBSCRIPTS

- 1 inlet
2 exit



INTRODUCTION

Within the last ten years a successful development of new blade design methods has been reported. Names like "Prescribed Velocity Distribution" (PVD), "Controlled Diffusion" (CD) and "Custom Tailored" (CT) Airfoils characterize this development in the turbomachinery world. This was possible because direct and inverse computational codes became available for high subsonic and transonic cascade flow fields which enabled the tailoring of blade geometries according to desired flow fields and boundary layer behaviours.

The idea of this technique is, of course, not a new one. In fact, the NACA airfoils for instance and especially the 6-series have been developed in the same way by prescribing the surface velocity distributions. But due to the lack of fast computers and computational codes it was necessary to adjust the profile geometry to the desired boundary conditions using empirical data and correlations to account for the unknown real flow effects. The drawback of this method is twofold. The high number of geometric as well as flow parameters of a cascade limits the empirical data base on one side and does generally not allow a design optimization with regard to loading, Mach number etc. on the other side. Therefore, quite often axial flow turbomachinery bladings were developed by a time consuming trial and error method.

Today we are in a better position with regard to our design tools. But still we have to learn how to handle them and how to overcome their existing limitations. In addition these new design tools are time consuming and it is therefore advisable not to start in each blade design from scratch but also to make use of past experience, especially that from experiment. The development of certain criteria for tailoring the best possible velocity distribution under given boundary conditions is such a way. These criteria result from theoretical considerations verified and completed by cascade and turbomachinery tests. The following chapters deal with this subject whereby the different inlet velocity ranges are treated separately.

Generally, the aim of the aerodynamic optimizations is the reduction of the total pressure losses to a minimum and the increase of the loading to a maximum which means a maximum pitch chord ratio or a minimum blade number. Additionally the off-design operating range should also be as large as possible. Depending on the requirements of the turbomachine the main attention is directed more to one or to the other point or a compromise has to be found. There is, however, little information available on off-design optimizations. So far, the main attention has been directed towards the improvement of the design-point operation.

SUBSONIC PRESSURE DISTRIBUTION

In the development of low drag airfoils extended laminar suction surface boundary layers were proposed and applied in the 50's. In 1959 this was supplemented by Stratford /1/,/2/ who published a way to optimize the turbulent boundary layer to reach a maximum diffusion. He derived a rapid method for the prediction of turbulent boundary layer separation which included the pressure rise and required only a single empirical factor. An extension led to the pressure distribution which just maintains zero skin friction throughout the region of pressure rise and which is now often called "Stratford distribution". The application of this distribution to blade or airfoil suction surfaces renders possible very different velocity distributions depending on the prescribed position of the transition point which is identical to the onset of the pressure recovery. Fig.1 from Liebeck /3/ shows as an example such different pressure distributions which were calculated for a fixed downstream pressure value. A transition point near the leading edge renders possible a very strong deceleration due to a thin laminar boundary layer at this point. Therefore the peak velocity can be very high. However, a transition point near the trailing edge limits the maximum velocity considerably due to a thick laminar boundary layer followed by a reduced turbulent diffusion capability. An integration of these curves leads to different lift coefficients with a maximum at a transition point position around 45% of chord.

Similar velocity distributions were also obtained by Fottner (published by Scholz /4/) who applied a constant near separation shape parameter H_{12} in the diffusion region as proposed by Eppler /5/. An integration of his curves yielded a maximum loading at a transition point position around 30% of chord, as shown by the bottom curve in Fig.2.

This optimum position of the transition point with regard to highest loading was also confirmed by Papailiou /6/ who used an inverse boundary layer method developed by Le Poll to optimize the suction surface velocity distribution. Fig.3 shows the dependency of his results on the transition point location and Fig.4 the optimum velocity distribution he used to design a high camber compressor stator blade section. The profile shape he obtained with the aid of a conformal mapping method is also shown in Fig.4. The geometry is typical for this so called flat or laminar roof top type of pressure distribution with a Stratford like recompression. It is characterized by high front and low rear camber. Due to a limited suction capacity of the cascade wind tunnel a complete experimental verification of this design failed but the results confirmed the design tools.

At the same time (around 1970) similar design methods and optimization techniques had already entered into practice in turbine development. Fig.5 shows as an example a 3-parameter velocity distribution applied to the design of a turbine blade as described by Payne /7/. The suction surface velocity exhibits the same basic idea of a laminar roof top distribution with a Stratford like recompression as proposed above for compressor blades.

However, it was later recognized that this distribution is very sensitive to turbulence levels due to transition point movement (Fig.6. Sharma, et al. /8/) and an accelerated - also called aft loaded - suction surface velocity distribution became the more favorite one. Typical examples are presented for instance by Cherry, Dengler /9/. As shown in Fig.7 from Eckardt, Trappmann /10/ the accelerated distribution of a LP turbine results in long laminar boundary layers even at high turbulence levels and consequently smaller momentum loss thicknesses and improved efficiencies.

The maximum velocity position has to be selected according to the pressure recovery capability of the boundary layer including a possible laminar separation bubble. The latter is especially important at low Reynolds numbers where the separation bubble may be long and requires a considerable length for reattachment. This may even lead back to the laminar roof top design as described by Patterson and Hoeger /11/ who called this "combination" loaded because it combines a mid and aft loaded design.

The pressure surface velocity distribution is generally selected according to strength and stiffness requirements of the blade section. In addition, of course, the integrated pressure difference between suction and pressure surface has to be in accordance with the desired flow turning and pressure drop or rise. Therefore, the final design pressure distribution is generally achieved only in an iterative process.

Thereby it has also to be considered that the final blade section has to have a certain operating range at positive and negative incidences. This is especially important for compressor blades. In Fig.8 the considerable changes of the surface Mach number distribution is shown in the operating range of a compressor stator blade section. In order to "adjust" the design point correctly within this range, either the above described optimum velocity distribution may be changed or the blade design could

be performed at an inlet flow angle which is different from the operating point in the turbomachine. The feasibility of the latter method has been proved by Rechter and Steinert /12/ who designed and tested a blade section at two different inlet flow angles but similar surface Mach number distributions. The measured performance curves are shown in Fig.9. The positive incidence range was thereby extended by the same amount as the design inlet flow angle was changed, whereas the negative incidence range was reduced, so that the higher camber resulted in a smaller overall operating range.

SUPERCritical PRESSURE DISTRIBUTION

Within the 70's numerical methods and computer systems became available which had the capacity to solve also compressible flow cases including local supersonic areas. In particular inverse codes now offered the possibility to develop, at least theoretically, shock free compressor blade sections. This stimulated the numerical blade design considerably. In the beginning the laminar roof top pressure distribution was also considered to be the best choice for the design of the so-called "supercritical cascades". Korn /13/ was the first who published such inverse designed compressor and turbine cascades applying also the Stratford distribution (Fig.10 and 11). However, in his turbine example he already applied an acceleration along the suction surface up to the peak velocity and not a roof top distribution. The compressor blade, on the other hand, exhibits a considerable rear loading which leads to a minimum blade thickness ahead of the thick trailing edge. The overall loading of this design is very high due to a pitch-chord ratio of 1.2. Based on this concept and by order of Pratt & Whitney, Korn developed a cascade which was tested in a cascade wind tunnel at the DFVLR in Köln to validate the design code.

In Fig.12 design and measured blade Mach number distribution are compared as reported by Stephens /14/. With the exception of the flat roof top and the correct exit Mach number the basic concept could be confirmed. The first difference was later detected as a result of a manufacturing inaccuracy of the blade leading edge whereas the second one was due to an increased axial velocity density ratio (AVDR) above the design value in the test. The latter was necessary to avoid strong boundary layer separation. In other words, the design diffusion rate according to the Stratford criterion was slightly too high and had to be reduced by increasing the AVDR.

The success of this supercritical design, especially with regard to the low loss level which was also attributed to the absence of shock waves (Fig.13), caused the DFVLR to develop its own blade section called SKG-DFVLR 1.3 (Rechter et al. /15/). The suction surface Mach number distribution was kept identical to the Korn blade whereas the rear loading of the pressure side had to be reduced in order to achieve a finite blade thickness (Fig.14). This was due to the velocity triangles chosen according to a realistic stator blade application. The blade geometry was calculated by E. Schmidt using an inverse full potential code /16/. The cascade test results, however, were very disappointing. The minimum loss coefficient was quite high and the off design behaviour was very bad. Fig.15 shows the dependency of the losses from the inlet Mach number. Thereby the differences between design and measured surface Mach number distributions were in the same order of magnitude as for the Korn blade (Fig.16). However, there is one important deviation and that is the suction surface Mach number near the leading edge. Contrary to the P&W blade, the DFVLR section exhibited a leading edge suction peak resulting in an upstream position of the transition point. From a boundary layer analysis it was derived that a forward movement of the transition point up to 10% of chord would lead to early turbulent separation. In Fig.17 the development of the boundary layer shape parameter H_{32} at two different transition point positions is shown. The final conclusion was that the suction peak, caused also by manufacturing errors of the leading edge, was responsible for the bad performance of this cascade.

Consequently Pratt & Whitney as well as DFVLR changed the flat roof top design of the velocity distribution to an accelerated one. Fig.18 shows the basic supercritical compressor blade design concept of P&W as published by Stephens and Hobbs /17/. Cascade tests performed at DFVLR confirmed this concept not only at design condition but also at off design. Some results of a stator blade section are shown in Fig.19 to 21 /17/. Fig.22 and 23 show the improvements of Mach number and incidence range of the Controlled Diffusion Airfoils as compared to standard series airfoils as published by Hobbs and Weingold /18/. These authors also report a significantly higher loading capability of the new airfoils.

The DFVLR concept was derived in the following way. Calculations of the boundary layer behaviour of the first 30% of the suction surface of an accelerated, a flat roof top, and a peaky Mach number distribution, revealed very different positions of instability and transition points. In Fig.24 from Weber et al. /19/ results are presented at a turbulence level of about 1.6% which leads to a Reynolds number difference of $Re = 100$ (after Granville) between instability I and transition point T. Most important is the long distance between I and T for the flat roof top distribution. This points to a high sensitivity of such designs according to inlet turbulence intensity, surface roughness and Reynolds number levels. If the before mentioned sensitivity of the transonic flow to small geometric variations and errors in the design code are considered as well as an often required positive incidence range, the accelerated distribution becomes the most attractive one. It offers low losses due to long laminar boundary layers, a stable transition point, a reasonable loading, and a two to three degrees of positive incidence range which is about half the total off-design value. The maximum Mach number was selected around $M = 1.25$ in order to avoid boundary layer separation in

case normal shock waves would occur.

The rear turbulent diffusion part of the suction surface was optimized also by a boundary layer calculation. Fig.25 and 26 show three important steps of this development /19/. The first step was the generation of a Stratford like Eppler distribution called SKG 2.3.18 with a nearly constant H_{32} -value from 35 to 100% of chord. This resulted in a very high diffusion rate down to a Mach number below $M_2 = 0.5$. However, the momentum loss thickness δ_{32} at the trailing edge was quite high in this case. Unloading the rear (SKG 2.3.1) reduced δ_{32} down to less than half the value before. But the very high diffusion rate between 30 to 35% was considered too dangerous with respect to a possible shock induced boundary layer separation. Therefore, a gradual decrease of the shape parameter H_{32} was selected which led to the final Mach number distribution SKG DFVLR 2.7. The resulting momentum loss thickness is about half way between those of the other two distributions.

The experimental verification was performed again in a wind tunnel. Cascade geometry and velocity triangles were identical to the SKG DFVLR 1.3 blade tests. In Fig.27 the design and measured surface Mach number distributions are compared. The agreement is quite good. Differences at the leading edge and on the suction surface were due to limitations of the design code of E. Schmidt at that time and due to a laminar separation bubble. Even though the minimum total pressure loss coefficient was half the value of the SKG DFVLR 1.3 cascade and also the off design behaviour was improved considerably (Fig.28). The local laminar boundary layer separation does obviously not affect the overall loss coefficient in this case where the chord Reynolds number was around one Million. However, if a low critical Reynolds number is required a more peaky pressure distribution has to be selected. An application of a special transition length within the pressure distribution having a moderate diffusion as proposed by Walker /20/ and shown in Fig.29 seems not to be necessary because the flow adjusts itself by building up a corresponding "fluid blade shape" by a laminar separation bubble.

The experience of P&W and DFVLR was later also confirmed by cascade tests at the NASA. Boldman et al. /21/ reported in 1983 the experimental investigation of a supercritical compressor stator cascade. The blades were designed by the method of Bauer, Garabedian and Korn (BGK) whereby the pressure distribution on the blade surface is prescribed as part of the input. The design surface Mach number distribution together with the blade shape is shown in Fig.30. Again a laminar roof top distribution with a Stratford recompression was selected. Also again, this distribution could not be reached in the cascade experiments. Instead, a long laminar separation bubble was observed near the 10 percent suction surface chord location. The related Mach number distribution as shown in Fig.31 exhibited two suction peaks and complete separation around 50% of chord at design inlet angle and Mach number. A measured total pressure loss coefficient in the order of 8% is therefore not surprising. By a small variation of the blade geometry, as shown in Fig.32 from the report of J.F. Schmidt et al. /22/, the flat roof top distribution was then changed to an accelerated one, shown in Fig.33. Besides an excellent agreement between measured and calculated surface Mach number distribution the total pressure loss coefficient of the redesigned blade went down to 3.5%. Also the off-design loss behaviour was improved considerably.

All the above described results indicate the superiority of the accelerated suction surface Mach number distribution for supercritical compressor cascades. But these data do not clearly answer the question about the maximum allowable suction surface Mach number at low losses. As Starken and Jawtusch /23/ have shown quite recently for controlled diffusion blades, the loss rise onset with inlet Mach number seems to depend on a so-called "intersection Mach number" M_{int} . M_{int} is obtained at the unique intersection point of the suction surface Mach number distributions derived at different inlet flow angles. It is therefore some kind of an average surface Mach number taking into account also the off-design behaviour of the cascade. An example of a controlled diffusion rotor blade calculated with an inviscid code is shown in Fig.34. Deriving M_{int} in this way at different inlet Mach numbers M_1 results in curves as presented in Fig.35 for different controlled diffusion blades (Fig.36).

The corresponding optimum loss rise curves, normalized by the minimum measured loss value, are shown in Fig.37. The onset of the loss rise varies between about $M_{int} = 0.68$ and $M_{int} = 0.92$. However, if these curves are plotted as a function of the intersection Mach number M_{int} the onsets coincide near $M_{int} = 1.0$ and the loss rise curves may be approximated by an average one (Fig.38). From these results a maximum inviscid M_{int} value in the order of 1.05 can be derived as design criterion for low loss supercritical compressor airfoils. The method is limited to CDA blades because it is based on the condition that the loss rise is caused primarily by the inlet Mach number. It does not apply to blade sections which exhibit boundary layer separations already at lower Mach numbers.

A direct calculation of the off-design surface Mach number distributions should always be performed to check the correct position of the design point inlet flow angle. Already the inviscid results, as for example those shown in Fig.34, allow a good estimate about the minimum loss inlet flow angle. It is generally connected with that incidence where the maximum suction surface Mach number has its minimum. If this check is not performed it may easily happen that the design incidence position is very near to choking or stalling of the cascade. This is also due to the fact, that with decreasing pitch-chord ratio, which is generally necessary with increasing flow turning, the maximum velocity point has to be moved upstream towards the leading edge. A typical example is the ONERA 115 cascade ($s/l = 0.28$, $\alpha = 50^\circ$) of Fig.37 with a predicted inviscid Mach number distribution as shown in Fig.39. At this low pitch chord ratio the

maximum velocity could only be at or around the 30% chord position under choked condition.

In conclusion the following criteria can be stated for the design of supercritical compressor blade suction surface pressure distributions:

- Maximum velocity around 30% of chord (at s/c above about 0,7). Further upstream position at low Re-number and pitch-chord ratios.
- Front part accelerating.
- Rear part decelerating with a continuously falling boundary layer shape parameter H_{32} .
- Maximum intersection Mach number M_g around 1,05.

TRANSONIC PRESSURE DISTRIBUTION

Until the end of the 50's sonic velocity has been considered as an upper limit for flows in compressor bladings. The experience had shown that higher local velocities led to an intolerable increase in total pressure loss coefficients and consequently in a severe drop in efficiency. The test results from cascade wind tunnels could even lead to the suggestion of a limiting barrier (Fig.37).

However, the efforts in the US in the development of supersonic compressors showed surprisingly good performance of these machines around sonic inlet velocities. This resulted in the development of the transonic axial flow compressor now extensively used in modern jet engines. It was possible by the development of new compressor blade sections. Fig.37 shows as an example also the loss coefficient of a typical transonic rotor cascade (Multiple Circular Arc L030-4) with a moderate loss increase with inlet Mach number passing sonic velocity without any difficulties. In order to understand the reason for this loss behaviour, the cascade and blade section geometry as well as the related surface Mach number distribution must be compared.

At first the cascade and blade section geometry is considered. In Fig.36 the geometry of the subsonic cascade called SKG-FVV 2.2 is presented. This cascade was designed and optimized for an inlet Mach number of 0.85 (Weber et al. /19/). It is a so-called "supercritical cascade" with local supersonic velocity on the suction surface and designed for shock free deceleration. A pitch-chord ratio of 1.0 and 20° turning were prescribed in this design. The MCA blade section of the transonic cascade L030-4 of Fig.36 (Schreiber, Starken /24/), however, looks quite different. The blade thickness as well as the blade camber distribution are different and especially the pitch-chord ratio is considerably lower ($s/c=0.62$).

All these geometrical differences result in very different surface Mach number distributions when compared at identical inlet flow velocities. Fig.40 shows these distributions around $M_1 = 0.83$. Due to the higher blade loading (larger pitch chord ratio and 4° higher turning) and also due to the thick leading edge and front thickness of the subsonic airfoil, the suction surface velocity exceeds sonic conditions whereas the velocity of the transonic airfoil remains everywhere subsonic. Nevertheless the loss coefficient of the supercritical design is smaller than that of the transonic one because of the higher pitch-chord ratio.

However, at increased inlet velocities as for instance around $M_1 = 0.91$, shown in Fig.41, the high blade loading becomes detrimental to the subsonic cascade. The suction surface Mach number reaches nearly $M = 1.3$ causing complete boundary layer separation behind a normal shock wave. On the contrary, the Mach number past the transonic airfoil remains below 1.2 and the boundary layer stays unseparated.

The final conclusion of these results is therefore: Any efficient transition of a compressor cascade to supersonic velocities requires a limitation of the suction surface Mach number to values below 1.3 at $M_1 \geq 1.0$. This, in turn, limits pitch-chord ratio, front suction surface camber, and leading edge radius as the responsible parameters.

In order to elucidate this even more, the influence of the blade suction surface and the pitch chord ratio is demonstrated by some test results obtained at subsonic and low supersonic velocities. In Fig.42 the measured total pressure loss coefficient is plotted as function of the inlet Mach number of three different double circular arc (DCA) blade sections with 30° , 15° and 10° meanline camber and various pitch-chord ratios (Starken /25/). In addition the results of the MCA, the FVV and of a wedge-type MTU cascade (Fottner, Lichtfuss /26/) are included. Some cascade and blade section geometries are shown in Figs. 43 to 46 together with Schlieren pictures taken around sonic inlet velocity. The Schlieren pictures show quite clearly the boundary layer separation and the dependency of this separation from the blade suction surface camber. By reducing the latter the total pressure losses can be reduced considerably.

The main reason for this is the reduced Mach number ahead of the shock waves. Fig.47 shows a correlation of the measured loss coefficients of several cascades as function of the measured maximum or pre-shock surface Mach number $M_{s,s}$. Plotted are the minimum losses which could be achieved so far at maximum back pressures. The correlation is based on a limited amount of data and should be considered as a preliminary one. But it shows

two facts quite clearly, that is the considerable loss increase above a pre-shock Mach number of 1.2 to 1.3 and an additional dependency of this increase on the maximum blade thickness.

Fortunately, the supersonic flow allows a deceleration and pressure rise without any flow turning and therefore efficient transonic blade sections could be developed for transonic compressor rotors having low camber. However, the design of a high turning (i.e. $\theta > 20^\circ$), low loss transonic decelerating blade section is still an unsolved problem.

This holds true also for supersonic inlet velocities. Similarly the surface Mach number should also be as low as possible in the higher Mach number range. Above inlet Mach numbers of about $M_1 = 1.4$ it is therefore advisable to apply negative suction surface camber. This reduces also the bow shock strength and allows the design of a low loss oblique passage shock in the entrance region making use of the strong oblique shock solution. An example of such a blade section is shown in Fig. 48 (Schreiber /27/). The design flow configuration has been verified experimentally by L2F measurements in a cascade wind tunnel. A detailed loss analysis revealed the shock losses as 55% of the overall loss coefficient of $\omega = 0.13$ at the design inlet Mach number of $M_1 = 1.5$. Although the turbulent suction surface boundary layer is completely separated behind the first passage shock, a considerable diffusion is achieved in the blade passage as shown in Fig. 49. This is a typical flow situation for compressor blade sections at supersonic inlet Mach numbers. Above sonic velocity it is generally impossible to avoid shock induced boundary layer separation. The efficient design of these airfoils may be therefore described more as a controlled separation rather than a controlled diffusion one.

Besides the surface curvature also the leading edge thickness influences the suction surface Mach number level. Fig. 50 gives an impression of this influence. The diagram shows the difference between suction surface and inlet Mach number as function of inlet Mach number and leading edge radius ratio of a flat plate cascade as derived by a unique incidence calculation described by Starken et al. in /28/.

LIST OF REFERENCES

- /1/ Stratford, B.S. "The Prediction of Separation of the Turbulent Boundary Layer." Journ. of Fluid Mech. Vol. 5, pp. 1-16 (1959).
- /2/ Stratford, B.S. "An Experimental Flow with Zero Skin Friction Throughout its Region of Pressure Rise." Journ. of Fluid Mech. Vol. 5, pp. 17-35 (1959).
- /3/ Liebeck, R.H. "Design of Subsonic Airfoils for High Lift." AIAA, J. Aircraft, Vol. 15, No. 9, pp. 547-561 (1978).
- /4/ Scholz, N. "Aerodynamik der Schaufelgitter." G. Braun, Karlsruhe (1965).
- /5/ Eppler, R. "Ergebnisse gemeinsamer Anwendung von Grenzschicht und Profiltheorie." Z. f. Flugwissenschaften 8, 247-260 (1969).
- /6/ Papailiou, K. "Optimisation d'aubages de compresseur à forte charge sur la base de theories de couches limites." VKI TN 55 (1969).
- /7/ Payne, D. "Axial Turbine Blading" in "Gas Turbine Blading Design". Symposium at Borough, Polytechnic, 1970.
- /8/ Sharma, O.P.; Wells, R.A.; Schlinker, R.H.; Bailey, D.A. "Boundary Layer Development on Turbine Airfoil Suction Surfaces." Trans. of ASME, Journal of Eng. for Power, Vol. 104, July 1982.
- /9/ Cherry, D.G.; Dengler, R.P. "The Aerodynamic Design and Performance of the NASA/GE E Low Pressure Turbine". AIAA-84-1162, June 1984.
- /10/ Eckardt, D.; Trappmann, K. "Strahltriebwerke für Verkehrsflugzeuge der nächsten Generation". Vortrag Jahrestagung der DGLR, Oktober 1982.
- /11/ Patterson, D.J.; Hoeger, M. "The Effect of Reynolds Number and Velocity Distribution on LP Turbine Cascade Performance". ASME Paper 86-GT-271, 1986.
- /12/ Rechter, H.; Steinert, W. "Auslegung und experimentelle Untersuchung hochbelasteter Unterschall-Verdichtergitter." DFVLR IB-325-02-86, 1986.
- /13/ Korn, D. "Numerical Design of Transonic Cascades." ERDA Research and Development Report C00-3077-72, 1975.
- /14/ Stephens, H.E. "Application of Supercritical Airfoil Technology to Compressor Cascades: Comparison of Theoretical and Experimental Results." AIAA Paper No. 78-1138, 1978.
- /15/ Rechter, H.; Schimming, P.; Starken, H. "Design and Testing of Two Supercritical Compressor Cascades." ASME Paper No. 79-GT-11, 1979.
- /16/ Schmidt, E. "Computation of Supercritical Compressor and Turbine Cascades with a Design Method for Transonic Flows." ASME Paper No. 79-GT-30, 1979.
- /17/ Stephens, H.E.; Hobbs, D.E. "Design and Performance Evaluation of Supercritical Airfoils for Axial Flow Compressors." United Technologies Corporation Report FR 11455, June 1979.
- /18/ Hobbs, D.E.; Weingold, H.D. "Development of Controlled Diffusion Airfoils for Multistage Compressor Application." ASME Paper 83-GT-211, 1983.
- /19/ Weber, A.; Rechter, H.; Starken, H. "Verlustarme, superkritische Verdichterprofile." FVW Forschungsbericht Heft 344-2, 1984.
- /20/ Walker, G.J. "A Family of Surface Velocity Distributions for Axial Compressor Blading and their Theoretical Performance." ASME Paper No. 75-GT-34, 1975.
- /21/ Boldman, D.R.; Buggele, A.E.; Shaw, L.M. "Experimental Evaluation of Shockless Supercritical Airfoils in Cascade." AIAA Paper 83-0003, 1983.
- /22/ Schmidt, J.F.; Gelder, T.F.; Donovan, L.F. "Redesign and Cascade Tests of a Supercritical Controlled Diffusion Stator Blade-Section." NASA TM 83635, 1984.

- /23/ Starcken, H.; Jawtusch, V. "Der Machzahl- und Winkleinfluß auf Umströmung und Verluste superkritischer Verdichtergitter." VDI Bericht NR. 706, 1988.
- /24/ Schreiber, H.A.; Starcken, H. "Experimental Cascade Analysis of a Transonic Compressor Rotor Blade Section." ASME Paper 83-GT-209, 1983. Trans. ASME, Journal of Eng. for Gas Turbine and Power, Vol. 106, pp. 288 to 294, 1984.
- /25/ Starcken, H. "Loss Development in Transonic Cascade." In VKI Lecture Series 88-03 on "Transonic Compressors", 1988.
- /26/ Fottner, L.; Lichtfuß, H.J. "Design of Transonic Compressor Cascade for Minimal Shock Losses and Comparison with Test Results." AGARD-CP-351, 1983.
- /27/ Schreiber, H.A. "Experimental Investigation on Shock Losses of Transonic and Supersonic Compressor Cascades". AGARD-CP-401, 1986.
- /28/ Starcken, H.; Zhong, Y.X.; Schreiber, H.A. "Mass Flow Limitations of Supersonic Blade Rows due to Leading Edge Blockage". ASME Paper 84-GT-233, 1984 and Turbo & Jet-Engines Vol. 2, No. 4, 1985.

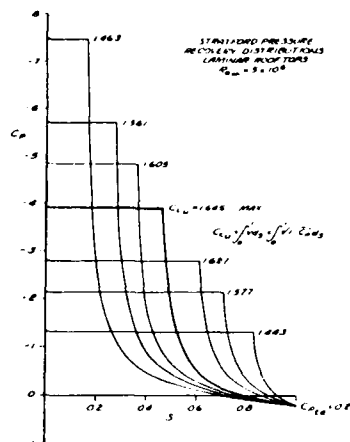


Fig. 1 Stratford pressure recovery distributions with laminar roof tops (Liebeck /3/)

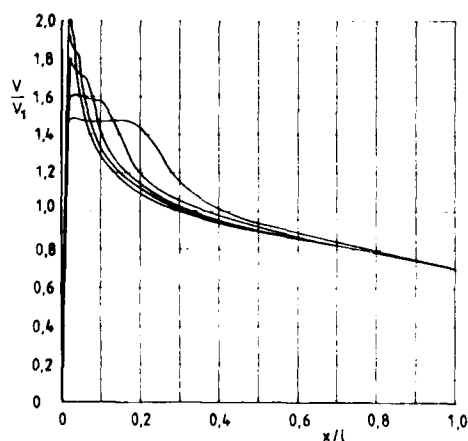


Fig. 3 Optimized velocity distributions computed by Papaliou /6/

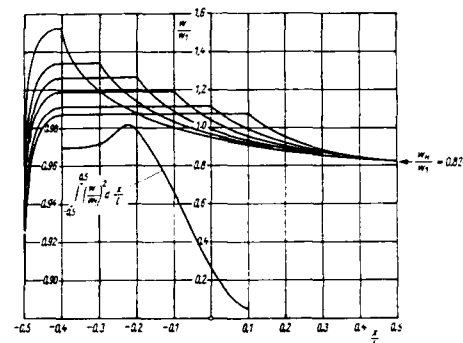


Fig. 2 Variation of optimum suction surface velocity distribution with transition point position at fixed overall velocity ratio computed by Fottner (Scholz /4/)

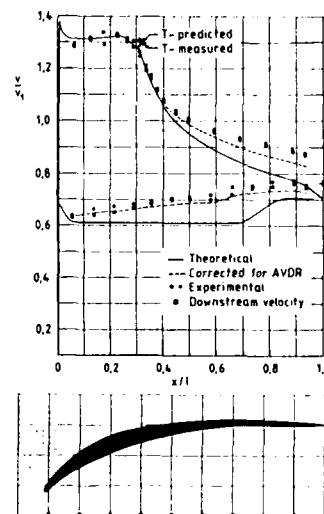


Fig. 4 Velocity distribution and blade shape of optimum loading compressor design by Papaliou /6/

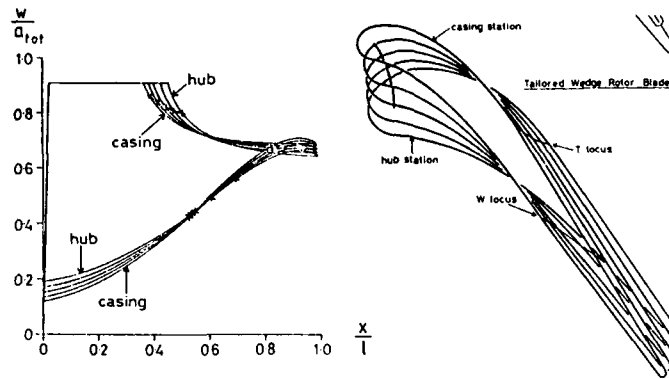


Fig. 5 Laminar roof top velocity distributions in the design of a turbine blade (Payne /7/)

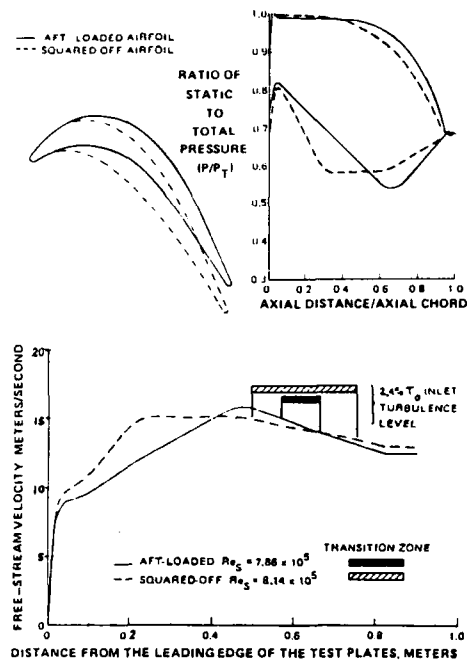


Fig. 6 Transition zones of laminar roof top (squared off) and aft loaded turbine airfoils (Sharma et al. /8/)

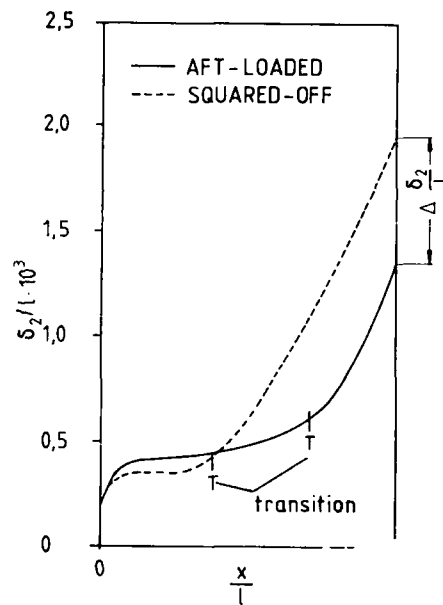


Fig. 7 Suction surface momentum loss thickness distribution of aft loaded and squared off velocity distribution (Eckard, Trappmann /10/)

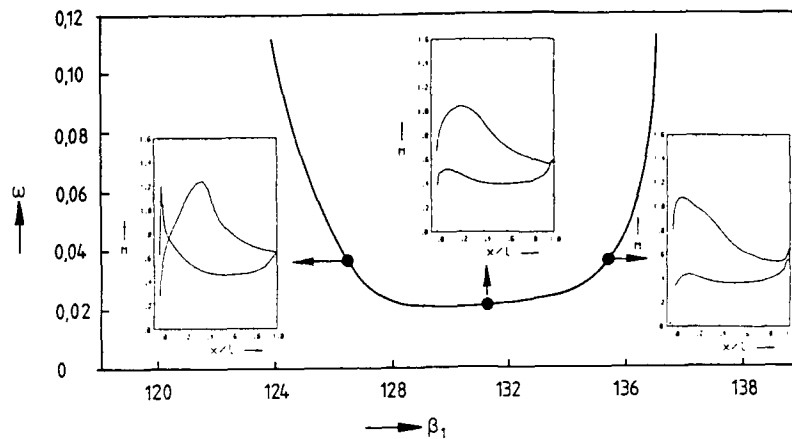


Fig. 8 Variation of surface Mach number distribution and loss coefficient with inlet flow angle of a compressor airfoil ($M_1 = 0.7$)

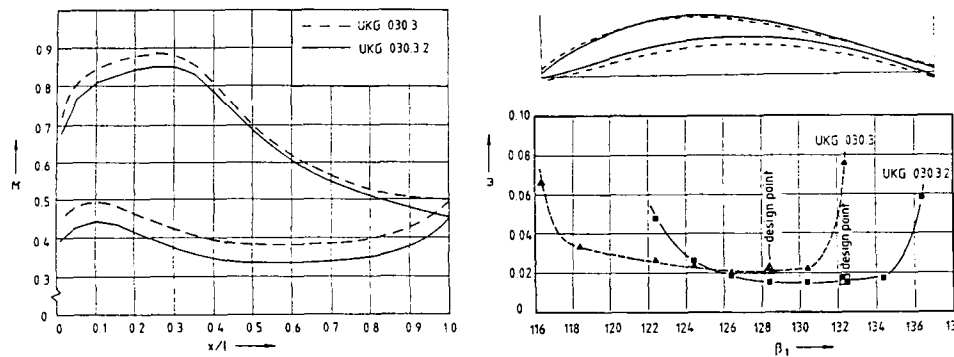


Fig. 9 Surface Mach number distributions, blade shapes, and loss curves of two Controlled Diffusion Airfoils designed at different inlet flow angles (Rechter, Steinert /12/)

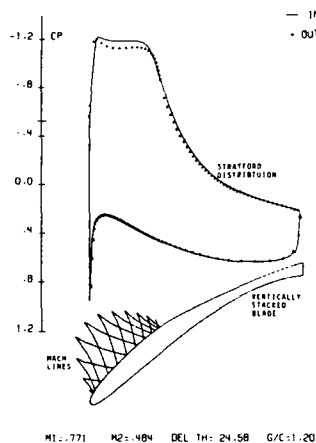


Fig.10 Laminar roof top distribution and airfoil shape of a supercritical compressor cascade (Korn /13/)

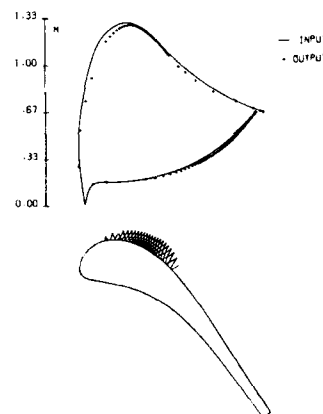


Fig.11 Surface Mach number distribution and blade shape of a supercritical turbine cascade (Korn /13/)

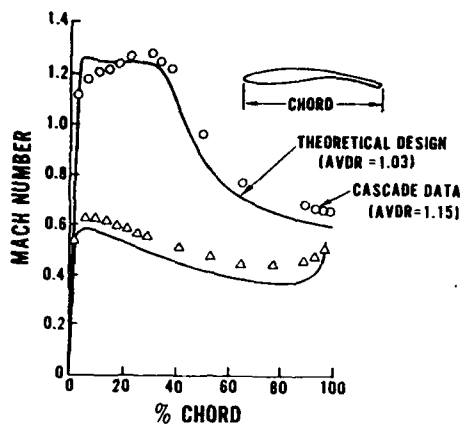


Fig. 12 Comparison of theoretical and measured Mach number distribution for the near-design test condition of a supercritical cascade (Stephens /14/)

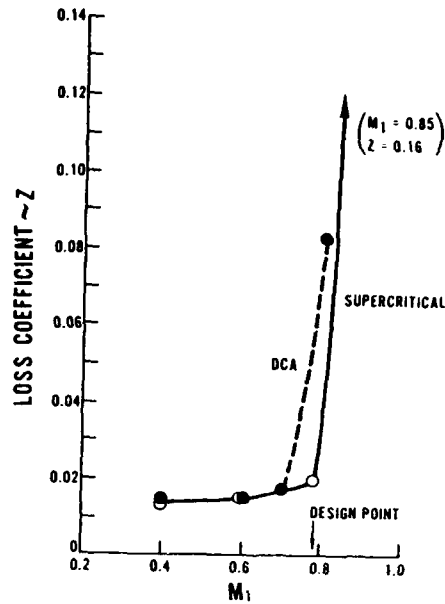


Fig. 13 Comparison of minimum loss performance for a supercritical and a DCA cascade (Stephens /14/)

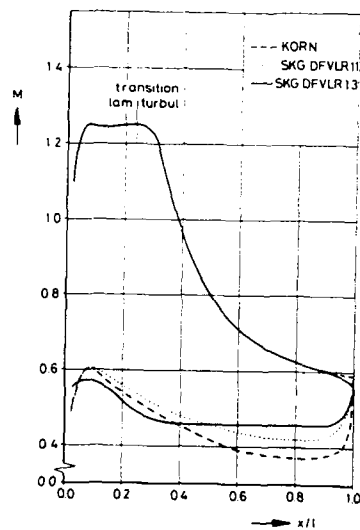


Fig. 14 Laminar roof top distribution SKG DFVLR 1.3 derived from the Korn design (Rechter et al. /15/)

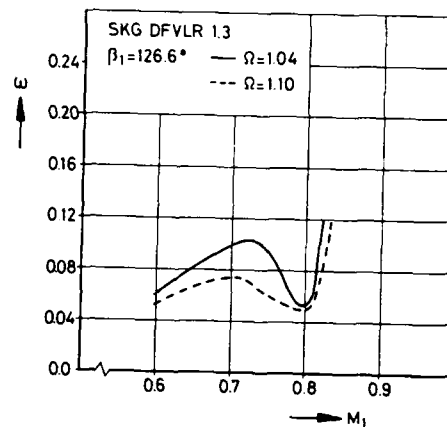


Fig. 15 Loss performance of the cascade SKG DFVLR 1.3 (Rechter et al. /15/)

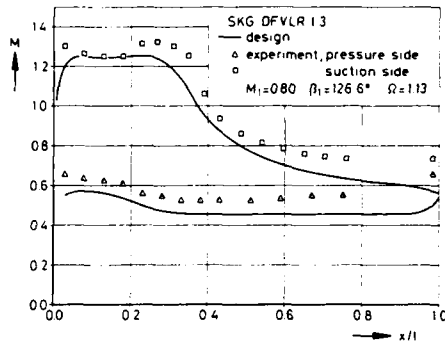


Fig. 16 Comparison of theoretical and measured Mach number distribution for the near-design test condition of the supercritical cascade SKG DFVLR 1.3 (Rechter et al. /15/)

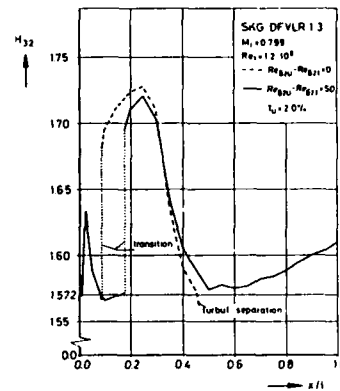


Fig. 17 Suction surface boundary layer shape parameter of the cascade SKG DFVLR 1.3 at two transition point positions (Rechter et al. /15/)

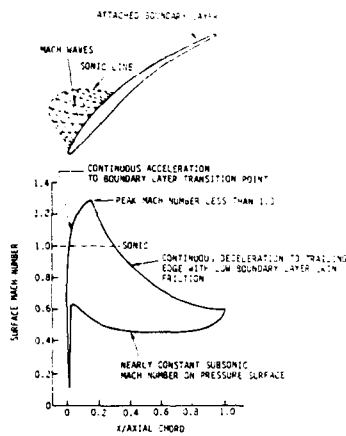


Fig. 18 Controlled Diffusion Airfoil aerodynamic design criteria of P&W (Stephens, Hobbs /17/)

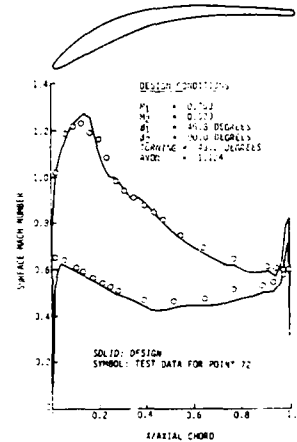


Fig. 19 Comparison of theoretical and measured Mach number distribution of a supercritical compressor exit guide vane (Stephens, Hobbs /17/)

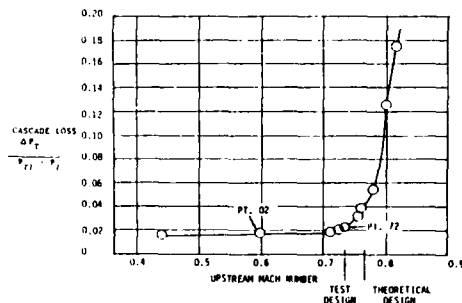


Fig. 20 Loss performance of a supercritical compressor exit guide vane (Stephens, Hobbs /17/)

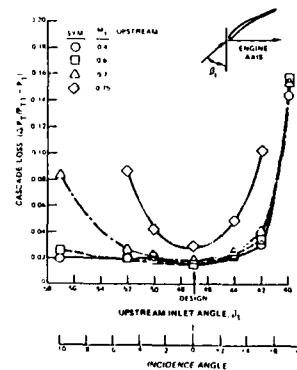


Fig. 21 Off-design loss performance of a supercritical compressor exit guide vane (Stephens, Hobbs /17/)

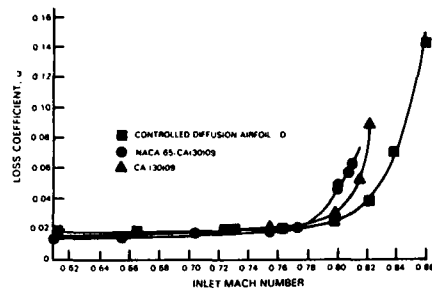


Fig. 22 Loss performance curve of Controlled Diffusion Airfoil D compared to standard series airfoils (Hobbs, Weingold /18/)

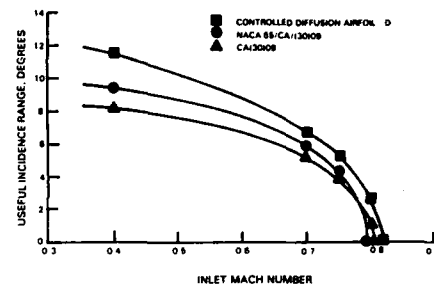


Fig. 23 Increased incidence angle range of Controlled Diffusion Airfoil D compared to standard series airfoils (Hobbs, Weingold /18/)

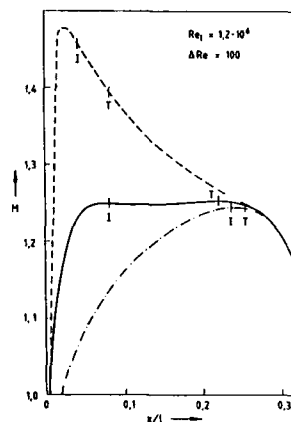


Fig. 24 Instability and transition point positions at different Mach number distributions (Weber et al. /19/)

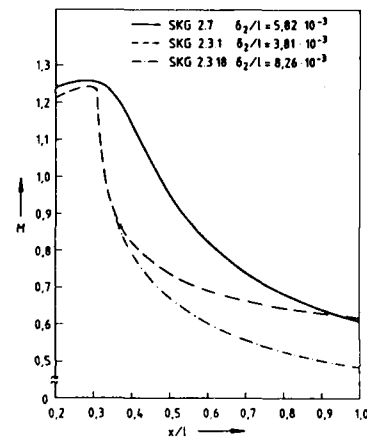


Fig. 25 Three different diffusion distributions and the resulting trailing edge momentum loss thickness (Weber et al. /19/)

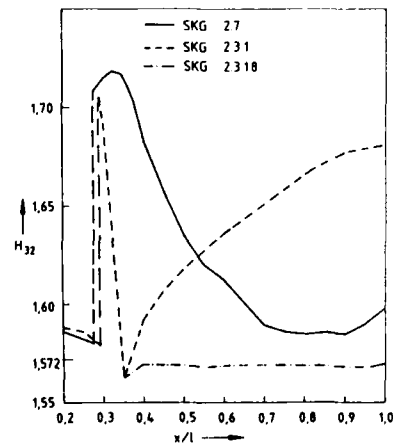


Fig. 26 Boundary layer shape parameter distribution of the diffusion curves of Fig. 25 (Weber et al. /19/)

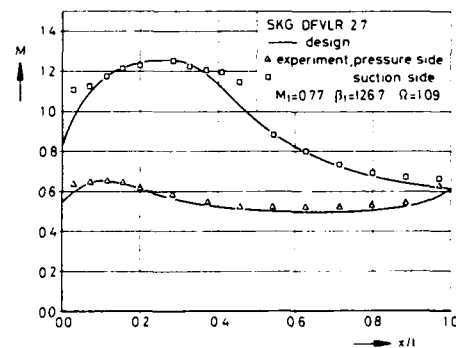


Fig. 27 Design and measured surface Mach number distribution of the supercritical cascade SKG DFVLR 2.7 (Rechter et al /15/)

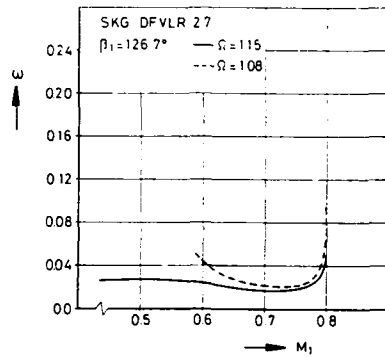


Fig. 28 Loss performance curves of the cascade SKG DFVLR 2.7 (Rechter et al. /15/)

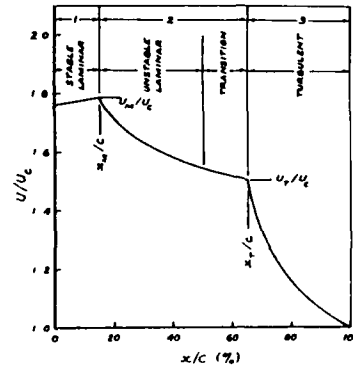


Fig. 29 Optimum suction surface velocity distribution proposed by Walker /20/

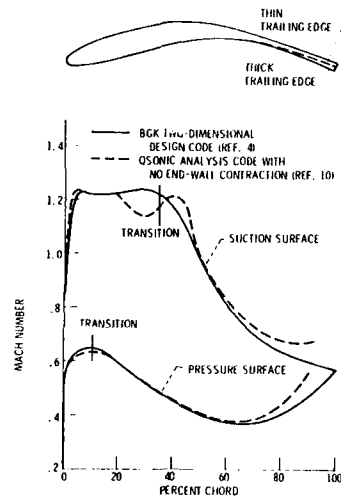


Fig. 30 Blade shape and surface Mach number distribution of supercritical NASA compressor cascade (Boldman et al. /21/)

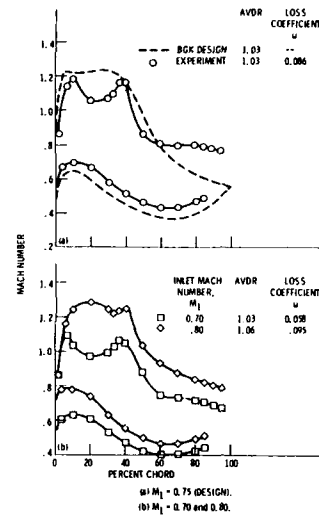


Fig. 31 Measured design and off design surface Mach number distributions of NASA cascade (Boldman et al. /21/)

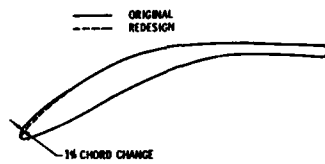


Fig. 32 Redesigned NASA blade shape (Schmidt /22/)

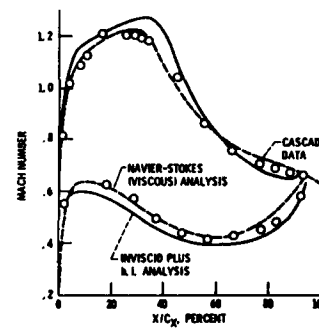


Fig. 33 Comparison of computed and measured near design surface Mach numbers of redesigned NASA cascade (Schmidt /22/)

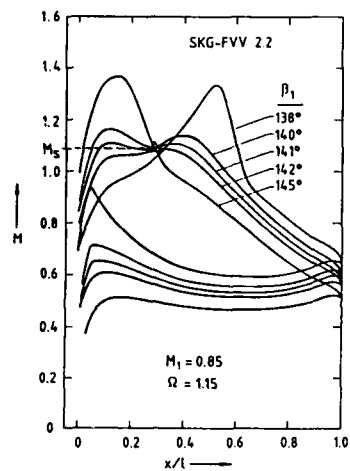


Fig. 34 Computed inviscid Mach number distributions of the supercritical compressor cascade SKG-FVV 2.2 at different inlet flow angles (Starken, Jawtusch /23/)

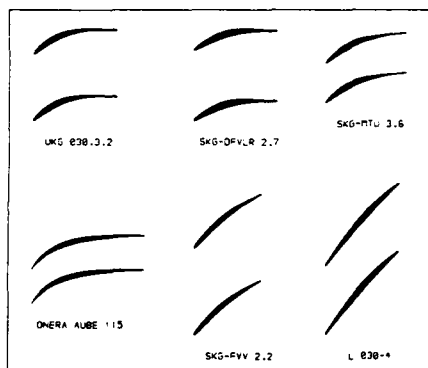


Fig. 36 Cascade sections of the Controlled Diffusion Airfoils of Fig. 35 (/23/)

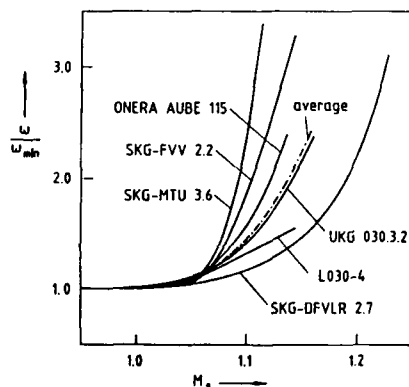


Fig. 38 Normalized loss performance curves correlated by the "Intersection Mach number" M_s (/23/)

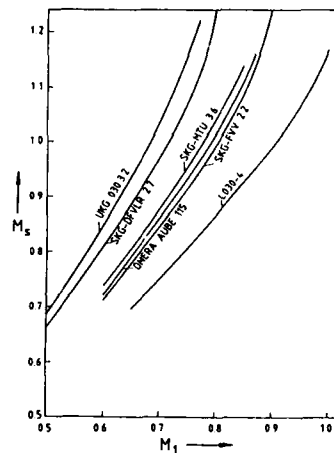


Fig. 35 Dependency of the "Intersection Mach number" M_s from the inlet Mach number for different Controlled Diffusion Airfoils (/23/)

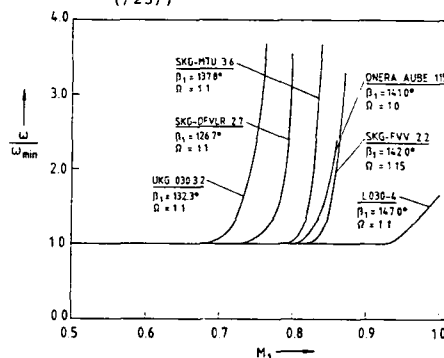


Fig. 37 Normalized loss performance curves of the Controlled Diffusion Airfoil Cascades of Fig. 36 (/23/)

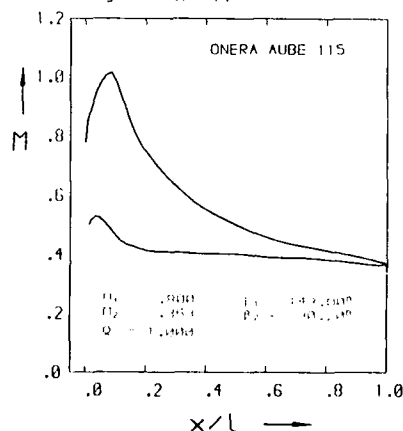


Fig. 39 Surface Mach number distribution of the low pitch chord ratio cascade ONERA AUBE 115

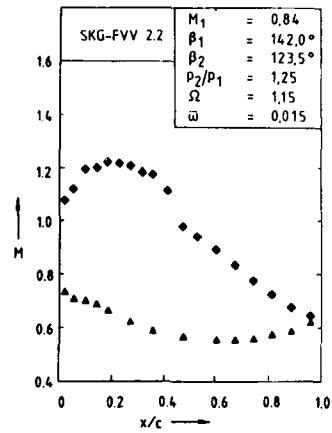


Fig.40 Surface Mach number distribution of supercritical and transonic blade section around $M_1 = 0.84$

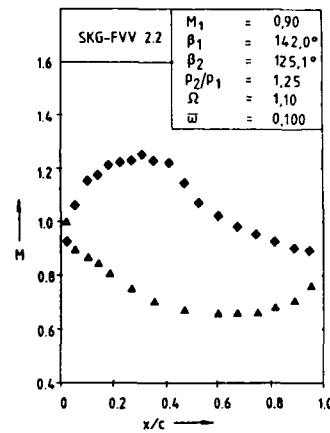
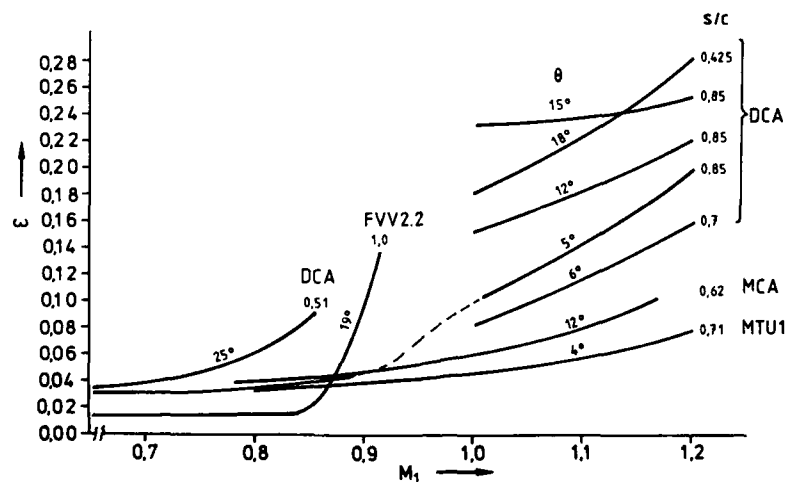
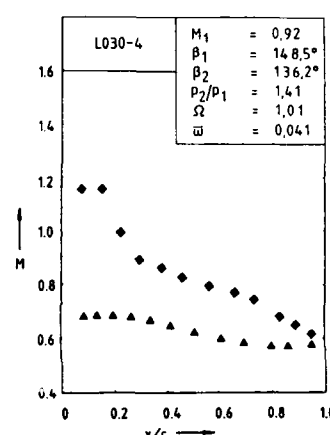
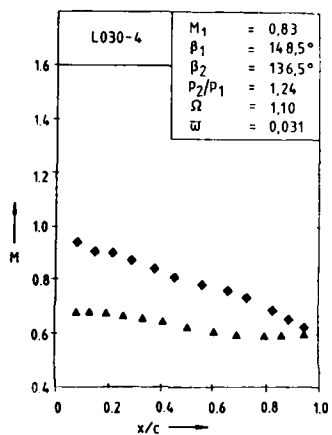


Fig.41 Surface Mach number distribution of supercritical and transonic blade section around $M_1 = 0.91$



ig.42 Loss performance curves of various cascade configurations around sonic inlet velocity (Starken /25/)

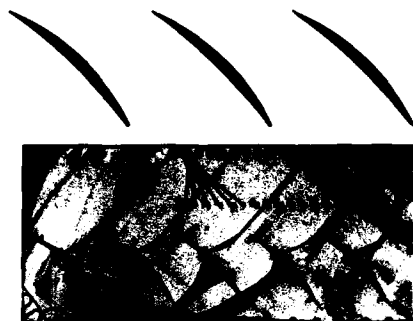


Fig.43 Cascade section and Schlieren picture of 30° camber DCA blade at sonic inlet velocity



Fig.44 Cascade section and Schlieren picture of 10° camber DCA blade at sonic inlet velocity

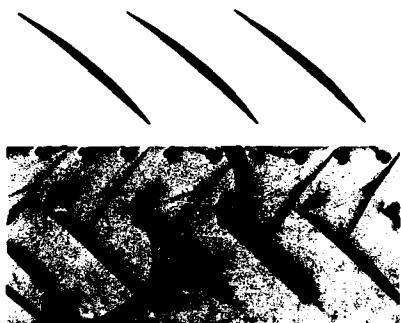


Fig.45 Cascade section and Schlieren picture of MCA blade at sonic inlet velocity

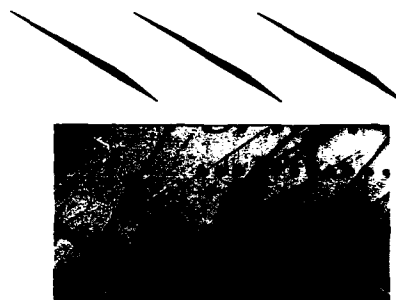


Fig.46 Cascade section and Schlieren picture of wedge type blade MTU 1 at sonic inlet velocity

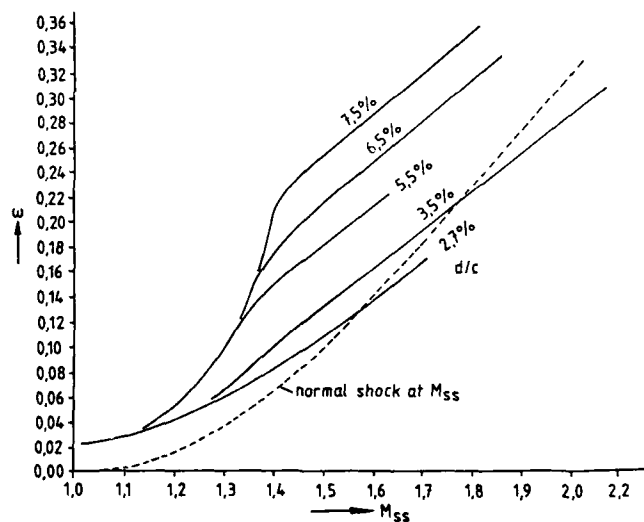


Fig.47 Dependency of measured minimum total pressure loss coefficient from pre-shock suction surface Mach number M_{ss} and relative blade thickness d/c (Starken /25/)

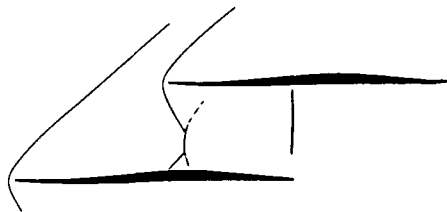


Fig. 48 Cascade geometry and shock pattern of supersonic precompression blade section PAV-1.5 (Schreiber /27/)

PAV-15

$M_1 = 1.529$ $p_2/p_1 = 2.13$ $\beta_2 = 150.8^\circ$
 $\beta_1 = 149.9^\circ$ $AVDR = 1.02$ $\omega = 0.144$
 $Re = 2.68 \cdot 10^6$ $\omega_s = 0.069$

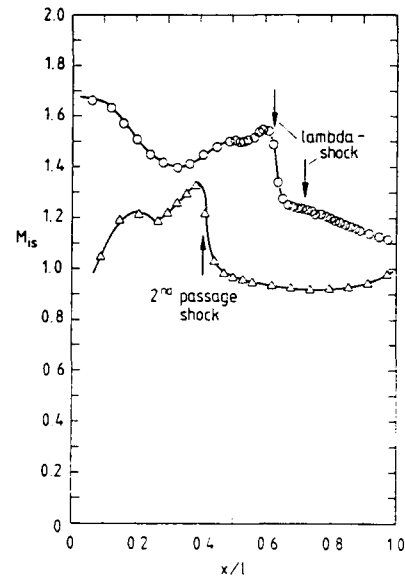


Fig. 49 Surface Mach number distribution of PAV-1,5 blade section at $M_1 = 1.529$ (Schreiber /27/)

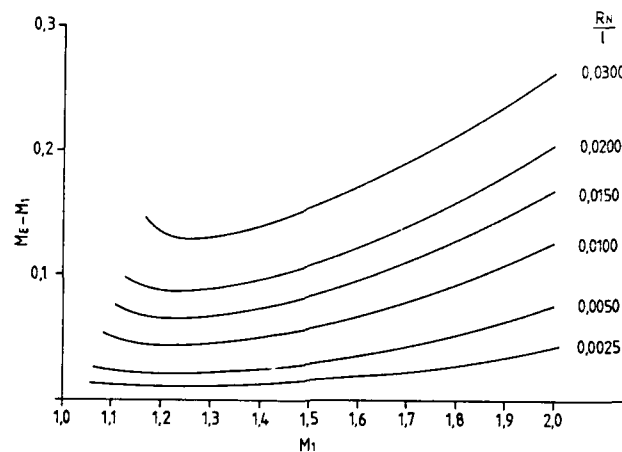


Fig. 50 Suction surface Mach number increase of a flat plate cascade due to leading edge bluntness

OVERVIEW ON BLADING DESIGN METHODS

G. MEAUZÉ

ONERA BP 72, 92322 Châtillon Cedex, France.

NOMENCLATURE

C_f	skin friction coefficient
C_p, C_v	specific heats
H	shape factor δ_1/δ_2
l	length
M	Mach number
r	radius
S	surface
T	temperature
t	time
V	absolute velocity vector
W	relative velocity vector
δ_1	displacement thickness
δ_2	momentum thickness
ρ	density
γ	ratio of specific heats C_p/C_v
ω	angular velocity
θ	tangential direction
ϕ	meridional angle

1 - INTRODUCTION AND SUMMARY

Rather than presenting an exhaustive catalogue on the design method calculations, this paper aims at discussing the possible ways to use calculation methods, as well as the problems of their practical applications.

The first part recalls the complexity of the flow behaviour through a turbomachine and the simplifications which must be adopted, i.e., a mean axisymmetric steady through flow hypothesis. The second part is devoted to the particular case of an isolated blade row with the possible use of a full 3D design approach. The well-known quasi 3D approach combining the mean through flow and the blade-to-blade calculations is discussed in the third part where some details are given on direct and inverse methods for both through flow and cascade flow.

2 - FLOW COMPLEXITY IN A TURBOMACHINE

The flow in a turbomachine is mainly viscous, 3D and unsteady. The viscosity effects are encountered of course on blade boundary layers and wakes. They are very important in the so-called secondary effects where the blade and hub or tip boundary layers are mixed under the tangential gradient influence (Fig. 1). Obviously, the flow is three dimensional, but the main characteristics of the true 3D flow corresponds to the warping of the stream surface across the blade passage: this phenomenon is due to the fact that the radial pressure gradients differ from the suction side of a blade to the pressure side of the following blade (Fig. 2). The secondary flow vortices are of course strongly 3D. The unsteady effect is mainly due to the series of fixed and rotating blade-rows (Fig. 3). It is important to point out that only one case can be considered as steady (in the relative frame): it corresponds to the particular configuration of an isolated blade-row when all the boundary conditions including a fixed rotational speed remain constant. In fact this case is very rare in a turbomachine: the unsteady effects can be neglected and the flow can be assumed as steady only in the first fan of a compressor or in the inlet guide vane of a turbine.

Very sophisticated, unsteady, 3D Navier-Stokes codes are generally needed to give a real physical representation of the flow properties. These codes have not been available for industrial use up to now and probably they will be for a long time to come.

Before reminding the reader of the simplified hypothesis which is necessary to make industrial codes, the following two important remarks have to be made.

The first remark concerns the aims of computational methods: one set of methods operates in the analysis mode where the flow properties are calculated for a given geometry in order to predict performance; these methods are also used to analyse in detail certain particular phenomena. A well-defined analysis mode is essential. Obviously, ever improved and more sophisticated methods are necessary for a better flow field analysis. The second aim of the numerical simulation is the design mode which is used for the geometry definition of an element of a turbomachine in order to obtain a required flow specification. As detailed later on, several methods can be imagined for the design mode the definition of which is the main purpose of this paper. Contrary to the analysis aim it is not evident that the design approach requires codes giving a very detailed physical description. For instance, it would seem rather difficult to design a blade-row using an unsteady approach. In fact, a simplified analysis is essential for the design mode, except in a few particular cases.

The second remark concerns the utilisation of a full 3D code in the general case of a multi-stage compressor or turbine.

A fundamental question is to know whether or not, it is realistic to apply a full 3D method on a current wheel like on an isolated one, i.e., without directly taking into account the influence of the upstream and downstream blade-rows.

In our opinion, the answer is negative mainly for two reasons: if the 3D flow is computed on a blade treated as an isolated wheel (Fig. 4), the warping of the inlet stream surfaces coming from the previous blade is completely neglected. (It should be noticed that the phenomenon is unsteady if the two successive wheels have a different rotational speed). This is not acceptable because the effect of the inlet flow field distortion on the flow behaviour is probably of the same order of magnitude as the internal warping in the blade passage of the considered blade-row. Besides, it is not easy to simulate the change of enthalpy and entropy due to the previous wheel.

A second reason is related to the problem of the boundary conditions which are necessarily applied at the inlet and the outlet of the calculation domain, namely, how to determine these boundary conditions, and how to verify the

validity of the computed results?

Consequently, it is, in our opinion, necessary to take into account all the blade-rows (at least one on each side of the considered wheel) to obtain a valid full 3D flow computation. This rule leads to the following statement: in general, full 3D flow involves unsteady flow. And moreover, the wheel blade numbers being usually different, the flow is not periodic in each passage of a wheel like it is for an isolated row. Thus, it is necessary to compute the unsteady flow in several blade passages of each wheel (see Fig. 5).

Therefore, the valid application of a full 3D calculation is, in fact, really complex and not as yet accessible for an industrial use.

All these reflexions imply that simplified assumptions are necessary, especially from the design point of view.

The main simplifying hypothesis consists in assuming a tangential space averaged flow. This model, which corresponds to a mean axisymmetric through flow, presents two advantages:

a) if the rotational speed and the inlet and outlet conditions remain constant, the simplified flow is steady (it is pointed out that it is always possible to add the unsteady effect, for instance, by taking it into account in the design criteria);

b) the stream surface warping phenomenon is neglected and an approximation of the 3D flow is obtained by the superimposition of the axisymmetric mean through flow and the blade-to-blade flow on all axisymmetric stream surfaces of the mean flow. These two sorts of flows (through flow and blade-to-blade flow) are essentially 2D in the sense that each one uses two space variables.

Three remarks are important:

- The through flow model is very old but we have shown by the previous reflexions that it is still essential, especially from the design point of view. This approach was the aim of an AGARD Working-Group (see [1]).

- This model corresponds mathematically to an infinite blade number and it is well defined from the reduction of 3D Euler equations when all the tangential gradients are cancelled. The same approach using the N.S. equations is more complex because several simplified hypotheses concerning the radial viscous terms have to be adopted.

- The mean axisymmetric flow concept involves all the average problems which were studied by an AGARD Working-Group (see [2]).

3 - FULL 3D CALCULATION OF AN ISOLATED BLADE-ROW

An isolated blade-row is the only case corresponding to a steady flow in the relative frame (rotational speed, inlet and outlet conditions have to be steady). Besides, since the flow is periodic in each blade-to-blade passage, it is thus sufficient to compute the flow in one passage only.

A full 3D computation is now feasible with the existing large computers and it is possible to directly use the actual 3D approach to design a compressor fan or an inlet guide vane turbine.

Direct mode calculation

The optimization of a blade profile through a 3D N.S. direct calculation by using an iterative process is, of course, theoretically possible but still very expensive. It is thus very interesting to examine the possible simplifications of the viscous effects. The use of 3D Euler solvers (inviscid flow) is very efficient if there is no risk of blockage due to the viscosity like in the transonic configurations. First of all, the improvement of an existing profile is easy to achieve. Once one gains experience, only a few iterations are needed to modify several blade sections from hub to tip in order to obtain an improved inviscid velocity distribution.

Very good results have been obtained on existing transonic axial compressors with small changes of the blade shape, leading to a decrease of the overvelocity on the suction side.

The design of a very new blade profile is also feasible but the viscosity effects have to be taken globally into account mainly for deviation, blockage and losses. A typical example of the design of a transonic fan with shrouds (Fig. 6) by using a direct 3D Euler solver is shown in a SNECMA paper [3] (see also [4 and 5]).

We would like to point out that there are now a lot of papers available on 3D Euler or N.S. calculations applied to turbomachines [6 to 17], but they concern essentially the direct analysis. A special AGARD Lecture Series was devoted to this subject [18].

The different ways to solve N.S. or Euler equations are analysed in the corresponding report for incompressible, compressible, transonic and supersonic steady or unsteady flows. Of course, all these methods can be used to design a blade profile via an iterative process.

Viscous losses simulations

Although in the design approach, the use of 3D N.S. codes are very expensive, on the other hand, there is some risk if the viscous effects are completely neglected. Thus it can be useful to improve the Euler solver by adding a viscous losses simulation.

The body-force concept is quite old, and as proposed by Denton [19], it is easy to include in the unsteady Euler solver a wall friction force in the momentum equation as follows:

$$\frac{\partial p}{\partial t} + \text{DIV}(\rho \mathbf{V} \otimes \mathbf{V} + p) = \mathbf{f}$$

The force can be directly related to the classical skin friction coefficient $|f| = \frac{1}{2} \rho V^2 C_f$.

The C_f value is given as constant or with a streamwise distribution. However, it has to be adjusted based on some experimental data assuming that it remains valid for similar configurations. The force is applied to blade suction and pressure side, hub and tip. Due to the numerical viscosity, an artificial entropy layer is created near the walls. Its behaviour is similar to that of an actual boundary layer. (It is to be noticed that the velocity on the wall has decreased compared to the external main velocity, but is not equal to zero as in the actual viscous layer).

The results given by this very simple simulation are very interesting especially when the external velocity accelerates or remains constant. However, if separations occur on the wall, the simulation is not realistic enough and we suggest the following improvement:

The dissipative force is in fact directly related to the increase of the momentum thickness $|f| = \frac{1}{2} \rho V^2 dS/d\ell d(\delta_1 + \delta_2)$. Thus by using the Von Karman equation and neglecting the skin friction if decelerated flows are considered, we can write the following equation:

$$Cf = \frac{d\delta_1}{dx} + \delta_1 \frac{(H+2-M_e^2)}{1 + \frac{\gamma-1}{2} M_e^2} \frac{dM_e}{M_e dx} = 0 \quad \Rightarrow \quad \frac{d(\delta_1 + \delta_2)}{\delta_1 + \delta_2} = \left[\frac{2\alpha M_e^2}{H+1} - \frac{H+2-M_e^2}{1 + \frac{\gamma-1}{2} M_e^2} \right] \frac{dM_e}{M_e}$$

We can also assume that $H = H_i + \alpha M^2$, with $\alpha = 0.4$ and $H_i \approx 2$.

So the force which must be applied on the wall is related to the external Mach number gradient provided that an estimation of the displacement thickness is known. This improved simulation has been included in the 3D Euler code performed at ONERA [16], which is an extension of the 2D code. (Some details are recalled in section 2.5). The losses simulation leads to realistic results. Some comparisons with experiments are given on Fig. 7 and 8 where the measured and calculated tangential averaged radial distributions of angles and total pressures are plotted. The Fig. 9 gives the detail of the main aerodynamic variable evaluations in the absolute and the relative-frame versus the tangential direction for different sections from hub to tip. The complexity of the flow field is well illustrated on this figure. The warping of the stream surface corresponding to the actual 3D effect, is shown by the tangential evolution of the meridional ϕ .

The occurrence of vortices result from the meridional and tangential angle distributions. More details on this simple but realistic viscous losses simulation will be published soon by the author. The 3D Euler code including the losses model has been recently used at ONERA to design a supersonic axial compressor fan with the following main characteristics:

- Pressure ratio ≈ 2 ; Inlet hub-to-tip ratio = .7; Tip speed = 415 m/s.

Several isentropic Mach number distributions on suction and pressure sides are given on Fig. 10 for different rotor blade sections. We notice that there is no over velocity and that there is a controlled deceleration. The design of this compressor is a part of a Chinese-French collaboration. The test apparatus is being manufactured in China in 1988/1989 and the experimental results are not yet available. The figure 11 shows the shape of the expected streamlines on the rotor blade pressure and suction sides.

Inverse or semi-inverse mode calculation

The inverse mode is quite an old concept which aims at avoiding the iterative process of the direct calculation design mode. In theory, an inverse calculation code gives, as a result, the geometry of a blade corresponding to an assigned pressure or velocity distribution on the profile. A great advantage is that the viscous effects can be directly included via the boundary layer concept: the inviscid inverse calculation gives a profile which takes into account the displacement thickness which is determined from the assigned velocity distribution.

As specified later on for the 2D case, there are different kinds of inverse approaches. Besides, in the 3D approach, the design procedure can be applied to the tip and the hub surface which are not necessarily axisymmetric.

The stacking of the blade sections is also an important parameter especially for non-rotating blades. Thus the application of the inverse mode is not so easy and that leads to some unsolved problems.

Full inverse mode (blade only)

The mean disadvantage of a full inverse calculation which gives the whole geometry of the blade profile is that the shape and particularly the thickness is not known in advance. The profile could be unrealistic and, in fact an adjustment of the assigned pressure distributions is needed. Up to now, no publication concerning a full inverse 3D method has been available. We can well imagine that some codes will be proposed in the future, but certain problems concerning their applications can be expected, especially for rotating blades where the radial thickness evolution must be controlled accurately.

Semi-inverse mode

In the semi-inverse approach, the pressure distribution is assigned only on a part of the profile and thus certain mechanical constraints such as the thickness can be taken into account. This technique which has already been used in 2D flow, seems to be easier than the previous one. There are no apparent difficulties when imagining such a method or the writing of the corresponding code but no paper has been published on this topic yet. It is pointed out that this semi-inverse mode can also involve the design of the tip and hub shape.

Full optimization method

The optimization method is probably the most tempting way to design the whole blade-row (including tip and hub shape) by using a full 3D calculation. This method is used for 2D flow [20].

It consists in determining by a direct analysis the influence due to an isolated variation of typical parameters and/or particular points carefully selected on the blade profile. Then, by using the matrix of the influence coefficients, it is theoretically possible to determine the whole blade-row geometry corresponding to a desired pressure field. Of course, it is rather difficult to carry out such a computation programme, but we are hopeful that some company will take an interest in this topic in the near future.

4 - QUASI 3D DESIGN CALCULATION

The flow is assumed to remain axisymmetric. An approximation of the 3D flow results from the combination of the mean through flow and the blade-to-blade flows which are computed on each axisymmetric stream surface. These two sorts of flow are study separately below.

4.1. Through flow calculation

Several remarks have to be recalled:

- i) Two main results are expected from a through flow calculation:
 - The radial evolution of temperature, pressure and velocity triangles in the absolute and the relative frame, particularly at the inlet and the outlet of each blade-row;
 - The geometry of the axisymmetric stream surfaces, i.e., their radius and thickness axial evolution (see an exemple on Fig. 12).
- ii) The shape of the stream surface is closely connected to the losses and, most essentially the secondary effects. They must thus be taken into account, even if only in a simplified manner.
- iii) A through flow calculation can be considered as direct or inverse.
 - In the direct mode, the geometry of the blade profile is known. Its influence is simulated in the calculation through the thickness and the mean angle variation in the relative frame inside the blade passage. The mass flow is given (even indirectly). The radial evolutions of the total temperature and the total pressure result from the calculation.
 - Different sorts of inverse mode can be imagined.
 - The axial location of the blade-row and its thickness distribution are usually given. The radial evolution of the total pressure or the total enthalpy ratio is also given. If the losses are not simulated, the radial evolution of the

efficiency must be given. The velocity triangles result from the calculation in the absolute and the relative frame.
In both cases, the stream surface geometry is computed.

- iiii) There is an important limitation concerning the validity of the direct method application. In most cases, the axial velocity remains subsonic, thus in the through flow model, the upstream flow depends on the downstream conditions. This is not necessarily true for the actual flow if there is a supersonic region in the blade passage. The phenomenon occurs for two typical configurations:
- Started supersonic relative flow at the inlet of the blade passage (supersonic compressor and turbine). If the solidity is not too small, the unique incidence phenomenon exists and the inlet velocity triangle is directly related to the suction side geometry of the blade.
 - Choked flow. Depending on the blade passage geometry (with a possible throttle) and the pressure ratio, a sonic line followed by a supersonic zone can occur. (Transonic compressor, transonic and supersonic turbine).
- For both cases, the inlet flow is not influenced by the downstream conditions and consequently, the mass flow must be a result of the computation. Rigorously speaking, a through flow calculation is not valid for these configurations but some modifications can be incorporated into the code in order to extend the validity domain. Theoretically, the application of the inverse mode is not limited because the blade profiles are supposed to be designed in order to correspond to the inlet and outlet velocity triangles for each section.

The steady 3D flow equation using the cylindrical coordinates can be written as follows:

$$\frac{1}{\rho} \frac{\partial p}{\partial r} = \frac{V_\theta^2}{r} = \frac{DV_r}{Dt}$$

$$\frac{1}{\rho} \frac{\partial p}{\partial \theta} = - \frac{D(rV_\theta)}{Dt}$$

$$\frac{1}{\rho} \frac{\partial p}{\partial z} = - \frac{DV_z}{Dt}$$

The mean through flow equations are deduced via the hypothesis $d/d\theta = 0$.

Several methods have been used to solve these equations, mainly finite-difference and streamline curvature methods.

It is not possible to give here a complete list of the publications concerning this topic. An AGARD meeting was devoted on the through-flow calculations in axial turbomachinery [21]. A large bibliography was given by SEROVY in [1].

For particular applications, it can be useful to use the radial equilibrium approach which is a simplification of the through flow equations. By a combination of the previous equations, the following relation can be written:

$$\frac{1}{\rho} \frac{\partial p}{\partial r} = \frac{V_\theta^2}{2} - \frac{DV_m}{Dt} \sin \phi - \frac{V_m^2}{R_m} \cos \phi$$

where V_θ = tangential component of the velocity
 V_m = meridional component of the velocity
 ϕ = meridional angle
 R_m = meridional streamline radius of curvature

By using the Mach number instead of velocity, this equation becomes:

$$\left(1 - \frac{M_n^2}{\cos^2 \phi}\right) \frac{\partial p}{\partial r} = \left(1 - M_n^2\right) \frac{M_n^2 \lg^2 \beta}{r} + M_n^2 \frac{\lg^2 \phi}{r} + M_n^2 \lg \phi \frac{\partial(\lg \phi)}{\partial r} - \frac{M_n^2 (1 - M_n^2)}{\cos^3 \phi - R_m}$$

where M_n = axial component of the Mach number
 $\beta = \lg^{-1}(V_\theta/V_m)$

We can observe that if the radial evolution of the radius of curvature R_m and the slope ϕ of the streamline are given, this equation is independent of the axial coordinate. It can be directly integrated if the radial distribution of the total pressure, the total temperature, and the tangential angle are given. Considering now the mass flow conservation, we obtain two differential equations, for instance, in the following form:

$$\frac{dr_2}{dr_1} = \frac{r_1 \cos \beta_1}{r_2 \cos \beta_2} \frac{P_{t_1}}{P_{t_2}} \sqrt{\frac{T_{t_2} \Sigma(M_2)}{T_{t_1} \Sigma(M_1)}} \quad \text{where } \Sigma(M) = \text{ratio of area on sonic area}$$

$$\frac{dp_2}{dr_1} = \frac{dp_2}{dr_2} \frac{dr_2}{dr_1}$$

Then, starting from a given station 1, it is easy to integrate these equations into a station 2. If there is no blade-row between the two stations, we consider the conservation of RV_θ . If there is a blade, we consider the conservation of the rothalpy ($C_p T + w^2/2 - \omega^2 r^2$) in the relative frame, with some loose correlations concerning the efficiency. This simple method can be used in direct or inverse mode. It very quickly gives a first approximation of the through flow field. (It is to be noticed that its extension, which consists in determining iteratively the radius of curvature and the slope, leads to the streamline curvature method).

4.2 - Blade-to-blade calculation

The stream surfaces computed by the through flow calculation generally offer a variable radius and thickness. The blade-to-blade calculation must then take into account these variations. The cascade methods, which are strictly 2D, are not valid for practical applications.

We will now give a short overview of blade-to-blade calculations by considering separately the inviscid and the viscous methods.

4.2.1 - *Inviscid blade-to-blade flow calculations.* As the methods described in the technical literature are numerous, such a survey will necessarily be incomplete, and will only address the main families of methods.

Direct calculation

We shall first review the direct methods currently recommended for blade-to-blade calculations in the following configurations:

- i) Subsonic conditions: the flow is subsonic throughout the whole field.
- ii) Supercritical conditions: the flow is quasi-subsonic throughout the whole field, with, at the utmost, supersonic pockets which do not extend from the upper surface of a blade to the lower surface of the next blade; in this case, the entropy variations associated with the passage through a possible shock wave can be disregarded.
- iii) Supersonic conditions: the supersonic area of the flow occupies at least one full section of an interblade channel. In this area, recompression shock waves are more intense, and the corresponding entropy jump cannot be disregarded.

There are essentially five categories of the blade-to-blade flow calculation methods; they differ by the numerical techniques used.

Singularity methods

Singularity methods are based on the principle of the superimposition of potential flow solutions; the potential from which the flow is derived is considered as the sum of elementary potentials corresponding respectively to:

- the basic uniform flow;
- sources, sinks or vortices located in adequately selected points of the flow fields.

The various singularity combinations proposed in the published literature are as follows:

- (1) Singularities located within the blade contour; this method applies essentially to low camber blades [22].
- (2) Singularities made up of vortices located on the blade contour. These methods lead generally to more accurate results than the previous ones. They were developed for flows in incompressible fluids, but can be extended to the case of subsonic flows of compressible fluid, by the addition of sources and sinks in the inter-blade channels, representing the compressibility effect [23, 24].

With such methods, the precision of the inviscid solution on the trailing edge makes it possible to determine the direction of the flow issuing from the cascade, with the help of Kutta-Joukowski or an equivalent condition. This condition can be easily introduced in the computation programme. This method offers an additional advantage: due to its high degree of accuracy, it permits a fine analysis of high velocity gradient zone (in the vicinity of the leading edge, for instance) which is important in view of the prediction of boundary layer transition. Its major drawback lies in the fact that it is limited to the case of subsonic flows without shock-waves.

Methods based on the curvature of streamlines

Streamline curvature methods are quite commonly used. Their starting point is a family of pseudo-streamlines deduced, by similarity, from the profile geometry. The transverse pressure gradients are connected to the curvature of these streamlines; a transverse velocity distribution is derived, and, by iteration on the continuity equation, the shape of the streamline is changed until a convergence of the process is reached [25, 26].

The main advantage of this method is the rapidity of the computation, also for subsonic compressible flows. For transonic flows, difficulties arise because of the discontinuity of the streamline curvature at the shocks and because of the ambiguity in the choice between a subsonic or supersonic solution. Another drawback lies in the lack of accuracy in areas of strong curvature (leading and trailing edges). As a result, local velocity peaks are smoothed out which limits the capability in predicted boundary layer behaviour.

Finite-difference or volume methods

It is necessary to distinguish between methods where entropy is assumed to be constant, and methods where entropy variations are taken into account.

A) Stationary irrotational flows

- i) Relaxation method using the stream function: the continuity equation allows definition of a stream function which combined with the condition of irrotationality provides a second-order, non-linear equation for compressible flow. This equation is generally discretized in an orthogonal grid, by means of a scheme suite for an elliptic type problem (subsonic flow). The finite-difference equation is solved by a relaxation technique [27] or by a matrix technique [28]. This well-proven type of method is relatively fast and shows good agreement with experiments. A second advantage is the ease of extension of these methods to rotational flow on non-cylindrical stream surfaces. The major drawback is the necessity to specify the outlet flow angle.
- ii) Relaxation methods using the velocity potential: this type of method has first been developed to calculate transonic flow around isolated airfoils. However, the number of references on this method are too numerous to be listed here. The ambiguity between the subsonic and supersonic solution, when using a stream function has been avoided by the use of a potential function. However, this requires the assumption of irrotational flow. The continuity equation provides a non-linear, second-order, partial derivation equation which is of the elliptic type in the subsonic field, and of the hyperbolic type in the supersonic field. Discontinuous solutions can be adopted for this equation although they do not satisfy the Rankine Hugoniot relations for shock waves. The methods recommended in the published literature differ essentially by the discretization method adopted:

- it is possible to use mixed discretization schemes, that is centered meshes in the subsonic flow, and eccentric meshes in the supersonic field [29]; with this method, it is necessary to subject to a special treatment the points where discontinuities appear (shock waves), for the scheme to remain conservative;
 - it is possible to put the scheme off center, systematically, by using a term of artificial viscosity; this type of method leads generally to a conservative scheme [30];
 - an original method [31] consists in using a discretization method of the finite volume type.
- Numerical results obtained by this method are very satisfactory if the Mach number upstream of the shock is only slightly supersonic. However, the use of a potential function makes it difficult to control the mass flow through the flow channels (conservation problem) which puts a limitation to the prediction of choking. Furthermore, the use of a potential function does not allow the application of these methods to rotational flow on non-cylindrical stream surfaces.
- iii) Pseudo non-stationary, isentropic method: the iterations of the relaxation method can be replaced by introducing in the equations time dependent derivatives which do not necessarily have a physical significance. The entropy is assumed to be constant in the whole field, even during transient periods, so that only the stationary asymptotic solution has a physical significance [32]. While this method, which requires a longer computation times, has a more extensive field of application than the previous methods, it is limited to the case of motions with only low intensity shock waves.

B) General solution to Euler equations under steady conditions

Until now, the problem raised by the mixed elliptic-hyperbolic nature of the Euler equations for steady transonic motion with intense shock could only be solved by non-steady type methods. Here again, we find the characteristic of the steady flow considered as the asymptotic state of a non-steady motion.

Such methods offer the great advantage of being applicable to any transonic flow; however, they require long computation times for the asymptotic condition to be achieved. As far as cascades are concerned, the computation time depends on rapidly with which disturbances get damped and disappear at the borders of the computation field. As the asymptotic solution is the only solution retained, the intermediate states do not need to have a physical significance, and the non-steady terms can be modified in order to accelerate the achievement of the final solution.

With these methods, shock waves are usually dealt with by means of a shock capturing method, with which they appear quite naturally, owing to the dissipative properties of the numerical schemes used (dissipative properties which are either natural or reinforced by an artificial viscosity term).

While this technique is simple, it is not accurate enough as regards the description of shocks; these do not appear as true discontinuities, but are somewhat spread out.

The use of a two-step calculation process [33, 34] offers the advantage of second-order accuracy.

Finite element methods

Finite element methods are of increasing interest for computations.

This method is based on an approximation of dependent variables in the form of polynomials, and on an integral definition of the problem [35, 36, 37].

The benefits expected from technique are as follows:

- possibility of giving an optimum design to the grid of the plane, especially by using curvilinear meshes;
- automatic treatment of natural boundary conditions;
- preservation of symmetry in the discretization of differential operators.

On the other hand, we risk increasing the computation time due to the complexity of the meshes used and to the number of terms of the polynomials.

Methods of characteristics

As supersonic flows lead to equations of the hyperbolic type, one can think about calculating the supersonic flow directly from the upstream boundary conditions. The field of dependence of each point is then defined by the characteristics issuing from it.

This very classical problem is described in numerous references and the application to two dimensional or three dimensional blades is described in [38] and [39].

The main difficulties encountered are as follows:

- the supersonic field must be perfectly well defined (fully supersonic flow), and upstream conditions (supersonic flow or sonic line) must be known;
- only oblique shock waves can be taken into account, since the flow is subsonic downstream of normal shocks; and the method is no longer applicable;
- the computation cannot be carried out unless the upstream boundary conditions are set. Thus, as regards turbine cascades, the sonic line has to be calculated first, for instance by a method of series development [40]: in this case, the subsonic portion of the flow is calculated by any method which can use the downstream boundary conditions as defined by the calculation of the sonic region.

For all these regions, the method of characteristics is only applicable to cascades with a well-defined minimum section where the sonic line can be calculated in a sufficiently accurate manner.

In addition, the use of other computation methods suited to calculate the subsonic flow field increases markedly the complexity to the computation process.

Inverse calculation

Improvement of the aerodynamic performance of turbomachine elements requires a correct tailoring of the velocity distribution on the walls of this element since this velocity distribution determines the behaviour of the viscous layers in which originate the losses.

Use of inverse methods is of great help in tailoring the velocity distribution and leads to the design of blades adapted to any operating conditions.

Inverse methods defining blade geometries corresponding to a given velocity distribution on the walls are known for many years [41, 42] and have been widely used [43, 44].

However, use of these methods has some drawbacks:

- great number of inverse methods can be used for isentropic flows only and are not well-suited for flows with strong shock waves;
- they are usually, fully inverse, i.e., the velocity distribution is given on all the wall of the channel or the blades and

quite often not realistic geometries come out of the computations, that most of the time do not satisfy requirements imposed by non-aerodynamic considerations.

Most of them apply to 2D flow fields only and are unable to take into account the change in stream tube thickness. It is quite impossible to give an exhaustive catalogue of the inverse or semi-inverse method. The main interesting papers on this field are given in Ref. [20, 45 to 55].

Several specialised meetings have been recently devoted on this topic [56, 57] and the corresponding publications give a very useful synthesis of the different inverse methods.

We will now recall a simple way to correct and to improve the velocity distribution on an existing profile. This very general method, based on the time marching Euler solution has been developed at ONERA [58, 59, 60].

Time marching methods are well-suited for the resolution of Euler's equations and can be used for transonic flows having both subsonic and supersonic domains, even with strong shock waves in-between. In direct mode, the boundary condition on a wall consists in imposing the normal velocity equal to zero. All other aerodynamic values, such as Mach number, pressure and temperature, are computed. At the opposite, in the inverse mode, we assign a local static pressure and we compute all the other values by using compatibility relations.

This treatment gives a large choice of conditions that we must assign on the boundary of the calculation domain. Passage from direct mode to inverse mode is easy and by tailoring the boundary conditions, semi-inverse methods can be used to satisfy geometric conditions, keeping unchanged for instance the pressure side of the blades and smoothing out the velocity distribution on the suction side. In some other cases, the blade thickness law will be kept. The mesh system has to be modified at each iteration and one should take into account the speed of displacement of the meshes. Numerical tests have shown that if the final asymptotic flow only is researched, this correction can be neglected.

A first solution consists in building the new wall using the flow angle computed at each boundary mesh. A second solution, which is more rigorous, consists in moving the boundary mesh in order to annul the normal velocity component.

Direct or inverse arrangement conditions do not present difficulties, i.e., semi-inverse applications can be imagined on different walls in the computed field. An inverse condition can follow a direct condition on one or several walls. The opposite is possible, but so far we have never needed it. An inverse condition can be assigned as a function of linear or curvilinear abscissae, possibly reduced. Thus, many applications can be assigned; however, some remarks should be considered.

It has to be emphasised, that during the whole computation the shape of the meshes must be continuous, otherwise a divergence of the computations may appear. Thus if the initial mesh network is very different from the final one, a special care should be taken for the evolution of the meshes.

In all the cases presented below, the meshed are displaced in the θ direction only for sake of simplicity and gain in computation time. Only small changes in the mesh system are then observed.

It has to be noted that for a given pressure distribution, there is not necessarily a corresponding blade.

Obviously, assigned pressure distributions must correspond to a physical reality. In particular, different cases can happen at the junction between direct and inverse application: if the flow is locally supersonic, a jump in static pressure is allowed (shock wave or expansion); if the flow is locally subsonic, a smooth evolution between imposed and computed pressures is required.

Another inverse application consists in determining the flow field corresponding to a given pressure distribution assigned on a given wall geometry. This does not correspond to our definition of inverse mode and its treatment by a time-marching code seems difficult.

Some typical applications are now analysed. In the case of the flow in a compressor or turbine blade cascade, the computation domain is limited by the suction side A_1F_1 and the pressure A_2F_2 of two adjacent blades (Figure 13) and lines B_1A_1 and B_2A_2 upstream of the blades, F_1C_1 and F_2C_2 downstream of the blades that satisfy the periodicity condition, i.e., at two points G_1 and G_2 of these lines situated at the same distance from the cascade, all the parameters have identical values.

The fully inverse approach consists in prescribing pressure distribution on lines A_1F_1 and A_2F_2 , periodicity conditions on B_1A_1 and B_2A_2 , as well as on F_1C_1 and F_2C_2 , and determining the corresponding boundary lines. Usually at the end of such a calculation, distance F_1F_2 differs from pitch A_1A_2 , which means there exists no actual blade that gives the prescribed pressure distributions. In fact, only one value of solidity corresponds to a closed profile for a given pressure distribution.

In practice, the adjustment of the cascade solidity (chord divided by pitch), in order to obtain a fixed blade thickness at the trailing edge, can be obtained (a) by adjusting the cascade pitch during the time-marching process or (b) by adjusting the pressure distributions.

An example of such a computation was reported in [59] for a turbine blade cascade. As shown in Figure 14, this is a high expansion ratio cascade and there was a non-regular pressure distribution on the suction side. Figure 14(a) shows, by means of a broken line, the initial blade and the pressure side of the adjacent blade.

In order to improve the cascade flow, the pressure distribution shown by solid line in Figure 14(b), downstream of the two arrows, was chosen (as a matter of fact, the pressure distribution on the pressure side was kept unchanged). The blade shapes corresponding to the modified pressure distributions are shown by solid lines in Figure 14(a). The pitch is slightly increased.

Another example is shown in Figure 15. This is a supersonic impulse turbine blade with a fixed solidity. The pressure distribution on the suction side is fixed; on the pressure side, it is assumed that the pressure is constant and its value is modified until a blade with satisfactory trailing edge thickness is obtained (remark: since the inlet and outlet Mach numbers are supersonic, there is no pressure continuity between pressure side and suction side).

The solution is very close to case III of Figure 15(b).

A more realistic example is shown on Figure 16 where the pressure side velocity distribution was adjusted in order to obtain a close profile with a non zero-thickness at leading and trailing edge. In fact whatever the process used for ensuring the profile closure at the trailing edge, the shape obtained may not be realizable, the thickness being either too large or too small, or even negative. However, it appears that, in most applications, one is mainly interested in the pressure distribution over the suction side, which is the most critical as regards the boundary layer, for compressors as well as turbines. This distribution is usually determined so as to minimise the losses due to viscous effects. A particular attempt is made to reduce over-velocities and avoid separation. As regards velocity distributions over the pressure side, they usually present no particular risk.

A new method was developed in which the pressure distribution is prescribed on the blade suction side only, the other one being obtained from geometrical considerations. A first application consists in prescribing the thickness evolution. We thus directly obtain a profile corresponding to a given velocity distribution over the suction side and having the required mechanical characteristics. We shall note that, the profile being automatically closed, the cascade solidity may be chosen in advance.

However, a problem appears because two solutions can exist. Numerical experiences show that only solutions corresponding to small deviations are stable. This is convenient for most of the compressor cases but only for few special turbine cases.

Another semi-inverse mode consists in assigning, as geometrical requirements, the trailing edge thickness and the geometry of a more or less long part of the pressure side near the trailing edge. The initial part of the pressure side is built using a continuous deformation. The pitch and axial chord are fixed. This technique gives good results for a turbine cascade, but obviously the thickness evolution is not controlled. An example is given in Figure 17.

If inverse or semi-inverse calculations give the blade shape with correct pressure distributions, one should not forget that it is impossible to assign values to all aerodynamic parameters. If the inlet velocity and blade surface velocity distributions are prescribed, the outlet velocity (axial as well as tangential components) results from the computation. If the outlet velocity triangle is also prescribed, then a few iterations are necessary in order to obtain the corresponding blade velocity distributions.

Therefore, starting with an approximately correct blade shape, that already satisfies the downstream velocity conditions, the semi-inverse method gives with few iterations a pressure gradient-wise optimized profile with the same performance. Typical examples of inverse or semi-inverse applications are given from the literature on Fig. 18 to 21 (HORSMANN and SMIDT [54], SANZ [52], CEDAR and STOW [20], JACQUOTTE [55]).

4.2.2 - *Viscous blade to blade calculations.* When it becomes necessary to take into account the viscous effects, two ways are open:

- solve the averaged N.S. equations (for instance [60]); this way is very expensive and probably not very useful (for design mode);

- use the coupling approach: the main flow is considered as inviscid, and the viscous effects are concentrated in the boundary layers close to the suction and pressure side, and in the wakes. (It is to be noticed that the most recent sophisticated coupling methods are equivalent to a N.S. solution, not needed for the main design applications).

Different kinds of coupling can usefully be considered. (For more details see [62]).

They depend on the one hand on the aim of the computation, and on the other hand on the flow pattern, according as it comprises a separation or not, and as the flow is supersonic or not.

The perfect flow and the viscous flow computations can both be applied either in direct or in inverse mode.

Four kinds of coupling can be distinguished a priori. But we must recall that whenever a separation occurs, boundary layer calculations have to be done in inverse mode.

Coupling method with an inviscid inverse flow computation

This problem corresponds to the design of the geometry, meeting imposed aerodynamic requirements. An inverse mode perfect flow computation is applied. Two cases have to be distinguished, according to the kind of requirements.

1) We look for a given perfect flow behaviour. For instance, we assigned a pressure evolution (or velocity or Mach number distribution) on the walls.

The choice of δ_1 as coupling frontier seems to impose itself, even though the other choices can be used a priori (Fig. 22).

The perfect fluid yields the δ_1 limit streamline. The boundary layer calculation gives the δ_1 evolution, but it can succeed only if there is no separation, else it is necessary to modify the assigned velocity distribution and to resume the process. The real geometry is easy to obtain by subtracting the δ_1 thickness to the computed limit streamline. This very classical kind of coupling has been used for a long time, particularly for all the cases where there is no risk for a separation to occur.

2) We look for a given boundary layer behaviour. For instance, it is the case of flows where we want to avoid the extended separation that may occur. Then we start with an inverse boundary layer calculation, that can even comprises a restricted separation.

From a given friction coefficient or shape factor evolution for instance, the computation yields both the velocity (or pressure) distribution, used then as a data by the inverse perfect flow calculation, and the evolution of δ_1 . Therefore the computation algorithm is represented on Fig. 23.

Then the wall geometry can easily be obtained. It has to be noticed that in the two cases, the problem is well set and that no iteration is needed between the perfect flow and viscous flow computations. In practice, when taking into account the technological constraints often imposed for blades design, these modes are applied just on parts of the studied flow (semi-inverse design).

Coupling method with an inviscid direct flow computation

In this case, we have an analysis mode: an iterative process is needed to design a cascade corresponding to a desired velocity distribution. The flow is computed in a cascade of well-known geometry, either when we give aerodynamic conditions on the upstream and downstream frontiers crossed by the flow (mass flow, pressure, temperature and so on), or when we look for a given shock pattern (for instance, when we want to impose the position of a normal shock in a supersonic cascade).

Important distinctions have to be done: whether there is a risk of separation or not, whether the perfect flow is fully supersonic or not.

i) Configuration without risk of separation

We use the coupling that associates the viscous an inviscid flow computations in direct mode.

The algorithm is as follows:

The iteration loop starts with given surface boundary conditions (i.e., conditions at or near the body). These conditions are known from the previous iteration step.

An inviscid flow calculation provides a pressure distribution which is then fed into the boundary layer calculation. This last condition furnishes new boundary conditions and the process is repeated.

It is clear that this method breaks down as soon as separation occurs since the boundary layer is always computed in the direct mode.

We can notice that we do not need to use an iterative perfect flow, boundary layer computation process if the perfect fluid flow remains fully supersonic. As a matter of fact, the inviscid fluid has an hyperbolic behaviour and the boundary layer a parabolic one. The computation can be done step-by-step, by directly solving the coupling relation. This is easy to apply if the perfect fluid is treated by simple waves or by the characteristics method (see some details in [63]).

ii) Configuration with a risk of separation (direct-inverse coupling)

The boundary layer has to be computed in inverse mode if a separation occurs. According to the present

procedure, the same displacement thickness distribution $\delta_1(x)$ (or the equivalent) is fed both in the boundary layer and in the inviscid flow calculations. Two pressure distributions $p(x)$ for inviscid flow and $\bar{p}(x)$ for B.L., are thus obtained. (They coincide when convergence is reached). Here a new iteration cycle is started by "guessing" a new $\delta_1(x)$ distribution from the "error" $p(x) - \bar{p}(x)$.

Concerning the viscous flow, direct mode is rather used if the viscous layer is not separated and thin. Inverse mode is used as soon as a separation occurs (or as the dissipative flow is strongly unbalanced).

These kinds of coupling methods at the walls or on displacement frontiers $\delta_1(x)$ have given very interesting applications, especially on cascades but some problems can rise when a shock boundary layer interaction produces a separation.

Basically, two cases can be distinguished according as the perfect flow near the reattachment (if there is one) is supersonic or not.

For further details, one can refer to the synthesis done in [63] and [64].

The condition downstream of reattachment point is not easy to obtain to a complex flow pattern.

It has to be noticed that in the case of a subsonic reattachment, depending on downstream conditions, in which the coupling process does not lead to problems a priori, can be considered in two different ways:

- either a downstream condition (most frequently the static pressure) is given : then the separated flow location will be a computation result.

- or we impose the beginning of the interaction, and the inverse-inverse mode calculation gives the downstream conditions.

This last possibility leads to interesting applications, mostly in internal aerodynamics, when strong shocks occur, because we often try to compute flow patterns corresponding to well determined locations of shock waves, or supersonic blade cascades).

Anyway, those two methods are equivalent, as far as the description of different working points is concerned.

The three above coupling techniques are said to be explicit in the sense that the boundary layer and the inviscid stream are computed in turn, the one after the other. Some supersonic methods were in fact implicit coupling procedures, since in these methods the two streams were determined simultaneously (see [63]). Extensions of the implicit procedure to elliptic flows, with a view to obtain higher convergence rates, are now available.

REFERENCES

- [1] Propulsion and Energetics Panel Working group 12 on through flow calculations in axial turbomachines. AGARD ADVISORY REPORT N° 725.
- [2] PIANKO, M., WAZELT, F., «Méthodes d'établissement de caractéristiques moyennes dans les écoulements internes hétérogènes». AGARD AR 182, 1983.
- [3] DERRIEN, T., «Calcul tridimensionnel dans les aubages de turbomachines avec nageoire». AGARD CP 401.
- [4] GOUTINES, M., «Design methodology for advanced HP compressor first stage». VKI Lecture Series 1988-03.
- [5] KARADIMAS, G., «Design of high performance fans using advanced aerodynamic codes». ASME 88 GT 14.
- [6] HAH, «A Navier-Stokes analysis of 3-D turbulent flows inside turbine blade rows at design and off-design conditions». Journal of Engineering for Gas Turbines and Power. (April 1984, Vol. 106).
- [7] DENTON, J.D., «An improved time marching method for turbomachinery flow calculation». ASME paper 82-GT-239.
- [8] RAI, M.M. «Unsteady 3-D Navier-Stokes simulation of turbine rotor-stator interaction». AIAA paper 87-2058.
- [9] SUBRAMANIAN, S.V., BOZZOLA, R. «Numerical simulation of 3-D flow fields in turbomachinery blade rows using the compressible Navier-Stokes equations». AIAA paper 87-1314.
- [10] DAWES, W.N., «A numerical analysis of the 3-D viscous flows in a transonic compressor rotor and comparison with experiment». ASME paper 86-GT-16.
- [11] HOLMES, D.G. and TONG, S.S., «A three-dimensional Euler solver for turbomachinery blade rows». ASME 84-GT-79.
- [12] ARTS, T., «Calculation of the 3-D, steady, inviscid flow in a transonic axial turbine stage». ASME paper 84-GT-76.
- [13] HIRSCH, C. and LACOR, C. «Rotational flow calculations in 3-D blade passages». ASME paper 82-GT-316.
- [14] BROCHET, J., «Calcul numérique d'écoulements internes tridimensionnels». La Recherche Aéronautique n° 1980-5 pp. 301-315, English translation ESA TT 673.
- [15] CHOI, D. and KNIGHT, C.J., «Computations of 3D viscous flows in rotating turbomachinery blades». AIAA 89-0323, Reno, January 9-12, 1989.
- [16] NI, R. and BOGOIAN, J., «Prediction of 3D multi-stage flow field using a multiple-grid Euler solver». AIAA 89-00203, Reno, January 9-12, 1989.
- [17] CHIMA, R. and YOKOTA, J., «Numerical analysis of three-dimensional viscous internal flows». AIAA-88-3522, AIAA/ASME/SLAM/APS 1st National Fluid Dynamics Congress, Cincinnati, July 25-28, 1988.
- [18] «3-D computation techniques applied to internal flows in propulsion systems». AGARD Lecture Series n° 140.
- [19] DENTON, J.D., «The use of a distributed body force to simulate viscous effects in 3-D flow calculations». ASME paper 86 GT 144.

- [20] CEDAR, C.D. and STOW, P., «The role of a mixed design and analysis method in a turbomachinery blade design system». International Conference on Inverse Design Concepts in Engineering Sciences, October 17-18, 1984.
- [21] «Through-flow calculations in axial turbomachinery». AGARD CP-195.
- [22] SCHLICHTING, H., «Berechnung der reibungslosen incompressible Strömung für ein vorgegebenes ebenes Schaufelgitter, VKI Forschungsheft 447- B/21, 1955.
- [23] VAN DEN BRAEMBUSSCHE, R., «Calculation of compressible subsonic flow in cascades with varying blade height». ASME Trans., J. Engineering for Power, Vol. 95, n° 4, 1973, pp. 345-351.
- [24] LUU, T.S., «Méthode d'équations intégrales en mécanique des fluides». Coupling Methods in Applied Sciences and Engineering. R. Glowinski and J.L. Lyons Eds., Lecture Notes in Economic and Mathematical System, Vol. 134, Springer, 1976, pp. 359-373.
- [25] WILKINSON, D.M., «Stability, convergence and accuracy of two dimensional streamline curvature methods using quasi orthogonal». Thermodynamics and Fluid Mechanics Convention 1970, Inst. Mech. Engrs., London, Vol. II.
- [26] BINDON, J.R., «Stability and convergence of streamline curvature flow analysis procedures». Int. J. for Numerical Methods in Engineering, Vol. 7, 1973, pp. 69-83.
- [27] KATSANIS, T., «Computer program for calculating velocities and streamlines on a blade-to-blade stream surface of turbomachines». NASA TN D 4525, April 1968.
- [28] CALVERT, W.J. and SMITH, D.J.L., «A digital computer program for the subsonic flow past turbomachine blades using a matrix method». ARC R & M 3838, 1976.
- [29] DODGE, P., «A transonic relaxation method for cascade flow systems, in Turbomachinery». VKI Lecture Series 59, May 1975.
- [30] IVES, D.C. and LIUTERMOZA, J.F., «Second ordre accurate calculations of transonic flow over turbomachinery cascades». AIAA paper 78-1149, 1978.
- [31] CASPAR, J.R., HOBBS, D.E. and DAVIS, R.L., «The calculation of two dimensional compressible potential flow in cascades using finite area techniques». AIAA paper 79-007, 1979.
- [32] VEUILLOT, J.P. and VIVIAND, H., «A pseudo unsteady method for the computation of transonic potential flows». AIAA paper 78-1150, 1978.
- [33] GOPALAKRISHNAN, S., «Fundamentals of time marching methods, in transonic flows in turbomachinery». VKI Lecture Series 59, 1973.
- [34] VIVIAND, H. and VEUILLOT, J.P., «Méthodes pseudo-instationnaires pour le calcul d'écoulements transsoniques». ONERA Publication n° 1978-4.
- [35] KRIMERMAN, Y. and ADLER, D., «Calculation of the blade-to-blade compressible flow field in turbo impellers using the finite element method». Fac. Mech. Eng. Technion, Israel Inst. of Technology, Haifa, 1976.
- [36] MORICE, Ph., «Une méthode numérique basée sur les principes variationnels pour des écoulements avec frontières libres». ONERA TP 1978-40.
- [37] HIRSCH, Ch., «Transonic flow calculations in blade rows with an optimal control - Finite element formulation». Bat-Sheva Seminar on Finite Element for Non-elliptic problems. Tel-Aviv Univ., July 1975.
- [38] FRUEHAUF, H.M., «A method of characteristic for three dimensional steady supersonic flow in rotating and stationary annular cascades». ESRO TT-44, July 1975.
- [39] MARTINON, J., «Use of the characteristics method for the prediction of the three dimensional flow field in high transonic compressors». ASME paper 79 GT 34, 1979.
- [40] MOORE, A.W., «The transonic flow in the throat region of a two dimensional nozzle with walls of arbitrary smooth profile. ARC R & M 3481, 1965.
- [41] LEGENDRE, R., «Calcul d'un profil pour ailette de turbine à partir d'un hodographe». La Recherche Aéronautique n° 84, 1961.
- [42] LE FOLL, J., «Inverse method for optimized blading calculations, transonic flows in axial turbomachinery». VKI Lecture Series 84, 2-6 February 1976.
- [43] STANITZ, J.D. and SHELDRAKE, L.J., «Application of a channel design method to high-solidity cascades and tests of an impulse cascade with 90° of turning». NACA Tech. Note 2652.
- [44] KARADIMAS, G., «Définition des profils d'aubages de turbomachine par une méthode analytique». 3e Symp. Franco-Soviétique, Paris, 1-4 décembre 1969.
- [45] STANITZ, J., «Design of two-dimensional channels with prescribed velocity. Distributions along the channel walls». NACA Report 115, 1952.
- [46] SCHMIDT, E., «Computation of supercritical compressor and turbine cascades with a design method for transonic flows». ASME paper n° 79-GT-30, 1979.

- [47] BAUER, F., GARABEDIAN, P. and KORN, D., «Supercritical wing sections». Vol. I, II, III. Springer-Verlag, New York, 1972, 1975, 1977.
- [48] WILKINSON, D.H., Calculation of blade-to-blade flow in a turbomachine by streamline curvature». Short Course on Advanced Flow Calculations, 23-27 March 1981. Fluid Engineering Unit, Cranfield Institute of Technology.
- [49] TONG, S.S. and THOMPSON, W.T. Jr., «A design calculation procedure for shock-free or strong passage shock turbomachinery cascades». ASME 82-GT-220, 1982.
- [50] KARADIMAS, G., «Calcul analytique des grilles d'aubes». 7th Applied Aerodynamics Conference, ECL, Ecully and ONERA, Modane, France, 1970.
- [51] HOBSON, D.E., «Shock free transonic flow in turbomachinery cascade», Cambridge Univ. Eng. Dept., CUED/A Turbo/TR65, 1974.
- [52] SANZ, J.M., «Improved design of subcritical and supercritical cascades using complex characteristics and boundary layer correction». AIAA Journal Vol. 22, n° 7.
- [53] JACQUOTTE, O.P., «A finite element inverse method for the design of turbomachinery blades». 7th International Conference on Finite Elements in Flows problems. April 3-7, 1989.
- [54] HORSMANN, M. and SCHMIDT, M., «Comparison between inverse design (PVD) airfoils and standard series airfoils for high loaded axial turbine nozzle application». AGARD-CP-401 *Transonic and Supersonic Phenomena in Turbomachines*.
- [55] JACQUOTTE, O.P., «Une méthode inverse pour la détermination d'aubes de turbomachines». Proceedings de l'AGARD-FDP Specialists Meeting on Computational Methods for Aerodynamics Design (inverse) and Optimization, Loen, Norvège, 22-23 mai 1989.
- [56] International Conference on Inverse Design Concepts in Engineering Sciences. ICEDES Oct. 17-18, 1984.
- [57] Second International Conference on Inverse Design Concepts and Optimization Sciences. ICIDES II Oct. 26-28, 1987.
- [58] MEAUZE, G., «Méthode de calcul aérodynamique inverse pseudo-instationnaire». La Recherche Aérospatiale n° 1980-1, English translation, ESA TT 651, pp. 23-30.
- [59] MEAUZE, G., «An inverse time marching method for the definition of cascade geometry». J. of Engineering for Power, Vol. 104, July 1982.
- [60] MEAUZE, G. and LESAIN, A., «Use of an inverse method for the design of high efficiency compressor and turbine blades with large change in radius». ASME paper 84-GT-167.
- [61] CAMBIER, L. and VEUILLOT, J.P., «Computation of cascade flows at high Reynolds number by numerical solution of the Navier-Stokes equations». AIAA paper 88-0364.
- [62] LE BALLEUR, J.C., «New possibilities of viscous-inviscid numerical techniques for solving viscous flow equations with massive separation». 4th Symposium on Numerical and Physical Aspects of Aerodynamics Flows, Long Beach, 16-19 January 1989.
- [63] «Shock-waves boundary layer interactions». AGARDograph n° 280, February 1986.
- [64] «Nato advance study institute on thermodynamics and fluid mechanics of turbomachinery». Izmir, Turkey, Sept. 17-28, 1984.

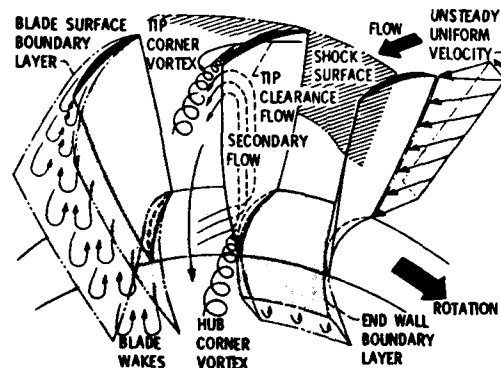


Fig. 1 - AXIAL-FLOW COMPRESSOR ROTOR FLOW PHENOMENA [1]

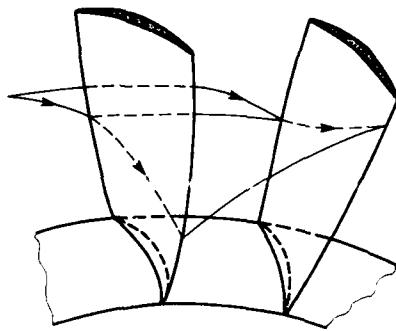


Fig. 2 - TRUE 3D FLOW
STREAM SURFACE WARPING PHENOMENON

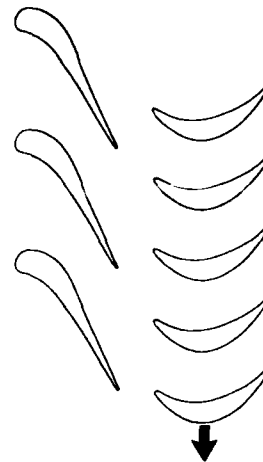


Fig. 3 - UNSTEADY EFFECT
AND NON PERIODIC FLOW

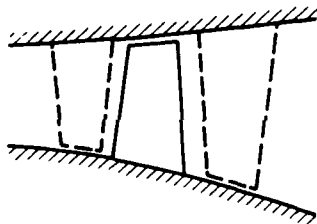
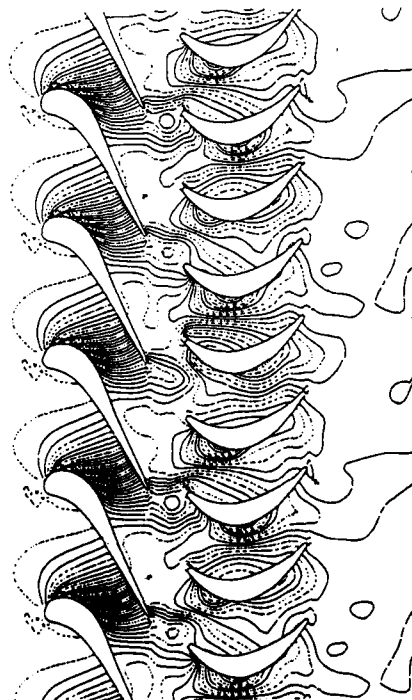
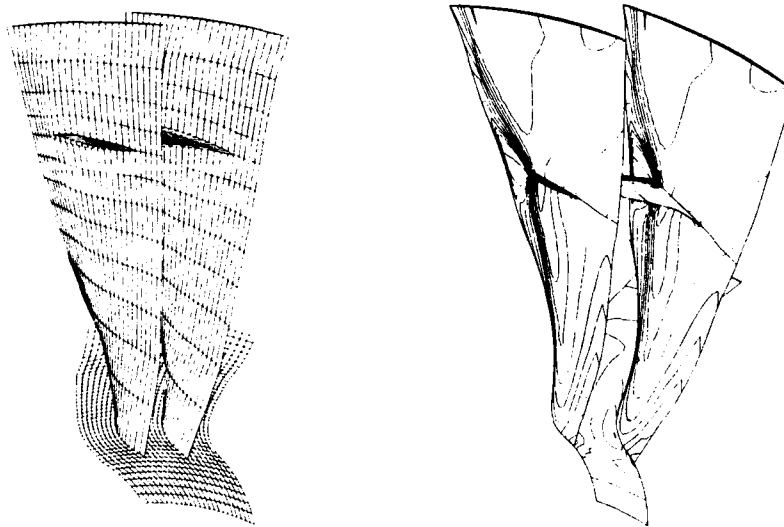


Fig. 4 - BLADE TREATED AS
AN ISOLATED WHEEL

Fig. 5 - STATIC PRESSURE FIELD AT A GIVEN
TIME. NON PERIODIC FLOW





a) FAN BLADE MESH

b) FAN BLADE FLOW ANALYSIS

Fig. 6 - FAN BLADE WITH SHROUD FROM [3]

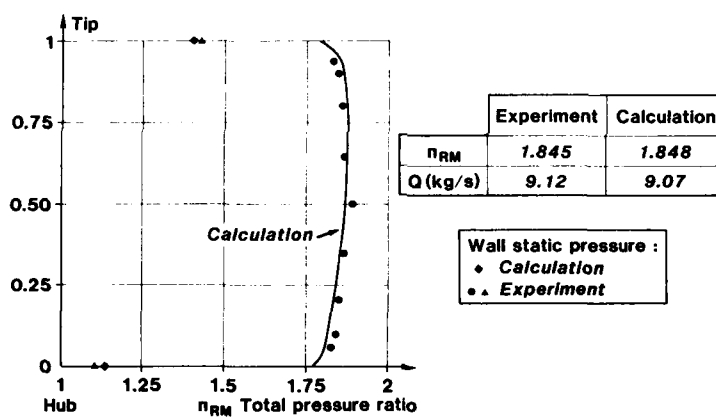
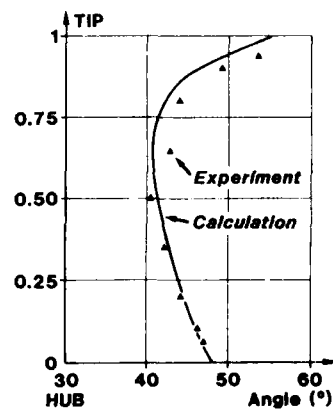


Fig. 7 - ISOLATED COMPRESSOR ROTOR

Fig. 8 - ISOLATED COMPRESSOR ROTOR



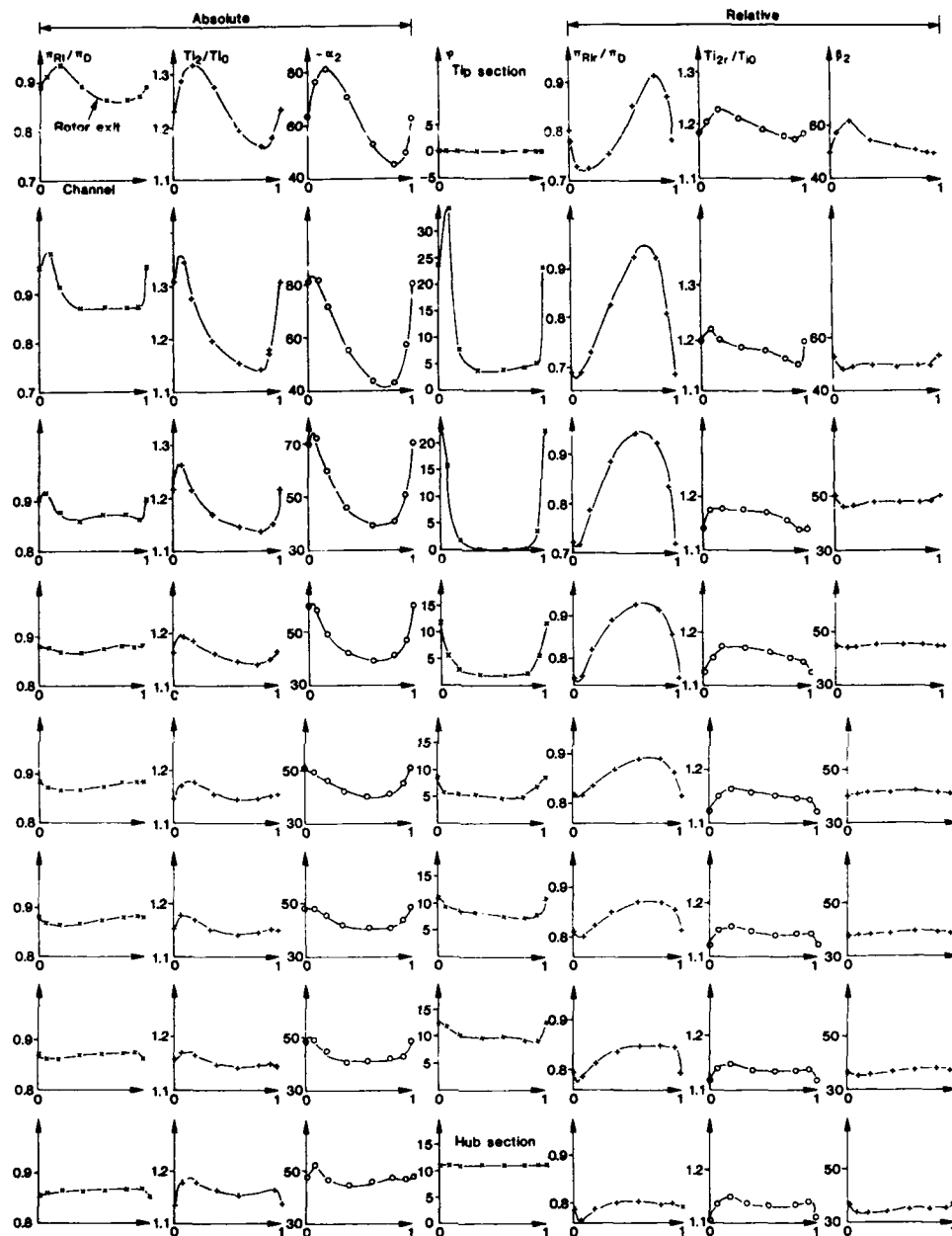


Fig. 9 - CALCULATED FLOW FIELD ON AN INTERBLADES CHANNEL DOWNSTREAM OF BARON ROTOR

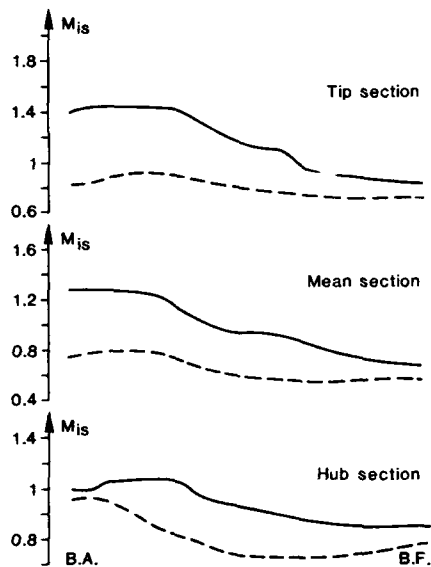


Fig. 10 - ISENTROPIC MACH NUMBER DISTRIBUTION ON THE ROTOR BLADE (NOMINAL POINT)

Fig. 11 - STREAM LINE PATTERNS ON THE ROTOR BLADE

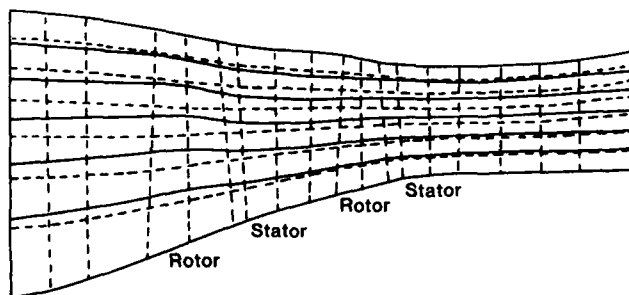
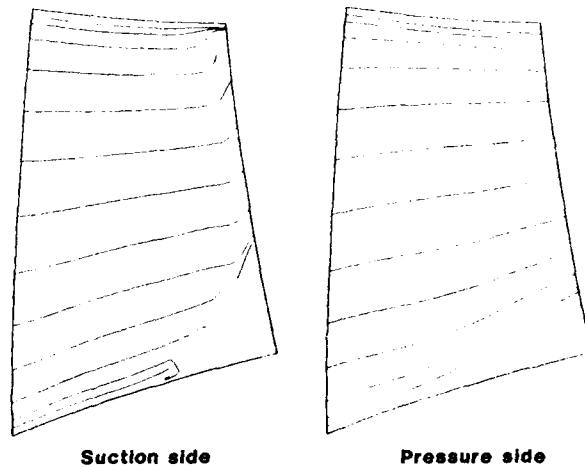


Fig. 12 - TWO-STAGE FAN GEOMETRY WITH ELEMENT BOUNDARIES AND CALCULATED STREAMLINES [from Hirsch and Warzee (1976)]

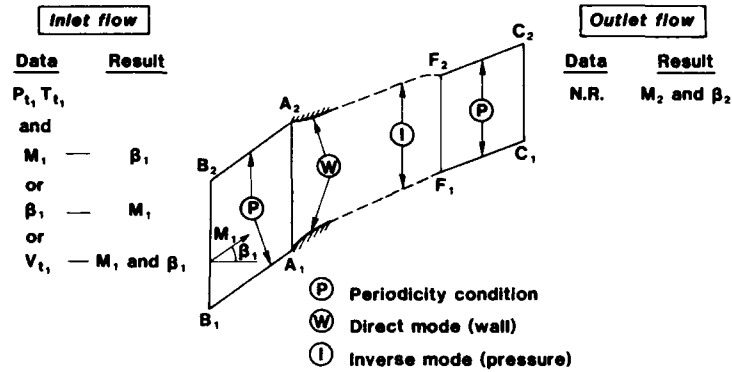


Fig. 13 - COMPUTATION DOMAIN FOR A CASCADE

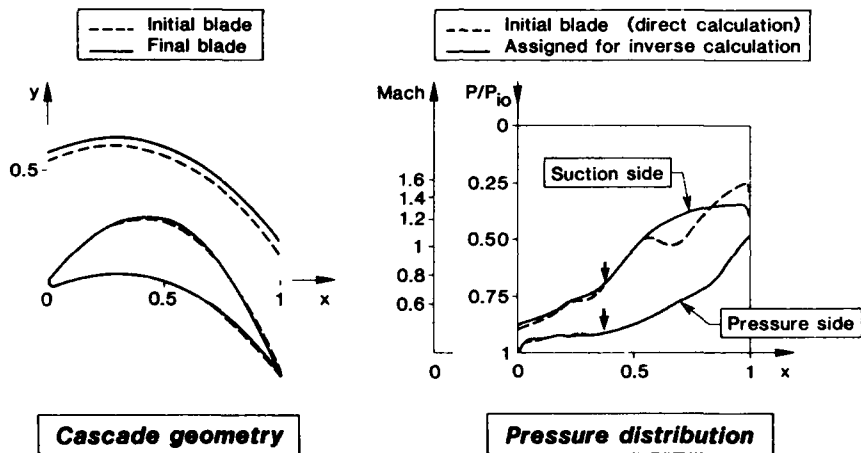


Fig. 14 - DEFINITION OF A TURBINE BLADE AND THE CASCADE PITCH, FOR PRESSURE DISTRIBUTIONS ASSIGNED ON THE PRESSURE AND SUCTION SIDES

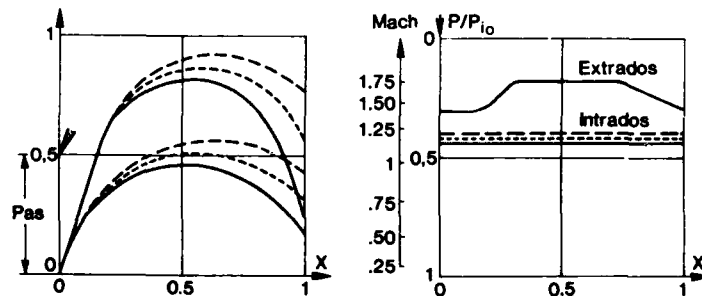


Fig. 15 - DEFINITION OF AN IMPULSE TURBINE BLADE, FOR PRESSURE DISTRIBUTIONS ASSIGNED ON THE PRESSURE AND SUCTION SIDES-PITCH AND AXIAL CHORD ARE FIXED

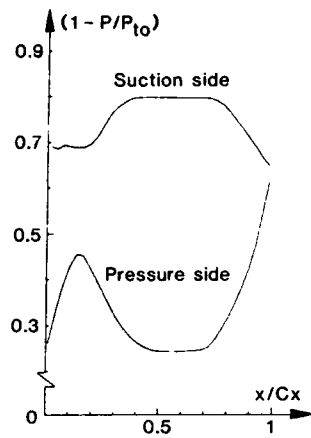


Fig. 16a - SECOND ROTOR DESIGN :
PRESSURE DISTRIBUTION (mid span section)

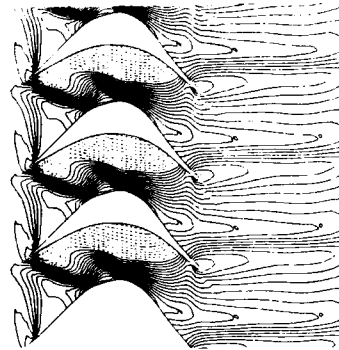


Fig. 16b - STATIC PRESSURE FIELD
IN A ROTOR CASCADE (unchoked)

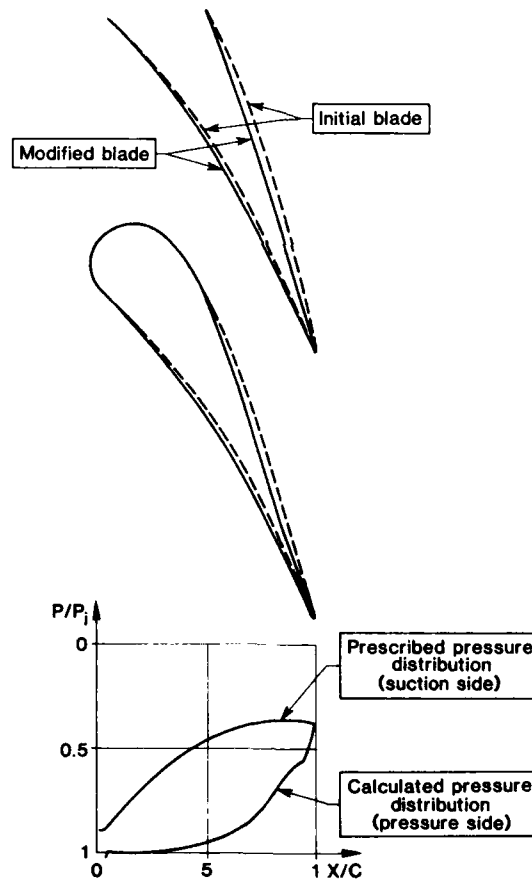


Fig. 17 - IMPROVEMENT OF A TURBINE CASCADE WITH A GIVEN
TRAILING EDGE THICKNESS AND A GIVEN PART OF THE SHAPE
OF THE PRESSURE SIDE

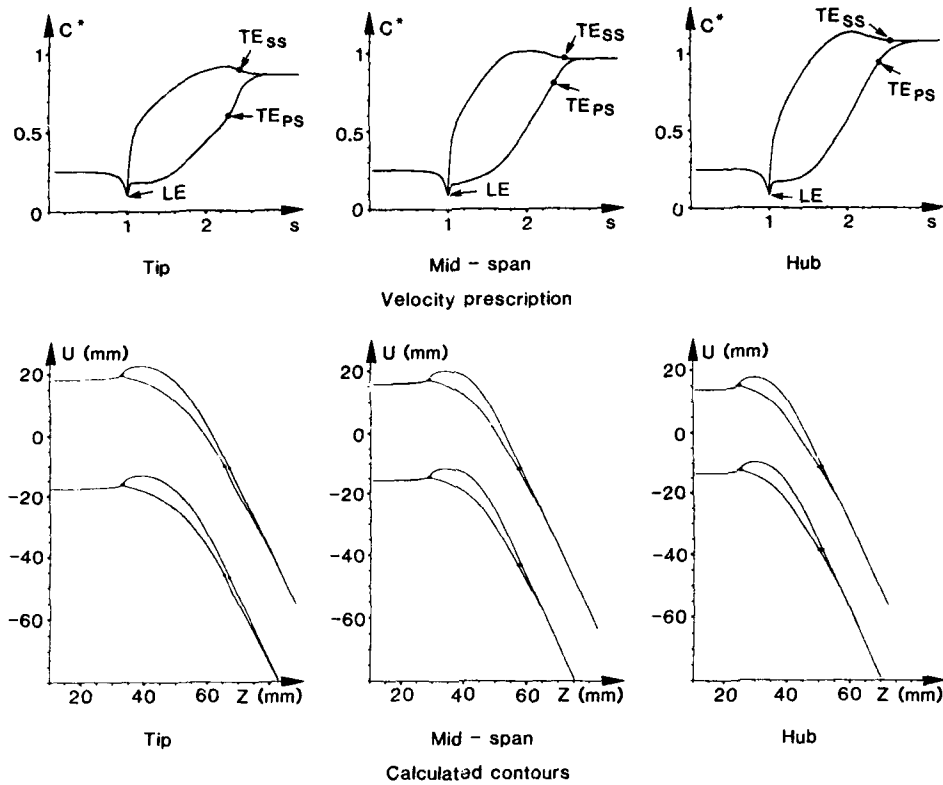


Fig. 18 - DESIGN OF AN TURBINE INLET GUIDE VANE (from Horsmann and Schmidt [54])

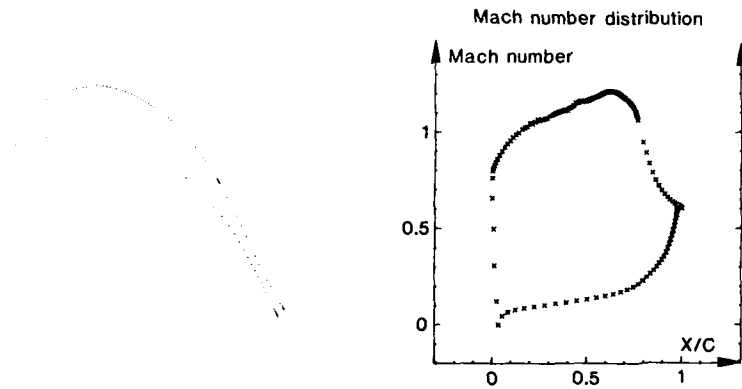


Fig. 19 - SANZ SUPERCRITICAL TURBINE BLADE

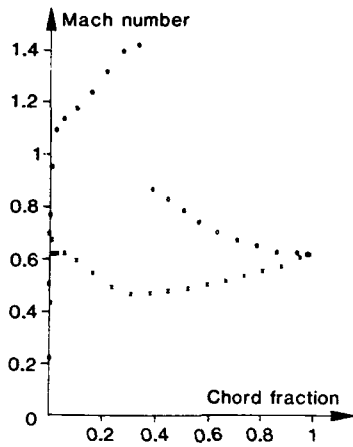


Fig. 20a - SUPERCRITICAL COMPRESSOR
BLADE WITH SHOCK

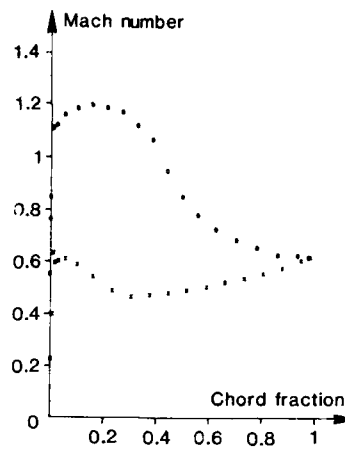


Fig. 20b - DESIGN MACH NUMBER
DISTRIBUTION

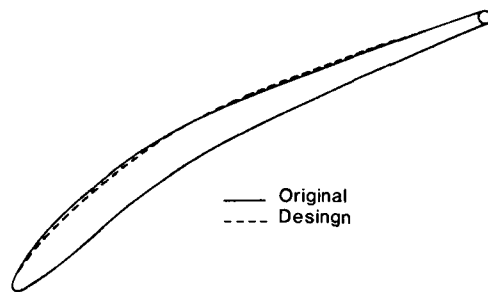


Fig. 20c - CHANGE IN BLADE SHAPE TO REMOVE SHOCK
(from Cedar and Stow [20])

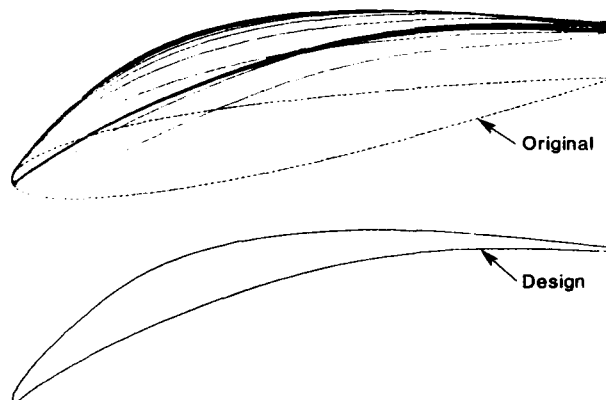


Fig. 21 - INVERSE STATOR BLADE DESIGN
(2.5 isentropic method from Jacquette [55])

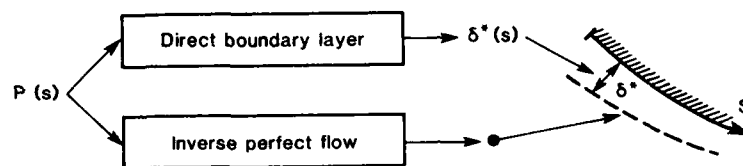


Fig. 22

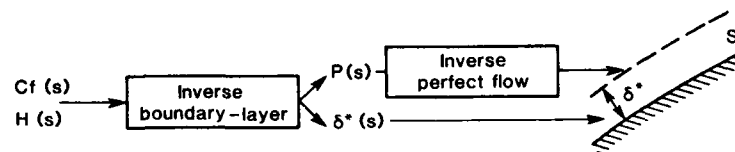


Fig. 23

PERFORMANCE PREDICTION FOR AXIAL-FLOW COMPRESSOR AND TURBINE BLADING

George K. Serovy
 Department of Mechanical Engineering
 Iowa State University of Science and Technology
 Ames, Iowa 50011
 United States of America

SUMMARY

The performance of compressor and turbine blading must be predicted in all of the levels of a conventional design system, beginning in the preliminary design phase before blade row geometry has been defined. Because of this requirement, many levels of complexity exist in both input and output of prediction methods, and alternative methods exist within each phase of design.

A brief review of performance prediction problems and current solutions is presented. Because details of equations and methods cannot and should not be included, references to original documents in readily available sources are classified according to their place in configuration design and analysis.

It is concluded that both quasi-three-dimensional and three-dimensional computational methods have a potential for future development in terms of configuration optimization. Additionally, it is concluded that experimental data correlation is not dead, and that improvement potential exists in every area of the performance estimation problem.

SYMBOLS AND NOTATION

c	blade section chord length
D	diffusion loading parameter
D_{eq}	equivalent diffusion loading parameter
h_o	total enthalpy per unit mass
i	incidence angle, measured from tangent to camber line at leading edge
M	Mach number
P	total pressure
p	static pressure
r	radial coordinate
s	blade spacing
V	absolute velocity
x	axial coordinate
z	spanwise coordinate
β	angle between relative fluid velocity and meridional plane
γ	blade setting angle (stagger angle)
δ	deviation angle, angle between fluid velocity and camber line tangent angle at trailing edge
Θ	boundary layer momentum thickness
κ	blade section camber line tangent angle measured from meridional plane
σ	cascade solidity, c/s
ϕ	blade section camber angle
$\bar{\omega}$	average total pressure loss coefficient

Superscripts

()	average value
*	at minimum loss incidence angle

Subscripts

m	component in meridional plane
max	maximum
r	radial component
rel	relative to rotating blade row
SS	suction surface
x	component in x-direction
z	component in z-direction
θ	tangential component
1	blade row inlet
2	blade row exit

INTRODUCTION

The subject of *blade row performance prediction* is reviewed in this lecture on the basis of the requirements of the various phases of compressor and turbine design. Discussion is limited to aerodynamic performance, but it should be

recognized that parallel prediction of stress and aeromechanical behavior must also occur. Performance prediction is defined here as the estimation by experimental data correlation or by flow field computation of fluid turning (deflection) and losses (entropy production) upstream, within, and downstream of the individual rows of rotating and stationary blades in compressors and turbines. In addition, methods for setting design blade section incidence angles, for predicting blade-to-blade passage choking, and for estimating stall margin should be recognized as part of the performance prediction problem.

Figures 1 and 2 are representative schematic illustrations of several flow phenomena influencing performance. Figure 1 has appeared frequently in papers on compressor aerodynamics, and Fig. 2 is a product of turbine aerodynamic research. These figures indicate the genuinely complex nature of both types of flow field; fortunately they are only schematic, and as drawn they exaggerate the secondary features of the flow. While the real flows are both three-dimensional and unsteady and the secondary flows are the source of both undesired flow angle distributions and entropy production, the "throughflow" velocity components V_m and V_θ in the "core" flow away from the wall, corner, and wake regions—where secondary flows are concentrated—move the major portion of the mass flow rate. The secondary flows disrupt and modify the "core" flow, but *control and detailed accounting* for secondary flow effects remain in the area of final-development-level geometry adjustments. Major portions of all compressor and turbine design systems do and will consist of design/analysis based on one-dimensional or two-dimensional (called quasi-three-dimensional) flow models.

Figures 3, 4, and 5 summarize the basis for the linear cascade model, which is an element in all quasi-three-dimensional design/analysis, and show the principal geometric and kinematic variables associated with the linear cascade. The first assumption basic to the linear cascade model is that computed stream surfaces of revolution can be generated for a circumferential-average, steady relative flow, and that adjacent surfaces can be used to generate a series of stream tubes of revolution in the hub-to-tip flow. The section of the blade intersected by two closely spaced surfaces can then be used with the computed entrance and exit velocity and property values to define a linear cascade of blades that can be used for performance prediction purposes and for experimental performance evaluation. This model, of course, cannot account for many of the secondary features of the flow fields in actual blade geometries as indicated in Figs. 1 and 2.

In subsequent sections of the lecture the requirements for and the present status of performance prediction methods are described for each phase of the design process. At the end of these sections a classified list of references is given, with more complete bibliographic information included at the end of the lecture text. References have been listed which are both historically and currently important, and nearly all of those selected are believed to be readily accessible.

PERFORMANCE PREDICTION IN THE THREE-LEVEL DESIGN SYSTEM: GENERAL COMMENTS

For prescribed overall design-point performance values, a new multistage compressor or turbine geometry is normally designed in a three-level, iterative optimization process. These levels, as shown in Fig. 6, might be described as follows:

1. **Preliminary Design:** Selection of possible stage design parameters and stage envelope geometry (hub and tip wall diameters and stage length), tentative blade row solidity and aspect ratio values, and spanwise velocity diagram estimates.
2. **Quasi-Three-Dimensional, Throughflow Design/Analysis:** Combined and iterative hub-to-tip velocity and property distribution computation based on stations within and between blade rows to fix hub and tip profiles, with initial blade row geometry definition.
3. **Three-Dimensional Throughflow Analysis:** Flow-field computation upstream, inside, and downstream of individual blade rows to evaluate flow path geometry and locate flow-field problems. First-build development blade row geometry is a product.

Requirements for performance prediction vary greatly between levels, and within a given level widely different approaches are both available and used.

Preliminary Design

Although not every "new" compressor or turbine requires a true preliminary design phase, the information on candidate configurations developed in preliminary design must be available before the second-level design/analysis can begin. Preliminary turbomachine design answers the questions "What might work, and could the roughly defined candidate geometries perform satisfactorily when integrated with other system (e.g., aircraft turbine engine) components?"

In preliminary design there may be, in addition to specified design operating point conditions, some restrictions on turbomachine outer diameter, length and rotational speed. However, *no* flow path or blade row geometry is known. In fact, these items are not the objective in preliminary design. Many choices must be made on the basis of the designer's experience. As a consequence any blade performance prediction criteria must be simple and based only on assumed preliminary blade row geometric parameters such as solidity, chord length, and aspect ratio. Only the simplest across-row velocity and property distribution calculations can be made, and these are often one-dimensional (mean-line) or simple radial equilibrium computations.

Performance prediction for blading when *there is no blading* is limited to setting experience-based limits on row-average or mean-line geometric and aerodynamic parameters. These limits are used to set trial design values for the parameters, and the design values might be used with experience-based correlations to predict average blade-row and individual stage performance.

Performance prediction requirements for preliminary design initiated the development of diffusion limit criteria that permit "safe" velocity diagram values to be computed. Examples are the Lieblein et al. (1953) and de Haller (1953) compressor cascade diffusion parameters and the Zweifel (1946) coefficient for turbine blade row solidity.

Mach number limits, which might include axial Mach number as well as relative Mach number maximum levels for individual blade rows, have increased substantially over the years, so that it is not a good idea to give currently accepted numerical values. It is a good idea to recognize that M limits depend on the application and on the experience of the designer's organization in development of high Mach number cascade geometries.

Minimum Reynolds number levels may be set, and in some cases manufacturing and damage-tolerance considerations may set minimum acceptable values of blade dimensions.

Overall compressor and turbine performance prediction at the preliminary design level is usually carried out by one-dimensional, mean-line calculations, again because of the lack of well-defined blade row information.

Quasi-Three-Dimensional, Throughflow Design/Analysis

The term "quasi-three-dimensional" has become the recognized designation for design or analysis calculation methods that use two-dimensional approximations to the flows in hub-to-tip surfaces and in blade-to-blade surfaces. Blade row performance prediction results are a part of the input to the hub-to-tip surface flow field solution. This input is in the form of hub-to-tip distributions of quantities that determine flow direction and entropy for calculation stations located in the spacing regions between blade rows, at stations corresponding to leading edge and trailing edge, and at stations internal to the blade rows.

The hub-to-tip flow direction and entropy distributions described can come only from a rather detailed knowledge or assumed knowledge of the blade-to-blade flow. This knowledge, in turn, can come only from experimental correlations of airfoil cascade data or from blade-to-blade surface flow field calculations capable of dealing with the effects of compressibility and viscosity. An immediately obvious problem with an unmodified quasi-three-dimensional analysis method is that it cannot, within its own structure, account for the secondary flows shown in Figs. 1 and 2 and the corresponding potential for secondary losses. These effects can only be artificially introduced into the computation system by flow angle and entropy production adjustments.

Three-Dimensional Throughflow Analysis

During the past ten years a *few* of the many turbomachine-oriented computation systems described by their developers as three-dimensional have actually under close inspection been found to be three-dimensional. Of the few, some are inviscid and can therefore only predict a very limited type of "performance" information. The three-dimensional, viscous computation systems appear to have a long development period ahead, in which fluid shear stress modeling and computation time reduction will play the same major part that they play in all computational fluid dynamics applications.

VARIABLES AND PARAMETERS OF INTEREST IN BLADE ROW PERFORMANCE PREDICTION

As shown in Figs. 1 and 2, in contemporary compressor and turbines the flow is viscous, compressible, and unsteady in complex three-dimensional passage geometries having relative motion of passage boundaries. When the present state of fluid shear stress modeling and the nature of the unsteadiness generated by varying blade numbers in the alternatively rotating and stationary rows is considered, there seems little chance that completely defined and correct compressor and turbine flows will be computed in the near future, thus finally solving the performance prediction problem. In view of this the need is apparent for continued evaluation and reevaluation of performance prediction based on the linear cascade model, with corrections arising from detailed experimental and computational studies of secondary effects.

If we want to consider the cascade flow problem in the geometrically two-dimensional context, and in a thorough manner, a list of the variables known to influence the experimental linear cascade model should be on hand. For this lecture, the first list is based on the linear cascade model, and the second list includes the secondary flow generators which can exist in finite length, finite-aspect ratio linear cascade test facilities, and *do* exist in compressor and turbine blade rows. These flows do affect the cascade performance. The lists should also be considered in planning linear cascade computational studies.

Linear Cascade Variables for Two-Dimensional, Steady-State Flow

Configuration (geometric) variables

Blade section geometry

Camber line shape

Chordwise location of maximum camber
Value of maximum camber (or camber angle)

Thickness profile

Distribution of profile thickness along camber line
 Ratio of maximum thickness to chord length
 Leading edge shape or radius
 Trailing edge shape or radius
 Manufacturing errors and tolerances
 Surface finish

Stagger angle (angle between blade chord line and cascade axial direction)

Solidity**Flow Variables**

Thermodynamic property characteristics of
 working fluid

p, v, T relationship
 Specific heats
 Viscosity characteristics

Isentropic exponent
 Other (e.g., water vapor content)

Entrance total pressure and temperature

Upstream flow angle measured relative to cascade axial direction

Mach number in leading-edge region

Reynolds number

Leading-edge region turbulence (intensity, scale, isotropy)

Incidence angle

Axial velocity-density ratio distribution (stream tube thickness variation)

Back-pressure (static pressure) ratio for started supersonic flow

All of the variables above are independent variables and are known to influence the dependent performance variables associated with the entrance region, internal, and downstream flow fields.

The usual dependent variables and parameters considered to be of probable interest as measures of performance are listed as follows:

- Leading edge plane angle distribution associated with average incidence angle
- Trailing edge plane velocity magnitude, flow angle and total pressure distributions with corresponding averaged exit angle and loss coefficient; trailing-edge suction and pressure surface boundary layer thickness parameters
- Downstream plane flow angle and total pressure distributions and averaged parameters (including "mixed-out" values)
- Blade surface static pressure distributions
- Shock wave characteristics (in supersonic flow regimes) in leading edge region, trailing edge region, and blade-to-blade passage
- Velocity magnitude, fluid angle, and pressure fields in blade-to-blade passage

There is also a long list of additional variables generally accepted as influencing the secondary flow and secondary loss patterns in the three-dimensional geometry of the compressor turbine blade.

Three-Dimensional Flow Generators

Aspect ratio-dihedral and sweep-related variables

Spanwise chord length distribution
 Spanwise stagger angle distribution
 Stacking axis shape and location in sections
 Spanwise variation in blade thickness

Blade tip clearance and tip shape

Hub fillet shape or radius

Spanwise variations in entrance velocity

CURRENT STATUS OF PREDICTION METHODS

Preliminary Design

Performance estimates during preliminary design are invariably derived from experience with existing cascade, compressor, or turbine configurations. In the rough definition of possible geometries it is typical to select limiting values of diffusion, or blade row and stage "loading" limits. A good example of such a limit is the original Lieblein (1953) diffusion parameter

$$D = 1 - \frac{V_2}{V_1} + \frac{\Delta V_\theta}{2\sigma V_1}$$

which was derived as a means for predicting the onset of excessive profile loss coefficients:

$$\omega = \frac{P_1 - \bar{P}_2}{P_1 - P_1}$$

For two-dimensional low-speed linear cascades of NACA 65-series airfoil sections, an upper limit of $D = 0.6$ was indicated, but for subsonic compressor blade rows also consisting of NACA 65-series sections, limits suggested were

$$\begin{aligned} D &= 0.45 \text{ for rotor tip region at } M_{rel} < 0.75, \\ D &= 0.55 \text{ for rotor mean and hub regions,} \\ D &= 0.60 \text{ for stator sections at } M_{rel} < 0.75. \end{aligned}$$

These values are given here because for the blade sections and conditions used in the original correlation, they could be considered as valid today. The parameter D was rapidly modified to account for radius change, and as airfoil profiles were developed for transonic relative flows the idea of limiting values with an associated limit on relative Mach number was revised. It is a fact that values of the D parameter, with modifications, continue to be used as limits in preliminary design and continue to be routinely calculated in most compressor data reduction programs. The Lieblein D contains the deHaller (1953) diffusion ratio as the second term.

A turbine blade loading parameter of corresponding character and stature is the Zweifel (1946) "tangential lift coefficient," normally used in setting initial blade row solidity levels. Wilson (1984) gives a clear explanation of the use of the Zweifel criterion.

Additional diffusion- and stall margin-related parameters used primarily in the preliminary design phase have been developed and are supported by data correlations. Useful examples for both compressor and turbine applications are listed at the end of this section.

In a second phase of preliminary compressor and turbine design, the limited geometry and velocity diagram information established for candidate designs is used to predict performance maps. This process usually is based on one-dimensional stage-by-stage calculations in which correlations of data relating to various categories of "loss" and effective passage area blockage due to end-wall "boundary layers" are used. In this area alternative methods exist in the literature for both compressors and turbines, and these methods continue to be developed because they are vital to cycle analysts and control designers.

Quasi-Three-Dimensional, Throughflow Design/Analysis

In this design system phase the blade performance input to a through flow (hub-to-tip computation surface) calculation is updated in successive runs as more and better information about the cascade (blade-to-blade) surface geometry and flow field is determined. Figure 7 shows the computing station locations used in one variety of hub-to-tip computation code. All of the variables and parameters listed for two-dimensional, steady-state linear cascade flow become relevant for this situation as the compressor or turbine geometry is more thoroughly defined. In addition, some of the secondary flow and loss effects can be approximated by correlations as the computation advances.

For both compressors and turbines, data correlations and/or blade-to-blade surface flow field computation methods for performance prediction have demonstrated capability at this level. Data correlations have resulted from linear cascade experiments and from single- and multi-stage test programs. For compressor blading, recent work on inviscid-viscous interactions codes and on Navier-Stokes solutions has improved in terms of both turning and loss prediction. In turbine blading, where surface pressure distributions from inviscid blade-to-blade computation can be valuable in airfoil section improvement, numerous Euler and Navier-Stokes computation systems have been used for blading definition.

The blade selection or design problem at this level is to specify, for a known blade leading-edge region flow, a cambered airfoil section and cascade solidity, set at a stagger and incidence that will produce the necessary exit velocity direction and magnitude. Data correlations are available for selection of cascade geometries in subsonic and transonic cases, but in most current design studies, especially of high-performance transonic and supersonic blade rows, arbitrary airfoil sections are determined by either iterative airfoil analysis or inverse airfoil design computation. Because these computations generally determine an equivalent linear cascade, the question of how to relate velocities and airfoil geometry in the equivalent linear cascade to the corresponding stream surface intersection velocities and airfoil section is important. One widely accepted procedure is shown in Fig. 8.

Fluid turning and loss prediction in quasi-three-dimensional methods are based on relatively complete input. Data correlation-based and simple flow model methods usually include a basic trailing-edge deviation angle prediction, possibly supplemented by hub and tip region adjustments. They also normally contain estimation methods for three classes of loss. These are the profile and wake-mixing losses due to suction and pressure surface boundary layer development with accounting for trailing-edge thickness; a shock loss prediction based on a simplified shock-wave model; and a one- or two-element loss increment prediction accounting for entropy production due to secondary flows.

Representative types of profile loss correlation for compressors are those based on an "equivalent" D-parameter such as the initial D_{eq} of Lieblein (1959) as shown in Fig. 9, where a trailing-edge momentum thickness parameter is plotted as a function of D_{eq} where D_{eq} is proportional to a blade suction surface velocity diffusion ratio $V_{max,ss}/V_2$. This correlation parameter concept, again initially developed for a data base consisting of a limited range of subsonic, two-dimensional cascade experiments, has subsequently been revised and its application extended to a wide range of compressor row geometries and flow conditions. Presently a variety of parameters called D_{eq} exist, among which the Koch and Smith (1976) variant may be the most widely used.

For turbines, there are also a number of blade-surface velocity diffusion parameters now in use that frequently derive from the data correlation proposed by Stewart, Whitney, and Wong (1960).

Shock loss modeling for compressors has developed from the simple normal shock model of Miller, Lewis, and Hartmann (1961) to more advanced models accounting for the three-dimensional nature of the wave pattern such as the method of Wennerstrom and Puterbaugh (1984).

The secondary loss correlation scene for both compressors and turbines in quasi-three-dimensional design/analysis can only be presented by indicating the variety of approaches described in the reference list.

Performance prediction by flow field computation for both compressor and turbine linear cascade geometries has become a reality during the last ten years, after a long period of advertised solutions having no useful results. In the compressor case the successive papers of Calvert (e.g., 1982 and 1983) show the nature of recent results. Similarly for the turbine case several groups have shown substantial results. In both the compressor and turbine computations, it should be understood that only linear cascade cases have been published, with consequent limitation to predicting "equivalent" cascade turning and loss.

A major contribution to blade-to-blade computation improvement has come from realistic boundary layer development prediction. Figure 10 is a "flow chart" for two-dimensional boundary layer development, and it is now understood that all of the eccentricities of the developing layer can and do occur in compressor and turbine blade rows. Simple models of characteristics such as transition length (Roberts 1975), as well as detailed in-row measurements (Hourmouziadis et al. 1987), have become extremely important in recent improvements in loss and turning prediction.

As shown in Fig. 7, all modern hub-to-tip surface flow field computation codes include computing stations between the blade row leading and trailing edges. At each of these locations there must be an input of a circumferential-average relative flow angle and an entropy value. Until recently these inputs were based on arbitrarily assumed distribution functions between the leading- and trailing-edge stations for each stream surface. The generation of in-row data by laser anemometry and to a limited extent by computation has now changed distributed-deviation and distributed-loss prediction to a more rational basis.

Three-Dimensional Throughflow Analysis

In the past decade, understandable and computationally attractive three-dimensional flow analysis codes have become a genuine contributing factor to compressor and turbine development. In AGARD Lecture Series 140 a number of survey papers showed the status of this subject in 1985 and more recent referenced publications show continued progress. Certainly, qualitative features of both compressor and turbine flows as shown in Figs. 1 and 2 have been duplicated by three-dimensional computation.

Classification of References

Preliminary Design

Development and selection of aerodynamic limits for design:

Carchedi and Wood 1982	Lieblein, Schwenk, and Broderick 1953
deHaller 1953	Schaffler 1980
Diakunchak et al. 1985	Schweitzer and Garberoglio 1984
Gostelow (1984)	Wilson 1987
Koch 1981	Zweifel 1946
Koch and Smith 1976	

One-dimensional performance prediction and related correlations:

Casey 1987	Horlock and Lakshminarayana 1973
Craig and Cox 1970-71	Kacker and Okapuu 1982
Dunham 1970	Lakshminarayana and Horlock 1963

Farokhi 1988
Grieb et al. 1975
Horlock 1960

Peacock 1983
Wilson 1984

Quasi-Three-Dimensional, Throughflow Design Analysis:

Design/Analysis by quasi-three-dimensional codes-application

Boyle, Haas, and Katsanis 1985	Horlock 1971
Calvert, Ginder, and Lewis 1987	Moustapha et al. 1987
Cetin et al. 1987	NATO/AGARD 1981
Crouse 1974	Stow 1985
Dunker et al. 1984	Sullery and Kumar 1984
Ginder and Calvert 1987	Wennerstrom 1984
Grahl 1977	

Correlation development and related experiments-profile and shock loss models-turning

Citavy 1987	Miller and Wasdell 1987
Denton 1973	Miller, Lewis, and Hartmann 1961
Denton, Cumpsty 1987	Papaliou 1975
Dunker 1987	Prince 1980
Howell 1964	Schreiber 1987
Klein 1977	Serovy 1978
Lichtfuss and Starken 1974	Traupel 1973
Lieblein 1959	Wennerstrom and Puterbaugh 1984
Lieblein 1960	Xu and Denton 1988
Lieblein 1965	

Blade profile improvement

Behlke 1986	Kiock et al. 1986
Hobbs and Weingold 1984	Serovy and Okiishi 1988
Huffman and Tramm 1974	

Allowances for three-dimensional effects

Adkins and Smith 1982	Robbins et al. 1965
Bardon, Moffat, and Randall 1975	Roberts, Serovy, and Sandercock 1986
Gregory-Smith 1982	Roberts, Serovy, and Sandercock 1988
Papaliou et al. 1977	Smith 1970

Prediction by blade-to-blade computation-boundary layer methods and data

Bradshaw 1974	Hourmouziadis et al. 1987
Calvert 1982	Roberts 1975
Calvert 1983	Sanger and Shreeve 1986
Davis, Hobbs, and Weingold 1988	Stewart 1955
Hansen, Serovy, and Sockol 1980	Stewart, Whitney, and Wong 1960
Hoheisel et al. 1987	Stow 1985a
Hoheisel and Seyb 1987	

Three-dimensional, throughflow analysis-experiments on secondary flow effects

Breugelmans et al. 1984	Pouagare and Delaney 1986
Denton 1985	Povinelli 1985
Dong, Gallimore, and Hodson 1987	Sharma and Graziani 1983
Gallimore and Cumpsty 1986	Sharma and Butler 1987
Gallimore 1986	Sieverding 1985
Karadimas 1988	Sieverding 1985a
Lakshminarayana et al. 1988	Sieverding 1985b
McNally and Sockol 1985	Smith and Yeh 1963
Northall et al. 1987	Wisler 1985
Peacock 1983	Wisler, Bauer, and Okiishi 1987

CONCLUSIONS

This lecture makes the following major points:

1. Performance prediction is defined here as the estimation of turning and entropy production (loss) due to blade row flow fields, selection of incidence angle, and estimation of choking and stall margins.

2. Many sources of loss and turning rate variation are three-dimensional in nature and cannot be related to the "equivalent linear cascade" cut by a stream surface approximation predicted in a quasi-three-dimensional throughflow solution.
3. Even though point (2) is true, there is still value in many old as well as contemporary performance prediction techniques as utilized in all levels of a typical compressor or turbine design system. Data correlations and the experimental support for them should continue to be an important element of research and development programs.

LIST OF FIGURES

- Fig. 1. Compressor blade row flow field characteristics (NASA-Lewis Research Center).
- Fig. 2. Turbine blade row flow field characteristics (NASA-Lewis Research Center).
- Fig. 3a. Definition of annular cascade arrangement.
- Fig. 3b. Definition of linear cascade arrangement.
- Fig. 4. Typical blade section profile terminology.
- Fig. 5. Typical linear cascade terminology.
- Fig. 6. Structure of a design system for axial-flow turbomachines.
- Fig. 7. Hub-to-tip computation results for a quasi-three-dimensional design/analysis method showing typical computing stations.
- Fig. 8. Definition of the linear cascade projection for a computed stream surface approximation (from Starken-DFVLR).
- Fig. 9. Example correlation curve for profile loss parameter.
- Fig. 10. Course of the boundary layer (from J. M. Robertson).

REFERENCES

- Adkins, G. G., Jr. and Smith, L. H., Jr., 1982, "Spanwise Mixing in Axial-Flow Turbomachines," *Jour. of Engr. for Power*, Trans. ASME, 104:97-110.
- Bardon, M. F., Moffat, W. C. and Randall, J. L., 1975, "Secondary Flow Effect on Gas Exit Angles in Rectilinear Cascades," *Jour. of Engr. for Power*, Trans. ASME, 97:93-100.
- Behlke, R. F., 1986, "The Development of a Second Generation of Controlled Diffusion Airfoils for Multistage Compressors," *Jour. of Turbomachinery*, Trans. ASME, 108:32-41.
- Boyle, R. J., Haas, J. E. and Katsanis, T., 1985, "Predicted Turbine Stage Performance Using Quasi-Three-Dimensional and Boundary-Layer Analyses," *J. Propulsion and Power*, 1:242-251.
- Bradshaw, P., 1974, "Prediction of Turbulent Shear Layers in Turbomachines," *Fluid Mechanics, Acoustics, and Design of Turbomachinery*, NASA SP-304, Pt. I, pp. 251-277.
- Breugelmans, F. A. H., Carels, Y. and Demuth, M., 1984, "Influence of Dihedral on the Secondary Flow in a Two-Dimensional Compressor Cascade," *Jour. of Engr. for Gas Turbines and Power*, Trans. ASME 106:578-584.
- Calvert, W. J., 1982, "An Inviscid-Viscous Interaction Treatment to Predict the Blade-to-Blade Performance of Axial Compressors with Leading Edge Normal Shock Waves," ASME Paper 82-GT-135.
- Calvert, W. J., 1983, "Application of an Inviscid-Viscous Interaction Method to Transonic Compressor Cascades," *Viscous Effects in Turbomachines*, AGARD CP-351, Paper 2.
- Calvert, W. J., Ginder, R. B. and Lewis, G., 1987, "Performance of a Civil Fan Rotor Designed Using a Quasi-Three-Dimensional Calculation System," *Proc. of the IME, I. Mech. E. Conf.*, 1987-G, Paper C257/87.
- Carchedi, F. and Wood, G. R., 1982, "Design and Development of a 12:1 Pressure Ratio Compressor for the Ruston 6-MW Gas Turbine," *Jour. of Engr. for Power*, Trans. ASME, 104:823-831.
- Casey, M. V., 1987, "A Mean Line Prediction Method for Estimating the Performance Characteristic of an Axial Compressor Stage," *Proc. of the IME, I. Mech. E. Conf.* 1987-G, Paper C264/87.

- Cetin, M., Ücer, A. S., Hirsch, C. H. and Serovy, G. K., 1987, "Application of Modified Loss and Deviation Correlations to Transonic Axial Compressors," NATO/AGARD Report AGARD-R-745.
- Citavy, J., 1987, "Performance Prediction of Straight Compressor Cascades Having an Arbitrary Profile Shape," *Jour. of Turbomachinery*, Trans. ASME, 109:114-122.
- Craig, H. R. M. and Cox, H. J. A., 1970-1971, "Performance Estimation of Axial Flow Turbines," *Proc. IME*, 185:32/71:407-473.
- Crouse, J. E., 1974, "Computer Program for Definition of Transonic Axial Flow Compressor Blade Rows," NASA TN-D-7345.
- Davis, R. L., Hobbs, D. E. and Weingold, H. D., 1988, "Prediction of Compressor Cascade Performance Using a Navier-Stokes Technique," *Jour. of Turbomachinery*, Trans. ASME, 110:520-531.
- de Haller, P., 1953, "Das Verhalten von Tragflügelgittern in Axialverdichtern und im Windkanal," *Brennstoff-Wärme-Kraft*, 5:333-337.
- Denton, J. D., 1973, "A Survey and Comparison of Methods of Predicting the Profile Loss of Turbine Blades," *IME Paper C76/73*, Conf. Proc. of the IME, 3:204-212.
- Denton, J. D., 1985, "The Calculation of Fully Three Dimensional Flow Through any Type of Turbomachine Blade Row," *3-D Computation Techniques Applied to Internal Flow in Propulsion Systems*, AGARD-LS-140, Paper 9.
- Denton, J. D. and Cumpsty, N. A., 1987, "Loss Mechanisms in Turbomachines," *Proc. of the IME, I. Mech. E. Conf.* 1987-G, Paper C260/87.
- Diakunchak, I. S., Young, J. Y. and Spedaler, P. S., 1985, "Aerodynamic Design of a Highly Loaded, High Efficiency, Cooled Single Stage Compressor Turbine for an Energy Efficient Industrial Gas Turbine," *CIMAC Intl. Cong. on Combustion Engines*, Oslo, June 1985, Paper T4.
- Dong, Y., Gallimore, S. J. and Hodson, H. P., 1987, "Three-Dimensional Flows and Loss Reduction in Axial Compressors," *Jour. of Turbomachinery*, Trans. ASME, 109:354-361.
- Dunham, J., 1970, "A Review of Cascade Data on Secondary Losses in Turbines," *J. Mech. Engr. Sci.*, 12:48-59.
- Dunker, R., Rechter, H., Starken, H. and Weyer, H., 1984, "Redesign and Performance Analysis of a Transonic Axial Compressor Stator and Equivalent Plane Cascades With Subsonic Controlled Diffusion Blades," *Jour. of Engr. for Gas Turbines and Power*, Trans. ASME, 106:279-287.
- Dunker, R. J., 1987, "A Shock Loss Model for Supercritical Subsonic Flows in Transonic Axial Flow Compressors," *Transonic and Supersonic Phenomena in Turbomachines*, AGARD-CP-401, Paper 27.
- Farokhi, S., 1988, "Analysis of Rotor Tip Clearance Loss in Axial-Flow Turbines," *J. Propulsion and Power*, 4:452-457.
- Gallimore, S. J., 1986, "Spanwise Mixing in Multistage Axial Flow Compressors: Part II-Throughflow Calculations Including Mixing," *Jour. of Turbomachinery*, Trans. ASME, 108:10-16.
- Gallimore, S. J. and Cumpsty, N. A., 1986, "Spanwise Mixing in Multistage Axial Flow Compressors: Part I-Experimental Investigation," *Jour. of Turbomachinery*, Trans. ASME, 108:2-9.
- Ginder, R. B. and Calvert, W. J., 1987, "The Design of an Advanced Civil Fan Rotor," *Jour. of Turbomachinery*, Trans. ASME, 109:340-346.
- Gostelow, J. P., 1984, *Cascade Aerodynamics*, Pergamon Press, Oxford.
- Grahl, K. G., 1977, "Über den Stand der Kennfeldberechnung Mehrstufiger Axialverdichter," *Zeit. Flugwiss Weltraumforsch*, 1:29-41.
- Gregory-Smith, D. G., 1982, "Secondary Flows and Losses in Axial-Flow Turbines," *Jour. of Engr. for Power*, Trans. ASME, 104:819-822.
- Grieb, H., Schill, G. and Gumucio, R., 1975, "A Semi-Empirical Method for the Determination of Multistage Axial Compressor Efficiency," *ASME Paper 75-GT-11*.
- Hansen, E. C., Serovy, G. K. and Sockol, P. M., 1980, "Axial-Flow Compressor Turning Angle and Loss by Inviscid-Viscous Interaction Blade-to-Blade Computation," *Jour. of Engr. for Power*, Trans. ASME, 102:28-34.
- Hobbs, D. E. and Weingold, H. D., 1984, "Development of Controlled Diffusion Airfoils for Multistage Compressor Application," *Jour. of Engr. for Gas Turbines and Power*, Trans. ASME, 106:271-278.

- Hoheisel, H., Kiock, R., Lichtfuss, H. J. and Fottner, L., 1987, "Influence of Free-Stream Turbulence and Blade Pressure Gradient on Boundary Layer and Loss Behavior of Turbine Cascades," *Jour. of Turbomachinery*, Trans. ASME, 109:210-219.
- Hoheisel, H. and Seyb, N. J., 1987, "The Boundary Layer Behavior of Highly Loaded Compressor Cascade of Transonic Flow Conditions," *Transonic and Supersonic Phenomena in Turbomachines*, AGARD-CP-401, Paper 4.
- Horlock, J. H., 1960, "Review of Losses and Efficiencies in Axial-Flow Turbines," *Intl. Jour. Mech. Sci.*, 2:48-75.
- Horlock, J. H., 1971, "On Entropy Production in Adiabatic Flow in Turbomachines," *Jour. of Basic Engr.*, Trans. ASME, Series D, 93:587-593.
- Horlock, J. H. and Lakshminarayana, B., 1973, "Secondary Flows: Theory, Experiment, and Application in Turbomachinery Aerodynamics," *Annual Rev. of Fluid Mechanics*, 5:247-280.
- Hourmouziadis, J., Buckl, F. and Bergmann, P., 1987, "The Development of the Profile Boundary Layer in a Turbine Environment," *Jour. of Turbomachinery*, Trans. ASME, 109:286-295.
- Howell, A. R., 1964, "Flow in Cascades," *High Speed Aerodynamics and Jet Propulsion*, Vol. X of *Aerodynamics of Turbines and Compressors*, Princeton University Press, Princeton, N.J.
- Huffman, G. D. and Tramm, P. C., 1974, "Airfoil Design for High Tip Speed Compressors," *Jour. Aircraft*, 11:682-689.
- Kacker, S. C. and Okapuu, U., 1982, "A Mean Line Prediction Method for Axial Flow Turbine Efficiency," *Jour. of Engr. for Power*, Trans. ASME, 104:111-119.
- Karadimas, G., 1988, "Design of High-Performance Fans Using Advanced Aerodynamic Codes," *Jour. of Turbomachinery*, Trans. ASME, 110:419-427.
- Kiock, R., Lethaus, F., Baines, N. C. and Sieverding, C. H., 1986, "The Transonic Flow Through a Plane Turbine Cascade as Measured in Four European Wind Tunnels," *Jour. of Engr. for Gas Turbines and Power*, Trans. ASME, 108:277-284.
- Klein, A., 1977, "Aerodynamics of Cascades," Translation and revision of "Aerodynamik der Schaufelgitter" by N. Scholz, AGARDograph 220.
- Koch, C. C., 1981, "Stalling Pressure Rise Capability of Axial Flow Compressor Stages," *Jour. of Engr. for Power*, Trans. ASME, 103:645-656.
- Koch, C. C. and Smith, L. H., Jr., 1976, "Loss Sources and Magnitudes in Axial-Flow Compressors," *Jour. of Engr. for Power*, Trans. ASME, Series A, 98:411-424.
- Lakshminarayana, B. and Horlock, J. H., 1963, "Review: Secondary Flows and Losses in Cascades and Axial-Flow Turbomachines," *Intl. J. Mech. Sci.*, 5:287-307.
- Lakshminarayana, B., Kirtley, K. R. and Warfield, M., 1988, "Computational Techniques and Validation of 3D Viscous/Turbulent Codes for Internal Flows," *Validation of Computational Fluid Dynamics*, NATO/AGARD-CP-437.
- Lichtfuss, H.-J. and Starken, H., 1974, "Supersonic Cascade Flow," *Progress in Aerospace Science*, Vol. 5, Pergamon Press, Ltd., New York, pp. 37-149.
- Lieblein, S., 1959, "Loss and Stall Analysis of Compressor Cascades," *Jour. of Basic Engr.*, Trans. ASME, Series D, 81:387-400.
- Lieblein, S., 1960, "Incidence and Deviation-Angle Correlations for Compressor Cascades," *Jour. of Basic Engr.*, Trans. ASME, Series D, 82:575-587.
- Lieblein, S., 1965, "Experimental Flow in Two-Dimensional Cascades, *Aerodynamic Design of Axial-Flow Compressors*," NASA SP-36, Chap. VI.
- Lieblein, S., Schwenk, F. C. and Broderick, R. L., 1953, "Diffusion Factor for Estimating Losses and Limiting Blade Loadings in Axial-Flow-Compressor Blade Elements," NACA RM E53 D01.
- McNally, W. D. and Sockol, P. M., 1985, "REVIEW-Computation Methods for Internal Flows With Emphasis on Turbomachinery," *Jour. of Fluids Engr.*, Trans. ASME, 107:6-22.
- Miller, D. C. and Wasdell, D. L., 1987, "Off-Design Prediction of Compressor Blade Losses," *Proc. of the IME, I. Mech. E. Conf. 1987-G*, Paper C279/87.
- Miller, G. R., Lewis, G. W. and Hartmann, M. J., 1961, "Shock Losses in Transonic Compressor Blade Rows," *J. of Engr. for Power*, Trans. ASME, Series A, 83:235-242.

- Moustapha, S. H., Okapuu, U. and Williamson, R. G., 1987, "Influence of Rotor Blade Aerodynamic Loading on the Performance of a Highly Loaded Turbine Stage," *Jour. of Turbomachinery*, Trans. ASME, 109:155-162.
- NATO/AGARD Propulsion and Energetics Panel Working Group 12, 1981, "Through Flow Calculations in Axial Turbomachines," AGARD-AR-175.
- Northall, J. D., Moore, J. G. and Moore, J., 1987, "Three-Dimensional Viscous Flow Calculations for Loss Prediction in Turbine Blade Rows," *Proc. of the IME, I. Mech. E. Conf. 1987-G*, Paper C267/87.
- Papailiou, K. D., 1975, "Correlations Concerning the Process of Flow Deceleration," *Jour. of Engr. for Power*, Trans. ASME, 97:295-300.
- Papailiou, K., Flot, R. and Mathieu, J., 1977, "Secondary Flows in Compressor Bladings," *Jour. of Engr. for Power*, Trans. ASME, 99:211-224.
- Peacock, R. E., 1983, "A Review of Turbomachinery Tip Gap Effects, Part 2: Rotating Machinery," *Intl. Jour. Heat and Fluid Flow*, 4:3-16.
- Pouagare, M. and Delaney, R. A., 1986, "Study of Three-Dimensional Viscous Flows in an Axial Compressor Cascade Including Tip Leakage Effects Using a SIMPLE-Based Algorithm," *Jour. of Turbomachinery*, Trans. ASME, 108:51-58.
- Povinelli, L. A., 1985, "Assessment of Three-Dimensional Viscous Codes and Loss Calculations for Turbine Aerodynamic Computations," *Jour. of Engr. for Gas Turbines and Power*, Trans. ASME 107:265-276.
- Prince, D. C., Jr., 1980, "Three-Dimensional Shock Structures for Transonic/Supersonic Compressor Rotors," *J. Aircraft*, 17:28-37.
- Robbins, W. H., Jackson, R. J., and Lieblein, S., 1965, "Blade-Element Flow in Annular Cascades," *Aerodynamic Design of Axial-Flow Compressors*, NASA SP-36, Chap. VII.
- Roberts, W. B., 1975, "The Effect of Reynolds Number and Laminar Separation on Axial Cascade Performance," *Jour. of Engr. for Power*, 97:261-274.
- Roberts, W. B., Serovy, G. K. and Sandercock, D. M., 1986, "Modeling the 3-D Flow Effects on Deviation Angle for Axial Compressor Middle Stages," *Jour. of Engr. for Gas Turbines and Power*, Trans. ASME, 108:131-137.
- Roberts, W. B., Serovy, G. K. and Sandercock, D. M., 1988, "Design Point Variation of Three-Dimensional Loss and Deviation for Axial Compressor Middle Stages," *Jour. of Turbomachinery*, Trans. ASME, 110:426-433.
- Sanger, N. L. and Shreeve, R. P., 1986, "Comparison of Calculated and Experimental Cascade Performance for Controlled-Diffusion Compressor Stator Blading," *Jour. of Turbomachinery*, Trans. ASME, 108:42-50.
- Schaffler, A., 1980, "Experimental and Analytical Investigation of the Effects of Reynolds Number and Blade Surface Roughness on Multistage Axial Flow Compressors," *Jour. of Engr. for Power*, Trans. ASME, Series A, 102:5-13.
- Schreiber, H. A., 1987, "Experimental Investigations on Shock Losses of Transonic and Supersonic Compressor Cascades," *Transonic and Supersonic Phenomena in Turbomachines*, AGARD-CP-401, Paper 11.
- Schweitzer, J. K. and Garberoglio, J. E., 1984, "Maximum Loading Capability of Axial Flow Compressors," *J. Aircraft*, 21:593-600.
- Serovy, G. K., 1978, "Deviation Angle/Turning Angle Prediction for Advanced Axial-Flow Compressor Blade Row Geometries," AFAPL-TR-77-81.
- Serovy, G. K. and Okiishi, T. H., 1988, "Performance of a Compressor Cascade Configuration With Supersonic Entrance Flow-A Review and Comparison of Experiments in Three Installations," *Jour. of Turbomachinery*, Trans. ASME, 110:441-449.
- Sharma, O. P. and Graziani, R. A., 1983, "Influence of Endwall Flow on Airfoil Suction Surface Midheight Boundary Layer Development in a Turbine Cascade," *Jour. of Engr. for Power*, Trans. ASME, 105:147-155.
- Sharma, O. P. and Butler, T. L., 1987, "Predictions of Endwall Losses and Secondary Flows in Axial Flow Turbine Cascades," *Jour. of Turbomachinery*, Trans. ASME, 109:229-236.
- Sieverding, C. H., 1985, "Recent Progress in the Understanding of Basic Aspects of Secondary Flows in Turbine Blade Passages," *J. of Engr. for Gas Turbines and Power*, Trans. ASME, 107:248-257.
- Sieverding, C. H., 1985a, "Secondary Flows in Straight and Annular Turbine Cascades," *Thermodynamics and Fluid Mechanics of Turbomachinery*, Vol. II, M. Nijhoff Publ., Dordrecht.

- Sieverding, C. H., 1985b, "Axial Turbine Performance Prediction Methods," *Thermodynamics and Fluid Mechanics of Turbomachinery*, Vol. II, M. Nijhoff Publ., Dordrecht.
- Smith, L. H., Jr., 1970, "Casing Boundary Layers in Multistage Axial-Flow Compressors," *Flow Research on Blading*, Elsevier Publ. Co., Amsterdam, pp. 275-304.
- Smith, L. H., Jr. and Yeh, H., 1963, "Sweep and Dihedral Effects in Axial-Flow Turbomachinery," *Jour. of Basic Engr.*, Trans. ASME, Series D, 85:401-416.
- Stewart, W. L., 1955, "Analysis of Two-Dimensional Compressible Flow Loss Characteristics Downstream of Turbomachine Blade Rows in Terms of Basic Boundary-Layer Characteristics," NACA TN 3515.
- Stewart, W. L., Whitney, W. J. and Wong, R. Y., 1960, "A Study of Boundary Layer Characteristics of Turbomachine Blade Rows and Their Relation to Overall Blade Loss," *Jour. of Basic Engr.*, Trans. ASME, Series D, 83:588-597.
- Stow, P., 1985, "Incorporation of Viscous-Inviscid Interactions in Turbomachinery Design," *Thermodynamics and Fluid Mechanics of Turbomachinery*, Vol. II, M. Nijhoff Publ., Dordrecht, pp. 887-921.
- Stow, P. 1985a, "Turbomachinery Blade Design Using Advanced Calculation Methods," *Thermodynamics and Fluid Mechanics of Turbomachinery*, Vol. II, M. Nijhoff Publ., Dordrecht, pp. 923-964.
- Sullery, R. K. and Kumar, S., 1984, "A Study of Axial Turbine Loss Models in a Streamline Curvature Computing Scheme," *Jour. of Engr. for Gas Turbines and Power*, Trans. ASME, 106:591-597.
- Traupel, W., 1973, "Prediction of Flow Outlet Angle in Blade Rows with Conical Stream Surfaces," ASME Paper 73-GT-32.
- Wennerstrom, A. J., 1984, "Experimental Study of a High-Throughflow Transonic Axial Compressor Stage," *Jour. of Engr. for Gas Turbines and Power*, Trans. ASME, 106:552-560.
- Wennerstrom, A. J. and Puterbaugh, S. L., 1984, "A Three-Dimensional Model for the Prediction of Shock Losses in Compressor Blade Rows," *Jour. of Engr. for Gas Turbines and Power*, Trans. ASME, 106:295-299.
- Wilson, D. G., 1984, *The Design of High-Efficiency Turbomachinery and Gas Turbines*, MIT Press, Cambridge, Chapters 7 and 8.
- Wilson, D. G., 1987, "New Guidelines for the Preliminary Design and Performance Prediction of Axial-Flow Turbines," *Proc. of the IME*, 201(A4):279-290.
- Wisler, D. C., 1985, "Loss Reduction in Axial-Flow Compressors Through Low-Speed Model Testing," *Jour. of Engr. for Gas Turbines and Power*, Trans. ASME, 107:354-363.
- Wisler, D. C., Bauer, R. C. and Okiishi, T. H., 1987, "Secondary Flow, Turbulent Diffusion, and Mixing in Axial-Flow Compressors," *Jour. of Turbomachinery*, Trans. ASME, 109:455-482.
- Xu, L. and Denton, J. D., 1988, "The Base Pressure and Loss of a Family of Four Turbine Blades," *Jour. of Turbomachinery*, Trans. ASME, 110:9-17.
- Zweifel, O., 1946, "Optimum Blade Pitch for Turbo-Machines with Special Reference to Blades of Great Curvature," *Brown Boveri Review, The Engineer's Digest*, 7:358-360 and 7:381-383.

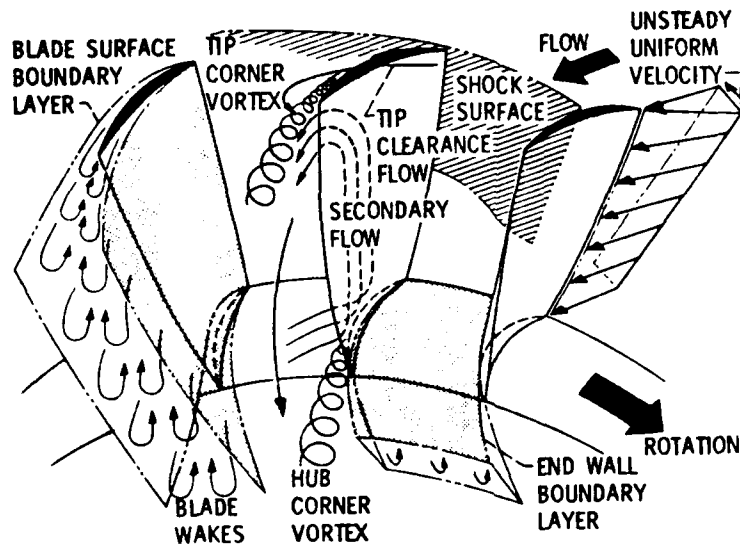


Fig. 1. Compressor blade row flow field characteristics (NASA-Lewis Research Center).

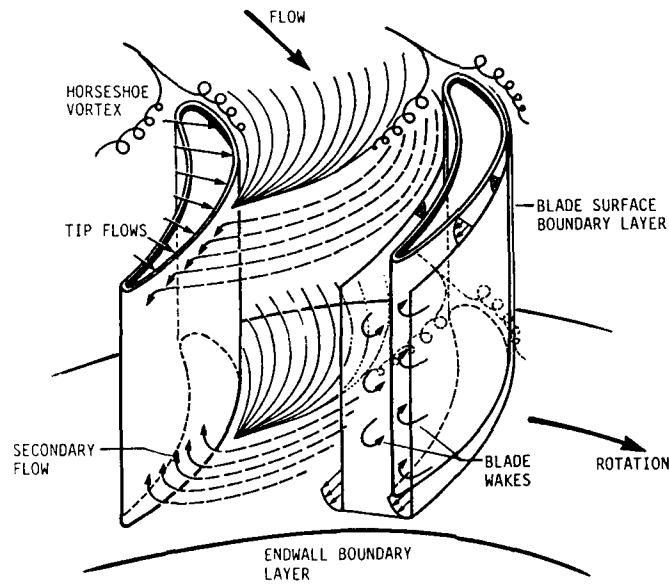


Fig. 2. Turbine blade row flow field characteristics (NASA-Lewis Research Center).

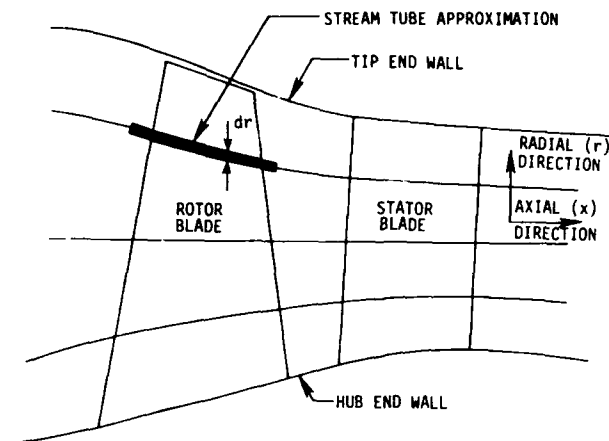


Fig. 3a. Definition of annular cascade arrangement.

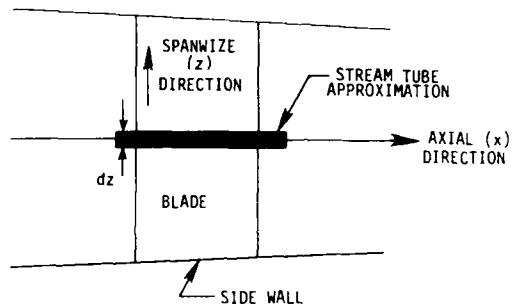


Fig. 3b. Definition of linear cascade arrangement.

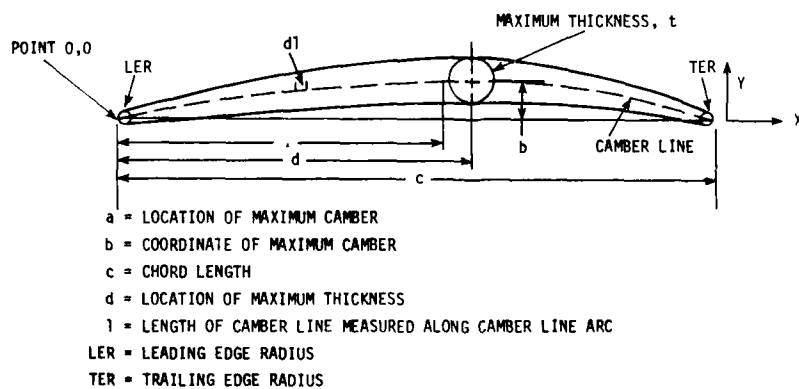


Fig. 4. Typical blade section profile terminology.

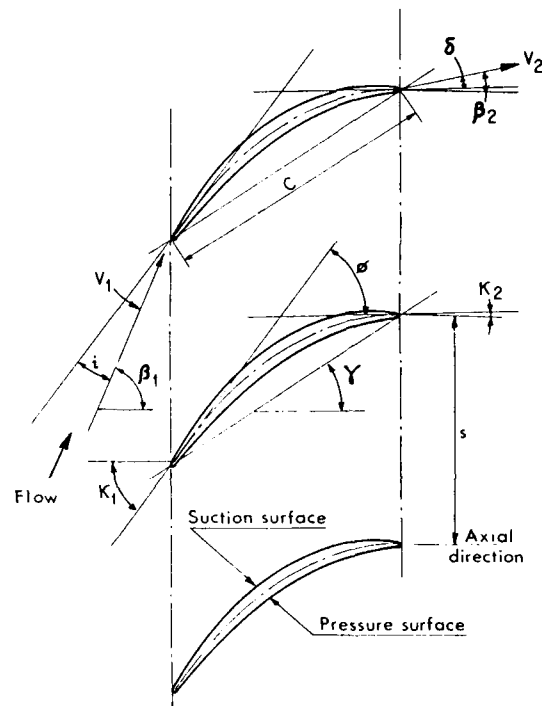


Fig. 5. Typical linear cascade terminology.

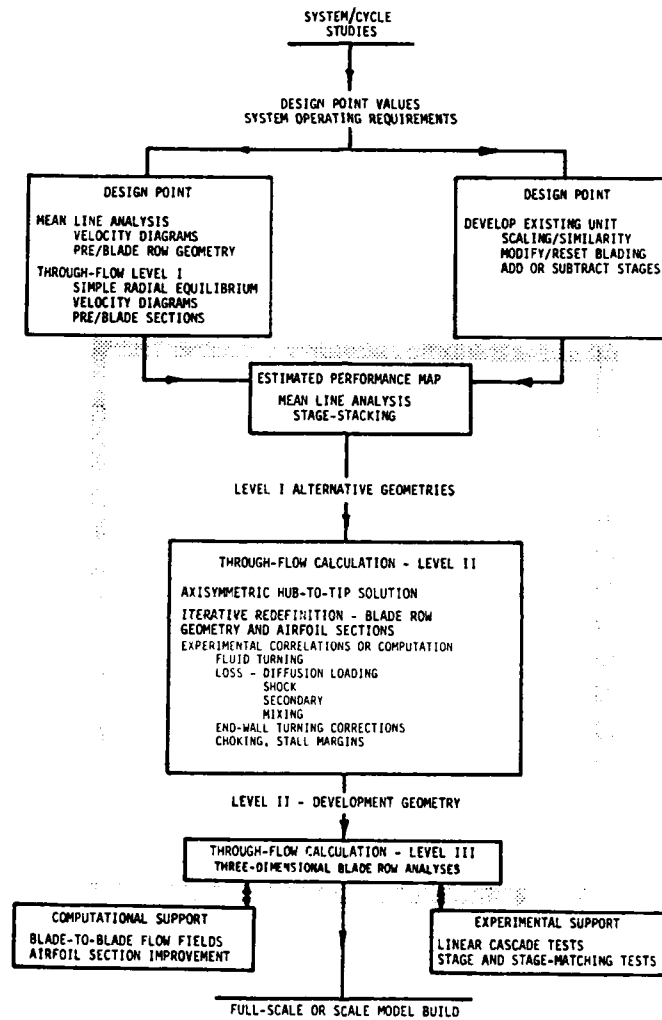


Fig. 6. Structure of a design system for axial-flow turbomachines.

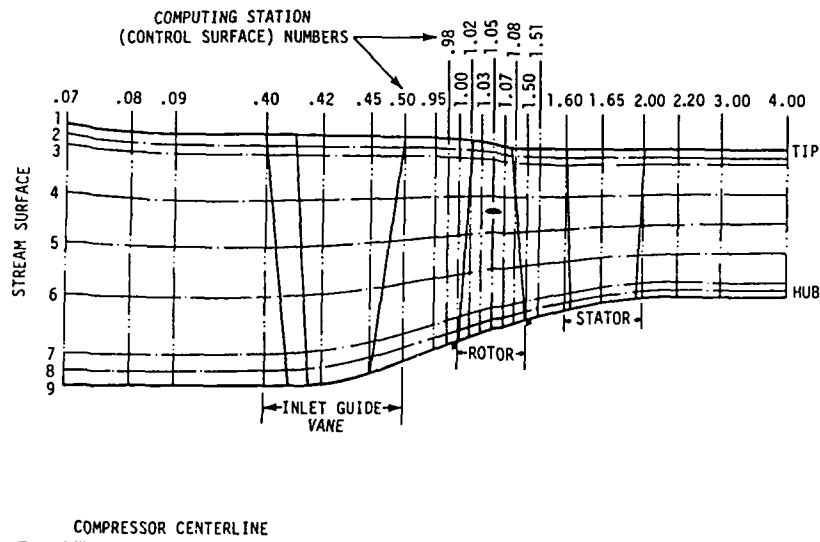


Fig. 7. Hub-to-tip computation results for a quasi-three-dimensional design/analysis method showing typical computing stations.

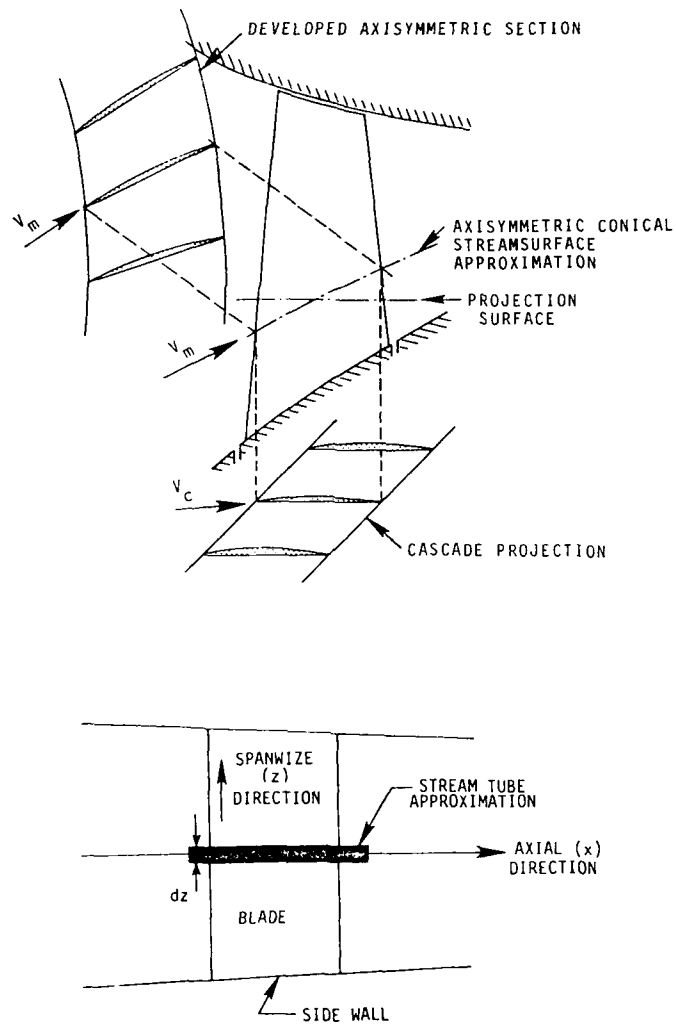


Fig. 8. Definition of the linear cascade projection for a computed stream surface approximation (from Starken-DFVLR).

```

graph TD
    1[1 INITIAL CONDITIONS  
STAGNATION POINT  
OR WEDGE FLOW] --> 2[2 LAMINAR LAYER  
DEVELOPMENT]
    2 --> 4a{4a TRANSITION}
    4a -- NO --> 2
    4a -- YES --> 4c[4c INITIAL CONDITIONS  
TURBULENT LAYER]
    2 --> 3a{3a SEPARATION}
    3a -- YES --> 3b[3b SEPARATION BUBBLE  
LAMINAR-TURBULENT  
FREE-SHEAR LAYER  
GROWTH]
    3a -- NO --> 4c
    3b --> 4b{4b RE-ATTACHMENT}
    4b --> 4c
    4b --> 7[7 TURBULENT  
SEPARATED AND BASE FLOW]
    4c --> 5[5 TURBULENT LAYER  
DEVELOPMENT]
    5 --> 6{6 SEPARATION}
    6 -- YES --> 7
    6 -- NO --> 5b{5b RELAMINARIZATION}
    5b -- YES --> 4c
    5b -- NO --> 5
    5 --> 7
    5 --> 8[8 TURBULENT  
WAKE]
    7 --> 8
    7 --> END_OF_BODY[END OF BODY]
    8 --> END_OF_BODY
    8 --> FINE_TRAILING_EDGE[FINE TRAILING  
EDGE]
    FINE_TRAILING_EDGE --> 8
    
```

Fig. 10. Course of the boundary layer (from J. M. Robertson).

BLADING DESIGN FOR MULTI-STAGE HP COMPRESSORS

Professor P. Stow
 Chief of Theoretical Science
 Rolls-Royce plc
 P.O. Box 31
 Derby
 DE2 8BJ
 UK

Summary

In this paper the subject of computer aided turbomachinery blade design is discussed with the emphasis on the mathematical models that are needed in order to account for the important physical phenomena. The various aspects of a typical blade design system are presented covering through-flow and blade-to-blade analysis.

The through-flow discussion covers aspects such as linked through-flow-blade-to-blade analysis, blade loss models, end-wall boundary layers, secondary flow analysis and spanwise mixing models.

Blade section design using mixed design and analysis methods is covered together with loss prediction using coupled inviscid boundary layer approaches. Limitations of the coupled approach are discussed together with the emerging role of Reynolds averaged Navier-Stokes methods aimed at removing these limitations.

The need for fully three-dimensional methods is covered together with their incorporation into the design system.

Finally areas for future development and application are discussed.

1.0 Introduction

Turbomachinery blading components are designed with the aid of theoretical methods and computer programs. If one is to have confidence in achieving design targets in practise using these methods then it is essential that the mathematical model employed adequately describes the physical processes involved. However, the flow in a turbomachine is very complex. There are rotating and non-rotating components. The blade geometries are three-dimensional with the sectional geometry and blade stagger varying from hub to tip. There are boundary layers on the annulus walls and blade surfaces, wakes from the trailing edges of the blades, over-tip leakage flows etc. Consequently the flow is unsteady, three-dimensional and has regions where viscous effects are important. The solution of the full equations of motion with the full boundary conditions represents a formidable task from both a computational and modelling point of view. As a consequence approximate models of the flow are adopted.

Many blade design systems are based on the work of Wu (1952) using quasi-3D through-flow and blade-to-blade programs, see Fig. 1. In this approach sections of a blade are designed on isolated axisymmetric stream-surfaces using a blade-to-blade program with information from a through-flow program being used to define the geometry of the stream-surfaces and the stream-tube height variation as well as to provide the inlet and outlet flow conditions to be achieved. The different types of blade-to-blade methods available will be discussed later together with models for loss analysis. Once the blade sections have been designed they are stacked radially and circumferentially to produce a three-dimensional blade geometry taking into account aerodynamic or mechanical constraints.

With such a design system and the models adopted there are a number of phenomena that cannot be accounted for, for example stream-surface twisting, the three-dimensional nature of the blade surface boundary layers, blade-annulus boundary layer interaction, blade over-tip leakage flows etc. In some cases valuable information about the effects of features such as the annulus geometry and blade lean can be assessed early in the design process using linked through-flow and blade-to-blade methods and this will be discussed later. However, many of the flow features can only be analysed adequately using fully three-dimensional methods; how such methods are linked to the traditional design system will be covered later.

Additional features not accounted for in the traditional blade design system are associated with the unsteady nature of the flow e.g. the effects of incoming wakes, blade row interaction from upstream and downstream blade rows etc. These effects can be important with regard to blade performance and blade row stability and the development of models to include the main features will be discussed in later sections.

2.0 Through-Flow Analysis

In the through-flow calculation the flow through a number of stages is considered. The flow is taken as steady in an absolute coordinate system for a non-rotating components and in a relative coordinate system for a rotating component. As a consequence the detailed effects of blade wakes and unsteadiness are ignored. The three-dimensional equations of motion are usually reduced to a two-dimensional form either by assuming fully axisymmetric flow or by adopting a passage-averaging (or mean stream-sheet approach). In the former only calculations outside the blade rows are performed and assumptions need to be made as to how stream-surface properties needed in a blade-to-blade calculation vary through the blade row. In the passage-averaging technique the equations within the blade row are integrated in the circumferential direction to produce equations for averaged quantities; in this way the effects of the blade, in terms of blockage, stack and boundary layer losses, on the through-flow can be accounted for.

For steady flow in a relative co-ordinate system the three-dimensional momentum equations are

$$\underline{\tilde{W}} \cdot \nabla \underline{\tilde{W}} + 2\Omega \underline{\tilde{A}} \underline{\tilde{W}} - \Omega^2 \underline{\tilde{R}} = -\frac{1}{\rho} \nabla p + \underline{\tilde{F}}_t \quad (1)$$

where $\underline{\tilde{W}}$ is the relative velocity vector and Ω is the blade speed and $\underline{\tilde{F}}_t$ is a dissipative force introduced to simulate losses through the blade row. The passage averaged form of the equation is

$$\tilde{W}_x \frac{\partial \tilde{W}_x}{\partial x} + \tilde{W}_R \frac{\partial \tilde{W}_x}{\partial R} = -\frac{1}{\rho} \frac{\partial \tilde{P}}{\partial x} + \tilde{F}_{B_x} + \tilde{F}_{t_x} - P_x \quad (2)$$

$$\tilde{W}_x \frac{\partial \tilde{W}_R}{\partial x} + \tilde{W}_R \frac{\partial \tilde{W}_R}{\partial R} - \frac{1}{R} (\tilde{W}_\theta + \Omega R)^2 = -\frac{1}{\rho} \frac{\partial \tilde{P}}{\partial R} + \tilde{F}_{B_R} + \tilde{F}_{t_R} - P_R \quad (3)$$

and

$$\tilde{W}_x \frac{\partial \tilde{W}_\theta}{\partial x} + \tilde{W}_R \frac{\partial \tilde{W}_\theta}{\partial R} + \frac{\tilde{W}_R}{R} (\tilde{W}_\theta + 2\Omega R) = \tilde{F}_{B_\theta} + \tilde{F}_{t_\theta} - P_\theta \quad (4)$$

where "-" denotes a passage averaged value and "~" denotes a density weighted passage average: \tilde{F}_B is the blade force and P involves averages of product of perturbations from the means, see Jennions and Stow (1984) for more details.

The continuity equation is

$$\nabla \cdot \rho \underline{\tilde{W}} = 0 \quad (5)$$

which after passage averaging becomes

$$\frac{\partial}{\partial x} (B \rho \tilde{W}_x) + \frac{\partial}{\partial R} (B \rho \tilde{W}_R) = 0 \quad (6)$$

where

$$B = 2\pi - \frac{Nt}{R} \quad (7)$$

where N is the number of blades and t is the blade thickness.

The above equations (2), (3), (4) and (6) together with an energy equation can be solved using a number of techniques e.g. streamline curvature, matrix through-flow, time-marching or finite elements.

Figure 2 illustrates the information flow in such a quasi-3D through-flow system, see Jennions and Stow (1984) and also Hirsch and Warzee (1978) for more details.

The stream-tube height and streamline radius variations through a blade row are affected by the blade geometry, i.e. blockage, turning and stack, as well as the annulus shape and consequently account needs to be taken of these. In the early stages of a design the effects are often included in an approximate manner with the system depicted in Figure 2 being used in the later stages once blade profiles exist. Fig. 3.1 shows results from the quasi-3D system developed by Jennions and Stow (1985) for the high pressure turbine nozzle guide vane shown in Fig. 3.2. It can be seen that good agreement exists with the experimental data. The linked analysis was inviscid with no account being taken of losses in either the through-flow or the blade-to-blade calculation. Further results from the system are shown in Jennions and Stow (1984) for a different stack of the blade sections in Fig. 3.2. It should be mentioned that the secondary flow deviations, i.e. the flow over-turning and under-turning associated with passage vortices, are not predicted with such a coupled system unless some specific account is taken of the secondary flow; this will be discussed later.

The coupled analysis discussed by Jennions and Stow has been extended to include various blade-to-blade programs available so that analysis of fans and subsonic and transonic compressors and turbines is possible. The fan analysis system follows closely that developed by Calvert and Ginder (1985) in which blade profile, mixing and secondary losses are included.

In order to provide an adequate description of the real flow it is necessary to supplement the above analysis using a number of models; these are discussed below.

2.1 Blade Loss Model

One commonly adopted procedure for accounting for viscous losses through a blade row is to include a dissipative force $\underline{\tilde{F}}_t$ in the equations of motion, as in equations (1), and relate this to entropy production.

It can be shown that

$$\underline{\tilde{W}} \cdot \nabla S = \underline{\tilde{W}} \cdot \nabla I - \underline{\tilde{W}} \cdot \underline{\tilde{F}}_t \quad (8)$$

where I is the rothalpy defined by

$$I = C_p t + \frac{1}{2} \tilde{W}^2 - \frac{1}{2} \Omega^2 R^2$$

t being the static temperature. For adiabatic flow the energy equation is taken as

$$\underline{W} \cdot \nabla T = 0 \quad (9)$$

so that

$$\underline{W} \cdot \underline{F}_T = -t \underline{W} \cdot \nabla S$$

If in addition the dissipative force is taken to act in the streamline direction i.e.

$$\underline{F}_T = F_T \underline{s} \quad (10)$$

then it follows that

$$F_T = -t \frac{\partial S}{\partial s}$$

Assuming that perturbation terms are negligible this gives

$$\underline{F}_T = -t \frac{\partial \tilde{S}}{\partial s} \quad (11)$$

from which the three components can be found for use in equations (2), (3) and (4).

The distribution of entropy through a blade can be obtained from a blade-to-blade analysis. Alternatives are to use loss correlations or to use experimental data in the form of loss-incidence curves for particular blade designs.

An alternative procedure for modelling the effects of the blade losses is to use the blade surface boundary layer displacement thicknesses in the form of a blockage in the through-flow calculation. For example, equation (7) becomes

$$B = 2\pi - N \frac{1}{R} (t + \delta_s^* + \delta_p^*) \quad (12)$$

where δ_s^* and δ_p^* are the suction and pressure surface displacement thicknesses. In this way the effect of the wake development downstream of the blade trailing edge can be accounted for. Note, however, that it will have to be assumed that the flow is circumferentially uniform by the leading edge of the following blade row.

Even with the blade boundary layer blockage model it is usual to account for any additional end-wall or secondary flow losses using the dissipative force model, see Calvert and Ginder (1985).

2.2 End-wall Boundary Layer

The usual manner in which the effects of the end-wall boundary layers are included is to calculate the boundary layer development using an integral method and represent the effects using a displacement model. In this the annulus is altered by the displacement thickness of the boundary layer and the inviscid flow calculated within the modified geometry.

The governing passage-averaged equations can be derived in a manner similar to that in Section 2.1. The boundary layer equations are first written in terms of a local meridional streamline co-ordinate system with the usual boundary layer assumptions that only gradients normal to the meridional direction are retained in the viscous terms. The equations can then be passage averaged by integrating from one blade to the next (skin friction effects on the blade surfaces being ignored). For example the momentum integral equations become

$$\frac{1}{BR_b} \frac{d}{dm} [BR_b \rho_e Q_e^2 \theta_{mm}] + \rho_e Q_e \delta_m^* \frac{dq_{me}}{dm} - \rho_e \frac{\sin \lambda_b}{R_b} (Q_e^2 \theta_{\theta\theta} + q_{\theta e} Q_e \delta_\theta^*) = F_m + (\tau_m)_w + P_m \quad (13)$$

$$\frac{1}{BR_b} \frac{d}{dm} [BR_b \rho_e Q_e^2 \theta_{\theta m}] + \rho_e Q_e \delta_m^* \frac{dW_{\theta e}}{dm} + \rho_e \frac{\sin \lambda_b}{R_b} Q_e (Q_e \theta_{m\theta} + q_{m\theta} \delta_\theta^*) = F_\theta + (\tau_\theta)_w + P_\theta \quad (14)$$

where m is the meridional co-ordinate see Fig. 4 R_b is the radius of the annulus, B is given by equation (7), F_m and F_θ are the components of the blade force defect and represent integrals through the boundary layer of differences of the blade force from the value at the edge of the boundary layer; τ_w is the wall shear stress, P_m and P_θ represent perturbation terms, Q is the absolute velocity given by

$$Q^2 = q_m^2 + q_\theta^2$$

W is the relative velocity and the subscript e denotes quantities at the edge of the boundary layer; it should be noted that the "-" notation has been dropped in the above equation. Appendix A gives the definitions of the momentum and displacement thicknesses.

The entrainment equation becomes

$$\frac{d}{dm} [BR_b \rho_e (q_{m_e} \delta - Q_e \delta^*)] = BR_b \rho_e Q_e C_E \quad (15)$$

It can be seen that in cases where the effects of the hade angle λ can be ignored the two momentum integral equations become uncoupled. If in addition the effects of averages of products of perturbations are ignored i.e. $F_m = 0 = F_Q$, and the blade force is taken as constant through the boundary layer i.e. $F_m = 0 = F_Q$, then particularly simple forms result. For example equation (13) becomes

$$\frac{1}{B} \frac{d}{dm} [B \rho_e Q_e^* \theta_{mm}] + \rho_e Q_e \delta^* \frac{dq_{m_e}}{dm} = (\tau_m)_w \quad (16)$$

see March and Horlock (1972). This equation can be solved together with the entrainment equation (15) assuming the usual two-dimensional boundary layer correlations to apply in the streamwise direction.

More sophisticated treatments including the effects of the blade force defect and cross-flows in the boundary layers are given for example by De Ruyck and Hirsch (1980) and De Ruyck, Hirsch and Kool (1979); see also Le Boeuf (1984).

2.3 Mixing Models

The effects of the mixing of various leakage flows, e.g. disc leakage, over-tip leakage, and of various ejected cooling flows needs to be taken into account in the through-flow analysis. As well as being a source of loss they can also affect the distribution of flow quantities, e.g. total temperature, pressure, whirl velocity, which are obviously important in determining the inlet flow conditions for the following blade row.

One approximate manner of accounting for the effects is to perform a simple mixing calculation, for example one-dimensional mixing in stream-tubes assuming the ejected flow, in terms of mass, momentum and energy, to be distributed radially between the stream-tubes. So for example the distribution of ejected mass flow may be taken as

$$m(R) = M_C \cdot f(R)$$

where M_C is the total mass flow ejected, $f(R)$ being a chosen distribution function with the constraint that

$$2\pi \int_{R_{hub}}^{R_{tip}} R \cdot f(R) dR = 1$$

The distribution function may be chosen using experimental information or using a more sophisticated viscous calculation to analyse the configuration. In theory the model can also account for axial mixing effects by making f a function of axial distance.

An alternative model to account for the effects of over-tip leakage is given by Adkins and Smith (1981). In the case of an unshrouded blade they calculate secondary flow vorticity based on the model of Lakshminarayan and Horlock (1965) and use this in a secondary flow calculations to determine secondary flow velocities, see later.

2.4 Secondary Flow Model

A quasi-three-dimensional blade design system assumes that stream-surfaces through a blade row are axisymmetric. In addition in calculating blade profile losses it is assumed that the boundary layer develops on the blade surface in a two-dimensional manner i.e. cross-flows in the boundary layer are ignored. In practice the stream-surfaces twist as they pass through the blade row so that there is flow through the blade-to-blade surfaces used, also boundary layers will be three-dimensional in nature. In addition the annulus end-wall boundary layer will separate near the blade leading edge to produce a horse-shoe vortex. The pressure side leg of this vortex tends to move across the passage and interact with the suction side leg; the blade surface boundary layers are also affected by the end-wall interaction, the extent being determined by the aspect ratio of the blade.

Secondary flow is a term often used to encompass all the three-dimensional effects mentioned which are not included in a quasi-three-dimensional approach. These effects give rise to additional or secondary losses as well as affecting the distribution of parameters such as total pressure, whirl angle etc., at exit to the blade row.

Secondary losses are usually accounted for in the through-flow analysis using a dissipative force model together with correlations or experimental experience. One simple way of attempting to account for the effects on the mean passage whirl angle is to use a distributed deviation on the predicted blade-to-blade flow. An alternative is to use inviscid secondary flow theory, see for example Lakshminarayan and Horlock (1973), Came and Marsh (1974) and Smith (1974). In this the quasi-three-dimensional through-flow is taken as the primary flow to convect inlet vorticity in the end-wall boundary layers giving rise to streamwise vorticity at the exit to the blade row; the effects of the secondary flow on the primary flow are assumed small. For example with the Came and Marsh theory the streamwise vorticity ξ_{sec} at exit to a blade row is given by

$$\xi_{sec} = \xi_{s1} \frac{\cos \alpha_1}{\cos \alpha_2} + \frac{\xi_{n1}}{\cos \alpha_1 \cdot \cos \alpha_2} [\alpha_2 - \alpha_1 + \frac{1}{2}(\sin 2\alpha_2 - \sin 2\alpha_1)] \quad (17)$$

where ζ_{n1} and ζ_{n1} are the inlet streamwise and normal vorticities and α_1 and α_2 are the inlet and exit whirl angles. It should be noted that the above model is derived for incompressible flow in a linear cascade, where the primary flow is irrotational, but can be extended, as can that of Smith, to include the effects of compressibility, radius change and blade rotation, see James (1981).

Once the distribution of exit streamwise vorticity is known the secondary flow velocities can be determined by solving the continuity equation in terms of a secondary flow stream-function. For example for incompressible flow the stream-function ψ satisfies

$$\frac{\partial^2 \psi}{\partial n^2} + \frac{\partial^2 \psi}{\partial z^2} = \zeta_{\text{sec}} \quad (18)$$

see Fig. 5 for the co-ordinate system and Appendix B for details of the analysis.

The results produced from inviscid secondary flow models are very dependent on the inlet conditions assumed, especially the inlet streamwise vorticity. This is particularly important when considering stage calculations as illustrated by the following example. The case considered is a compressor stage described by Freeman and Dawson (1983) consisting of an inlet guide vane, rotor and stator all double circular arc blades. Fig. 6 shows results for the inlet guide vane from James (1982) using a method based on that of Came and Marsh. It can be seen that the radial distribution of the pitchwise mass averaged whirl angle is well predicted. In this case the inlet boundary layer was taken as collateral. We consider now predictions for the stator. It can be seen from Fig. 7 that even for the case of a collateral hub boundary layer out of the upstream rotor the absolute inlet velocity will exhibit skew because of the change from a rotating to a stationary hub. This gives rise to streamwise vorticity at inlet to the stator; the effects of secondary flow in the upstream rotor will add to this effect. If the streamwise vorticity is included in the analysis, as in equation (17), then it can be seen from Fig. 8 that poor predictions result near the hub and tip where considerable underturning is predicted and the sense of the inlet skew is maintained. The reason for this is the effects of viscosity. Considering again Fig. 7 it can be seen that since the velocity on the stationary hub is zero then intense shearing will take place in the region near to the hub which will tend to unskew the inlet boundary layer reducing the streamwise vorticity. Even if the skew is maintained up to the leading edge the process will continue through the blade row assisted in the case of a compressor rotor by the blade force. Fig. 8 shows results from the calculation where the inlet streamwise vorticity is suppressed. It can be seen that the trend is now improved even though the level is wrong in the middle of the stator (it is felt that this is caused either by errors in the experimental measurements or deviation that is not taken into account in the analysis). Also shown in Fig. 8 are results assuming that the inlet boundary layer is collateral in the stator frame, the inlet skew being completely destroyed by viscosity. Again even though the overturning is exaggerated and the mid-passage level is incorrect the trends are encouraging. The results shown and the mechanisms described above have been substantiated by Birch (1984) using a three-dimensional viscous program for this example. The conclusion is that care must be exercised in using inviscid secondary flow theory for stage calculations. In fact this is true for any inviscid calculation where the effects of an inlet boundary layer are being simulated.

It is interesting to note that in the case of a turbine nozzle or rotor the effect of viscosity is again to tend to destroy the inlet skew from an upstream blade row but now the effect of the blade force is opposite to that of the compressor stator or rotor and tends to increase the skew. It is found that the latter effect tends to dominate and as a consequence good predictions can be obtained using an inviscid program, see for example the work of Boletis, Sieverding and Van Hove (1983) and Birch (1983) using three-dimensional programs. It should be mentioned that for a turbine the effects of the secondary flow on the "primary" flow can be large and that because these are ignored in an inviscid secondary flow analysis the results must be used with care (these effects are obviously included in a full three-dimensional analysis).

The above discussion has concentrated on the analysis of blades. It is however, possible to use the approach in a design sense to calculate blade angles in the end-wall regions to reduce the effects of boundary layer over-turning. As discussed earlier care is needed in applying such an analysis to the flow in a blade stage where the effects of viscosity between the blades becomes important in determining the inlet vorticity to each blade row.

2.5 Spanwise Mixing Model

A spanwise mixing model is aimed at accounting for two effects,

- (i) turbulent diffusion in the radial direction not accounted for in a blade-to-blade analysis,
- (ii) an inviscid secondary flow effect arising from the fact that in general there will be a component of velocity normal to the axisymmetric blade-to-blade surfaces used in the design of the blade sections.

Consider firstly the second effect mentioned above. It can be shown that the passage averaged energy equation may be written as

$$\psi_m \frac{\partial f}{\partial m} = - \frac{1}{BRP} \frac{\partial}{\partial R} \left[\frac{BR}{\cos \lambda} \rho V_k I \right] \quad (19)$$

where m is the meridional direction along the axisymmetric blade-to-blade surface see Fig. 4 and V_k is the velocity normal to this surface. In the usual quasi-three-dimensional design system the blade-to-blade surface is assumed to be a streamsurface and V_k is taken as zero, leading to the familiar energy equation.

In a similar manner it can be shown that the passage-averaged circumferential momentum equation becomes

$$\frac{w}{R} \frac{\partial}{\partial m} (R \dot{q}_\theta) = - \frac{1}{BR^2} \frac{\partial}{\partial R} \left[\frac{BR}{\cos \lambda} \rho V_L R \dot{q}_\theta \right] - F_{B\theta} + \bar{F}_{T\theta} \quad (20)$$

It would be possible to determine V_L using an inviscid secondary flow analysis but it should be noted that the distribution through a blade row is needed, at least in theory. An alternative approach is given by James (1982) where it is shown that equation (19) may be written as

$$\frac{w}{m} \frac{\partial \dot{q}}{\partial m} = \frac{1}{BR} \frac{\partial}{\partial R} \left[BR \bar{\rho} \epsilon \frac{\partial \dot{q}}{\partial R} \right] \quad (21)$$

where ϵ is related to the velocity normal to the blade-to-blade surface, being determined by the secondary flow through the blade row.

It is possible to include the effects of turbulent diffusion in the above model by considering ϵ to be an effective diffusion coefficient. In order to determine this using experimental data a more appropriate form is

$$\frac{\partial \dot{q}}{\partial m} = \epsilon^* \frac{\partial^2 \dot{q}}{\partial R^2} \quad (22)$$

Adkins and Smith (1981) derive equation (22) using a Taylor expansion analysis based effectively on tracing streamlines through the blade row taking into account secondary flow. They use diffusion equations for total temperature, total pressure and $R\dot{q}_\theta$, determining the mixing coefficients empirically to account also for the effects of viscosity on the secondary flow and interaction with downstream blade rows. They show that the model has a significant effect on predictions.

An alternative approach is due to Gallimore (1986a, 1986b). Suppose in equation (1) we express the viscous force \bar{F}_T as

$$\bar{F}_T = \bar{F}_T^{(1)} + \bar{F}_T^{(2)}$$

where with an effective turbulent viscosity model $\bar{F}_T^{(1)}$ is composed of derivatives in a stream-surface and $\bar{F}_T^{(2)}$ of derivatives normal to the stream-surface. We suppose that $\bar{F}_T^{(1)}$ can be determined either from a blade-to-blade calculation, as indicated earlier, or from a prescribed loss model for example using cascade loss correlations e.g.

$$\bar{F}_T^{(1)} = -t \frac{\partial S^{(1)}}{\partial S} \frac{\partial}{\partial R} \quad (23)$$

where $S^{(1)}$ is a prescribed entropy distribution. The second part of the viscous force $\bar{F}_T^{(2)}$ is expressed in terms of derivatives of velocity components, which for small λ involves components in a stream-surface.

Rothalpy is given by

$$I = I^{(1)} + I^{(2)} \quad (24)$$

where, consistent with equation (23),

$$w \cdot \nabla I^{(1)} = 0 \quad (25)$$

and where, for small λ $I^{(2)}$ satisfies

$$\rho \bar{w} \cdot \nabla I^{(2)} = \frac{1}{R} \frac{\partial}{\partial R} \left(k_e \frac{\partial I}{\partial R} \right) + \frac{1}{R} \frac{\partial}{\partial R} \left[R \mu_e \left(w_x \frac{\partial w_x}{\partial R} + w_\theta \left(\frac{\partial w_\theta}{\partial R} - \frac{w_\theta}{R} \right) \right) \right] \quad (26)$$

where, k_e and μ_e represent effective turbulent conductivity and viscosity respectively. Passage averaging has been dropped for the purposes of clarity.

Entropy is given by

$$S = S^{(1)} + S^{(2)} \quad (27)$$

where $S^{(1)}$ is prescribed and $S^{(2)}$ can be determined from

$$t \bar{w} \cdot \nabla S^{(2)} = \bar{w} \cdot \nabla I - \bar{w} \cdot \bar{F}^{(2)} \quad (28)$$

The similarity of equations (26) and (22) can be seen if we take an effective Prandtl number of unity.

The importance of including spanwise mixing effects in a through-flow calculation can be seen in Fig. 9 taken from Gallimore (1986a). Calculations have been performed for two 3-stage research compressors differing only in aspect ratio; 3S1 had an aspect ratio of 0.81 while 3S2 had an aspect ratio of 1.22. Design loss coefficients and flow angles were used together with measured inlet flow profiles. Exit total temperature predictions with and without spanwise mixing are shown. It can be seen that results using the spanwise mixing model agree closely with experiment while those without mixing show a totally misleading total temperature distribution.

3. Quasi-3D Blade-to-Blade Analysis

In the design process a through-flow analysis gives the necessary inlet and outlet flow conditions for each section of each blade row in order to achieve parameters such as stage or blade pressure ratio or work output. This means that the desired lift of each blade section is known. The design freedom lies with the lift distribution from blade leading to trailing edges which in turn determines the characteristics of the blade surface boundary layers and the efficiency of the blade. It is important therefore that a designer has methods that enable him to determine the boundary layer characteristics and that allow him to quickly analyse the effects of changes to his design variables.

3.1 Inviscid Analysis

Inviscid blade-to-blade methods generally fall into two categories, design and analysis. With the former the desired blade surface velocity is prescribed and the method produces the blade geometry. With the latter the blade geometry is prescribed and the method produces the blade surface velocity distribution. A design method in many ways offers advantages from a pure aerodynamics point of view, where desirable boundary layer development can be reflected in the velocity prescribed, whereas an analysis method is often needed in order to satisfy mechanical or blade cooling constraints. A method with compatible mixed design and analysis modes combines the best features of both and offers considerable advantages for practical design. Such a method based on a finite element full velocity potential analysis is described by Cedar and Stow (1985). In this the geometry can be prescribed over part of the blade, in which case the method produces the surface velocity, and the velocity can be prescribed over the remainder, the method producing the geometry. In the basic analysis mode the system of non-linear equations arising from the finite element method is solved using a Newton-Raphson procedure which ensures rapid convergence. Simple three node triangular elements are adopted which means that the areas integrals involved and the Jacobian matrix in the Newton-Raphson procedure can be calculated analytically.

In the design mode, changes to the blade shape are modelled using a surface transpiration technique which avoids mesh re-construction each time the geometry changes in the iterative design procedure. The transpiration mass flux is related to changes in the blade geometry in the same manner that a transpiration boundary layer is modelled. This is easily included in the finite element method through the boundary conditions. The surface transpiration mass flux is in turn related to desired changes in the blade surface velocity using what is called an influence matrix; this is determined efficiently using a slight adaptation of the Newton-Raphson procedure. The iterative solution is fast to converge giving rise to a very versatile interactive design tool.

The way of using such a method is to start with an analysis of an initial blade geometry. Loss producing features can be identified using a coupled boundary layer analysis. A velocity distribution can then be prescribed, over part of the blade, aimed at improving boundary layer development and the blade geometry determined. Fig. 10 from Cedar and Stow shows how the method has been used to remove a shock wave identified from an analysis of a blade whilst maintaining the same lift. Fig. 10.1 gives the surface Mach number distribution for the original blade; it also shows the desired design distribution which has been changed only over part of the suction surface. Fig. 10.2 shows the original and resulting blade shapes. It can be imagined that to achieve this result using only an analysis type of approach would have been difficult and time consuming.

A further application is shown in Fig. 11 to remove a Mach number over-speed around the leading edge of a blade in order to improve the boundary layer behaviour at design and off-design conditions.

Similar mixed design and analysis modes can be added to other blade-to-blade methods, e.g. streamline curvature, time-marching etc.

3.2 Boundary Layer Analysis

Some of the main physical features that need to be described by a boundary layer method are as follows,

- (i) Laminar flow
- (ii) Laminar separation and reattachment
- (iii) Start and end of transition
- (iv) Turbulent flow
- (v) Turbulent separation
- (vi) Re-laminarization

Boundary layer methods fall into two main categories, integral and finite difference approaches. In the former, boundary layer parameters like momentum thickness θ and displacement thickness δ^* are determined from ordinary differential equations formed by integrating the boundary layer equations through the boundary layer. For example in the case of two-dimensional flow the momentum integral equation takes the form

$$\frac{d}{ds} [(\rho u^2)_{\delta} \theta] = \tau_w - (\rho u)_{\delta} \delta^* \frac{du_{\delta}}{ds}$$

where s is the distance along the blade surface, τ_w is the skin friction and the subscript δ refers to conditions at the edge of the boundary layer.

The advantage with this approach is that the solution of the equations is fast and this means that combined with an inviscid method that is itself fast an interactive viscous-inviscid design program can be produced. The integral equations, however, need to be supplemented by correlations from experiment for quantities like skin-friction, form factor and features such as laminar separation and reattachment, the start and end of transition, and re-laminarization also need to be described in terms of correlations.

With finite difference approaches the boundary layer equations are solved numerically. For example the momentum equation for two-dimensional flow takes the form

$$\frac{\partial}{\partial s} (\rho u^2) + \frac{\partial}{\partial n} (\rho uv) = - \frac{\partial p}{\partial s} + \frac{\partial \tau}{\partial n}$$

where n is normal to the blade surface and u and v are the velocity components in the s and n directions and τ is the shear stress. As a consequence the solution time is longer than for integral methods, dependent largely on the accuracy of the procedures adopted. For turbulent flow the equations need to be supplemented with a turbulence model which will rely heavily on experimental data. Laminar separation usually involves adopting a "fix" of one sort or another in order to formally keep the method working but as the boundary layer equations breakdown locally in the region of separation the results need to be used with caution. With many methods correlations are still needed for determining the start and end of transition or re-laminarization. With methods adopting a turbulent kinetic energy equation then the means exist for trying to describe these phenomena using a differential equation; this will be discussed later.

3.3 Inviscid - Boundary Layer Coupling

There are three choices in deciding where to couple the solutions to the boundary layer and inviscid mainstream equations namely at the boundary layer edge, the edge of the boundary layer displacement thickness or the blade surface, see Murman and Bussing (1983) for details.

In the main the effect of the boundary layer on the inviscid mainstream calculations is represented either by a displacement effect or by transpiration. In the former the blade is thickened by the boundary layer displacement thickness and the inviscid flow calculated in the reduced passage area. This is equivalent to coupling at the edge of the displacement thickness. It is assumed in this model that changes in the mainstream variables between the edge of the displacement thickness and edge of the boundary layer are negligible. In the transpiration model transpiration through the blade surface of mass, momentum and energy is used to simulate the effects of the boundary layer on the mainstream; this is equivalent to coupling at the blade surface. It is assumed that changes in the mainstream quantities between the blade surface and edge of the boundary layer are negligible. In the case of two dimensional flow the transpiration velocity v_0 normal to the blade surface is given by

$$(\rho_0)_0 = \frac{d}{ds} [(\rho u)_\delta \delta^*]$$

It can be shown from considerations of conservation of momentum and energy that the transpiration streamwise velocity u_0 should be the local inviscid velocity i.e.

$$u_0 = u_\delta$$

and that the transpiration total enthalpy H_0 should also be the local inviscid value i.e.

$$H_0 = H_\delta$$

In practice only small differences will arise between the two main methods of coupling the equations and the choice is governed mainly by features or properties of the inviscid method. For example, in the case of a streamline curvature method a displacement model is used since the edge of the displacement thickness now becomes the new effective blade streamline. In a finite element approach where mesh generation is often quite expensive then a transpiration model is advisable, see Stow and Newman (1987). In time-marching methods, like that of Denton (1982), either approach can easily be used, see for example the work of Haller (1980) using a transpiration model and that of Calvert (1982) using a displacement model.

In addition to considering how to represent the effects of the boundary layer on the mainstream flow one needs to consider how the two calculations should be iteratively coupled. In some cases the effects of the boundary layer on the mainstream flow will be so small that useful boundary layer information can be obtained from a single call to a boundary layer routine after the inviscid calculation is converged. In general, however, the boundary layer will have an effect on the inviscid flow in terms of blockage, deviation etc. and the two calculations must be iteratively coupled together. The type of coupling is determined in the main by the magnitude of the boundary layer effect and different modes of coupling have been developed to cater for this.

3.3.1 Direct Mode Coupling

In this case the effects of the boundary layer on the inviscid mainstream are important but are still second order. The direct manner of coupling is illustrated in Fig. 12. In this case the boundary layer equations are used in the standard form. So for example the form of momentum integral equation used is

$$\frac{d}{ds} [(\rho u^2)_\delta \theta] = \tau_w - (\rho u)_\delta H_\theta \frac{du_\delta}{ds}$$

and the entrainment equation is

$$\frac{d}{ds} [(\rho u)_\delta H_\theta] = (\rho u)_\delta C_E$$

The input to the boundary layer calculation is the inviscid velocity at the "effective" edge of the boundary layer (where this is either the edge of the displacement thickness for a displacement model or the blade surface for a transpiration model); the input to the inviscid calculation is the boundary layer displacement thickness used to determine either a new effective blade surface or to calculate transpiration quantities.

Stow and Newman (1987) give details of the approach for the finite element method described in Cedar and Stow using an integral boundary layer method and surface transpiration model. The integral method adopted handles laminar and turbulent flow with transition correlations based on the work of Abu Ghannam and Shaw (1979) being used to predict the start and end transition and the starting conditions for turbulent flow. Laminar separation bubbles are handled using correlations due to Roberts (1980). The integral method is continued downstream of the trailing edge to calculate the wake development. A near wake "jump" model, due to Newman (1986), is adopted in order to calculate starting conditions for the wake calculation from those at the trailing edge. With this model the conservation equations are written in a jump form enabling the effects of the trailing edge base pressure to be incorporated.

Fig. 13 shows predictions for a low pressure turbine blade tested in cascade by Hodson (1984). Fig. 13.1 shows the mesh used with Fig. 13.2 indicating the good agreement of the predicted blade surface Mach number with experiment. Fig. 13.3 shows a comparison of the predicted and measured suction surface boundary layer momentum and displacement thickness, it can be seen that good agreement is found. In this example the leading edge velocity over-speed creates a laminar separation bubble with almost immediate relaminarisation after re-attachment and later natural transition towards the blade trailing edge.

It is found that in many cases the trailing edge base pressure can have an important influence on the predicted loss and should be included in any calculation. Fig. 14 shows the effect for typical turbine and compressor blades; the effect is much larger for the turbine blade because of the larger value of the blade trailing edge thickness to boundary layer momentum thickness. Currently the base pressure must be supplied by a designer or a correlation used.

3.3.2 Inverse Mode Coupling

Inverse mode coupling needs to be adopted in cases where the effects of the boundary layer on the inviscid calculation are not second order. If direct mode coupling were used in such cases then either the procedure would not converge or would require such heavy damping as to make convergence very slow. Often "fixes" have to be adopted (for example by putting an upper limit on the form factor) in order to avoid convergence problems; however, this means that the results are suspect and must be used with caution. Typical examples are cases where shock boundary layer interaction is important or where large turbulent separations occur. In such cases inverse mode coupling avoids the problems found with direct coupling. In general inverse coupling is needed only in certain areas of the flow where strong interactions occur, the direct mode of coupling being used elsewhere. There are a number of procedures that can be used but common to these is the use of an inverse boundary layer approach. Although inverse approaches in the main adopt integral boundary layer methods finite difference approaches can also be used, see for example Drela and Thompson (1983).

The input to the boundary layer routine is the boundary layer displacement thickness, the output being the velocity at the edge of the boundary layer to achieve this. For example the entrainment equation is used in the form

$$\frac{\partial}{\partial s} \frac{du_0}{ds} = \frac{1}{F_2} \left(\frac{d\delta^*}{ds} - F_1 \right)$$

together with the standard momentum integral equation

$$\frac{d}{ds} [(\rho u^3)_0 \theta] = \tau_w - (\rho u)_0 H \theta \frac{du_0}{ds}$$

and the usual correlations hold.

How this is used in the inviscid calculation depends on the details of the method and whether a design mode exists. In the case where such a mode does exist then full inverse coupling can be used. Calvert (1982) has developed such an approach based on the Denton inviscid time-marching method and an inverse integral boundary layer based on the lag-entrainment method of East, Smith and Merryman (1976).

Le Balleur (1983) has proposed a semi-inverse approach. This uses the direct mode of the inviscid calculation together with an inverse mode of the integral boundary layer in regions where separation is expected, the direct mode being adopted elsewhere. A semi-inverse mode of coupling has been developed for the finite element discussed earlier and is presented in Newman and Stow (1985). Fig. 15 shows the coupling procedure adopted and indicates that a correction technique must be applied to the displacement thickness to ensure that the velocity distributions from the inviscid and boundary layer calculations agree. The inviscid influence matrix, mentioned earlier in connection with the design mode, is used in this procedure. A similar boundary layer influence matrix can be determined numerically by perturbing the boundary layer equations and relating changes in velocity to those in displacement thickness. With the semi-inverse approach described rapid convergence is found and the resulting program can be used in a completely interactive manner. An alternative pointwise correction scheme due to Carter (1979) in which corrections are based on differences in the inviscid and boundary layer velocities has also been used successfully; however, convergence rates are heavily dependent on the relaxation factors used. Fig. 16 shows results for a compressor blade with a large suction surface diffusion; it can be seen that the predictions of the suction surface boundary layer parameters are in good agreement with experiment. The main limitations with such an approach lie not with problems in the coupling procedure but with limitations of the boundary layer method in handling flows with large turbulent separations. Evidence of this is apparent in the predictions shown in Fig. 16.3 where the rate of growth of the turbulent boundary layer is under predicted. A similar level of agreement is shown by Calvert (1982) using the same basic boundary layer method.

3.4 Reynolds Averaged Navier-Stokes Methods

The main reasons for interest in 2D flow in using a Reynolds averaged Navier-Stokes method are for the prediction of off-design losses, where laminar separation bubbles may occur near the leading edge and in some cases fairly extensive turbulent separation towards the trailing edge, and for the prediction of trailing edge base flow mixing losses. These are two areas where a coupled inviscid boundary layer approach has limitations.

Shortcomings in the prediction of the rate of growth of a turbulent boundary layer in a strong adverse pressure gradient have already been seen in Fig. 16.3. Shortcomings in the prediction of losses due to laminar separation bubbles can be seen in Fig. 17 showing loss against incidence for a controlled diffusion compressor blade shown in Fig. 18; details of the blade and test results are given in Sanger and Shreeve (1986). Shown in Fig. 17 are results from Walker (1987) using the finite element coupled boundary layer analysis discussed earlier. It can be seen that near design incidence a good prediction is produced but that this becomes progressively worse as the incidence increases both positively and negatively. The shortcomings are due to limitations in the correlations for laminar separation bubbles. With this blade, even at design conditions, leading edge separation bubbles exist on both surfaces. As the incidence increases positively the extent of laminar separation and associated losses increases on the suction surface with the pressure surface bubble disappearing. As the incidence increases negatively a similar situation occurs but this time on the pressure surface. With the correlations employed a burst separation bubble is predicted on at least one surface at all operating conditions. In the model employed immediate reattachment as a turbulent boundary layer is taken which means that transition is effectively anchored to the position of the leading edge velocity spike. As a consequence the losses associated with the bubble are not seen. It should be mentioned that in the case of a blade designed to avoid leading edge velocity spikes at design conditions, the limitations of the correlations would not occur until larger off-design incidences than seen in this example. Also shown in the figure are results from Ho (1988a) using a Navier-Stokes analysis which will be discussed later.

There are two main approaches being developed to solve the Reynolds averaged Navier-Stokes equations, pressure-correction techniques and time-marching techniques.

The pressure-correction method is based on the work of Caretto et al. (1972) and Patankar and Spalding (1972). With this technique an iterative linearization of the momentum and energy equations is adopted which effectively uncouples the equations and allows an implicit formulation to be adopted in order to determine the velocity components and total enthalpy; the pressure is determined from the continuity equation using abbreviated forms of the momentum equations. Turbomachinery applications of the method have been pursued by Hah (1983) and Moore and Moore (1984), especially for three-dimensional flow.

With the time-marching approach the unsteady form of the equations of motion are solved together usually with a steady form of the turbulence model. Both cell centred schemes, attributed to Jameson et al (1981), and cell node based scheme, attributed to Ni (1982) are under development; see Dawes (1986) and Norton et al (1984) for more details on the cell centred approach and Carrahar and Kingston (1986) and Davis et al (1980) on the cell node based approach. In addition various time-marching strategies for advancing the solution in time are available, for example a fully coupled implicit scheme in two-dimensions see Dawes and Norton et al, and explicit multi-step Runge-Kutta and two-step Ni-type Lax-Wendroff schemes in two and three-dimensions. With explicit methods the theoretical stability limit means that small time steps are needed in the viscous regions especially if fine grids are adopted. With implicit methods no such restriction exists and the time step can be chosen to achieve maximum convergence rate. In the approach implicit correction techniques are adopted to solve the fully coupled finite difference equations, very similar to a Newton-Raphson technique. Block matrix equations result from the basic formulation which can be fairly expensive to invert. Differential operator splitting techniques have been developed to some extent to reduce computational times, see for example Dawes (1984) and Chaussee and Pulliam (1981). In an attempt to improve convergence times of explicit schemes semi-implicit techniques have been developed where the basic uncoupled equations arising from the explicit approach are solved in an implicit manner; see for example Dawes (1986) where a pre-conditioning matrix is applied to each equation to improve coupling between corrections at grid nodes.

Grid systems with the various codes range from a simple H-grid to more elaborate embedded O-C-H grids, see Fig. 18, designed to give good spatial resolution around the leading and trailing edges of the blade.

Currently only relatively simple turbulence models are adopted, for example a Baldwin-Lomax or Cebeci-Smith mixing length model or one-equation kinetic energy-mixing length model, see for example Birch (1987). Transition is usually modelled using an intermittency function with various options for determining the region over which it is applied. One option is to specify the start and end of transition. An alternative is to predict the start and end using either a correlation, as discussed earlier in the integral boundary layer approach, or a kinetic energy model, see for example, Birch (1987) showing the relative performance of the two approaches for predicting turbine blade surface heat transfer.

The usual transition correlations account for the major effects of free stream turbulence and pressure gradient, and are reasonably adequate in determining natural transition. There are, however, shortcomings for large adverse pressure gradients and as one moves towards laminar separation promoted transition associated with off-design operation. Good results have been found using the kinetic energy model over a range of operating conditions. Fig. 17 shows results from Ho (1988a) using this model in an explicit cell centred time-marching scheme for the blade shown in Fig. 18; the grid system and number of points used can be seen from the figure. The result at near design incidence indicates that the model is probably slightly too sensitive to the small leading edge velocity spike that occurs. However it can be seen that it is able to predict the additional losses associated with the laminar separation bubble at off-design incidences reasonably well.

Further results from the code and model from Ho (1988) are given in Figs. 16.2 and 16.3 where it can be seen that there is closer agreement with experiment than with the coupled boundary layer approach.

Fig. 19 gives results for a case where the incidence has been increased. It can be seen that the model agrees quite well with experiment; the coupled boundary layer approach performs poorly in this case.

Transition and turbulence modelling are important in determining the quality of profile loss prediction i.e. loss up to the blade trailing edge. Modelling of the trailing edge base flow region is important in determining the quality of the overall loss including the base pressure and mixing effects. In many cases it is found that the flow in the trailing edge region is unsteady. Using a constant time-step in an implicit method discussed earlier it has been found that very realistic results can be produced in terms of the unsteady periodic flow structure around and downstream of the trailing edge and that the shedding frequency agrees closely with that expected, see for example Stow, Northall and Birch (1987). However this is a costly procedure to adopt especially in three-dimensional flow and especially with conditionally stable explicit time-marching methods. In addition it is the mean flow effects, loss etc., that are of main interest, at least at this stage. As a consequence mechanisms for producing the mean flow effects are being considered. It has been found that the unsteady nature of the trailing edge flow can be suppressed by adding smoothing or numerical viscous effects in that region. Care must be taken, however, so as not to generate significant spurious loss using such a technique. Fig. 20 from Connell (1985) shows predictions from an explicit cell centred time-marching code described by Norton et al for HP turbine blade tested in cascade by Nicholson et al (1982). About 7,000 points were used with the start and end of transition specified. It can be seen that there is good agreement in the overall mixed out loss. Also shown in the figure is the predicted profile loss indicating the importance of the trailing edge region, at least near sonic conditions, in determining the overall loss characteristics. It should be mentioned that a similar level of agreement is found using the coupled inviscid-boundary layer technique if the measured base pressure is input into the mixing loss calculation. The difference with the Navier-Stokes approach is that no such input data is required.

Further studies have been completed on the effects of trailing edge thickness on the overall loss indicating that the approach adopted agrees very well with the experimental findings in both magnitude and trends, see Fig. 21, from Stafford and Birch (1987).

It is clear from the developments and applications being undertaken that Reynolds averaged Navier-Stokes methods offer great promise in terms of loss and heat transfer prediction, understanding of flow phenomena and modelling opportunities. The methods are, however, much slower than current design methods adopting coupled techniques and consequently tend to be used more as research tools, at least in two-dimension, the situation being different in three-dimensional analysis. It is clear, however, that future developments in solution algorithms, convergence techniques and the application of super-computers will reduce elapsed time sufficiently to ensure more widespread application within design systems.

4. Three-Dimensional Analysis

As already discussed above, in the Quasi-3D design system blade sections are designed on isolated axisymmetrical stream-surfaces. In reality the stream-surfaces will twist under the influence of stream-wise vorticity, from upstream blade rows or created within the blade row, and the blade force etc.; this means that there will be flow through the surfaces used for designing. In addition, in the blade-to-blade boundary layer analysis adopted the effects of cross-flows normal to the stream-surface are assumed small and ignored; in some cases, however, they may be significant e.g. near the tips of rotors. A further complication comes from the blade-annulus interaction where the annulus boundary layer separates ahead of the blade to form a horse-shoe vortex which affects the development of the blade boundary layers through the blade passage. In order to account for these effects a three-dimensional analysis system is needed. Fig. 22 shows the elements of such a system and how it links to the conventional quasi-3D design system. Also indicated are the routes back into the conventional system to allow changes to the blade sections or to the blade stack after a three-dimensional analysis.

In general in a three-dimensional analysis one is interested in studying the effects of changes in design parameters, e.g. blade stack, annulus curvature, on the secondary flows and secondary losses of a blade row. However, very useful information can often be obtained using an inviscid analysis in which the effects of the annulus boundary layers are accounted for only at inlet to the blade row. In such an approach the inlet boundary layer is modelled by adopting an approximate inlet total pressure profile which gives rise to low momentum fluid but still has some slip velocity at the wall. The low momentum fluid is then acted on by the blade force within the blade row giving rise to secondary flows at the exit. The effects of numerical viscosity are to accelerate the inlet low momentum fluid and consequently these must be controlled by the using a refined grid near the end wall and avoidance of excessive smoothing. It is found that good predictions of secondary flow angles can result from the procedure at least for isolated blade rows.

Care is needed, however, in applying such a technique to stage calculations where the effect of each blade row is to produce a skewed inlet end-wall boundary layer to the following row. As discussed earlier the effects of viscosity are very important in determining the development of the inlet boundary layer. In a compressor the blade force and viscosity tend to have opposite effects on the skew in the boundary layer and large errors can arise in the prediction of the secondary flow using a purely inviscid analysis due to neglecting the action of viscosity on the skew. In turbines the blade force and viscosity tend to act in the same manner on the skew in the boundary layer and the effects of ignoring viscous action is less dramatic than in a compressor. Although some compensation for the effects of viscosity can be made in either case, the situation is unsatisfactory and indicates that a viscous analysis should be adopted.

The situation with regard to the development of methods for the solution of the Reynolds averaged Navier-Stokes equation in 3D is basically as described earlier in 2D, with pressure-correction and time-marching techniques being developed, with the 2D methods and developments leading naturally into 3D.

With the time-marching technique, as discussed earlier, cell centre based and cell node based schemes are being applied and further developed. In general explicit multi-step Runge-Kutta and two-step Lax Wendroff time-marching approaches are adopted with semi-implicit smoothing or coupling schemes being adopted in some cases in an attempt to improve convergence rates. With the pressure-correction technique two basic approaches are available a semi-elliptic space-marching technique, see for example Moore and Moore (1981), and a fully elliptic technique, see Moore and Moore (1985) and Hah (1983). The space-marching technique is ideally suited to flows where separation does not occur in the streamwise marching direction; separations in planes normal to this direction can be handled. This means that secondary flows found in ducts, exhausts etc. are well modelled with the technique. When applied to blade rows the effects of separations near the leading edge, due to the end-wall horse-shoe vortex, or reversed flows near blade trailing edges are handled only in an approximate manner; even so valuable information on secondary flows is still produced. In order to remove these limitations fully elliptic procedures have been developed capable of handling the flow separations that are found at the leading and trailing edges of blades and over the tip of rotating blades.

5. Future Developments

The work described above has tended to concentrate on areas where capabilities have been developed and have been evaluated. At this stage it would be useful to discuss briefly areas where further development is under-way or is needed in the future and to indicate the mathematical and numerical modelling problems to be addressed.

In 2D and 3D steady blade-to-blade flow analysis extensions to both turbulence and transition models adopted in Navier-Stokes methods are required in order to handle both attached and separated flows associated with design and off-design behaviour. For example any transition model needs to be able to handle natural transition, laminar separation promoted transition and transitional separation. It is contemplated that in addition to extending existing simple models, higher order turbulence models, i.e. algebraic and Reynolds stress models will be adopted; it will be important, however, to assess at each stage what advances are being made in relation to the additional computational costs of the higher order methods.

The work discussed so far has concentrated on steady flow analysis although unsteady analysis in connection with flutter and forced response, i.e. incoming wake excitation, is undertaken routinely; for example the full potential finite element program mentioned in Section 3 adopts a linearised unsteady analysis for flutter. Development of other methods and techniques described earlier is already underway aimed at both linearized and full non-linear analysis of the unsteady flow associated with flutter and blade row interaction. Single blade row analysis will be performed initially, with the inclusion of the wake from the upstream blade row, but eventually full stage interaction is envisaged. See for example Hodson (1974), Giles (1987, 1988), Rai (1987) and Rai and Madaran (1988). In considering unstalled flutter and forced response analysis, inviscid models are adequate, whereas for stalled flutter and blade row interaction effects on blade loss and heat transfer characteristics, viscous models are needed. With regard to the latter turbulence and transition models are needed to describe the major phenomena. Initially quasi-steady models are envisaged but later models capable of describing the unsteady features of the interaction will be needed.

As more is learned about blade interaction effects then the more one will start to design individual blade rows or stages with the interaction taken into account. The subject presents particular challenges in the areas of algorithm development, grid systems, turbulence and transition models with progress being dictated by physical understanding and by the speed of computers.

References

- Abu-Ghannam, B.J., and Shaw, R. Natural Transition of Boundary Layers - The Effects of Turbulence, Pressure Gradient and Flow History. *Journal of Mechanical Engineering Sciences*, Vol. 22, (1980)
- Adkins, G.G., and Smith, L.H. Spanwise Mixing in Axial-Flow Turbomachines. ASME 81-GT-57, (1981)
- Birch, N.T. The Effects of Viscosity on Inlet Skew in Axial Flow Turbomachinery Calculations. Institute of Mechanical Engineers Conference on Computational Methods in Turbomachinery, University of Birmingham, England, (1984).
- Birch, N.T. Navier-Stokes Predictions of Transition, Loss and Heat Transfer in a Turbine Cascade. ASME-GT-22. (1987).
- Boletis, E., Sieverding, C.H., and Van Hove, W. Effects of a Skewed Inlet End-wall Boundary Layer on the 3-D Flow Field in an Annular Turbine Cascade. AGARD Rep "Viscous Effects in Turbomachinery." (1983)
- Calvert, W.J. An Inviscid-Viscous Interaction Treatment to Predict the Blade-to-Blade Performance of Axial Compressors with Leading Edge Normal Shock Waves. ASME Paper 82-GT-135 (1982).
- Calvert, W.J. and Ginder, R.B. A Quasi-three-dimensional Calculation System for the Flow Within Transonic Compressor Blade Rows. ASME Paper 85-GT-22 (1985).
- Came, P.M., and Marsh, H. Secondary Flow in Cascades - Two Simple Derivations for the Components of Vorticity. *Journal of Mechanical Engineering Sciences*. Vol. 16, (1974).
- Carrahar, D. and Kingston, T.R. Some Turbomachinery Blade Passage Analysis Methods - Retrospect and Prospect. 'Transonic and Supersonic Phenomena in Turbomachines' AGARD, Munich (1986)
- Caretto, L.S., Gosman, A.D., Patankar, S.V., and Spalding, D.B. Two Calculation Procedures for Steady Three-Dimensional Flow with Recirculation. Proceedings of the Third International Conference on Numerical Methods in Fluid Dynamics, Paris. Volume II, page 60, (1972).
- Carter, J.E. A new boundary layer inviscid interaction technique for separated flow. AIAA 79-1450. (1979).
- Cedar, R.D. and Stow, P. A compatible Mixed Design and Analysis Finite Element method for the Design of Turbomachinery Blades. *Int. J. for Num. Methods in Fluids*. Vol. 5, 331-345 (1985).
- Chaussee, D.S., and Pulliam, T.H. Two-Dimensional Inlet Simulations Using a Diagonal Implicit Algorithm. AIAA Journal, Volume 19, Number 2, (1981).
- Connell, S.D. An evaluation of FANSI-2 Implicit Navier-Stokes Code over a Range of Exit Mach Numbers. Rolls-Royce, Private Communication. (1985).
- Dawes, W.N. Computation of Viscous Compressible Flow in Blade Cascades using an Implicit Iterative Replacement Algorithm. Published in "Computational Methods in Turbomachinery". Institute of Mechanical Engineers, Birmingham University, England, April (1984).
- Dawes, W.N. A Numerical Method for Analysis of 3D Viscous Compressible Flow in Turbine Cascades; Application to Secondary Flow Development in a Cascade with and without dihedral. ASME Paper No. 86-GT-145 (1986).
- Davis, R.L., Ni, R.H. and Carter, J.E. Cascade Viscous Flow Analysis Using the Navier-Stokes Equations. AIAA-86-0033 (1986).
- Easton, J.D. An Improved Time-Marching Method for Turbomachinery Flow Calculation. ASME 82-GT-239 (1982)
- De Ruyck, J., Hirsch, C., and Kooel, P. An Axial Compressor End-wall Boundary Layer Calculation Method. ASME Journal of Engineering for Power. Vol. 101, April (1979).
- De Ruyck, J., and Hirsch, C. Investigations of an Axial Compressor End-wall Boundary Layer Prediction Method. ASME Journal of Engineering for Power. Vol. 103, January (1980).
- Giles, M. Calculation of Unsteady Wake/Rotor Interaction. AIAA Paper 87-0006 (1987).
- Giles, M. Calculation of Unsteady Turbomachinery Flow. Conference on Numerical Methods for Fluid Dynamics. 21-24 March, 1988. Editors K.W. Morton and M. Baines. Oxford University Press, (1988).
- James, P.W. Derivation of Expressions for Secondary Streamwise Vorticity which Allow for Blade Rotation and Streamwise Entropy Gradients. Rolls-Royce Report (1981).
- James, P.W. Rolls-Royce, Private Communication (1982).
- Jameson, A., Schmidt, W. and Turkel, E. Numerical Solution of the Euler Equations by Finite Volume Methods using Runge-Kutta time stepping Schemes. AIAA Paper 81-1259, (1981).
- Jennions, I.K. and Stow, P. A Quasi Three-Dimensional Turbomachinery Blade Design System. Part I - Through-Flow Analysis ASME 84-GT-26. Part II - Computerised System ASME 84-GT-27 (1984).

- Jennions, I.K. and Stow, P. The Importance of Circumferential non-uniformities in a Passage-averaged Quasi-three-dimensional Turbomachinery Design System. ASME-85-IGT-63, Beijing (1985).
- Lakshminarayan, B., and Horlock, J.H. Leakage and Secondary Flows in Compressor Cascades. Aeronautical Research Council R & M No. 3483, (1965).
- Lakshminarayan, B., and Horlock, J.H. Generalised Expressions for Secondary Vorticity Using Intrinsic Co-ordinates. Journal of Fluid Mechanics, Vol. 59, Part 1, pp. 97-115, (1973).
- Le Belleur, J.C. Numerical Viscous-Inviscid Interaction in Steady and Unsteady Flow. 2nd Symposium on Numerical and Physical Aspects of Aerodynamic Flows. Long Beach, California, January (1983).
- Le Bneuf, F. Annulus End-wall Boundary Layer Theory. VKI Lecture Series 05, Secondary Flows in End-wall Boundary Layers in Axial Turbomachines. (1984).
- Marsh, H., and Horlock, J.H. Wall Boundary Layers in Turbo-machinery, Journal of Mechanical Engineering Science, Vol. 14, No. 6, pp. 411-422, (1972).
- Moore, J. and Moore, J.G. Calculations of Three-Dimensional Viscous Flow and Wake Development in a Centrifugal Impeller. Trans. ASME, Journal of Engineering for Power. Volume 103, pp. 367-372 April (1981).
- Moore, J.G. and Moore, J. Calculation of Horseshoe Vortex Flow without Numerical Mixing. ASME Paper No. 84-GT-141 (1984).
- Murman, E., and Bussing, T.R.A. On the Coupling of Boundary Layer and Euler Equation Solutions. 2nd Symposium of Numerical and Physical Aspect of Aerodynamic Flows. Long Beach, California, January (1983).
- Newman, S.P. Addition and Evaluation of an Integral Wake Calculation in FINSUP. Rolls-Royce, Private Communication (1986).
- Newman, S.P. and Stow, P. Semi-inverse Mode Boundary Layer Coupling. I.M.A. Conference on Numerical Methods for Fluid Dynamics. University of Reading, England. (1985).
- Ni, R.H. A Multiple-grid Scheme for Solving the Euler Equations. AIAA, Jnl. Vol. 20, No. 11, (1982).
- Nicholson, J.H., Forest, A.E., Oldfield, M.L.G. and Shultz, D.L. Heat Transfer Optimised Turbine Rotor Blades - An Experimental Study using Transient Techniques. ASME 82-GT-304. (1982).
- Norton, R.J.G., Thompkins, W.T. and Haimes, R. Implicit Finite Difference Schemes with Non-simply Connected Grids. A Novel Approach, AIAA, 22nd Aerospace Sciences Meeting, January, (1984) Reno.
- Patankar, S.V., and Spalding, D.B. A Calculation Procedure for Heat, Mass and Momentum Transfer in Three-Dimensional Parabolic Flows. International Journal of Heat and Mass Transfer Volume 15, pp. 1787-1806 (1972).
- Rai, M.M. Unsteady Three-Dimensional Navier-Stokes Simulations of Turbine Rotor-Stator Interaction. AIAA Jnl. Propulsion and Power, Vol. 3, No. 5, (1987).
- Rai, M.M., and Madavan, N.K. Multi-Airfoil Navier-Stokes Simulations of Turbine Rotor-Stator Interaction. AIAA-88-0361, 26th Aerospace Sciences Meeting, Reno (1988).
- Roberts, W.B. Calculation of laminar Separation Bubbles and Their Effect on Airfoil Performance. AIAA, Vol. 18, No. 1 (1980).
- Sanger, N.L. and Shreeve, R.D. Comparison of calculated and experimental performance for controlled diffusion compressor stator blading. ASME Journal of Turbomachinery Vol. 108, July 1986, pp. 42-50.
- Smith, L.H. Jr. Secondary Flow in Axial Flow Turbomachinery. Trans. ASME 77, (1955).
- Stafford, R.J. and Birch, N.T. An Investigation of the Effects of Thick and Thin Trailing Edges in Compressor Cascades. Rolls-Royce, Private Communication (1987).
- Stow, P. and Newman, S.P. Coupled Inviscid - Boundary Layer Methods for Turbomachinery Blading Design. Joint IMA/SMAI Conference on Computational Methods in Aeronautical Fluid Dynamics. University of Reading, April (1987).
- Stow, P. Northall, J.D. and Birch, N.T. Navier-Stokes Methods for Turbomachinery Blade Design. Joint IMA/SMAI Conference on Computational Methods in Aeronautical Fluid Dynamics, University of Reading, April (1987).
- Walker, G.J. Performance calculation for a NASA controlled diffusion compressor cascade and comparison with experiment. Rolls-Royce, Private Communication (1987).
- Wu, G.H. A General Theory of Three-Dimensional Flow in Subsonic and Supersonic Turbomachines of Axial, Radial and Mixed Flow Types, Trans. ASME pp. 1363-1380, November (1952).

APPENDIX A. Definitions of Momentum and Displacement Thicknesses

The momentum thickness in the meridional and circumferential directions are defined as

$$\theta_{mm} = \frac{1}{\rho_e Q_e} \int_0^\delta \rho q_m (q_{m_e} - q_m) dz$$

$$\theta_{\theta\theta} = \frac{1}{\rho_e Q_e} \int_0^\delta \rho q_\theta (q_{\theta_e} - q_\theta) dz$$

and the two coupled thickness as

$$\theta_{m\theta} = \frac{1}{\rho_e Q_e} \int_0^\delta \rho q_\theta (q_{m_e} - q_m) dz$$

$$\theta_{\theta m} = \frac{1}{\rho_e Q_e} \int_0^\delta \rho q_m (q_{\theta_e} - q_\theta) dz$$

The displacement thicknesses are defined as

$$\delta_m^* = \frac{1}{\rho_e Q_e} \int_0^\delta (\rho_e q_{m_e} - \rho q_m) dz$$

and

$$\delta_\theta^* = \frac{1}{\rho_e Q_e} \int_0^\delta (\rho_e q_{\theta_e} - \rho q_\theta) dz$$

APPENDIX B Secondary Flow Stream-Function

For incompressible flow the continuity equation is

$$\frac{\partial u}{\partial s} + \frac{\partial n}{\partial n} + \frac{\partial w}{\partial z} = 0 \quad (B.1)$$

where the co-ordinate system is shown in Fig. 5. It is usually assumed that

$$\frac{\partial}{\partial s} \equiv 0 \quad (B.2)$$

so that from equation (B.1) a stream-function ψ can be introduced such that

$$u_n = -\frac{\partial \psi}{\partial z}, \quad w = \frac{\partial \psi}{\partial n} \quad (B.3)$$

The secondary streamwise vorticity ζ_{sec} is given by

$$\zeta_{sec} = \frac{\partial w}{\partial n} - \frac{\partial u_n}{\partial z} \quad (B.4)$$

so that from equation (B.3) ψ satisfies.

$$\frac{\partial^2 \psi}{\partial n^2} + \frac{\partial^2 \psi}{\partial z^2} = \zeta_{sec}$$

Knowing the distribution of ζ_{sec} , for example from equation (17), ψ can be determined and the secondary velocities found from equation (B.3). The boundary conditions are

$$\psi = 0$$

on the boundaries of the domain.

The above analysis can be extended to cylindrical polar co-ordinates and to include the effects of compressibility.

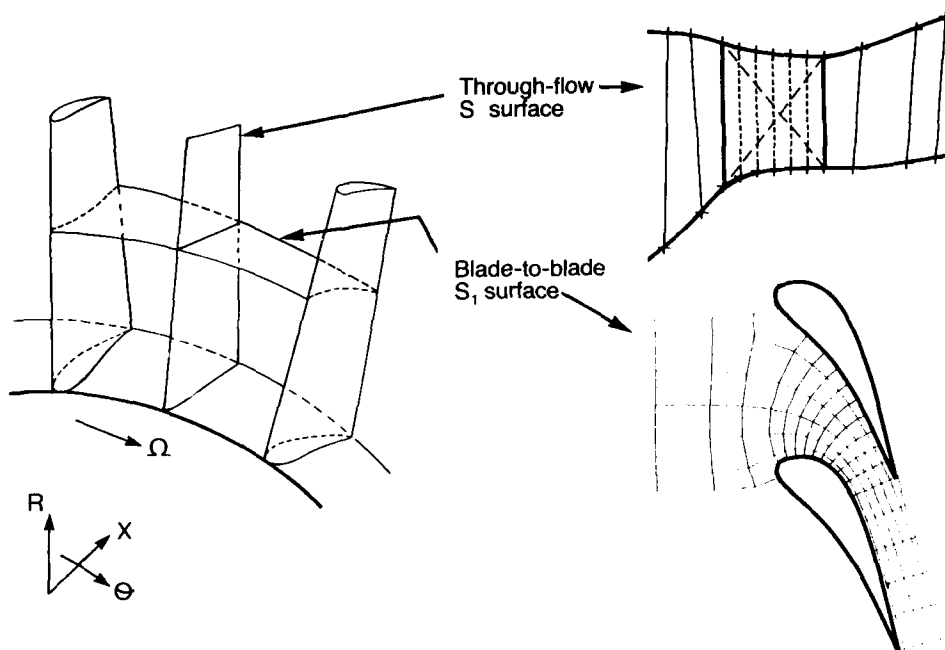


Fig. 1. Quasi-3D Geometries

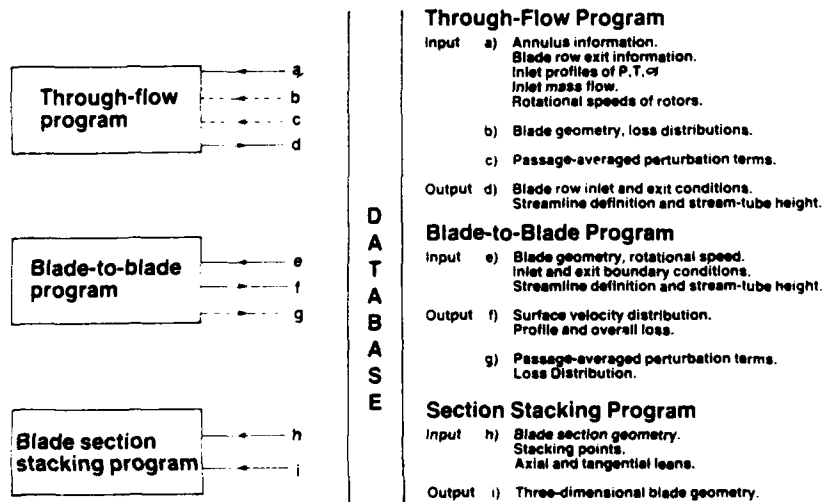


Fig. 2. Quasi-3D Through-Flow System

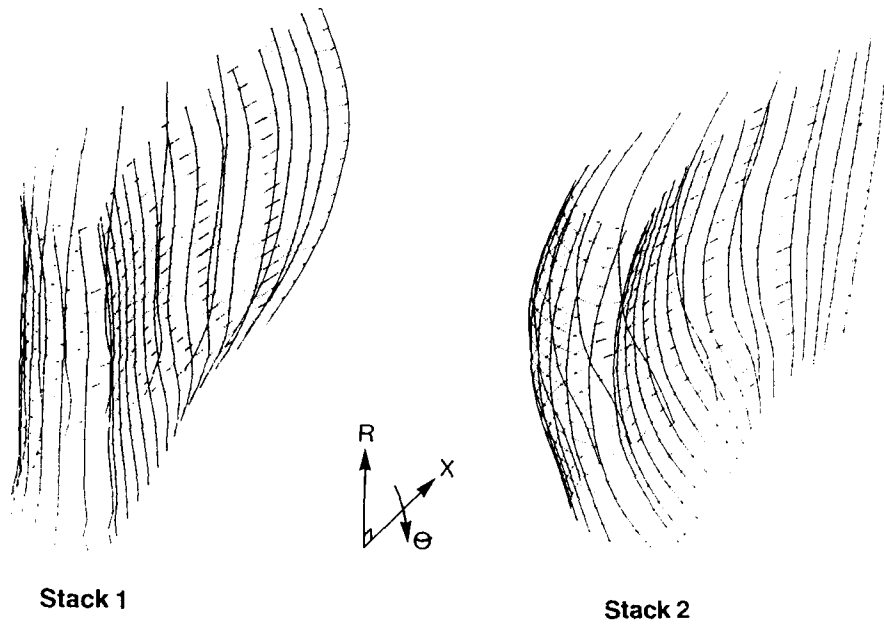


Fig. 3.1 Vane Geometries

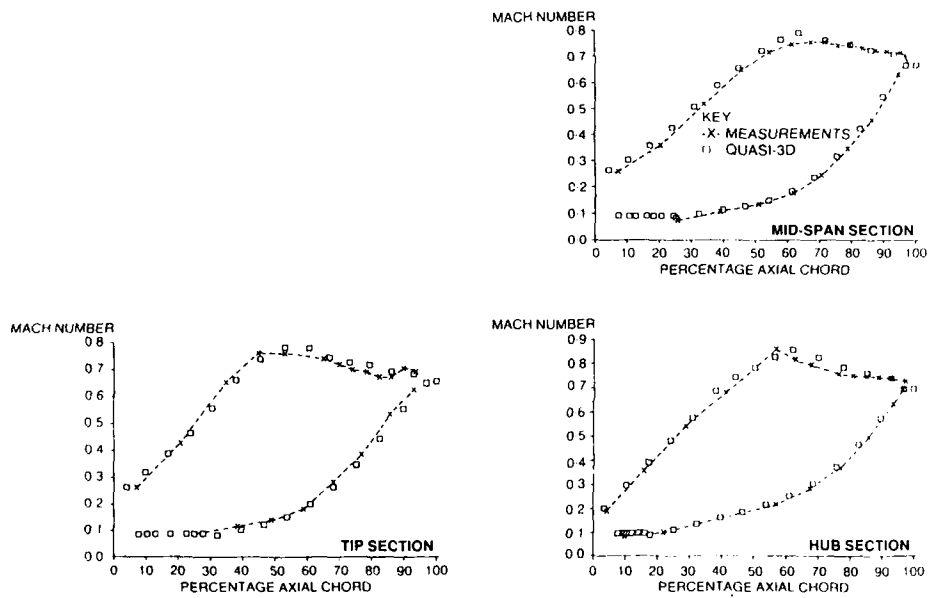


Fig. 3.2 Surface Mach Number Comparison for the Stack 2 Vane

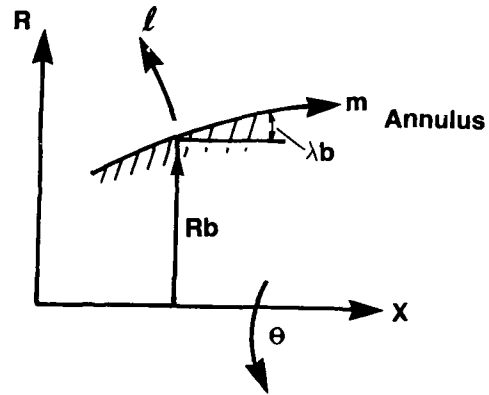


Fig. 4 Meridional Coordinate System

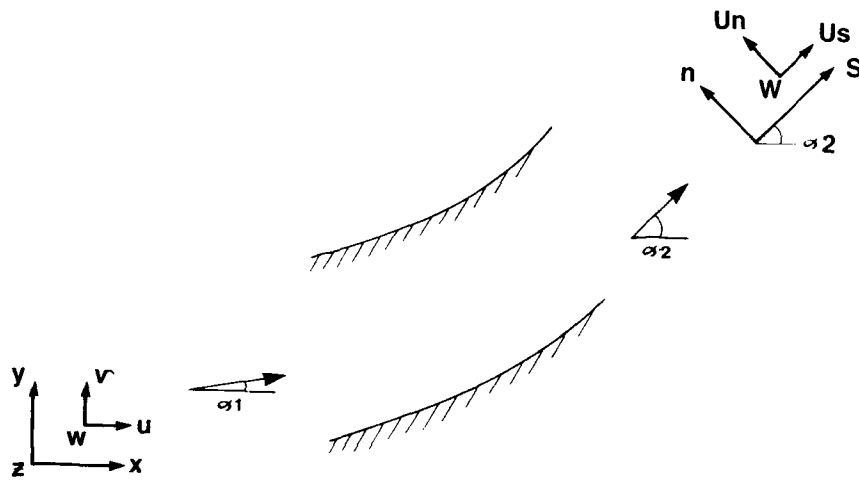


Fig. 5 Streamline Coordinate System

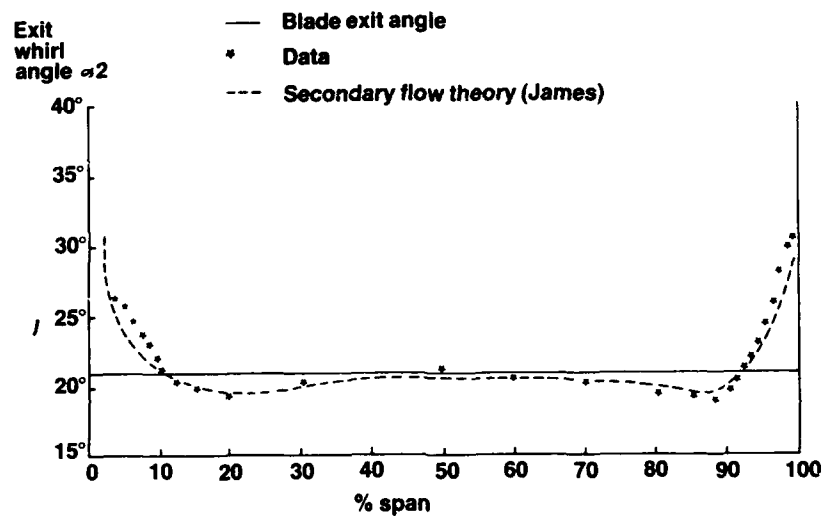


Fig. 6 Compressor Inlet Guide Vane

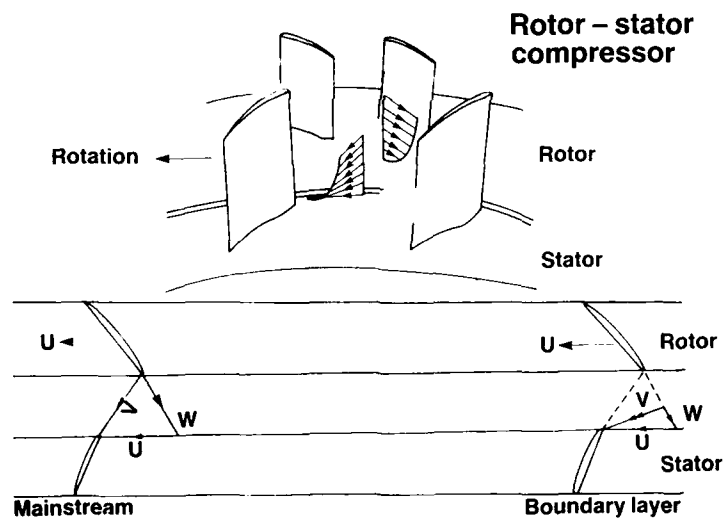


Fig. 7 Boundary Layer Skewing

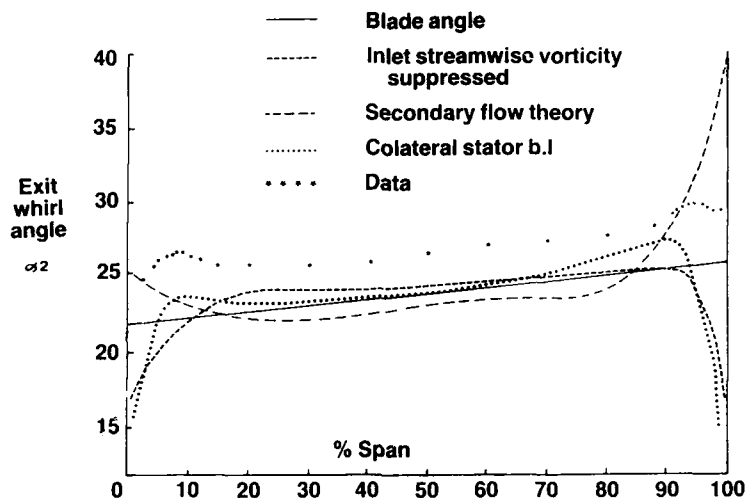


Fig. 8 Compressor Stator

Exit total temperature distribution from 3-stage compressor with different aspect ratios

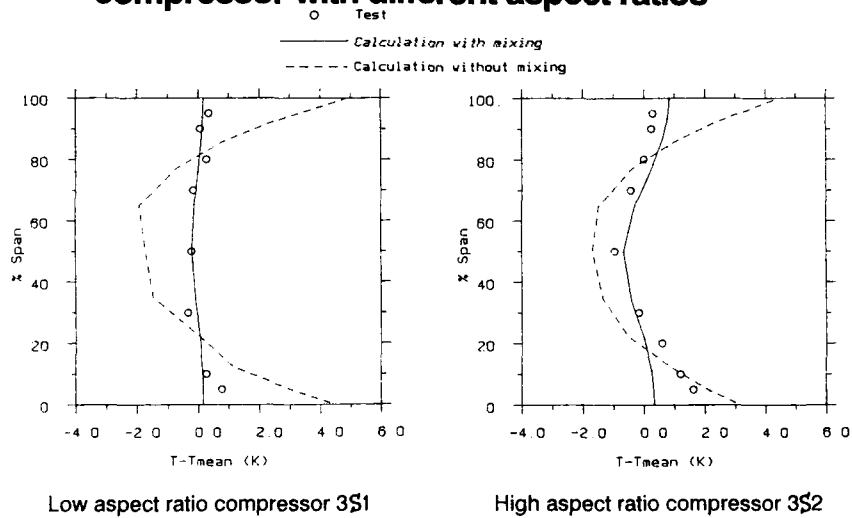


Fig. 9

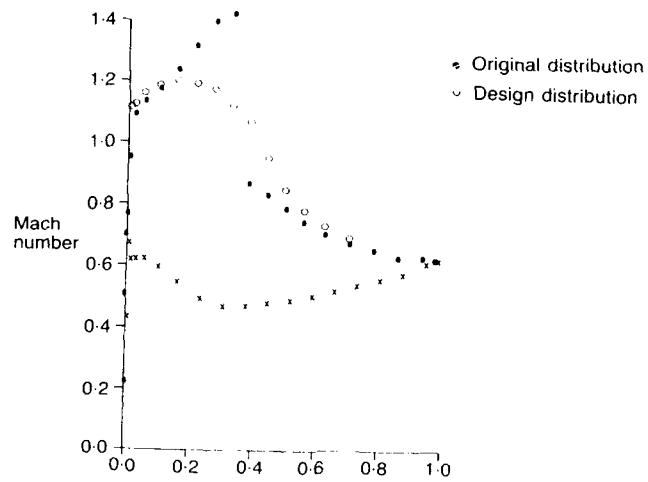


Fig. 10.1 Supercritical Compressor Blade with Shock

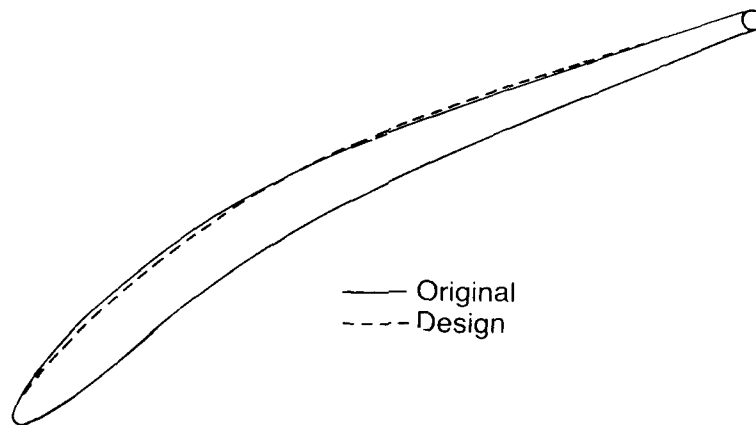


Fig. 10.2 Change in Blade Shape to Remove Shock

Redesigned blade to remove leading edge spike

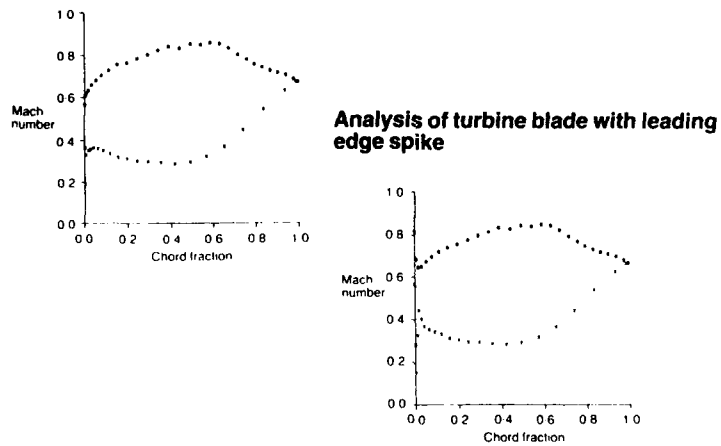


Fig. 11.1 Design of Leading Edge

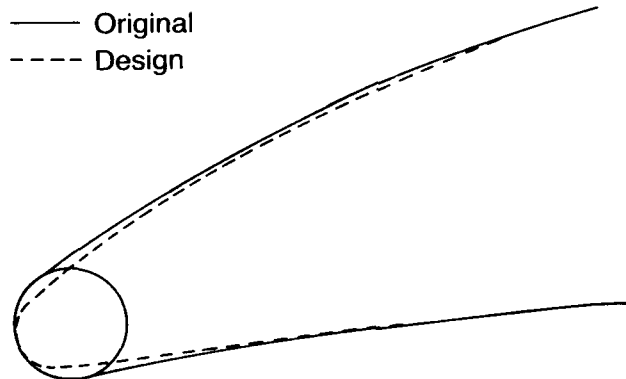


Fig. 11.2 Change in Blade Shape to Remove Leading Edge Spike

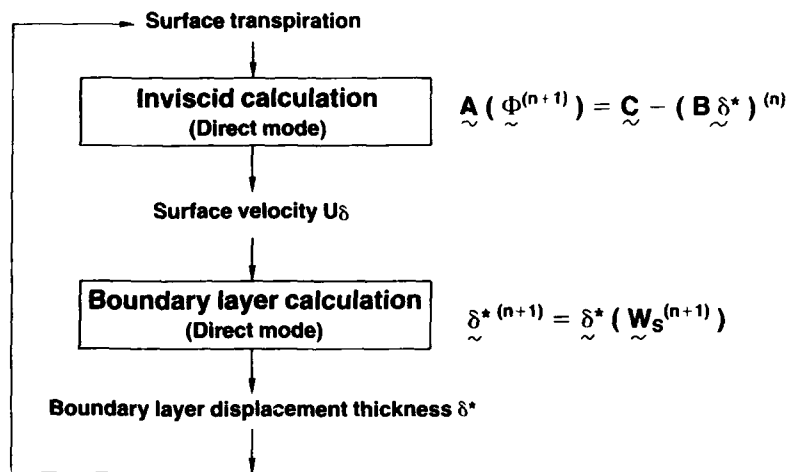


Fig. 12 Direct Mode Boundary Layer Coupling

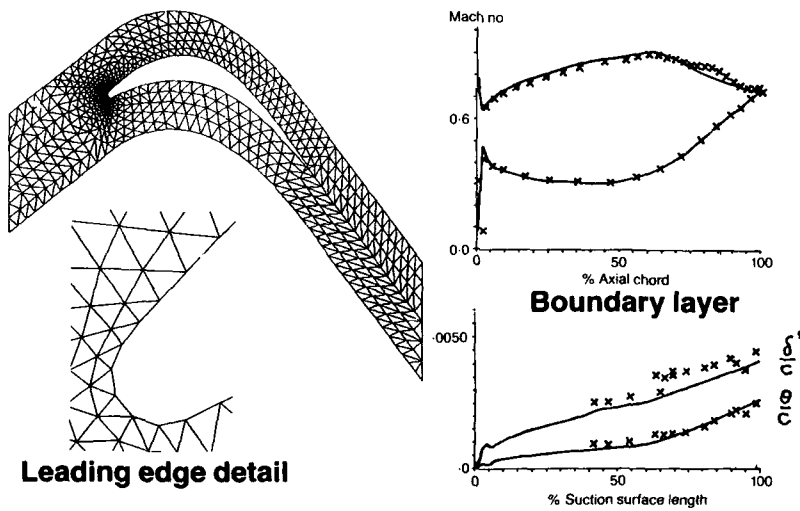


Fig. 13 LP Turbine

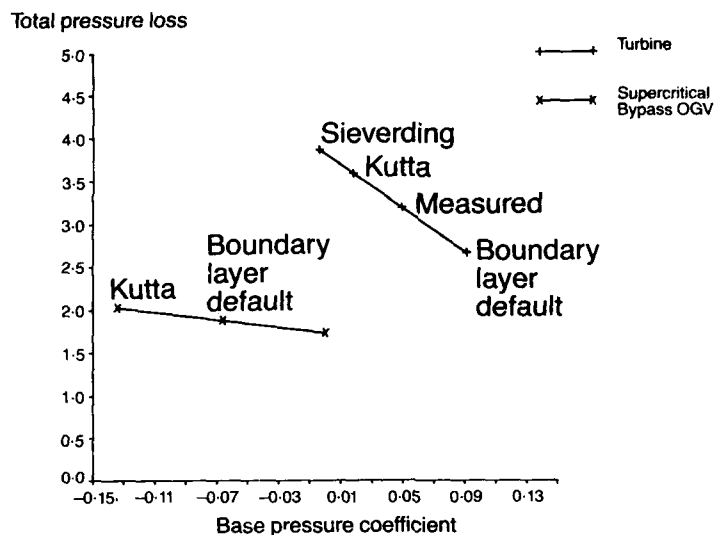


Fig. 14 Effects of Base Pressure on Loss

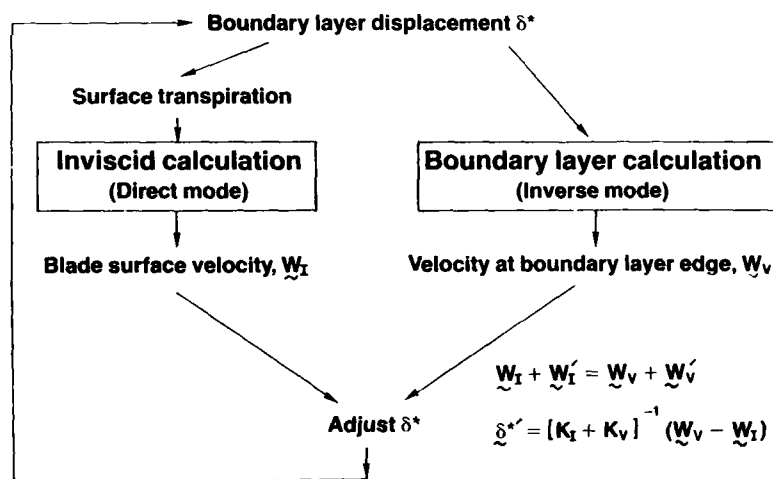


Fig. 14 Effects of Base Pressure on Loss

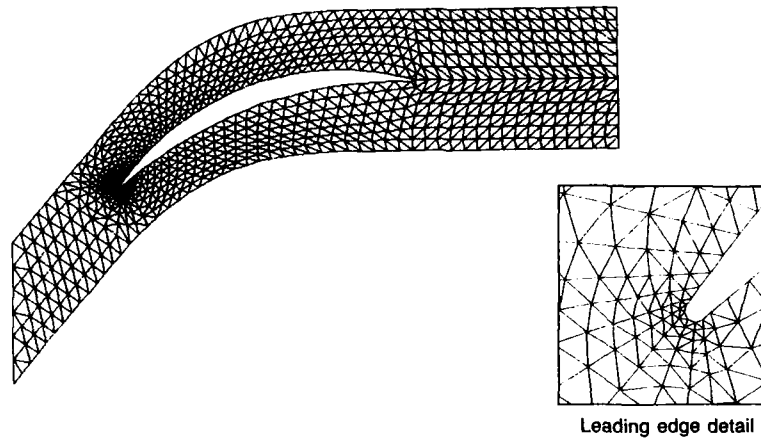


Fig. 16.1 V2 Compressor Cascade

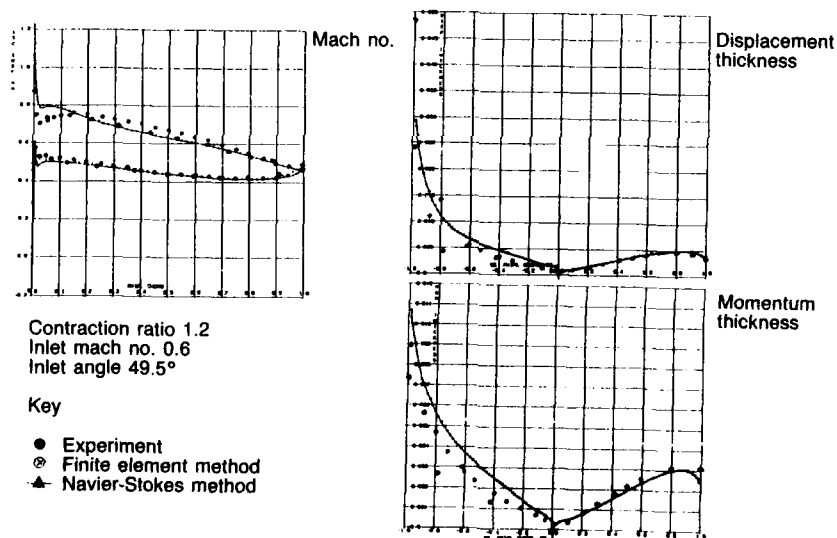


Fig. 16.2 Mach Number Distribution

Mach number and boundary layer parameters

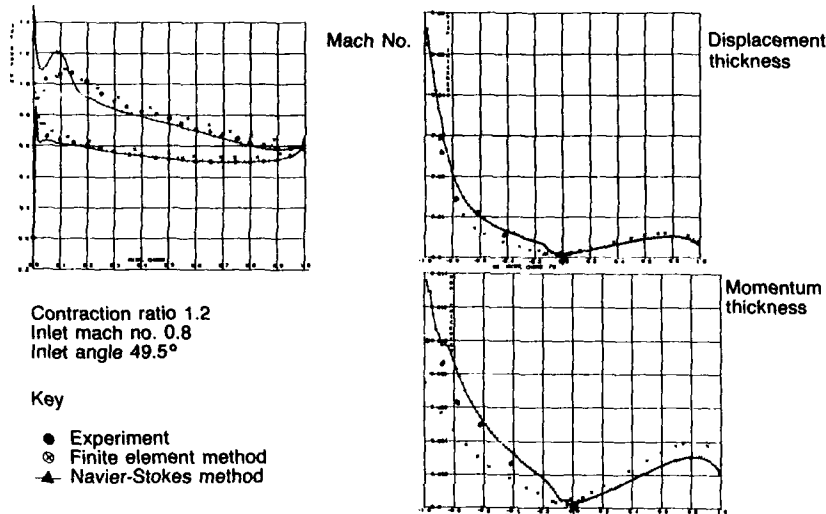


Fig. 16.3 Mach Number Distribution

Loss against incidence

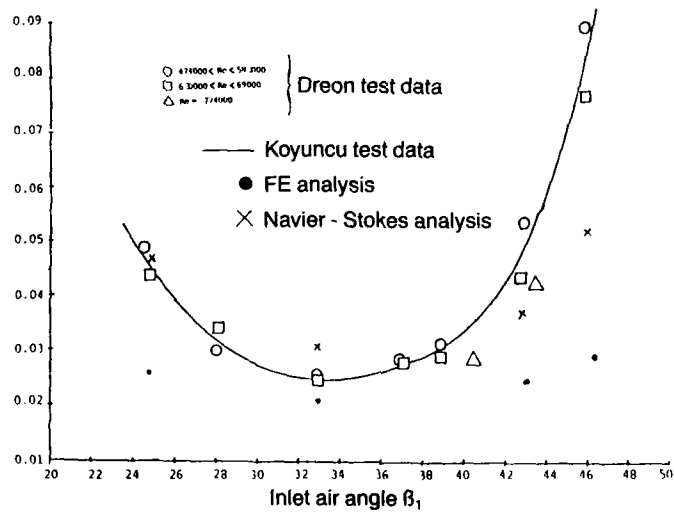


Fig. 17

Controlled diffusion compressor blade

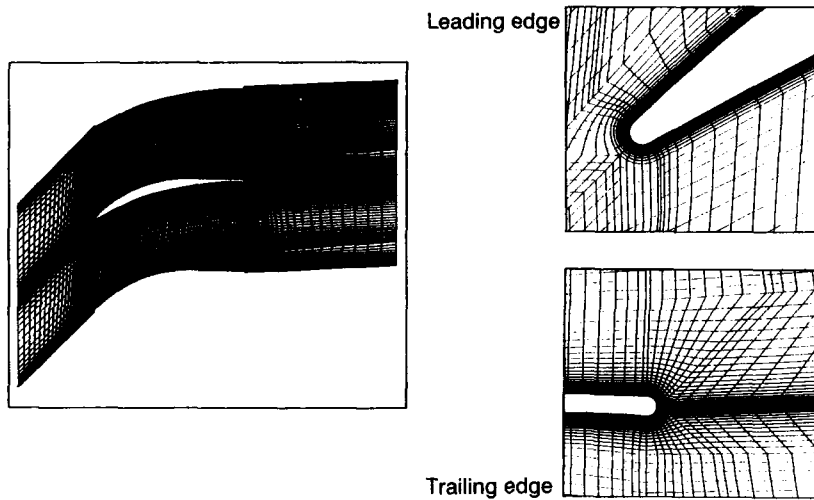


Fig. 18

Mach number and boundary layer parameters

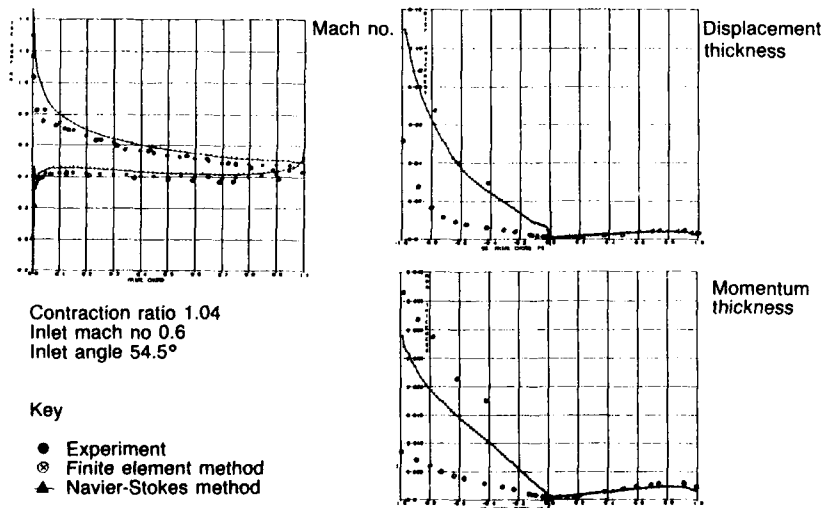


Fig. 19

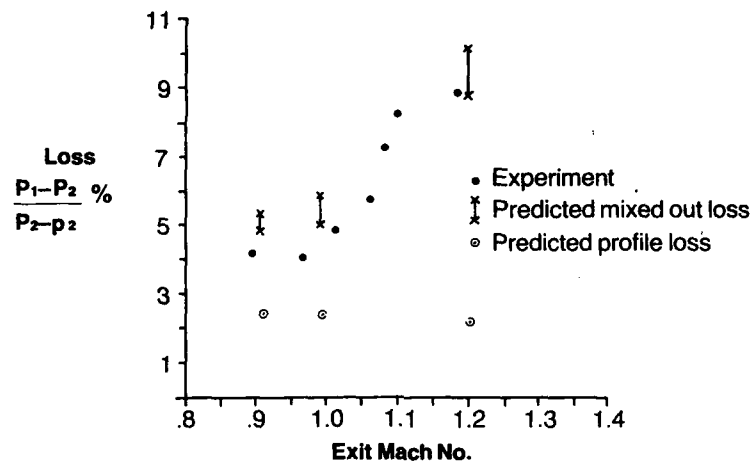


Fig. 20 Loss Prediction against Exit Mach Number

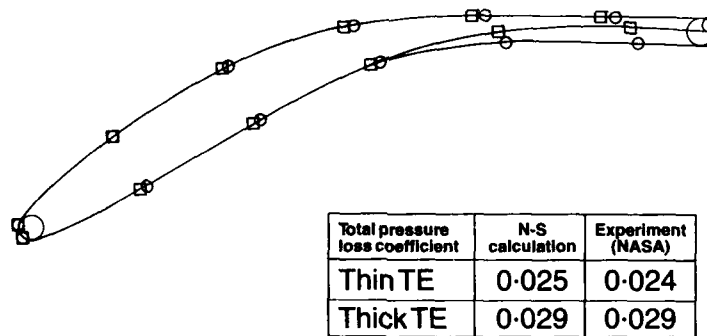


Fig. 21 Compressor Blade with Thick/Thin trailing Edge

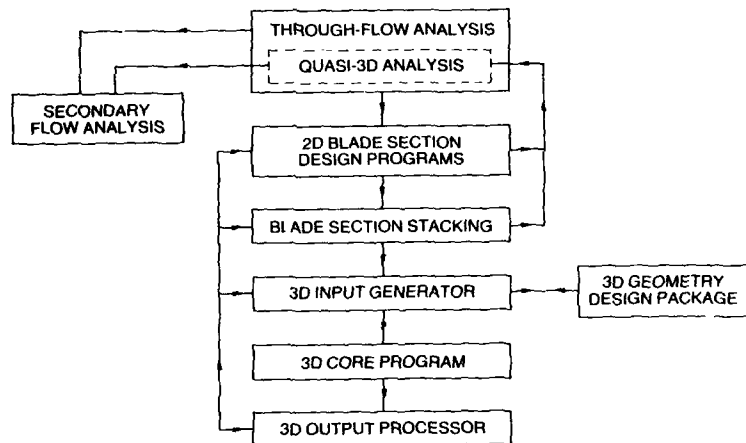


Fig. 22 Three-Dimensional Aerodynamic Design System

TRANSONIC AND SUPERSONIC COMPRESSOR BLADING DESIGN

by A. J. Wennerstrom, AFWAL/POTX, Wright-Patterson AFB, OH 45433, USA

Introduction

This lecture concerns the design of axial compressor stages for which the achievement of high performance is both critical from the standpoint of a thermodynamic cycle and also difficult because of high aerodynamic loading, Mach number, or both. In aircraft turbine engines, this would typically include the fan of a turbofan and the inlet stages of a turbojet. However, in principle, the methods could be applied to the design of any critical turbomachine stage, even a hydraulic machine, although in the latter case one would have to introduce additional criteria to deal with such problems as cavitation. The type of method we are concerned with is often termed a "through-blade" design procedure. It differs from an "across-blade" approach in that conditions are specified and calculated at a series of computing stations between the leading and trailing edge of each blade row as opposed to only at blade row edges. It can employ traditional geometrically-defined airfoils, but will more commonly employ airfoils of arbitrary geometry.

This lecture presumes that a preliminary design of the compressor has already been accomplished to the level of accuracy associated with across-blade design techniques. Thus, at the point where the detail design method starts, we already have an approximate definition of the flowpath, the loading of each stage, spanwise distributions of angular momentum changes and losses, aspect ratios and solidity levels. All of these parameters will typically undergo refinement during the detail design. In general, the flow rate will have been specified at the outset based upon the cycle requirements, and a wheel speed will normally have been chosen based upon structural considerations. The wheel speed of a high-bypass-ratio turbofan can also be limited by shock losses associated with high tip Mach numbers.

The first subject covered will be the general methodology employed including the computational framework. Next, the kinds of information derived from empiricism will be discussed, followed by those areas where design guidance is lacking and one must resort to logical assumptions. The foregoing can theoretically result in an infinite range of solutions and so an optimization criteria is presented through which one strives to obtain the one best solution. Three examples are shown covering the Mach number range of about 0.7 to 1.6 to illustrate the success of the approach. Several other factors which must be taken into account in a design are mentioned. Also, several glaring weaknesses in present design methods are identified. The lecture concludes with some comments on current design trends and computational goals.

General Methodology

The design computations will typically be performed assuming steady flow and using an axisymmetric system of equations. These are mathematically two-dimensional although their use is often termed a quasi-three-dimensional design approach. Variables in the circumferential direction are eliminated by either formulating the equations initially in axisymmetric form such as Wennerstrom [1] or by averaging circumferential variables such as Smith [2] or Jennions and Stowe [3]. The presence of blades is represented in the momentum equation by distributed body forces which account for the fact that, if the blade is not exactly radial, a radial component of force will be imposed on the fluid related to the pressure difference across a finite number of blades. Of course the largest part of the blade force is expended in changing the angular momentum of the fluid and in sustaining the static pressure rise across each blade row. The presence of blades is represented in the continuity equation by a blockage term which accounts for the area which the finite thickness of blades will subtract from the annulus.

In principle, the system of equations can be solved with equal accuracy by streamline curvature methods such as described by Novak [4] or by a matrix method such as described by Marsh [5]. However, the streamline curvature method is the one most widely used throughout the world because of the ease with which it accommodates the boundary conditions on a series of axisymmetric streamsurfaces. With the streamline curvature method, a fixed matrix of computing stations is defined which define the annulus and blade row leading and trailing edges. A sufficient number of these are placed throughout the annulus to ensure a reasonable definition of the streamsurface curvature. For a through-blade computation, several are also included within the meridional extent of each blade row. The computing stations may be curved or leaned to facilitate matching any geometry. The axisymmetric streamsurfaces represent the second set of coordinates. Except for the hub and tip streamsurfaces, streamsurfaces are free to float during the course of the iterative solution such that continuity is preserved within each stream tube. A schematic of this computational mesh is illustrated in Figure 1 with only a few streamlines shown to retain clarity.

Equation (1) illustrates one way of presenting the so-called radial equilibrium equation of turbomachinery. This is derived from the Momentum Equation in intrinsic coordinates, the Energy Equation for steady adiabatic flow, and an enthalpy-entropy relation.

$$V_m \frac{dV_m}{dl} = \sin \mu V_m \frac{\partial V_m}{\partial m} + \cos \mu \frac{V_m^2}{r_c} - \frac{V_\theta}{r} \frac{d(rV_\theta)}{dl} + \frac{dH}{dl} - T \frac{ds}{dl} - \frac{dH}{dl} \sin \mu \frac{d\mu}{dl} - \cos \mu \frac{d\mu}{dl} \quad (1)$$

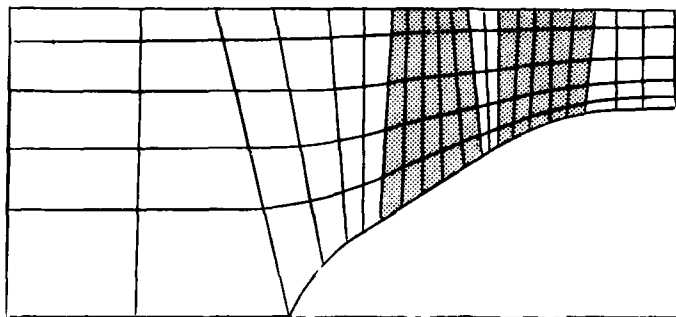


Figure 1. Typical Streamline/Computing-Station Mesh

With the streamline curvature method, we would be solving for the meridional velocity V_m along each computing station, defined by the l direction. The terms not shaded are those of first order importance in influencing the meridional velocity profile. These comprise, from left to right, the streamline curvature term (rc is the radius of curvature of the streamsurface), the gradient of angular momentum, the enthalpy gradient, and the entropy gradient. The angle μ is a measure of the non-orthogonality of a computing station and a streamsurface at each mesh point. Thus, where streamsurfaces and computing stations are nearly orthogonal, terms multiplied by $\sin \mu$ become vanishingly small. Of the shaded terms, the first is sensitive to the meridional acceleration of the fluid, the second takes into account the meridional component of the blade force, and the third and most important one takes into account the force normal to the streamsurface caused by a non-radial blade surface.

The equations are usually solved in one of two ways. The relative flow angles may be specified within bladed regions and the enthalpy and angular momentum changes through each blade row comprise a result. Alternatively, the enthalpy change may be defined through rotors, and the angular momentum change through stators, and the relative flow angles comprise part of the results. If one wishes to analyze an existing geometry, the first approach with relative flow angles specified is the most logical choice. Some designs have also been created in this fashion where it was desired to use airfoils of some prescribed geometric family such as multiple circular arcs. In this instance, one would assume a geometry based upon the preliminary design, analyze the flow through it, and then proceed to revise the geometry in a series of iterations until some optimization goal was achieved. However, this is an extremely laborious approach to optimizing a design and one is very likely to assume some geometries for which the solution will fail computationally because of choking or excessive spanwise gradients in some parameters. Also, a further drawback of solving with relative flow angles specified is that the solution has two branches: a subsonic and a supersonic one just like one-dimensional flow in a duct. When meridional Mach numbers are relatively high, i.e. approaching 1.0, many streamline curvature codes may have difficulty converging to the correct solution, even for a valid geometry.

A much more straightforward approach which circumvents these difficulties is the second method wherein enthalpy or angular momentum changes are specified and the relative flow angles are computed. Not only does this produce a unique solution but it virtually always produces some solution, given reasonably sensible input data, since it is rarely affected by the types of numerical convergence difficulties associated with the other method. In order to be able to exploit this solution, one must have the flexibility to define airfoils of arbitrary geometry, compatible with the calculated relative flow angles. This is rapidly becoming the most popular method with which to design high performance stages, although it is not really new. The first commercial fan designed according to this approach was reported by Wright and Novak [6] in 1960.

In order to define airfoils from a matrix of relative flow angles defined over the blade surface, one must either calculate or assume a deviation (or departure) angle within the blade row which gives the difference between the metal angle and the circumferentially averaged relative flow angle. This will be discussed later. One also needs to define a thickness distribution which will typically be selected on the basis of structural and aerodynamic considerations. Accepting these two as given for the moment, the distributions of relative flow angle and deviation angle over the blade surface will define the camber line metal angle at every mesh point. One way in which the geometry can be defined is as follows. If we define the metal angle distribution on each streamsurface by its first derivative or tangent, the values from leading to trailing edge at each streamsurface/computing station intersection point can be mathematically spline fit. Since we now have an analytical description of the first derivative of the camber line, a single integration serves to define the actual coordinates of the mean line surface in cylindrical polar form. A thickness distribution can then be symmetrically placed on this camber line. The actual design process involves many iterations between aerodynamic calculation and blade design to insure that the metal blockages of the final blade geometry are consistent with those used for the throughflow computation. This is normally easily accomplished during the course of the iterations required for design optimization. The optimization itself will also be discussed later.

Empirical Inputs

The traditional empirical inputs are the deviation angle, the losses related to diffusion, and the blockage distribution associated with boundary layers and wakes. These are listed in order of criticality in terms of how large an effect an error may have on the end result. The deviation angles are still commonly predicted with some version of the classic Carter's Rule, often with an "experience factor" added. This experience factor has sometimes been predicted by an inviscid secondary flow computation in lieu of pure empiricism.

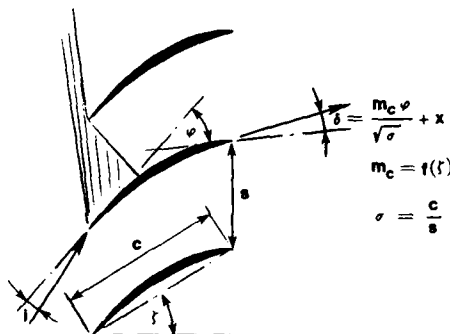


Figure 2. Deviation Angle Correlation

The parameters employed in Carter's Rule are illustrated in Figure 2. The deviation angle, δ , is proportional to a constant, m_c , (which is itself a function of the blade stagger angle, ξ) times the camber angle, Φ , divided by the square root of solidity, σ , (chord divided by spacing). The "experience factor" is x . The magnitude of deviation angle will usually range from a low of 1.0 or 2.0 degrees for a nearly uncambered fan tip to a high of possibly 12.0 or 13.0 degrees for a highly cambered hub influenced by a secondary flow field.

Diffusion losses are most commonly correlated in the Lieblein fashion of loss parameter versus diffusion factor, although the correlations are usually defined by more recent data than used for Lieblein's original correlation of the 1950's.

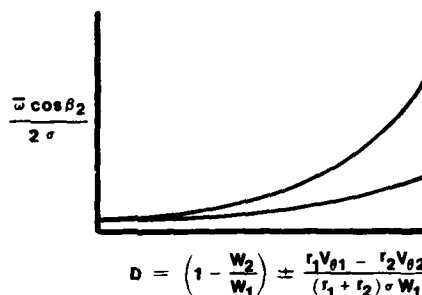


Figure 3. Loss Parameter/Diffusion Factor Correlation

The Lieblein type of correlation is shown in Figure 3 where the loss parameter is represented on the vertical axis and the diffusion factor on the horizontal axis. Different curves are often used as a function of spanwise position and also to reflect differences between rotors and stators. The variables represented in the loss parameter are:

\bar{w} = relative total pressure loss coefficient

$$\bar{w} = \frac{(P_{02})_{ideal} - P_{02}}{P_{01} - P_1}$$

β_2 = relative exit flow angle

σ = solidity = chord/spacing

The relationship between the relative total pressure loss coefficient and the loss parameter can be visualized as follows. Using the illustration of Figure 4,

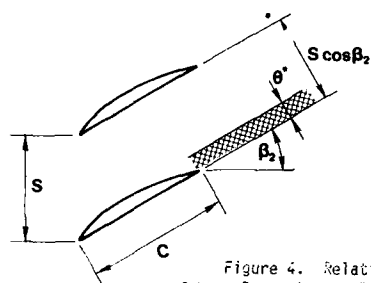


Figure 4. Relationship of Loss Parameter to Relative Total Pressure Loss Coefficient

consider \bar{w} to be directly proportional to the ratio of wake thickness to staggered blade spacing which we write.

$$\bar{w} \sim \frac{\theta^*}{S \cos \beta_2}$$

For a given cascade and level diffusion, θ^* is directly proportional to chord length. Also, assume that θ^* will increase in proportion to the loss parameter P .

$$\theta^* \sim C \cdot P$$

Combining the above we have

$$P \sim \frac{\theta^*}{C} \sim \frac{\bar{w} S \cos \beta_2}{C} = \frac{\bar{w} \cos \beta_2}{\sigma}$$

(The number 2 in the denominator of P is a residue of its original derivation from incompressible turbulent boundary layer theory. It is obviously irrelevant to the correlation.) In the expression for diffusion factor, subscripts 1 and 2 represent inlet and exit conditions, W represents the relative velocity, V represents the swirl component of relative velocity and the formulation shown includes the effect of radius change. The magnitude of diffusion losses can range from relative total pressure loss coefficients of only a few hundredths at low diffusion factors and low stagger angles to values exceeding 0.1 at higher loadings and staggers. More elaborate, but still empirical, correlations are also used, such as that of Koch and Smith [7]. The Koch and Smith model includes blade profile losses due to surface diffusion and trailing edge thickness as well as losses due to end-wall boundary layers and clearances. When part-span shrouds are employed, losses accounting for these should also be included.

Boundary layer and wake blockage are sometimes predicted on the basis of methods derived from flat plate boundary layer theory such as Jansen [8] or Stratford [9]. However, these methods are sufficiently unreliable that blockage is often defined on the basis of past experience under similar circumstances. Blockages will typically be on the order of only 1.0 or 2.0 percent upstream of a stage. However, they will often rise to 8.0 to 12.0 percent within a machine and sometimes higher. After the first few stages of a multi-stage compressor, a repeating pattern is often reached due to secondary flow and mixing. This may approach a plateau in stages of about 50 percent reaction or it may develop a cyclic pattern, rising in rotors and falling in stators, in high reaction stages.

Shock losses

In the 1950's, the first research compressors operating with rotor relative Mach numbers in excess of one were designed and tested. Shock waves were expected and were indeed observed. It was soon determined that shock waves were responsible for a significant fraction of the losses encountered. This stimulated formulation of the first openly published shock loss model by Miller, Lewis, and Hartmann in 1961 [10]. In experiments it had been observed that, near peak efficiency, the shock wave near the rotor tip appeared to be approximately normal to the flow and slightly detached from the leading edge. For purposes of the model, the shock was assumed to be perpendicular to the camber line at the leading edge in the cascade plane. The upstream Mach number was assumed to be the average of the relative inlet Mach number at the leading edge and the Mach number estimated to exist at the suction surface where the shock intersects it. This latter Mach number was obtained by assuming that the fluid near the suction surface undergoes a Prandtl-Meyer isentropic expansion through an angle equal to the difference between the relative inlet angle and the suction surface metal angle at the point of

shock impingement. Note that, by averaging these two Mach numbers, the model takes into account the effects of solidity, camber, and stagger as well as Mach number. Figure 5 illustrates the assumed flow pattern.

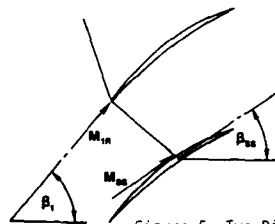


Figure 5. Two-Dimensional Shock Loss Model

The loss is predicted by the standard normal shock equation

$$\frac{P_{oy}}{P_{ox}} = \left[\frac{\frac{k+1}{2} M_x^2}{1 + \frac{k-1}{2} M_x^2} \right] \frac{\frac{k}{k-1}}{\left[\frac{2k}{k+1} M_x^2 - \frac{k-1}{k+1} \right]^{\frac{1}{k-1}}} \quad (2)$$

where

$$M_r = (M_{1r} + M_{2r})/2 \quad (3)$$

M_{1r} = relative inlet Mach number

and M_{ss} is found by expanding M_{lr} through the angle $(\beta_l - \beta_{ss})$ using the Prandtl-Meyer relations.

The above model results in the discontinuous onset of shock loss at the sonic radius. In reality, some degree of shock loss will exist inboard of the sonic radius at high subsonic Mach numbers. A transition model was proposed by Creveling and Carmody in 1968 [11].

$$M_x = \frac{M_{1r}}{2} (M_{1r} + M_i) \quad (4)$$

where M_i is the Mach number resulting from a Prandtl-Meyer expansion from Mach 1.0 through an angle equal to the relative turning angle ($\beta_i - \beta_{ss}$) and M_{lr} is again the relative inlet Mach number. This transition model is used in the region within which the relative inlet Mach number is less than 1.0 but where the shock upstream Mach number calculated according to Eq. (4) is greater than 1.0.

A more sophisticated model was proposed by Koch and Smith in 1976 [7]. They hypothesized that shock losses arise from leading-edge bluntness effects and from the blade passage shock structure. They suggest the following equation attributable to Prince for the leading-edge bluntness loss.

where $\frac{\Delta S}{R} = -\ln \left\{ 1 - t_{LE}/(\text{bcos}\beta_1) \times [1.28(M_{1r} - 1) + 0.96(M_{1r} - 1)^2] \right\}$ (5)

where

S = entropy
R = the gas constant
tLE = leading edge thickness
b = tangential blade spacing

According to the authors, "this expression represents the trend of results from a method-of-characteristics-type analysis of the leading-edge flow field. It includes the loss due to local strengthening of the leading-edge shock that is contained within the passage as well as from the shock structure which propagates upstream of the leading-edge plane." For several experimental configurations examined, Eq. (5) predicted about two-thirds of the measured efficiency loss. The second part of this model represents the shock-related losses associated with the diffusion process. Koch and Smith assumed that this loss was equivalent to the entropy rise of one oblique shock that reduces a representative passage inlet Mach number to unity Mach number. This applies as long as the relative exit Mach number is subsonic or sonic. When the exit Mach number is supersonic, the oblique shock is assumed to reduce the Mach number to the relative exit value. The representative passage inlet Mach number is assumed to be a weighted average of the maximum suction surface Mach number and the relative inlet Mach number. The weighting factor selected to give reasonable agreement with limited high-speed single-stage experience weights the Mach number estimated on the suction surface six times as heavily as the relative inlet Mach number. The normal shock model tends to be adequate for fan and compressor stages designed for military engines where the loading

levels are quite high. However, for lighter loading levels such as would be characteristic of a commercial turbofan, the passage shock is swept back in the passage and the Koch and Smith model would be likely to produce better results.

All of the above models are cascade-plane models; i.e. they are purely two-dimensional. This has normally proven adequate for compressor blade rows having aspect ratios of 2.0 or greater and having conventional leading-edge shapes. This would be representative of the vast majority of transonic compressors designed until quite recent times. However, in the mid-1970's several low-aspect-ratio designs were evaluated which developed remarkably good efficiencies. It was finally observed by Prince [12] that spanwise obliquity of the shock surface might account for much of this improvement. This can easily be visualized by referring to Fig. 6.

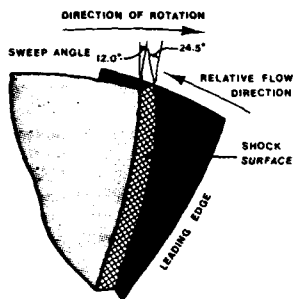


Figure 6. Three-Dimensional Shock Surface Geometry

Pictured is a rotor with an inlet hub-tip radius ratio of 0.31, a relative inlet flow angle at the tip of about 60 degrees, and an average aspect ratio of 1.32. This was the specific geometry of one of the stages tested in the mid-1970's with better-than-expected performance. Prince had further noted that, near peak efficiency, the passage shock still appeared to be approximately normal in the cascade plane. Thus, the shock surface illustrated in Fig. 6 represents a normal shock on each streamsurface in the cascade plane. (The fact that the shock vanishes near the hub has been ignored for purposes of this purely geometric illustration.) Note that, since the solidity is high at the hub and the stagger angle is low, the shock impinges near the leading edge of the suction surface near the hub. In contrast, at the tip with a much lower solidity and a higher stagger angle, the shock impinges much further aft on the suction surface. Thus, even if the leading edge were a radial line, the shock surface where it impinges on the suction surface could have significant spanwise sweep or obliquity just because of the airfoil twist and solidity variation. If the leading edge has some sweep in addition, the overall effect is exaggerated still further.

These observations led to the three-dimensional shock loss model of Wennerstrom and Puterbaugh [13]. For simplicity, it was patterned after the normal shock model of Miller, Lewis, and Hartmann, however, with appropriate correction for the spanwise obliquity of the shock. The angle of the shock surface relative to the upstream flow is calculated at the leading edge and the shock impingement point on each streamsurface using Eq. (6).

$$\Lambda = \cos^{-1} [\cos \beta \cos \epsilon \sin(\phi - \gamma) - \sin \beta \sin \epsilon] \quad (6)$$

The variables used in Eq. (6) are illustrated in Figs. 7 and 8

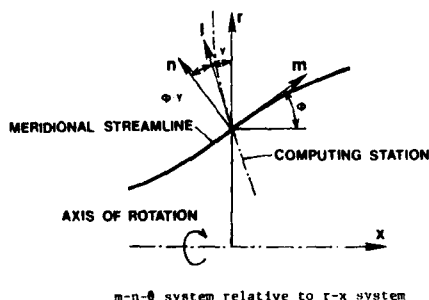


Figure 7. Meridional Plane

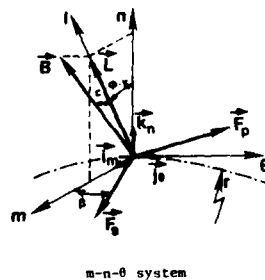


Figure 8. Intrinsic Coordinates

The angle Λ , which is 90 degrees plus the sweep angle, is a function of streamsurface slope, ϕ , the blade lean angle, ϵ , the relative flow angle, β , and either the computing station lean angle, γ , at the leading edge or the impingement line lean angle on the

suction surface. The blade lean angle used is that relative to the computing station at the leading edge or the impingement line on the suction surface. Properties across the shock are then calculated in the standard fashion for oblique shocks using the normal shock relations and an upstream Mach number equal to

$$M_x = M |\sin \Lambda| \quad (7)$$

where M is the approach Mach number at the point in question.

In addition to introducing shock obliquity, one more departure was made from the Miller, Lewis, and Hartmann model. In the original model, the two Mach numbers obtained on each streamsurface were simply averaged according to Eq. (3) to obtain an upstream shock Mach number for calculating the total pressure ratio. In the three-dimensional model, the authors integrated the total pressure ratio from leading edge to suction surface since the total pressure is not a linear function of either Mach number or obliquity. The Mach number and the spanwise shock obliquity were assumed to vary linearly from leading edge to suction surface. Then a three-point Simpson Rule integration was used to define the shock total-pressure ratio on each streamsurface. The effect of integrating along the surface is shown in Fig 9.

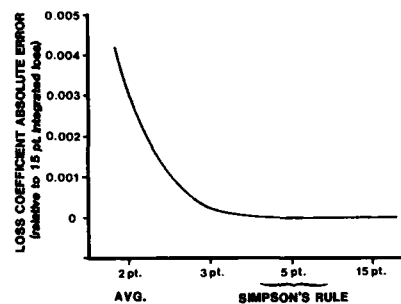


Figure 9. Loss Error from Averaging

The three-point integration produces a more conservative result (i.e. a higher loss) than the simple average. However, more than three points is not warranted in view of the absolute accuracy of such a loss estimate. The transition region for high subsonic Mach numbers was treated analogously to Eq. (4). Adjusted for sweep, this now becomes:

$$M_x = \frac{M_{1r}}{2} |\sin \Lambda| (M_{1r} + M_i) \quad (8)$$

Within the transition region, a blade-to-blade integration was not performed. The average (mid-passage) value of Λ was used in Eq. (8). The magnitude of the changes in predicted quantities caused by consideration of spanwise obliquity is shown in Tables 1 and 2 for the rotor illustrated in Fig 6. In column four of Table 1, the relative total pressure loss coefficient attributable to the shock is shown for the Miller, Lewis, and Hartmann two-dimensional model. Columns five and six show the magnitude of the sweep angles calculated at the leading edge and impingement line respectively. Column seven shows the loss coefficients as adjusted for spanwise shock obliquity.

Table 2 shows the difference in predicted overall stage performance with roughly two points in efficiency being attributable to the obliquity of the shock surface.

Table 1.

Table 2.

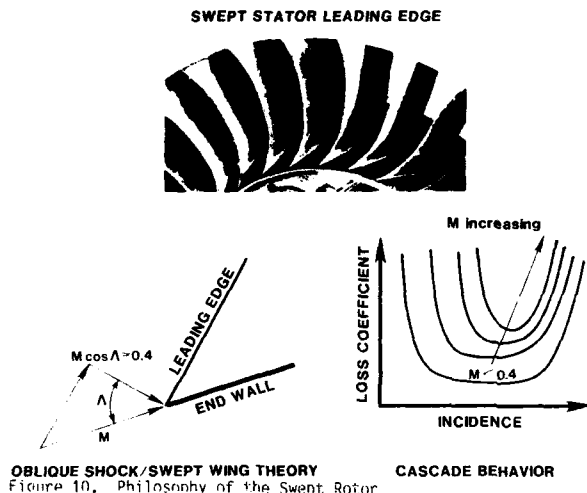
Shock Loss Calculation Parameters Performance Comparison for Transonic Stage

STREAMLINE NUMBER	INLET REL. MACH NO.	EXPANSION ANGLE	M-L-H SHOCK LOSS	L-E SWEEP	IMPINGEMENT LINE SWEEP	SWEEP SHOCK LOSS
1	0.861	3.557	0.0	38.86	40.85	0.0
5	0.746	7.020	0.0	32.97	32.01	0.0
9	0.864	7.726	0.008	21.19	20.96	0.001
13	1.223	5.796	0.043	16.14	21.19	0.024
17	1.466	2.771	0.104	15.84	21.43	0.073
21	1.567	-0.763	0.180	12.04	24.50	0.123

	M-L-H MODEL	NEW MODEL	EXPER. RESULTS
TOTAL PRESSURE RATIO	2.026	2.061	2.058
ISENTROPIC EFFICIENCY, %	86.96	89.07	88.90

The whole idea of correcting for sweep or shock surface obliquity derives from classic concepts derived for swept wings and oblique shocks. Namely, it is the component of Mach number perpendicular to the shock surface which determines the static pressure rise and total pressure loss. Consequently, the same concepts can readily be applied to

more sophisticated models such as that of Koch and Smith [7]. Also, although rotors will typically experience the highest Mach numbers and therefore can best exploit shock obliquity, the same principles can be applied to stators to alleviate locally high Mach numbers at the hub. In [14], Wennerstrom has described a stage design in which the stator leading edge was deliberately swept forward at the hub in order to reduce the component of Mach number normal to the leading edge consistent with swept wing theory. The concept is illustrated in Fig. 10.



The design logic ran as follows. NACA data for subsonic cascades illustrated that cascade incidence range increased in inverse proportion to Mach number down to approximately $M = 0.4$. At lower Mach numbers, no further increase was observed. Therefore, the stator leading edge sweep at the hub was set at an angle which resulted in the Mach number component normal to the leading edge being approximately 0.4; the absolute Mach number was approximately 1.02. The leading edge was then curved back forward for two reasons. First, a leading edge intersecting a casing wall at an acute angle is likely to be a high source of loss even at subsonic Mach numbers. Second, it minimized the axial length of the stage while allowing adequate solidity to be maintained at the stator tip. This expedient was completely successful in eliminating any observable hub shock loss. A subsequent design which applied the same logic to a different configuration has operated at hub Mach numbers as high as 1.2 without observable shock losses.

Through-blade Assumptions

The area where the designer's intuition and judgement become most important concerns the interior of the blade row in a through-blade design. The parameters which must be distributed, listed in approximate order of importance, are departure angle, losses, and blockage. We will use the term departure angle within a blade row to define the difference between the circumferential average relative flow angle and the camber line angle. However, recognize that this equals the incidence angle at the leading edge and the deviation angle at the trailing edge. Very little data exists on the distribution of these parameters within blade rows. What little does exist is generally derived from laser velocimetry measurements, and this data is both incomplete and of debatable accuracy for this purpose. Computational fluid dynamics, comprised of both viscous-inviscid interaction methods and Reynolds averaged Navier-Stokes codes, shows promise of providing this information in the not too distant future. However, most through-blade designs done up to now depend on assumptions and these are what will be discussed here.

The departure angle is by far the most critical assumption. Small errors in angle at high stagger angles, near a fan tip for example, can result in large variations. We have approached this as follows. At the leading edge, the departure angle must equal the incidence angle. At the trailing edge, it must equal the deviation angle. A third boundary condition which can be imposed is that, in order to satisfy the Kutta condition at the trailing edge, the rate of change of departure angle approaching the trailing edge must be approximately the same as the rate of change of the camber-line angle in order to unload the airfoil. A fourth and final condition is that we know that the departure angle within the fully covered portion of the blade passage, especially at higher solidities, must be very small. In fact, for S-shaped blades typical of modern fan tips, it can even be argued that the departure angle should be slightly negative in portions of the passage. At this point, if one now thinks of a plot of departure angle versus meridional distance from leading edge to trailing edge, we now have four boundary conditions to define a curve: a level at the leading edge, a level at the trailing edge, an approximate and very small level in the middle region of the passage, and a slope at

the trailing edge. Given these four conditions, it is up to the designer to use his judgement in drawing a sensible and smooth curve. An example of the departure angle distribution is shown in Figure 11.

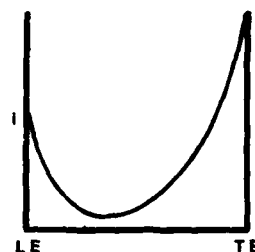


Figure 11. Typical Departure Angle Distribution

The interior meridional distribution of losses within a blade row has a much smaller effect on the results. A great many successful designs have been accomplished with nothing more elegant than a linear distribution of the overall blade-element loss from leading to trailing edge. A good piece of advice is that unless you have a very good reason to make a more elaborate assumption, select the simplest possible one. A logical basis for a slightly refined assumption might be the following. Once a design has been roughed out, by assuming a shock geometry in the cascade plane, one can identify what portion of the meridional cross-section of the blade passage the shock wave will cover. The shock portion of the loss can be assumed to be linearly distributed over that portion. Most of the diffusion loss will occur downstream of the shock. It will also include some mixing loss downstream of the trailing edge in the blade wake. Thus, the remainder of the loss could be assumed to be linearly distributed from where the shock loss terminates to either the trailing edge or some distance downstream of it, depending on where one wishes to distribute the mixing loss.

Blockage is another parameter which it is difficult to distribute on any firm scientific basis. Many designs have simply distributed it linearly across blade rows. It is probably just as often distributed non-linearly based upon a designer's evaluation of past experiments with similar machines. The safest approach is similar to that recommended for losses; namely, unless you have a good reason to use something more elaborate, stick to a linear distribution.

Design Control and Optimization

There are, in principle, an infinite number of designs which might satisfy all of the foregoing criteria for a given blade row or stage. One of the designer's goals is to have some rational basis for selecting the one best design to meet his objectives. The preliminary design will normally have established solidity levels and loading levels such that stall margin and other design goals can reasonably expect to be met. Structural design considerations will have largely defined blade and edge thickness distributions. At this point in a design, the major aerodynamic optimization goal will generally be to achieve the desired performance with minimum losses.

If one could calculate losses directly without resort to empiricism, then a rational search procedure could be devised to minimize losses themselves. However, the state-of-the-art has not yet advanced to this point. A shortcoming of the empirical loss prediction schemes is that they are not particularly sensitive to nuances in a design. A wide range of designs may be predicted to have the same performance. Thus, a more indirect approach is called for. The next most obvious approach would be to look at the boundary layer behavior and attempt to minimize separation. However, reasonably good methods of dealing with strong viscous effects coupled with high Mach numbers are just now beginning to reach fruition. What will be described here is a simpler method developed over fifteen years ago when good cascade plane computations for high Mach number viscous flows were only a faint hope on the horizon. The method has been very successful and several examples of its use will be illustrated.

The logic of the method presented is as follows. What we would really like to do is to minimize adverse pressure gradients on the airfoil surfaces. However, let us assume that the cascade plane computations available are not sufficiently reliable. Therefore, let us further assume that, if the meridional static pressure gradient as calculated by an axisymmetric through-flow analysis is minimized, we will have made a major step toward also minimizing gradients on the airfoil surfaces. Now, the absolute minimum would be a linear increase in static pressure from leading to trailing edge. However, this is an unachievable objective because the Kutta condition would not permit an airfoil to sustain loading all the way to the trailing edge. Therefore, let us assume that our objective will be to achieve as linear as possible a gradient from the leading edge to approximately the three-quarter chord position. From that point to the trailing edge, the gradient should gradually taper off in deference to the Kutta condition. A distribution having this character is illustrated in Figure 12.

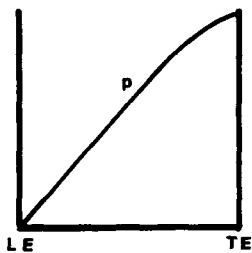


Figure 12. Static Pressure
Optimization Objective

Design control in order to achieve this objective is achieved largely through three variables. The most important are the enthalpy rise through a rotor and the angular momentum variation across a stator. The third variable is the annulus wall shape, although it is usually desirable to keep annulus wall curvatures to an absolute minimum. Consequently, we most often introduce only very subtle changes in wall shape. Also, for practical reasons of maintaining tip clearances, it is usually desirable to keep the annulus over rotor tips cylindrical, or at worst conical, but not curved in the meridional direction.

A very convenient and practical starting point for a new design is to begin by assuming a linear enthalpy increase on each streamsurface across rotors and a linear angular momentum decrease across stators. Although this will not be an optimum solution, it will be close enough to a realistic one that it provides an excellent basis from which the design iterations aimed at optimization may proceed. An optimum solution defined as above will normally have non-linear distributions of enthalpy and angular momentum, but they will not be far from linear and will normally deviate smoothly.

The annulus wall shape chosen to begin a design should be as simple as possible consistent with the aspect ratios chosen and the contraction ratios required. Wall curvature should be minimized. In fact, if aspect ratios are chosen which are initially too high or are poorly distributed axially, undesirable static pressure gradients may be calculated which can only be avoided by reducing some aspect ratios. An example case for which subtle changes in wall shape may prove of great benefit is at the hub of a rotor turning near to the axial direction relative to the rotor. When a rotor turns the flow to approximately axial, the pressure distribution in the last half of the blade row becomes very insensitive to even significant changes to the meridional enthalpy distribution. In such a case, once somewhat reasonable enthalpy distributions have been defined optimizing most of the blade row, further small adjustments to the hub contour may prove the key to achieving the optimization objective.

The next two figures illustrate the extent to which the optimization objective was achieved for the rotor shown earlier in Figure 6. Figure 13 shows the final design pressure distributions at the hub, mid-span, and tip as obtained from the axisymmetric through-blade computation. At the mid and tip radius, the optimization objective was reasonably well achieved. At the hub, because the rotor had a steep 32 degree ramp angle and turned the flow approximately to axial, the static pressure gradient could not be reduced without actually removing work from the air which would have been undesirable.

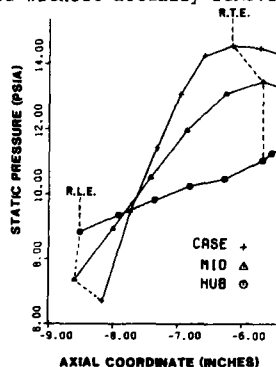


Figure 13. Rotor Design Meridional Static Pressure Distributions

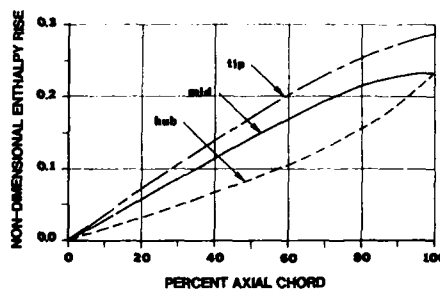


Figure 14. Rotor Design Meridional Enthalpy Distributions

Figure 14 illustrates the final design meridional enthalpy distributions which resulted in the static pressure distributions shown in Figure 13.

They are not far from linear and thus it is evident why a linear distribution is often a convenient starting point with which to begin the detail design process. Although at first glance, one might assume that a work distribution at the hub which was decreasing

in slope, or at least linear, instead of increasing in slope might have made it possible to achieve the original optimization objective at the hub, this was not the case. A more nearly linear hub distribution would have resulted in the static pressure rising more steeply, then flattening out or even falling, only to rise again near the trailing edge. This was felt to be undesirable and thus the minimum gradient was essentially linear from leading to trailing edge.

Sample Results

The methods outlined above have proven such a simple and direct, as well as effective, design approach that they have been applied without variation to inlet guide vanes, rotors, and stators covering an inlet Mach number range from approximately 0.6 to more than 1.6. Three examples will be illustrated which span most of this range. They include a subsonic stator section, a supersonic fan tip section, and a supersonic rotor section with substantial camber. All three met design objectives and did so with low losses.

Figure 15 shows the static pressure distribution around a subsonic stator section at approximately mid-span operating in a full compressor stage at near design-point conditions. The approach Mach number for this operating condition is approximately 0.85 and the diffusion factor was about 0.4. What one should observe is a modest suction surface expansion confined to a region near the leading edge followed by a smoothly decreasing rate of diffusion with no sign of separation. The gradient is steepest where the boundary layer is best able to handle it and then decreases smoothly as the boundary layer grows. If one would compare the appearance of this blade in the cascade plane with a circular arc it would have more camber in the aft portion of the blade. Figure 16 shows the pressure distribution around a fan tip section as tested in a two-dimensional cascade wind tunnel. The cascade has an S-shaped camber line.

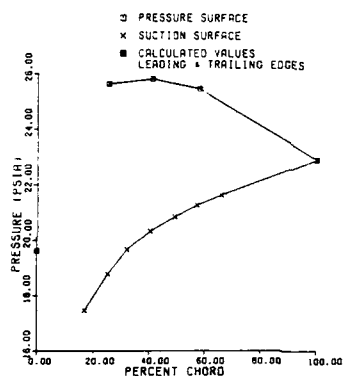


Figure 15. Stator Mid-Span Static Pressure Distribution

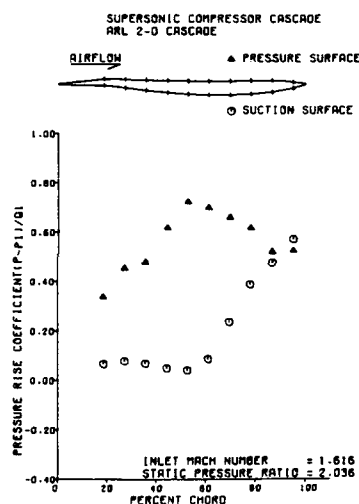


Figure 16. Supersonic Fan Tip Static Pressure Distribution

This type of airfoil is often called a precompression airfoil because of the negative camber in the leading edge region causing a focussing of supersonic compression waves from the suction surface. It was designed for a Mach number of about 1.62 and a diffusion factor of about 0.52. The important thing to note in this figure is that the pressure on the suction surface from the leading edge to the passage shock impingement point is practically constant and at a value slightly in excess of the upstream value. Thus, there is no significant supersonic expansion upstream of the shock impingement point, actually a very small precompression, and then suction surface diffusion proceeds smoothly all the way to the trailing edge.

Figure 17 illustrates the third example. This airfoil was also tested in a cascade wind tunnel, but not two-dimensionally.

This section in the actual rotor had approximately fifty percent contraction in the stream tube area across the blade row. This contraction ratio was duplicated with the cascade wind tunnel sidewalls, and all measurements were made in mid-passage in the plane of symmetry. This was designed for an inlet Mach number of 1.46 and a diffusion factor of about 0.58. It had about 25 degrees of camber and did not have any negative camber. Once again, observe that the suction surface pressure is nearly flat up to the shock impingement point. Following that, diffusion is smooth and gradually declining all the way to the trailing edge.

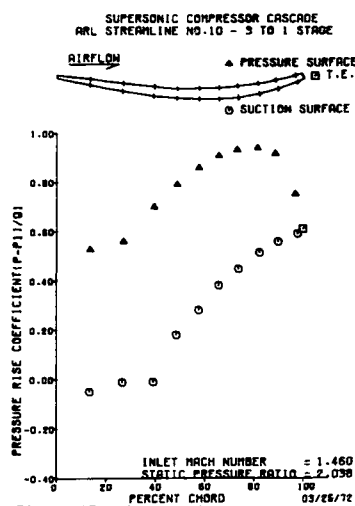


Figure 17. Supersonic Rotor Static Pressure Distribution

An interesting conclusion which can be drawn is that the simple optimization method described herein is capable of defining desirable airfoils over a broad band of Mach numbers. Better methods are available for very low Mach numbers. Other somewhat superior methods currently employed for high subsonic Mach numbers are much more time consuming, e.g. "controlled diffusion" airfoils. It is not yet apparent that alternate methods available for supersonic Mach numbers are in any way superior.

Other Aerodynamic Considerations

There are a variety of other factors primarily of aerodynamic concern which must be taken into account in the design process. Five of them will be discussed here. The mass flow through any streamtube in which the Mach number relative to the blades is supersonic is controlled by the inlet wave pattern if: (1) the flow is "started", i.e. the passage shock has been swallowed, and (2) the cascade throat area is sufficient to avoid choking. In fact, if the throat is too small, the passage will never achieve the started condition. All efficient supersonic blade sections operate in the started condition at their design point. The foregoing design process in most cases automatically leads to an adequate throat margin. What it does not automatically provide is the correct incidence angle. The inlet wave system controlling the flow consists of a bow shock propagating upstream from the suction surface aft of the leading edge up to what is termed the first captured Mach wave. The first captured Mach wave is that wave which first encounters the leading edge of the next blade. Any waves further inside the cascade cannot propagate upstream and thus cannot influence the flow swallowing capacity of the cascade. This wave pattern is illustrated in Figure 18.

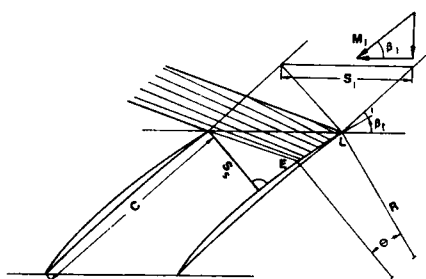


Figure 18. Supersonic Cascade Inlet Wave Pattern

For a given streamtube contraction ratio, sometimes called axial-velocity/density ratio, and a given inlet Mach number, any given cascade will have a unique incidence. This may or may not correspond to the flow which the designer wanted going through that streamtube. An incidence distribution must first be selected based upon past experience. For most supersonic blade sections, this will correspond to a value of about 1.0 to 2.0 degrees relative to the suction surface. However, once a design has been laid out, the designer should do a cascade plane analysis of the inlet wave pattern at several radii to

see if each section passes the flow intended. The flow in this region is largely inviscid. The most accurate method is probably the method of characteristics. However, time dependent computations have also been used successfully for this purpose. If the correct flow is not passed, the incidence must be adjusted up or down and a new design accomplished.

Solidity is another important parameter which the designer must consider. Since the solidity is included in the loss parameter which is usually correlated with diffusion factor, in some instances one can compute an "optimum" solidity in the sense of that one resulting in minimum loss. However, in most practical cases, the resulting value is too low because it may lead to insufficient stall margin. One rule of thumb used for many years has been to set the tip solidity of a transonic rotor at a value approximately equal to the relative inlet Mach number at the tip. This rule of thumb was gleaned from observation of many of the more successful NACA transonic rotor designs of the 1950's. However, depending on the amount of turning required and the level of diffusion, the best value may be higher or lower. Where a lot of turning is coupled with high Mach number, significantly higher solidity may be required to keep shock losses down by minimizing suction surface expansion upstream of the passage shock. Another way of arriving at the solidity level for a fan tip section, which may have a very high Mach number but nearly zero turning in the relative frame, is to insure that the solidity is high enough so that a weak oblique shock wave from the leading edge of one blade will impinge on the suction surface of the next blade upstream of its trailing edge. A weak oblique shock corresponding to the relative inlet Mach number and the angle of incidence to the pressure surface is the weakest shock likely to exist in the blade passage. This situation is illustrated in Figure 19.

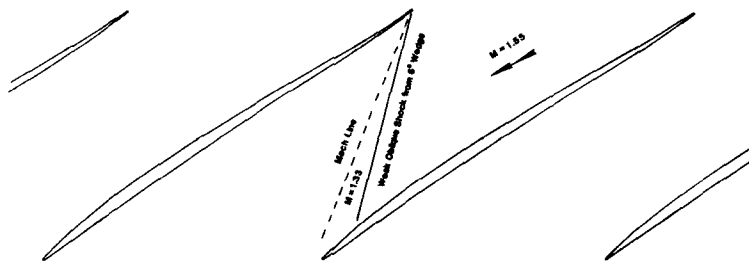


Figure 19. Weak Oblique Shock at Pressure Surface Wedge Angle

An impingement point about ten to twenty percent chord upstream of the trailing edge is an intuitively made arbitrary choice intended to insure that the shock will always be contained in the passage and to leave some margin to satisfy the Kutta condition. Most designs for which the solidity level has been low enough to allow a passage shock to miss the next blade have been rather unsuccessful. The example shown in Figure 19 is from the same compressor illustrated in Figures 6 and 16 and described by Wennerstrom [14]. For multistage designs, solidity is often roughly defined by stall margin criteria introduced into preliminary design procedures such as that of Koch [15] or Schweitzer and Garberoglio [16]. However, values arrived at in this manner usually need to be refined in the detail design process based upon more precise loss models, etc.

The ramp angle is the angle of the hub flowpath relative to the axial direction. The pressure ratio of a stage and the loading distribution between blade rows will approximately determine the area contraction required across each blade row. The choice of aspect ratio will then approximately determine the ramp angles, presuming little or no radius change at the tip. There is a reluctance to design for a ramp angle greater than about thirty degrees for an axial flow compressor. Most designs fall well under that value. More important than the absolute value perhaps is the smoothness of the hub flowpath. Ideally, one would like to see ramp angles declining monotonically from inlet to exit. A staircase shaped flowpath configuration would be among the least desirable but is not always avoidable. The main objective is to minimize streamline curvature effects along the flowpath. Every expansion around a convex surface in excess of what is required must necessarily be followed by a diffusion. Since every blade row in a compressor is a diffuser (neglecting inlet guide vanes), every effort should be made to avoid any unnecessary diffusion which will detract from overall loading capability or stall margin. Hence, the smoother the better is a good rule of thumb for flowpath design.

Figure 20 illustrates the flowpath of the single stage compressor described by Wennerstrom [14]. Note that the hub is conical over the rotor and is a circular arc through the stator.

Although in many flow situations it is desirable to avoid discontinuities in surface curvature, i.e. to maintain continuous second derivatives, for this design it was determined that maximizing radii of curvature had a more beneficial effect on velocity profiles.

Another example is shown in Figure 21 for a three stage compressor.

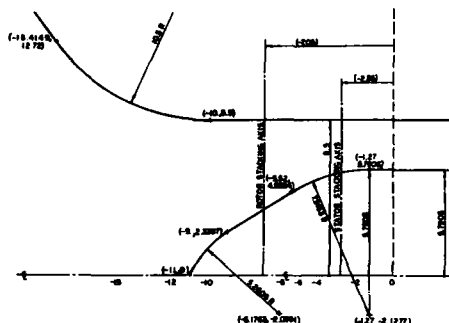


Figure 20. Single-Stage Compressor Flow-Path

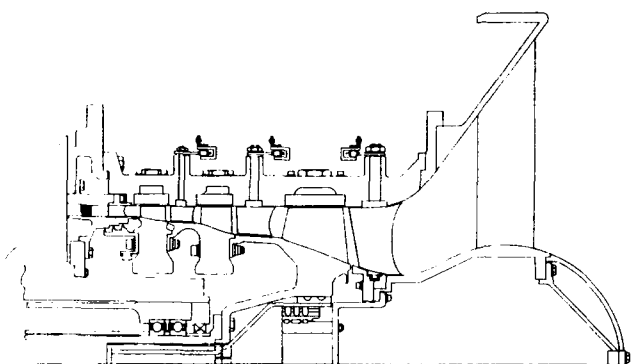


Figure 21. Three-Stage Compressor Flowpath

This was a highly loaded relatively high Mach number design where it was necessary to contract the flowpath much more across rotors than across stators in order to maintain a good loading distribution between blade rows. Here a staircase shaped hub flowpath was unavoidable, but every effort was made to minimize local extremes in curvature.

The smoothness of distributions is not only important for the flowpath. It is of vital importance for every single parameter employed in a compressor design. This is rather obvious with respect to airfoil mechanical design parameters such as chord length and thickness distribution. It is less obvious but equally important in distributing such things as the enthalpy rise across rotors and the angular momentum change across stators. Any lack of smoothness in either chordwise or spanwise distributions will be reflected in peculiarly shaped airfoils and some loss in performance. One technique which has been found successful for insuring smooth enthalpy and angular momentum distributions over airfoils is an adaptation of thin plate deflection theory from stress analysis. At the same time, it minimizes designer effort required to adjust these distributions. The technique works as follows. The grid composed of computing stations and streamsurfaces which defines an airfoil is mapped into a rectangle. One edge of this rectangle is fixed and assigned the leading edge values of the distribution. The opposite edge is fixed and assigned the trailing edge values of the distribution. Then, by imposing a deflection (read parameter variation) at a very few points on this surface, the entire surface will smoothly deform in a way insuring minimum gradients over the entire surface consistent with the boundary conditions. In stress analysis, this is termed a surface of minimum strain energy. This is illustrated in Figure 22.

If the initial distributions are analytically defined in some simple way, for example linearly, then their smoothness can be guaranteed. Then if this technique is used to adjust these distributions as the designer attempts to optimize a design, smoothness will be preserved and the number of quantities which the designer has to input are also minimized.

Airfoil stacking is another factor which the designer must consider. The so-called stacking axis is a radial line to which the coordinates of an airfoil are referenced. Thus, when a series of airfoils distributed along the span are referenced to a stacking axis, the three-dimensional shape of the airfoil is defined. In rotors, the designer has very limited latitude in that the centroid of each cross-section cannot depart far from this stacking axis or unacceptable centrifugal stresses will be developed. Centroid stacking is usually the starting point for rotors. However, subsequent stress analysis may indicate that modest off-sets from the stacking axis in some spanwise locations may

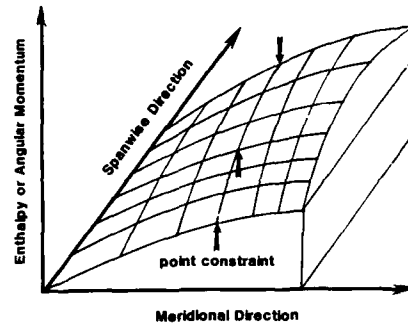


Figure 22. Stress Analogy for Work or Momentum Distribution

reduce stresses, deflections, and untwist. With stators of fixed geometry, the designer has a wide latitude to stack the blades any way which suits his purpose. For example, the stators installed in the booster stages between a high bypass fan and core compressor are often in an inward sloping flowpath. Here the stators are often deliberately leaned circumferentially so that the blade force terms in the radial equilibrium equation will help turn the flow inward toward the core. With variable geometry stators, here again there is less freedom. The stacking axis cannot depart too far from the mid-chord position or unacceptable end-wall clearances will result when the stator is set at certain angles.

Mechanical Design Considerations

The last factor which will be discussed is structural considerations. It is relatively obvious that the designer must choose his material, thickness, and chord distributions such that adequate margin exists between the centrifugal stress and the yield strength of the material at the temperature at which the machine must operate. This margin is to permit a vibratory stress to be superimposed on the steady state stress while still retaining infinite fatigue life. Prevention of high cycle fatigue is a major aim of the structural designer. Problems in this area account for a significant percentage of development and operational costs of a gas turbine engine. The two principal types of vibration which can cause high cycle fatigue are forced vibration and flutter. Forced vibration is defined as an externally excited oscillating motion where there are forces acting on the component which are independent of the displacement. Where the forces acting on the component are functions of the displacement, velocity, or acceleration of the component and these forces feed energy into the system, the self-induced oscillations are classified as flutter. Most of the material discussed in this section was abstracted from Snyder and Burns, Chapter XXII of [17]. However, for more complete coverage of the present state-of-the-art in this area, the reader is referred to the entire two-volume set comprising this reference.

Forced vibration is the result of external forces acting on the blade, disk, or vane component. Accurate calculation of the undamped natural frequencies and mode shapes is required if one hopes to achieve an acceptable minimum weight geometry subject to forced response. The most common sources of forced vibration are shown in Table 3.

TABLE 3	TABLE 4
Sources of Unsteady Forces in Rotating Turbomachinery Structures	STEP 1 IDENTIFY POSSIBLE SOURCES OF EXCITATION
o Aerodynamic sources	STEP 2 DETERMINE OPERATING SPEED RANGES
o Upstream vanes/struts (blades)	STEP 3 CALCULATE NATURAL FREQUENCIES
o Downstream vanes/struts (blades)	STEP 4 CONSTRUCT RESONANCE DIAGRAM
o Asymmetry in flowpath geometry	STEP 5 DETERMINE RESPONSE AMPLITUDES
o Circumferential inlet flow distortion (pressure, temperature, velocity)	STEP 6 CALCULATE STRESS DISTRIBUTION
o Rotating stall	STEP 7 CONSTRUCT MODIFIED GOODMAN DIAGRAM
o Local bleed extraction	STEP 8 DETERMINE HIGH CYCLE FATIGUE (HCF) LIFE (FINITE OR INFINITE)
o Mechanical sources	STEP 9 REDESIGN IF HCF LIFE IS NOT INFINITE
o Gear tooth meshes	STEP 10 CONDUCT STRAIN-GAGED RIG/ENGINE TEST TO VERIFY PREDICTED RESPONSE AMPLITUDE
o Rub	

There are ten basic steps involved in designing to prevent high cycle fatigue due to forced vibration. These are itemized in Table 4.

These steps involve evaluating the environment in which the component must operate (Steps 1, 2, & 5), predicting the aeroelastic characteristics of the component (Steps 3-8), investigating possible design changes (Step 9), and finally the actual measurement of the dynamic response of the component in the engine environment (Step 10). Step one calls for an identification of possible sources of excitation drawn from the inventory of Table 3. Step two concerns the speed ranges which the component will actually experience in service. Step three for most advanced designs will usually be done using a finite element analysis. Where disk flexibility is a factor, this must also be included. A typical example of a finite element mesh for a compressor blade is shown in Figure 23.

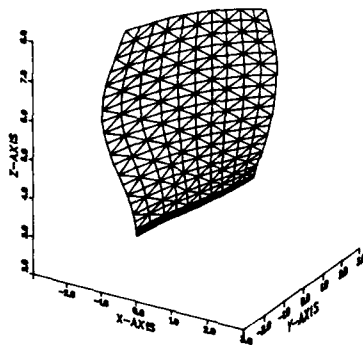


Figure 23. Example of Finite Element Mesh

This particular example used triangular plate elements and assumed a rigid disk. Depending upon the complexity of the airfoil, volumetric elements are also often used. Disk flexibility is often a factor and, when this is so, additional elements representing the disk are also included. The stiffness and mass matrices formed by these elements are solved to compute the natural frequencies. The more elements used, the more precise is the mathematical model.

Step four involves a presentation of the results of Step three in some manner which facilitates the identification of potential problems. This is most often accomplished by construction of a blade (and disc) resonance diagram often called a "Campbell" diagram. This is illustrated in Figure 24.

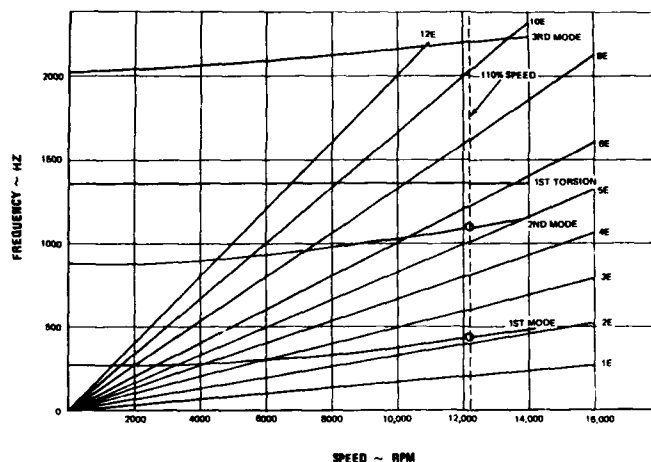


Figure 24. Blade and Disc Resonance Diagram

Note that the resonant frequencies of the airfoil increase non-linearly with speed; this is a result of the increasing stiffness of the airfoils as centrifugal stress increases. One of the designer's goals is to attempt to minimize the intersection of any airfoil resonant frequencies, particularly the lower order modes, with any excitations likely to be experienced in the compressor's operating range. This goes from 1-per-rev associated with unbalance, 2-per-rev associated with a common inlet distortion pattern, to N-per-rev associated with immediately adjacent blade rows up-and-downstream. All of the items listed in Table 3 represent potential excitation sources which bear examination.

Step five of Table 4, determination of the response amplitudes, is typically where we must resort to experience and empiricism. This empiricism may group typical blades by common mode shape, damping, type of source, and distance from the source to correlate with response experience. The use of an empirical method for estimating response is due to a current inability to adequately predict the strength of the forcing functions produced and the damping present in the gas turbine environment. The estimation of the blade stress distribution, Step six, is made by introducing the empirical estimates of Step five into a finite element stress computation. A modified Goodman Diagram is constructed from the properties of the material chosen, Step seven. An example is illustrated in Figure 25.

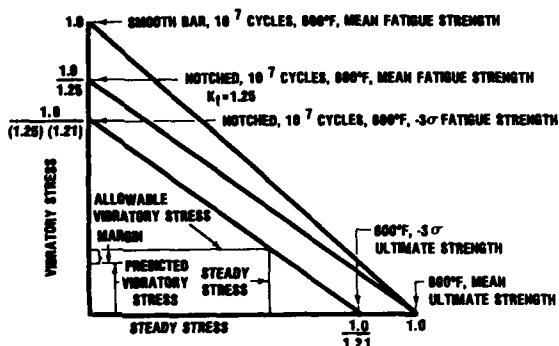


Figure 25. Typical Modified Goodman Diagram

From that, the vibratory stress margin is estimated permitting Step eight to be accomplished. If the result of Step eight is not satisfactory, Step nine must be accomplished. Otherwise, the final result is evaluated in Step ten from rig and/or engine tests. If redesign were required to obtain infinite fatigue life, a menu of possible changes is illustrated in Table 5.

TABLE 5

Typical forced vibration redesign considerations

- o Proximity of sources (gap/chord, P/Q)
- o Number of sources (resonance speed)
- o Geometry of sources (lower disturbance)
- o Geometry of resonant piece (stiffness and mass distributions)
- o Boundary conditions (type of fixity)
- o Increase system damping (coating, fixity)
- o Amplitude limitation (shroud gap)
- o Increase fatigue strength (geometry, material, temperature)

With respect to flutter, the designer is primarily interested in predicting its onset rather than attempting to predict a specific vibratory response level as with forced vibration. The object with flutter is to avoid it entirely whereas some level of forced vibration is unavoidable and must be dealt with. As mentioned earlier, the condition of flutter exists when the energy absorbed by an airfoil due to negative aerodynamic damping equals or exceeds the energy dissipated due to structural damping at the equilibrium vibratory stress level. Since, in most systems, the structural damping is not large, the design criteria essentially becomes designing for positive aerodynamic damping.

The five most common types of fan/compressor flutter are illustrated on a compressor map in Figure 26.

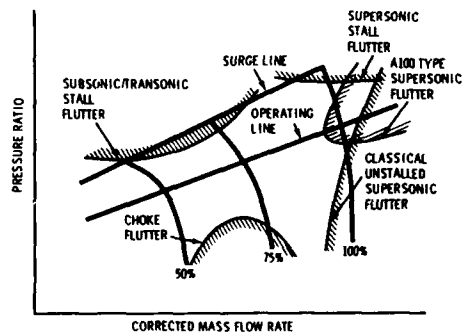


Figure 26. Types of Fan/Compressor Flutter

There are five design parameters dominant in the prediction of flutter. They are:

1. Reduced Velocity
2. Mach number
3. Blade loading parameter
4. Static pressure/density
5. Vibratory mode shape

The first four parameters are all aerodynamic. The fifth, the vibratory mode shape, is necessary since the vibratory displacement directly affects the magnitude and sign of the unsteady aerodynamic work per cycle. All five parameters are relevant to each type of flutter and are important elements of a flutter design system.

The first two parameters are dimensionless and appear in the governing equations for unsteady flow over a vibrating airfoil. Reduced velocity is defined as the ratio of relative inlet velocity to the product of blade vibratory frequency and blade semi-chord length (semi-chord equals chord/2). In general, the reduced velocity parameter will have a value between 1 and 5 at the flutter stability boundary.

$$\text{Reduced Velocity} = \frac{V}{b\omega}$$

A variety of blade loading parameters have been used for flutter correlations. These have included incidence or non-dimensional incidence, pressure ratio, diffusion factor, choke margin, and others. Either static pressure or density has been used as the fourth parameter. The primary effect of changing air density (or pressure) is a proportional change in unsteady aerodynamic work per cycle and therefore in aerodynamic damping. Increasing gas density is stabilizing if aerodynamic damping is positive; it is destabilizing if aerodynamic damping is negative.

The final dominant design parameter is vibratory mode shape. Since the blade unsteady surface pressure distribution is also a function of the blade mode shape (motion), the aerodynamic damping is also a strong function of the vibratory mode shape. The mode shape may be pure bending, pure torsion, or a coupled complex mode combining both bending and torsion. The low aspect ratio fan and inlet stages now entering service are particularly subject to these coupled modes if flutter is experienced.

Of the types of flutter illustrated in Figure 26, classical unstalled supersonic flutter is the only type of flutter for which a reasonably accurate analytical design system exists. The term unstalled is used because unstalled supersonic flutter is encountered when the stage is operating at a low pressure ratio relative to its potential. Classical is used because of its similarity to classical aircraft wing flutter. The existing analytical design system contains a blade-disk-shroud vibrational analysis, an unsteady flat plate cascade analysis, and an aerodynamic damping calculation. The result is the capability to calculate the aerodynamic damping for each mode (and nodal diameter if necessary) of a compressor blade/disk assembly. The simplest empirical classical unstalled supersonic flutter design system consists of plotting available data on a plot of reduced velocity versus inlet Mach number and drawing a curve (flutter boundary) which best separates the flutter and non-flutter data points. Such a curve is illustrated in Figure 27.

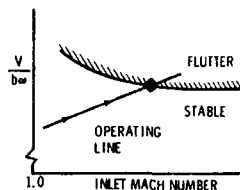


Figure 27. Typical Empirical Flutter Correlation

Any point below the curve should indicate freedom from flutter. Data points indicating the onset of flutter should be clustered about the shaded line. In general, all blades flutter at a common frequency.

Another of the types of flutter depicted in Figure 26 which can be empirically correlated by this approach is the A100 type supersonic stall flutter. The designation A100 derives from the model number of a particular engine in which this type of flutter was first observed. It is characterized by a torsional vibration of a shroudless blade. Its aerodynamic characteristics are unique in that there are stable operating points at both high and low loading but there is an intermediate range of loading at a given corrected speed which is unstable. All blades tend to vibrate at the same frequency and interblade phase angle in this mode.

The simplest form of correlation for the remaining three types of flutter depicted in Figure 26 is a plot of reduced velocity versus incidence angle such as shown in Figure 28. The first type illustrated in Figures 28 and 29 is subsonic/transonic stall flutter. Experience has shown that with such a correlation with parameters chosen at a representative spanwise location, it is possible to separate most of the flutter and non-flutter data with a curved line. The points A, B, and C shown in Figure 28 are the same ones shown in Figure 29 on a conventional compressor map. This type of flutter can prevent acceleration up an engine operating line. An unacceptable design can be corrected by design changes which decrease the reduced velocity, the blade loading or incidence, some combination of both, or by rematching the engine to lower the engine operating line on the map.

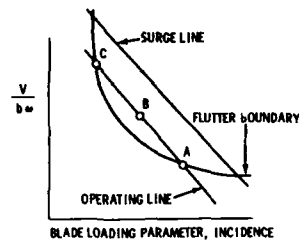


Figure 28. Empirical Flutter Correlation

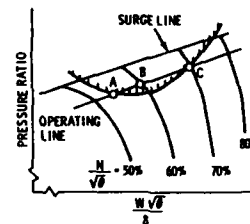


Figure 29. Subsonic/Transonic Stall Flutter

Vibratory mode shape is also a dominant subsonic/transonic stall flutter design parameter. For a given reduced velocity, a bending mode is much more stable than a torsional mode with the nodal line located near mid chord. This is illustrated in Figure 30 and requires that the designer evaluate the flutter margin in both modes. If bending and torsional modes are coupled by the presence of a flexible disk or part-span shroud or tip shroud, the ratio of bending to torsional motion and the phase angle between them must be considered in the flutter analysis. This is illustrated in Figure 31.

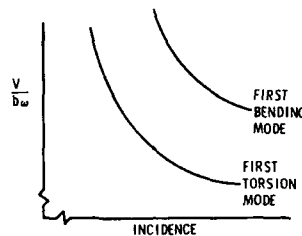


Figure 30. Flutter Correlation for Shroudless Blades

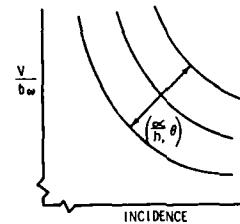


Figure 31. Flutter Correlation for Modes Coupled Through a Flexible Disc or Shrouds

Characteristics of subsonic/transonic stall flutter include non-integral order vibratory response, sporadic amplitude with time, stress levels which may remain constant or increase with blade loading, and blades which may vibrate at different frequencies and amplitude in the same mode, whether bending, torsion, or coupled.

Supersonic stall flutter can be empirically correlated in the same way as subsonic/transonic stall flutter. However, like unstalled supersonic flutter, all blades tend to vibrate at a common frequency. Experience indicates that the mode is generally first bending.

The last type of flutter, choke flutter, can also be correlated in the manner of Figure 28 as a function of reduced velocity and incidence. In the transonic flow regime, this usually corresponds to a negative incidence condition. Design changes to avoid this condition are the opposite of those to avoid stall flutter; namely an increase in reduced velocity or an increase in incidence would move one away from a choke flutter boundary.

Prior to manufacturing, for most designs, it is also important to correct the aerodynamic design for deflections due to steady state stresses and temperatures so that in the hot running condition the geometry will conform to the designer's intent. This means that the parts as machined will be slightly different. For high aspect ratio airfoils with shallow ramp angles, beam theory is often adequate to compute stresses and deflections. The corrections for deflection are then limited to a restagging of the airfoils. However, at lower aspect ratios and particularly with steeper ramp angles, a full finite element stress analysis must be accomplished and the deflection corrections must be applied over the whole surface. Thus both camber and stagger distributions are modified to define the cold static geometry.

Design System Weaknesses

The greatest weakness in axisymmetric design systems is the fact that they are axisymmetric and do not normally take secondary flows into account. Secondary flows are defined for this purpose as any flow which violates the assumption of flow confined to concentric streamtubes with no spanwise mass, momentum, or energy exchange. However, major progress has been made toward removing this deficiency in recent years. This also permits inclusion of end-wall losses where they actually occur since mixing precludes their accumulation in end-wall streamtubes. The improvements have resulted in a hybrid type of computation through which simplified empirical models of the more important

secondary flow features are incorporated through superposition on an axisymmetric computation. Since the computation with a streamline curvature code is inherently iterative, this is relatively straightforward to accomplish. The solution is typically started in the normal axisymmetric fashion and then, at some point before convergence is achieved, these corrections are introduced in the remaining iterations until the solution, hopefully, converges. The types of corrections introduced in this fashion include inviscid secondary flow, wake centrifugation, end-wall boundary layers, and turbulent diffusion, among others. The best published examples are those of Adkins and Smith [18] and Gallimore [19].

The next most important weakness in through-blade design systems is the lack of real data on parameter distributions inside a blade row. These include departure angle, losses, and blockage. As discussed earlier, at present one is forced to rely on logical assumptions which are only partly augmented by computations and experiments. The day appears not too far off when some combination of computational fluid dynamics and non-intrusive measurements will be able to answer these questions. However, this may still require several years.

The last significant weakness in contemporary design systems is their inability to take non-steady flow features into account. Non-steady flow has been found to influence the flow-swallowing capacity of transonic and supersonic stages and is also suspected to influence losses. It is not uncommon for a modern aircraft multi-stage compressor to have three or even four transonic or supersonic stages downstream of the inlet stage. The impact of a downstream stage overflowing is shown in Figure 32.

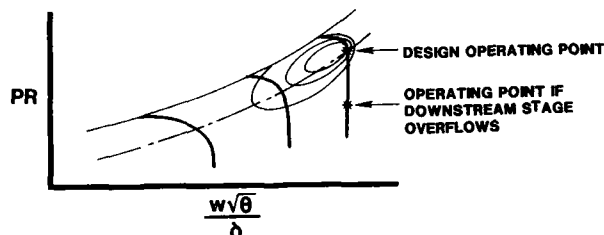


Figure 32. Effect of a Downstream Stage Overflowing

This compressor map illustrates the impact on an upstream stage, or block of stages, if a downstream stage overflows. The upstream stage or block is forced to a lower operating point on its characteristic. The efficiency is poorer and the work which this upstream stage or block could have accomplished is not achieved.

Lacking any other rational explanation for this behavior, it was hypothesized that this phenomenon was due to non-steady characteristics of the flow. It was further assumed that, since the flow-swallowing capacity of a supersonic cascade is normally defined by the inlet wave pattern, the non-steady wave pattern may be the primary cause of the change. This is illustrated in Figures 33 and 34.

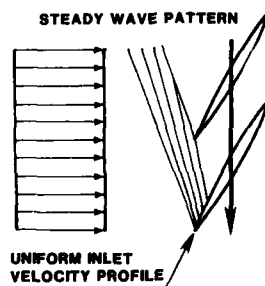


Figure 33. Steady Inlet Wave Pattern

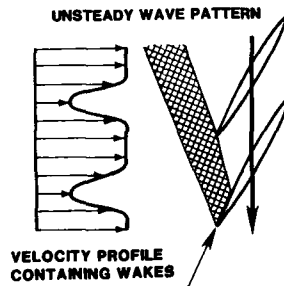


Figure 34. Non-Steady Inlet Wave Pattern

A numerical experiment was accomplished to examine this hypothesis. A non-steady Reynolds-averaged Navier-Stokes code was used to evaluate one particular cascade with one set of circumferentially mass-averaged inlet conditions. A non-dimensional inlet wake pattern was assumed for which the ratio of wake depth to wake width was held constant. The results are illustrated in Figure 35.

As the magnitude of the wake was increased from zero (equals a uniform steady flow) to higher values, note that the mass flow first increased, and then decreased below the uniform value. This effect is not yet fully understood and is now the focus of several computational and experimental efforts.

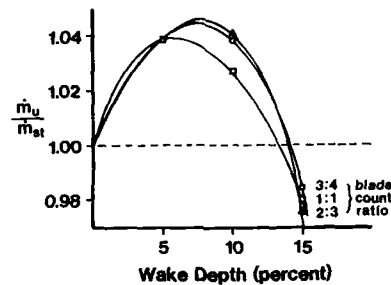


Figure 35. Variation in Cascade Mass Flow with Wake Depth

Current Design Trends

New compressors now under development, particularly for advanced military aircraft applications, exhibit three conspicuous trends. First, the aspect ratio of the blades is declining. Second, Mach numbers within the machine are increasing. Third, higher levels of diffusion are being employed. The first and third trends go hand in hand. It was finally recognized in about 1970 that at lower aspect ratios one could sustain significantly higher levels of diffusion due to three-dimensional secondary flow effects. Thus, with lower aspect ratios, one could reduce the number of stages required for a multi-stage compressor to achieve a given overall pressure ratio. The total length of a multi-stage compressor has only been reduced slightly in that the increased length of the low-aspect-ratio stages has almost equaled the length saved by reducing the number of stages. However, what has been dramatically reduced is the number of total airfoils required. Also, the airfoils of the low-aspect-ratio design are naturally much larger and more rugged than those of its high-aspect-ratio ancestor. Efficiencies have been reasonably well maintained. The higher Mach numbers are primarily a result of two factors. First, materials and mechanical design technology have both improved, permitting higher wheel speeds. Second, aerodynamic design technology itself has improved substantially so that we can now do a much better job of creating efficient designs for higher Mach numbers. For example, one variable now routinely considered is leading edge sweep, analogous to aircraft swept wing theory. Ten years ago, among compressor designers, this was almost unheard of.

Current Computational Goals

From the compressor designer's viewpoint, there are three major current computational goals. The axisymmetric throughflow code of the streamline curvature type is the work horse of the industry. Improvements to these codes of the hybrid type, such as those of Adkins and Smith [18] or Gallimore [19], are a number one priority. In this fashion, the most important three-dimensional effects can be incorporated into fast running codes efficient for design use. However, at present, there is no unanimity of opinion concerning which mathematical model--and they are very different--is more correct. The truth probably lies in some combination of both. A second major goal is an adequate treatment of non-steady flow effects. It was only in recent years that this was really recognized as being of some potential importance. Work in this area will probably be confined to two-dimensional cascade-plane computations of the non-steady flow. At this point, it is not yet clear how much of this effect is inviscid, and how much is a viscous effect. A third important area is three-dimensional computational flow models which are capable of taking into account the influence of adjacent blade rows. Most three-dimensional computations currently focus on a single blade row. It is very difficult to obtain an adequate representation of inlet and discharge boundary conditions. To make reliable use of three-dimensional computations in blade rows, major improvements need to be made in the treatment of boundary conditions.

References

1. Wennerstrom, A.J., "On the Treatment of Body Forces in the Radial Equilibrium Equation of Turbomachinery," Traupel-Festschrift, Juris Verlag, Zurich, 1974.
2. Smith, L.H. Jr., "The Radial Equilibrium Equation of Turbomachinery," ASME Transactions, Journal of Engineering for Power, Vol. 88A, No. 1, 1966.
3. Jennions, K. and Stow, P., "A Quasi-Three-Dimensional Blade Design System," ASME Transactions, Journal of Engineering for Gas Turbines and Power, Vol. 107, No. 2, 1985, pp. 301-316.
4. Novak, R.A., "Streamline Curvature Computing Procedures for Fluid Flow Problems," ASME Transactions, Journal of Engineering for Power, Vol. 89A, 1967, pp. 478-490.
5. Marsh, H., "A Digital Computer Program for the Through-Flow-Fluid Mechanics in an Arbitrary Turbomachine Using a Matrix Method," Aeronautical Research Council, R&M No. 3509, 1968.

6. Wright, L.C. and Novak, R.A., "Aerodynamic Design and Development of the General Electric CJ805-23 Aft Fan Component," ASME Paper 60-WA-270, 1960.
7. Koch, C.C. and Smith, L.H. Jr., "Loss Sources and Magnitudes in Axial Flow Compressors," ASME Transactions, Journal of Engineering for Power, Vol. 98A, No. 3, 1976, pp. 411-424.
8. Jansen, W., "The Application of End-Wall Boundary Layer Effects in the Performance Analysis of Axial Compressors," ASME Paper 67-WA/GT-11, 1967.
9. Stratford, B.S., "The Use of Boundary Layer Techniques to Calculate the Blockage from the Annulus Boundary Layers in a Compressor," ASME Paper 67-WA/GT-7, 1967.
10. Miller, G.R., Lewis, G.W. Jr., and Hartmann, M.J., "Shock Losses in Transonic Blade Rows," ASME Transactions, Journal of Engineering for Power, Vol. 83A, No. 2, 1961, pp. 235-242.
11. Crevelling, H.F. and Carmody, R.H., "Axial Flow Compressor Design Computer Programs Incorporating Full Radial Equilibrium, Part II," NASA CR-54531, June 1968.
12. Prince, D.C. Jr., "Three-Dimensional Shock Structures for Transonic/Supersonic Compressor Rotors," Journal of Aircraft, Vol. 17, No. 1, January 1980, pp. 28-37.
13. Wennerstrom, A.J. and Puterbaugh, S.L., "A Three-Dimensional Model for the Prediction of Shock Losses in Compressor Blade Rows," ASME Transactions, Journal of Engineering for Gas Turbines and Power, Vol. 106, No. 2, 1984, pp. 295-299.
14. Wennerstrom, A.J., "Experimental Study of a High-Throughflow Transonic Axial Compressor Stage," Journal of Engineering for Gas Turbines and Power, ASME Transactions, Vol. 106, July 1984, pp. 552-560.
15. Koch, C.C., "Stalling Pressure Rise Capability of Axial Flow Compressor Stages," ASME Transactions, Journal of Engineering for Power, Vol. 103, No. 4, 1981.
16. Schweitzer, J.K. and Garberoglio, J.E., "Maximum Loading Capability of Axial Flow Compressors," Journal of Aircraft, Vol. 21, No. 8, 1984, pp. 593-600.
17. Platzer, M.F. and Carta, F.O. ed., AGARD Manual on Aeroelasticity in Axial Flow Turbomachines, AGARD-AG-298, Vols. I&II, 1988.
18. Adkins, G.C. and Smith, L.H. Jr., "Spanwise Mixing in Axial Flow Turbomachines," ASME Transactions, Journal of Engineering for Power, Vol. 104, No. 1, 1982, pp. 104-110.
19. Gallimore, S.J., "Spanwise Mixing in Multistage Axial Compressors: Part II - Throughflow Calculations Including Mixing," ASME Transactions, Journal of Turbomachinery, Vol. 108, No. 1, 1986.

BLADING DESIGN FOR COOLED HIGH-PRESSURE TURBINES

par

P.F. BRY
S.N.E.C.M.A.
Centre de Villaroche
77550 Moissy Cramayel
France

1 - INTRODUCTION

The past fifty years have seen the tremendous development of jet engine propulsion. In this half century of research and development, two specific periods can be discerned: the first one, which lasted until the mid-sixties, can be characterized by a mostly empirical approach to the problems. Component design relied very heavily on systematic testing and flow calculations were carried out by using analytical methods and linearized theories; these were the only tools available before the generalized introduction of computational methods. Many impressive results were obtained through this approach which called for experience and intuition. Around 1965, the massive use of computers to determine the flow characteristics through a turbomachine marked the beginning of a new era. The first computational methods dealt with through-flow and incompressible blade-to-blade flow analyses. Then progressively, the simplifying assumptions were dropped one by one, and today, very sophisticated codes enable us to design blading for turbomachine as never before. It should, of course, be kept in mind that the advent of computational tools has not made obsolete the use of testing. However, testing should now be regarded not only as a means of checking performance for a given design but also as an opportunity to calibrate the complex computational methods used in design. The objective here is for the design tools to become so foolproof that a very reduced number of tests will be necessary to achieve optimal design.

For this purpose, testing has become very complex and has paralleled the increasing complexity observed in the domain of computational methods. As an example, we can cite the validation of 3-D viscous codes which requires very detailed flow descriptions including the measurements of turbulence components. Test rigs are therefore expensive facilities where advanced measuring techniques must often be implemented.

The above is true for the various engine components and especially for the cooled high pressure turbine which must operate under extremely rough conditions and demonstrate high performance, reliability and durability. The dramatic increase, over the past years, of the turbine inlet temperature, as illustrated in figure 1, has made the turbine designer's task extremely difficult. Unfortunately, meeting the various requirements, especially those demanding high performance and long life cycles, calls for contradictory design optima. High performance for highly loaded turbines can best be achieved by rather thin blades especially in the trailing edge region. Durability can only be guaranteed by reasonable surface temperature levels and gradients in the critical leading and trailing edge regions. Cooling of the trailing edge region can then only be achieved by bringing the internal coolant as close as possible to the critical point which means that the trailing edge region must be thick enough to accommodate a core. This simple example shows that the best compromise must be found for the inner and outer shapes of the nozzles and blades. And this can really only be achieved if internal and external designs are carried out by an integrated team of specialists.

The purpose of the present paper is to describe the tools that are available for helping today's design engineers to reach this objective. Examples of what can be achieved will be presented. Both theoretical and experimental aspects will be addressed since they are an integral part of the design process.

It is further pointed out that the present paper will extend somewhat beyond what is stated in its title. In fact we will not only cover the design of cooled HP turbines but also focus some of our attention on the design of the first LP nozzle behind the HP turbine because interaction problems between the HP and the LP turbines can be considered as a major design challenge. The HP turbine and the first LP nozzle cannot be treated separately and actually belong to the same component.

2 - DESIGN PROCEDURE

Compressors and turbines are designed using theoretical tools and computational methods. It is clear, however, that no current computer program can match the complexity of real flow through a turbomachine. Strong three-dimensional and viscous effects appear within and downstream of the simplest blade passage, for example secondary flows, 3D boundary layers on blades and endwalls and wakes from the blade trailing edges, just to mention a few. In addition, interactions between rotating and non-rotating components bring unsteady effects into the picture.

In the case of high temperature HP turbines, cooling adds a new dimension to the challenge of modelling internal flows through the machine.

The analytical solving of the entire problem cannot be envisioned for many years to come. Consequently, today's design is based on some fairly rough simplifications of the real flow that make it amenable to resolution on the current generation of computers.

Most design systems are based on the model introduced by Wu (1) for single blade rows. The model consists in breaking down the overall 3D problem into two problems where the flow is solved successively on two intersecting families of stream-surfaces S1 and S2 as shown in figure 2. The S1 surfaces correspond to blade-to-blade surfaces. On the S2 surfaces, the so-called through-flow is calculated.

Although it would be possible to solve the 3D problem using an iterative procedure linking the S1 and S2 surfaces, most designers have only been working with a single S2 stream-surface through the machine

and a number of S1 surfaces along the span, the latter being then axisymmetric. This design procedure, which is very widely used throughout the industry, is referred to as a 2.5D or quasi-three-dimensional design approach. It is still the starting point of any new design, although as will be seen, 3D-computations do come into play in the analysis mode.

It is a well established fact that the design of cooled high pressure turbines is a complicated process due to the fact that not only must aerodynamic problems be addressed, but also thermal aspects linked to high inlet temperature must be taken into account from the start. This leads to an intricate design procedure where various iterative loops interfere with one another. An attempt to depict this situation is presented in figure 3. The present paper will only deal with the external blading design and the cooling will be taken into consideration only from the point of view of its impact on the external shape of the blade and the external flow.

The various aspects encountered while defining a geometry can be classified into two categories: the first one corresponds to more specific design tasks where a geometry is actually determined from given constraints; in the second one, the geometry is thoroughly analyzed using methods which are usually more accurate than the design ones used in the previous step.

These two complementary stages will now be investigated in the following and each individual step will be presented.

3 - TURBINE DESIGN SYSTEM

3.1. Through-flow calculation

In most design systems, the initial design starts with the resolution of the through-flow on a S2 surface as defined previously.

The flow is always considered as steady in the frame relative to the considered blade row. The three-dimensional problem is reduced to a two-dimensional one by either neglecting the circumferential gradients in the general equations or by adopting a passage-averaging which introduces some fluctuation terms. The first approach can only be used outside of the blade row, while the second one can be applied within the blade row and therefore can provide valuable information about the effects of the blade geometry on the flow.

A very widely used method to compute the through-flow is the so-called streamline curvature method for which the radial position of the streamlines in any given axial station is determined through an iterative procedure in such a way that the flow equations are fulfilled and convergence is achieved.

For turbine design, this computation requires the specification of certain parameters for each blade row, for example the radial distribution of angular momentum at the HP nozzle exit and the radial distribution of work for the rotor. In order to minimize the effects of endwall phenomena, i.e., secondary flows, parabolic types of vortex radial distribution must be adopted on blade rows. These optimized distributions lead to opening the stators at the hub and at the tip to allow more flow in these endwall regions. Basically, this will have the effect of reducing the metal deviation close to the walls and lead to three-dimensional geometries.

The radial work distribution in the rotor will also be tailored in a such a way that endwall sections will be unloaded compared to the mid-span ones.

The loss distribution for each row must also somehow be specified. It can either be a given set of data or a correlation which is introduced as input or the result of some internal calculation linked to the computed flow properties as will be seen further on for the secondary losses.

Choice of reaction is naturally essential for any type of turbine stage. For high pressure turbine, its selection should not only be based on HP turbine performance but also on LP first nozzle-even first stage-efficiency. This is especially true for very highly loaded HP turbines where Mach number levels are very high and interaction problems between the HP and the LP turbines can take on some importance. Reduction of reaction from the optimal value for HP turbine can then bring an improvement to the overall performance through reduction of the LP first nozzle inlet Mach number and flow deviation.

For specific cooled turbine applications, cooling flows and parasitic flows must be specified in the through-flow calculation. These are characterized by their mass flows, temperatures and pressures as well as by the angles under which they are introduced into the main flow. The axial locations where this cooling air is introduced in the computation is of importance since it will have an effect on the turbine flow function and power output.

The design through-flow computation must still be considered as a basis for preliminary blade section design. It yields an approximation to the axisymmetric streamlines and stream-tube thicknesses through the blading. This piece of information is essential for quasi-three-dimensional blading design, but it must be stressed that the evolution of these parameters depends strongly on the assumptions made for the axial distributions of losses and turning through the blading as well as blade stack.

An example of such a through-flow computation is presented in figure 4 for an HP/LP turbine combination. Cooling flows are represented by small arrows distributed along the span. The streamlines obtained after convergence are likewise shown. For this application, a contoured flow-path in the HP nozzle has been used. The objective of this contouring is to reduce the secondary flow losses via action on the three-dimensional static pressure gradient through the blade row.

3.2. Flow-Path contouring

Back in 1960, work by Dejc (2) gave some indication on how to improve the efficiency of high hub-to-tip ratio turbines through flow-path contouring. This information was summarized in a set of curves (presented in figure 5) which linked the efficiency gain to the contraction ratio of the converging flow-path and to the aspect ratio of the blade row based on the exit blade height.

Since then, some in-depth research has been devoted to the understanding of the mechanisms that govern the flow through a contoured flow-path. We can cite, for example, Morris and Hoare (3), Kopper and Milano (4), Haas (5), Haas and Boyle (6), Boletis (7), Moustapha (8) and Arts (9) for theoretical and/or experimental analyses.

All authors agree that, when compared to classical cylindrical flow-path, outer flow-path contouring on a nozzle with constant inner radius has a small effect on the hub blade surface velocity distribution whereas large differences can be observed in the tip region close to the contour. Figure 6 from (7) is a classical example which shows how the suction side velocity distribution at the outer radius of the nozzle can be influenced by the geometry of the outer casing.

However, the situation is not as clear when one considers the radial loss distributions measured or estimated by the various authors. Most notice a small change of the losses in the contoured tip region of the blade row although a dramatic shift in the loss radial distribution may occur. This is not consistent with the strong effect of the contouring on the profile velocity distribution which would indicate a probable reduction of the secondary loss through reduction of the circumferential static pressure gradient. It should be noted, however, that the drastic change in suction side velocity in the first half of the blade may be compensated by an increase in the diffusion in the aft-portion of the profile. For the special case of transonic blades, this diffusion, if not carefully kept under control, can lead to a strong shock in the nozzle.

Outer flow-path contouring has a strong effect on the losses in the root region of a contoured nozzle. Secondary losses are greatly reduced although the mechanisms that lead to this reduction are not completely understood.

The overall gain through contouring can be expected to be of the order of half a point in turbine efficiency. However, for highly loaded HP turbines, it should be kept in mind that this gain could be offset by shock losses. Flow-path contouring may not be the best solution for high exit Mach number nozzles unless already highly forward loaded in cylindrical flow-path. Effect of induced curvatures on the rotor flow should also be taken into account.

For more conventional transonic blades, contouring can bring about an improvement but requires a fully integrated design of blade and flow-path in order to keep in check any undesirable overspeeds and the occurrence of strong shocks.

3.3. Blade section design

In the through-flow calculation, the velocity triangles at the inlet and the outlet of each blade row are determined along the span. These steady axisymmetric flow conditions will now be used as boundary conditions for designing blade sections that must also satisfy various aerodynamic and geometric constraints. For cooled turbine applications, these geometric constraints take the form of a thickness distribution in the leading edge but mostly the trailing edge region. In the latter, the internal cooling cavity must be brought as close as possible to the trailing edge which often must also accommodate a pressure side or a trailing edge slot.

The methods that deal with the aerodynamic designer's task of defining more efficient airfoils fall into two categories : the first approach is based on optimization techniques whereas the second one uses inverse design methods.

3.3.1. Optimization methods

The basis for the optimization methods is the use of a blade-to-blade analysis method coupled with a so-called optimization procedure which will successively modify the geometry until a given constraint is satisfied. The computation starts with a blade shape which is usually not too far from the final solution. It then proceeds by changing the overall geometry or only part of the profile to minimize, for instance, the difference between the computed and a desired blade surface velocity distribution.

Examples of such mixed mode methods have been presented by Tong and Thomkins (10) and Meauzé (11) using time-marching schemes to update the geometry. For each change of the latter, the computational mesh is updated until convergence is achieved. This procedure can be costly in computer time but some interesting results have been obtained as demonstrated in figure 7 from (11).

More recently, Cedar and Stow (12) proposed a mixed mode approach using a finite element velocity potential method. Update of the grid is avoided by use of a transpiration model to change the velocity potential boundary conditions on the blade surface.

Such optimization methods can also be extended to three-dimensions as in the contributions by Zannetti and Ayele (13).

3.3.2. Design methods

In this approach, one specifies the surface pressure distribution and the method calculates

the corresponding airfoil geometry. The first such design method was introduced by Lighthill (14) in 1945 for incompressible flow. He showed that one cannot prescribe any arbitrary velocity distribution in order to obtain a solution, but rather a given prescribed velocity distribution on the blade surface must satisfy certain constraints that deal 1) with the compatibility of the velocity distribution and the specified free-stream velocity and 2) with the closure of the profile. It has been shown that the same holds for compressible flow. Surface boundary layers can be taken into account within the design procedure via any fast integral boundary layer computation. The calculated displacement thickness is subtracted after smoothing from the computed profile to yield the final metal airfoil.

Examples of such design methods include the contribution by Stanitz (15), Schmidt (16), Giles and Drela (17).

Figure 8 gives an example of a first stage LP turbine nozzle designed with a method based on the work of Stanitz (15).

3.4. Blade stacking

In the usual design procedure, several SI stream-surfaces are used along the blade span to define blade sections. The final three-dimensional geometry of the blade is then obtained by stacking these blade sections in such a manner that some mechanical and aerodynamic constraints are fulfilled. In addition, for cooled blades, manufacturing problems related to the inner geometry of the cooling system must be taken into account.

When no such manufacturing constraints exist, great freedom can be applied in the stacking problem to optimize the radial loading distribution for the blade. In particular, leaning has been shown to be a powerful tool in influencing the radial loss distribution both for cylindrical and diverging side walls. Tests have been carried out for various values of blade lean angle (18). Figure 9, from Hourmouziadis and Hübner (19), gives a summary of these experiments. The loss improvement observed for blades having a lean angle such that the pressure side faces the inner/outer band can be traced back to a modification of the radial load distribution and of the radial static pressure gradient. According to Zhong-Chi Wang et al. (18) and Han Wanjin et al. (20), the latter causes the low energy boundary layer fluid near the walls to be sucked into the main stream zone with the effect of reducing the end-wall loss. Comments by Hourmouziadis and Hübner (19) do indicate, however, that leaning the blade as indicated previously may add another driving force to the mechanism leading to passage vortex formation and subsequent near wall suction side separation.

According to computations carried out by Hourmouziadis and Hübner, the main effect of leaning is a redistribution of the blade radial load. Quasi-three-dimensional Euler predictions of pressure distributions were obtained for a classical radial vane and a 15 degree leaned vane with the pressure side facing the hub. The results are presented in figure 10 from (19) and show a strong reduction of aerodynamic loading at the hub and the opposite effect at the tip. These computed results agree qualitatively with the measurements obtained at the hub of a 20 degree leaned vane and presented in figure 11 from (19).

These various observations have led some authors (18) to propose a blade with a curved stacking axis such that the pressure side faces the walls at the inner and outer radii and the middle part is radial. In such a design, the radial static pressure distribution encounters a minimum at the mean section, whereas the minimum is encountered at the hub for a conventional radially stacked blade. Figure 12 from (19) illustrates this concept. Dawes (21) performed a 3D Navier-Stokes analysis on just such a blade. Results are qualitatively in agreement with those reported in (18), (19), (20) concerning the reduction of loading in the endwall regions. The computation shows a strong increase of the loading at midspan as clearly demonstrated in figure 13 from (21). This increased loading causes a thickening of the suction side boundary layer.

The computation does not indicate a real improvement due to leaning. Computed total pressure contours are very similar for the radial and the leaned configurations. Furthermore, an increase of the secondary flows is observed, as clearly visible in figure 14 from (21) which compares the velocity vectors near the endwall with and without dihedral. This increase can be traced back to a shift of the saddle point separation away from the leading edge and to the driving force already mentioned by Hourmouziadis, which is caused by the inverted radial static pressure gradient.

It should be pointed out, however, that these computations were carried out with a very coarse mesh for a 3D Navier-Stokes code and thus some details of the flow may have been overlooked. In addition, the simple parabolic stacking selected for the sake of simplicity is probably not the optimal choice.

Cold flow performance tests of an HP turbine stage reported by Morgan (22) indicate a stage efficiency improvement of .8 percent with an optimized stacking versus a classical one for the HP nozzle. In this study, comparison is made between 1) a blade which is stacked along a straight line trailing edge, and 2) a geometry where the uncovered suction surface is concave over the span of the stator but the suction surface throat line is almost straight (see figure 15 from (22)).

Blade stack is obviously a powerful means of influencing the loading and loss distributions along the span of a given blade. However, the various aspects of the problem need to be assessed through experiment and detailed 3D computations. Furthermore when contemplating application to cooled turbines, it should not be forgotten that introducing complex stacking techniques will complicate the manufacturer's task even further due to the existence of the internal cooling system. This may limit the designer's freedom in his quest for improved performance.

As an illustration of the above, figure 16 gives a typical example of a cooled nozzle for the first stage of an LP turbine. This geometry has been designed for optimal adaptation to the HP turbine exit swirl. However, complex 3D stacking could not be incorporated due to the increased complexity this would have implied in the manufacturing process.

3.5. Constraints due to the internal cooling system

Current high pressure turbines that operate at very high temperatures must be cooled to guarantee durability. Cooling is achieved via internal convection, impingement and film cooling where the coolant is injected into the main flow via rows of discrete holes. To enhance internal convection, complex internal geometries are needed where heat transfer coefficients must be optimized- increased or not, depending on the overall configuration. Generally speaking, the internal coolant must be able to reach all portions of the blade and this requirement will have a direct impact on the blade outer shape. Of main concern for thermal design are the leading and trailing edges: the leading edge because this is where the pressure difference between internal and external flows is smallest, the heat flux is very high as well as the flame radiation for a nozzle; the trailing edge because it is the thinnest part of the blade, where the heat load can be felt from the suction as well as from the pressure side of the blade. In addition, this is also the hardest place for the coolant to reach due to thinness of the blade. For the leading edge, the requirements for a special outer blade shape are not as stringent as in the trailing edge region. In fact, the outer blade shape will more or less dictate the kind of cooling arrangement that will be selected. For pure convective cooling with turbulence enhancers, the blade nose should not be too thick in order to accommodate a small cavity in the leading edge where Reynolds numbers and heat transfer coefficients are high. In addition, the curvature of the profile when just leaving the stagnation point region should not be too high so as to allow drilling the film cooling holes at a small angle relative to the blade surface. This will help increase the film effectiveness and reduce the cooling losses induced by the perturbation of the boundary layer caused by the coolant ejection.

Cooling the trailing edge is usually more difficult because the geometry does not afford as many possibilities as in the leading edge region. Typically, current blades have a trailing edge thickness of roughly 1 mm, unless cooled via a slot in the trailing edge. For high Mach number profiles, the thickness in the aft-part of the blade is one of the main factors that will or will not lead to the occurrence of strong shocks in the blade passage. Minimizing this thickness and the trailing edge wedge angle is therefore necessary from the strict point of view of performance. For cooling purposes and durability, coolant must be brought as close as possible to the trailing edge. This then poses the problem of manufacturing the trailing edge cavity in a thin blade with skin thicknesses of the order of 0.5 to 1 mm. Tremendous difficulties are thus encountered when casting the blade with a thin core that has to be held in the right position. The trailing edge can therefore be said to best exemplify the necessity of finding a compromise between performance, durability and manufacturing requirements.

4 - LOSS PREDICTIONS

As indicated in figure 3, designing a turbomachine is the result of iterations between design and analysis procedures. The inverse procedure described above is typical of current practices used in the industry to obtain the first basic geometry of the blade. Following this initial task, a loss assessment must be completed at both design and off-design conditions. A whole new set of methods must now be implemented to determine the performance of the blading which may or may not fulfill the prescribed requirements. In the latter case, the geometry will have to be corrected and this will be achieved via the design loop.

It is obvious that one of the best ways to assess the loss of a given blade is to run a three-dimensional compressible Navier-Stokes code. A bit farther on, some attention will be devoted to this approach which will probably be available to future designers on a current basis. However, considering the present cost of such a procedure, not to mention certain technical problems that remain to be solved, more simplified methods are still widely used. In these procedures, the basic aerodynamic losses fall into two categories:

- 1) the profile loss linked to the surface velocity distribution, essentially a blade-to-blade problem, and
- 2) the secondary loss, which is strongly linked to the through-flow

In addition, for cooled turbine application, whatever the procedure, cooling losses must of course be taken into account in the loss assessment, which greatly complicates matters.

4.1. Quasi-3D and full 3D inviscid blade-to-blade analyses

A great deal of effort has been devoted in the past twenty years to the computation of the blade-to-blade flow through a turbomachine blade row. Back in the late sixties, Katsanis (23) made some pioneering contributions to the subsonic problem. Since then, many codes have been developed with specific applications and the various simplifications that were adopted in the early days have been progressively abandoned.

A whole set of blade-to-blade codes is now available for the designer, covering subsonic to transonic/supersonic flows, inviscid to viscous, two-dimensional to three-dimensional, and more recently, steady to unsteady. It is not our purpose here to describe all these methods. Instead, we will concentrate on a few examples of what can be achieved when using this computational approach. This affords us the opportunity to bring to light the problems that are currently encountered in blade profile design.

For inviscid subsonic and low transonic blade-to-blade analysis, the Katsanis code was for many years the standard method. In the past ten years, it has been progressively replaced by more advanced methods of the potential type such as the one developed by Luu and Monfort (24) for the quasi-three-dimensional case. The classical decomposition of the flow into an incompressible rotational part and a compressible irrotational one is applied. A finite-difference scheme is used to discretize the equations which are then solved on an orthogonal mesh obtained by a singularity method. Coupling with an integral boundary layer calculation is achieved via a transpiration model. Figure 17 shows an example of a comparison between the experimental and the computed (via Luu's method) surface velocity distributions on the nozzle for the first stage of an LP turbine at the mean-line. Although the results can be considered as satisfactory, there is still room for improvement in the leading edge region where the mesh is ill-adapted. Poor design in this region can lead to velocity spikes especially at off-design conditions. Great care should be taken to limit leading edge over-speeds both on the suction and the pressure sides, since they can cause laminar separation bubbles and increased loss. These spikes can be removed through a change in the geometry via a design method as illustrated in figures 18, 19 and 20 from Cedar and Stow (12).

Knowledge of the flow situation in the leading edge region is even more necessary for blades like HP nozzles where shower-head cooling is used in the leading edge area. In this case, the position of the stagnation point will not only influence the velocity distributions in the area but also the way the coolant will divide itself between the suction and pressure sides. In order to "capture" this stagnation point on a thick leading edge, C or O type meshes, such as the one presented in figure 21 for a transonic HP nozzle, must be implemented. However, it should be pointed out that even though the computation does yield plausible results in the immediate proximity of the stagnation point, it is hard to demonstrate the validity of the solution in this region due to measuring difficulties.

Figure 12 shows a comparison of the computed and experimental surface velocity distributions for the HP nozzle of figure 21. The calculated results were obtained with a time-marching method based on work by Viviani and Vuilliot (25). The quasi-three-dimensional unsteady inviscid Euler equations are solved with either a finite-difference or a finite-volume scheme. The multi-zone technique as well as the multi-grid scheme introduced by Ni (26) are used to optimize speed and accuracy. The experimental results were obtained in the VKI CT2 two-dimensional blow-down wind tunnel.

When computing quasi-three-dimensional inviscid flows through a turbine blade row, one has to deal with two problems: the first one is related to the stream-tube contraction while the second one concerns the trailing edge shock prediction. The first problem stems from the fact that the blade-to-blade computation does not take into account any loss production, except in the cases where shock losses are actually computed by the program or where a boundary layer code is coupled with the main stream computation. Even then, only part of the loss is taken into account while the rest of the entropy generation is ignored. To counter this deficiency, the stream-tube contraction obtained from the through-flow computation has to be corrected. This correction will naturally depend on the axial loss distribution which is prescribed for the blade. It should be kept in mind that uncertainties will remain concerning this distribution especially for the secondary loss and the HP/LP interaction loss. Furthermore, this assumption of loss distribution through the blade will also have an effect on the computed turbine flow function.

The other worrisome aspect of inviscid blade-to-blade computation is encountered in transonic turbines where trailing edge shock waves appear. A complex trailing edge flow structure linked to the blade thickness and boundary layer separation/reattachment must then be considered. The pressure side leg of the shock system will travel across the blade passage to impinge on the suction side of the adjacent blade. This causes a strong alteration of the velocity distribution. The boundary layer may then separate and in any case, will undergo transition at this very spot with an increase of the heat transfer coefficient. Prediction of this mechanism is therefore important for the overall design of the blade. Thus is the designer confronted with trying to solve a viscous related problem with an inviscid code. This can be accomplished in different ways:

The first solution is to adapt the blade trailing edge cusp which has to be introduced anyway to avoid unrealistic pressure distributions in this area. The problem here is that one never knows for sure whether the computed shock intensity is correct;

The second solution calls for models which can be based on base pressure correlations like the one proposed by Sieverding (27).

An alternative, of course, is to use a viscous blade-to-blade analysis. We will return to this point further on.

Naturally, similar problems are encountered with three-dimensional inviscid codes. Their utilization, however, brings such improvements to the design that they have become standard items in industrial design systems. Three-dimensional computer programs can calculate the flow in any complex geometry where strong radial equilibrium effects occur such as axial asymmetry of the stream surfaces or the presence of intense local radial flows. They can yield badly needed information about three-dimensional shock waves and help in the understanding of the choking condition of an annular turbine blade-row.

There is still some controversy over their ability to supply information about certain aspects of secondary flows. We will come back to this point later on.

Most of the three-dimensional calculations are based on the resolution via a time-marching method, of the three-dimensional unsteady or pseudo-unsteady compressible Euler equations. Different techniques are used by different authors; for example see Denton (28), (29), Van Hove (30), Brochet (31), Arts (32), Krouthen (33).

The method used at SNECMA solves the time-dependent Euler equations with a finite-difference or a finite-volume scheme. The compatibility equations are used to handle the boundary condition problem. For more information, see Brochet (31).

Povinelli (34) provides a partial assessment of the Denton code which may be considered as a standard program in the industry. Two test cases are considered.

The first one corresponds to a 67° turning annular stator cascade. Comparisons of experimental and computed results show very good agreement over the span of the blade. Naturally the greatest differences occur at the endwall and at the blade exit where secondary flows induce three-dimensional effects.

Good agreement was also obtained by Arts (32) with a low aspect ratio annular cascade having approximately the same turning as Povinelli's and a contoured tip endwall similar to the ones discussed earlier. In addition, a non-uniform inlet total pressure distribution corresponding to the test conditions was used in the computation carried out with a finite-volume code developed by Arts (32). The conclusion proposed by Arts is that three-dimensional inviscid analysis is able to compute three-dimensional rotational flows as well as the main secondary effects appearing in such flows, providing the mesh resolution is high enough to capture the strong radial gradients introduced via the non-uniform inlet total pressure or temperature. The results obtained tend to confirm the hypothesis that the main secondary flows (horse-shoe and passage vortex) are mainly an inviscid phenomenon due to the rotational character of the inlet flow, although viscosity is responsible for this rotational nature.

It seems however that Povinelli's second test case does not confirm this conclusion. This test case corresponds to the computation of the exit flow leaving a rotor in a low-aspect ratio turbine stage. Comparisons with experimental data were made for two operating conditions of the stage, i.e., a uniform and non-uniform radial temperature distribution at the stator inlet. For both cases, the nozzle inlet total pressure was also non-uniform. The measured inlet conditions specified for the computations are presented in figure 23.

The rotor inlet conditions for the 3D computations were obtained from the computed exit conditions of the nozzle 3D calculation. These nozzle exit conditions were circumferentially mass-averaged to yield steady inlet conditions for the rotor. Both stator and rotor exit velocities were matched to experimental data. The results for the rotor exit flow are presented in figure 24 from (34) which shows that the exit total temperature profiles are fairly well predicted, whereas the flow angle predictions are poor.

In contrast with Arts's conclusion, the discrepancy is attributed by Povinelli to the strong secondary effects that exist in the low aspect ratio stage and which cannot be taken into account by the inviscid calculation. Although it is not easy to reach a final conclusion, it should be noted that the mesh used by Povinelli has only 19 points distributed along the span, whereas the one used by Arts contained 31. Thus some information may have been lost with the coarser mesh. In addition, mass-averaging the nozzle exit flow induces a non-realistic stress upon the flow. As pointed out by Meauzé in this very Lecture Series, the only realistic way of calculating a turbine rotor flow is to take into account the stator-rotor interaction by computing the entire unsteady flow through the stage. We will address this problem further on.

Before closing this paragraph on inviscid blade-to-blade computations, the problem of the correction for the entropy generation in three-dimensional calculations must be considered. As mentioned previously, the entropy correction for quasi-three-dimensional blade-to-blade analysis is completed via modification of the stream-tube contraction. For three-dimensional analyses, the correction can be introduced by means of a distributed body force as proposed by Denton (35). This simple model enables viscous effects to be simulated at little extra computational cost. Taking into account these effects is not only necessary to compute realistic blade surface pressure distributions, but is also of major importance in turbine stage calculations in order to obtain the stage reaction ratio.

4.2. Boundary layer computations, cooling and related problems

Although some viscous blade-to-blade methods already exist, most design systems still rely on boundary layer calculations to determine the profile losses. These computations are usually two-dimensional and are coupled with the main stream calculations like in the case presented in section 4.1. The boundary layer analyses are then mostly integral methods which allow shorter computational time. For turbine application where the boundary layer is relatively thin, the coupling can be achieved using a direct mode for the main stream and the boundary layer calculations.

A great number of boundary layer codes have been developed over the years and it would be beyond the scope of the present paper to try to give an overview of these methods. Instead, we will try to review some of the problems which are encountered when dealing with the boundary layer on turbine blades.

4.2.1. Boundary layers and related topics

For turbine applications, predictions of losses always come together with predictions of external heat transfer coefficients. This leads to some specific problems regarding the prediction of transition and, as a consequence, turbulence modelling. The situation is further complicated by cooling. The high inlet temperature of current turbines requires that blades and vanes be protected not only by internal convective cooling, but also by blade surface film cooling. With the latter, the coolant is injected into the primary flow. This cooling flow may stay within the boundary layer or go through it; in any case

it will induce strong perturbations in the viscous layer. Experimental studies by Wittig and Scheier (36) and Pietrzyk, Bogard and Crawford (37) among others, clearly demonstrate this point.

Even without taking cooling into account, the thermal boundary layer problem is far from having been totally solved. Good results are usually obtained with most boundary layer codes as long as 1) the blade surface pressure distribution is smooth enough to allow transition to be clearly located; 2) curvature effects are not too large; 3) operating conditions of the blading do not lead to strong relaminarization of the flow like in the case of low Reynolds number conditions on the strongly accelerated pressure side of a blade; and 4) separation or strong shocks do not occur.

The problem of the turbulent model to be used is naturally one of the main aspects of boundary layer research. A difference must be made between models which do not predict transition between laminar and turbulent flows and those which compute this transition. To the first group belongs the classical mixing length model of which many versions exist. These models are combined with transition criteria such as the ones of Dhawan and Narasimha (38) or Abu-Ghannam and Shaw (39) among others. These criteria are based on a large body of experimental data obtained for various configurations ranging from flat plates without pressure gradient to realistic turbine blades. Studying various models for transition onset and length as well as curvature effects, Eckert, Goldstein and Simon (40) came to the conclusion that

- i) the Abu-Ghannam and Shaw model gives the best prediction for the start of transition;
- ii) the Dhawan and Narasimha model predicts the transition length and intermittency better than the others;
- iii) the Adams and Johnston (41) curvature model compares well with experimental data

Although these results can be considered as encouraging it must be kept in mind that simple models will probably never yield systematically good results for the numerous complex situations encountered in turbomachine design. In addition, for the specific cooled turbine applications, where durability depends largely on the boundary layer behaviour, more detailed information is often required than that provided by these models.

Thus one has to go over to more complicated models like the classical $k-\epsilon$ model for which the evolution of turbulence within the boundary layer is depicted via two transport equations for the turbulent kinetic energy and the dissipation respectively. Greatly improved versions of the basic model, not to mention advanced higher order ones, are now available. However, calibration of the constants that intervene in the models is still difficult. To put it simply, the more complex the model, the more coefficients have to be determined in order to match experimental data.

Figure 25 gives an example of the heat transfer coefficient computed on the suction side of a HP vane at two different levels of the Reynolds number. Calculations were run with the standard STAN 5 code (42) for which transition is imposed via a transition Reynolds number and with a finite-difference code developed at SNECMA (43) which computes the location of transition with the Mc Donald and Fish (44) model of transitional boundary layer together with the Adams and Johnston curvature model. Experiments were obtained in the CT2 two dimensional transient wind-tunnel of the Von Karman Institute.

The results presented in figure 25 can be considered as very satisfactory. Less satisfactory is the computation shown in figure 26 which corresponds to the heat transfer coefficient on the pressure side of a HP rotor blade section also tested in the CT2 wind-tunnel. The calculation was performed with the method mentioned above (43). For this application, laminar separation occurs near the leading edge, followed by reattachment. The boundary layer never really becomes fully turbulent due to the acceleration along the blade surface. The computation is clearly not capable of dealing with the strong gradients that occur in the region of separation.

For this special purpose, a new boundary layer method has been developed at the "Ecole Centrale de Lyon". The computation is based on a method proposed by Keller (45). The originality of the improved version is the introduction of coupling between the boundary layer and the simulated outer flow via a so-called "equation of interaction" which depicts the effect of the growth of the boundary layer along the blade surface. With this approach, leading edge separation bubbles can be partially taken into account as shown in figure 27. The large variations of the heat transfer coefficient due to the bubble can be reasonably well predicted. This ability of the code to describe boundary layer flows with strong local pressure gradients is a great advantage for the blade film cooling problem. In fact, injecting cooling flows into the primary blade-to-blade flow causes local separations that classical boundary layer calculations either oversee or cannot overcome.

4.2.2. Boundary layer with cooling

Prediction of boundary layer behaviour with film cooling is one of the main concerns of today's turbine designers. Not only must the loss, including cooling loss, be estimated, but so must the film effectiveness and the heat transfer coefficient in the presence of film. At current mean turbine inlet temperatures of 2000 K, between 7 and 12% of the HP compressor inlet flow is used as coolant to protect the HP turbine vane. This cooling air, after picking up heat within the blade via forced convection, is evacuated into the main flow and used as a protecting film on the blade surfaces. A certain number of rows of cooling holes are distributed along the surface according to the results of a complex optimization process which takes into

account the internal as well as the external thermal properties of the cooling air. In addition, cooling losses - i.e., losses induced by the introduction of cooling air into a hot blade-to-blade flow - must be considered all along so that the best achievable compromise can be reached between cooling and performance requirements.

Some contributions have already been made to the problem of the behaviour of a thermal boundary layer with cooling air from a row of discrete holes; see for instance Herring (46) and Miller and Crawford (47). The latter proposed an extension of the above-mentioned STAN 5 code in order to include an injection model. The comparisons between the computed results obtained with these models and experimental data show good agreement but only for blowing rates smaller than 1 or large relative spacings for the cooling holes or injection angles smaller than 45°. Applicability of these models to actual turbine design is therefore limited.

More recently, Schönung and Rodi (48) proposed an approach in which a finite-volume boundary layer computation is coupled with a cooling model taking into account two aspects of the flow via an injection model and a dispersion model. The injection model deals with the initiating of the boundary layer profiles after the injection while the dispersion model handles the three-dimensionality of the flow via additional terms which simulate the lateral mixing within the region of the jets. The originality of the method lies in the systematic use of a three-dimensional jet computation to obtain the information necessary for the development of the two above-mentioned models. Comparisons of computed results with experimental data show good agreement for the film effectiveness and the heat transfer coefficient as demonstrated in figure 28 for the film effectiveness and figure 29, for the heat transfer coefficient; both figures are taken from (48). Results were obtained on a highly curved turbine blade.

It should be noted, however, that models such as the one developed by Schönung and Rodi are still in the research stage although one might conclude from the quality of the comparisons between experiments and theoretical results that application to actual design will follow shortly.

In most design systems, prediction of cooling losses, film effectiveness and heat transfer coefficients are still based on simplified models and experimental correlations.

For cooling losses, mixing models have been developed in the past by various authors; see, for example, Hartsel (49). These models are often one-dimensional and take care of the thermodynamic mixing loss that is observed when mixing two flows having different thermodynamic properties and different directions. These models can be coupled with classical boundary layer computations which may take into account the aerodynamic effect of the film injection usually via displacement of the transition up to the location where the film is injected.

4.2.3. Cooling problems

Experimental correlations are also commonly used to deal with cooling. They are obtained in two- or three-dimensional cascade tests where the blowing ratio is varied for various film configurations, i.e., film location on the blade surface and injection angle. Figures 30 and 31 show examples of results obtained at NASA for the cooling losses on a core vane (50). This figure illustrates the well-known result that suction side cooling is detrimental to the blade efficiency, especially for films that are located close to the throat. This correlates well with results presented by Haller and Camus (51) which show the strong perturbation induced by film cooling in the region of the throat on the suction side velocity distribution; see figure 32 from (51).

Film effectiveness and heat transfer coefficients in the presence of film can also be determined experimentally. Correlations of the type presented in figure 33 can be obtained in two- or three-dimensional cascade tests. However measuring these characteristics, especially the heat transfer coefficient, is usually not as straightforward as measuring the cooling loss. A common practice is to use a transient technique where the blade surface temperatures are recorded while the flow establishes itself like in the above-mentioned VKI wind-tunnel. The problem is then to have a good knowledge of the blade internal conditions in terms of heat transfer. This is fairly easy as long as the transient is short enough and the blade is solid. However, the situation is much more complicated when one contemplates modern multi-cavity blades which can in no way be considered as a semi-infinite medium. The data reduction of the temperature transient will then strongly depend on the internal boundary conditions to which less research effort has been devoted.

Cooling problems are even harder to solve in the leading edge region of turbine blades. The stagnation point of a turbine blade is one of the most critical areas as it is exposed to an important level of heat flux. Considerable attention is always devoted to this region where strong internal convection is applied together with external film cooling. Obviously, cooling jets have a strong effect on the fluid mechanics of the stagnation point region. Detailed measurement of the blade surface heat transfer coefficient in the shower-head region of a HP rotor blade have been performed by Camci and Arts (52) in the VKI transient cascade wind-tunnel. These experiments show the importance of being able to locate precisely the stagnation point at the design stage as already pointed out in section 4.1. It should be mentioned, however, that HP vane leading edge thermal design should try to do without external film cooling whenever possible. The reason is naturally to be found in the low internal to external total pressure ratio that exists at the vane leading edge: it is of the order of 1.015 to 1.03. With such low pressure margins, hot gas ingestion at the leading edge becomes a hazard that has to be seriously weighed for very high temperature operation. We wish to close this chapter by addressing the problem of trailing edge cooling which is the other main difficulty that confronts the designer. Two technologies of trailing edge cooling arrangements are currently available: slots

or holes which are installed within the thickness of the trailing edge or on the pressure side.

The advantage of slots or holes in the trailing edge is evident from the cooling point of view. The cooling effect is more symmetrical with respect to the suction and pressure sides and is also more efficient. The main disadvantage comes from the increased trailing edge thickness which is necessary to accommodate the slots or holes. For uncooled operation in the transonic regime, this invariably leads to a dramatic increase in the trailing edge loss. Cooling has a strong effect on the flow in the trailing edge region and especially on the complex shock structure that is encountered in transonic and supersonic operation, as clearly shown by Sieverding (53). The ejection of coolant through the trailing edge considerably affects the base pressure in turbine cascades. An increase of the base pressure which should correspond to a decrease in losses is observed for a small amount of flow ejection. However, it is not quite clear whether this compensates for the increase in trailing edge loss due to the blade thickness. See Xu and Denton (54) for a discussion on this point.

Consequently, designers often prefer to use pressure side trailing edge slots which do not require thick trailing edges. Like in the case of the trailing edge slot, coolant blowing has an effect on the shock structure in the trailing edge region. In addition, the presence of ribs between the slots can be clearly felt and leads to a three-dimensional exit flow. It seems that the coolant flow has the effect of weakening the trailing edge shocks.

Measurements of cooling losses associated with pressure side trailing edge cooling indicate that this solution is favorable from the point of view of blade efficiency; the measured loss is generally very small.

4.3. Secondary flows

Secondary flow prediction has been a deep concern of the turbomachine designer for many years now. The basic effects of the secondary flows - i.e., loss production, over/under turning of the flow at the blade exit and blockage - were recognized early in the development of compressors and turbines. A great amount of research has been devoted to the problem both in the experimental and theoretical fields. A summary of some recent experimental investigations on the subject can be found in Sieverding (55).

Experiments show that secondary effects can be very large in a turbine blade passage and therefore should be taken into account in the early stage of the design process.

To compute the secondary phenomena, the designer is faced with the alternative of running a three-dimensional Navier-Stokes code or using a simplified approach. The first option is naturally very time consuming and assumes that the blading has already been designed. It may be argued that the three-dimensional Navier-Stokes code can be replaced by a three-dimensional Euler code according to the conclusion of Arts (32). This point has already been discussed in Section 4.1. In any case, the taking or not taking into account of the viscous terms in the flow equations will not change the requirement for a full three-dimensional geometry which will only be available after an initial loop of the design process.

In order to fulfill the requirement for secondary flow information at the early stage of design, the second option - i.e., a simplified secondary flow theory - is necessary. These models can be coupled with through-flow computations and yield information on blade exit angles, losses and additional blockage.

One such method is the one developed by Leboeuf (56) which has been in use for many years at SNECMA both for compressor and turbine design. Figure 34 shows an example of the exit angle computed in the inlet nozzle of a low pressure turbine where secondary flow effects are usually very strong and are felt up to a distance corresponding to approximately 25 percent of the span from the side walls. Such results are valuable when available at the very start of a design since they leave room for correction to compensate for these effects, i.e., optimization of the vortex distribution and adaptation of the following blade row.

No matter how accurate these simplified methods may be, they cannot fill the need for more detailed methods. This is especially true for cooled turbine design where one of the main concerns is how the cooling flows will be swept away by the secondary phenomena in the endwall regions since cooling the wrong part of the blade may have a tremendous effect on its longevity. This prediction can only be achieved with complex three-dimensional codes. The resolution of the full three-dimensional Reynolds-averaged Navier-Stokes equations will certainly bring about a solution to this complex problem.

4.4. Navier-Stokes blade-to-blade computations

Numerous solutions to the Reynolds-averaged Navier-Stokes equations have been proposed in the past five years both for two and three-dimensional applications. Once again, it is not the purpose of the present paper to describe these methods in detail. We will try instead to show how these recent computations can help in solving some of the problems that were mentioned previously. It should be kept in mind, however, that these complex methods, at least for three-dimensional applications, cannot be considered as much of an integral part of the design system as, for instance, the Euler three-dimensional computations. The reason for this is naturally to be found in the cost and time involved in the running of these computations, but also in the problems that remain to be solved.

However, it is already felt that real optimization of converging side walls, three-dimensional

stack and, generally speaking, complex blade geometries will only be achieved through use of these powerful tools.

For intensive use in a design loop, progress remains to be made in numerical methods, especially for three-dimensional flow computations, and in computer performance. Of course, the improvement of turbulence models is still one of the main concerns in the development of Navier-Stokes codes not only for three-dimensional, but also for two-dimensional applications. Much work remains to be done in the areas of transition, free stream turbulence effects, trailing edge and wake regions, skewed inlet boundary layers and turbulence associated with coolant ejection. One question that arises when running Navier-Stokes computations is related to the separation of real viscous effects and numerical viscous effects which is necessary in the assessment of the turbulence models. Improvement of both numerical methods and turbulence models is therefore closely related.

In spite of these shortcomings, impressive results have already been obtained with viscous flow computations. Figures 35 and 36 present results obtained by Weinberg et al. (57) with a solver using an implicit scheme for the two-dimensional time dependent Reynolds-averaged Navier-Stokes equations. The comparison of measured and computed velocity distributions on the classical C3X vane are shown in figure 35. Good agreement is observed although the computation exhibits some difficulties in the overspeed region at $X/CX = 0.6$. This would tend to indicate that the trailing edge shock system is not well predicted. Computed results concerning the heat transfer coefficient are compared to measurements in figure 36. Computations were run first, assuming a fully turbulent flow along the blade surface, then, transitional flow. The already mentioned model of Dhawan and Narasimha (38) was used for the intermittency in the transitional region together with a standard Prandtl mixing length model. Obviously, the assumption of fully turbulent flow over the blade surface is not relevant and even simple modelling can yield a satisfactory representation of the blade surface heat transfer distribution.

Such is not always the rule, however, and confidence in any turbulence model will only be built on numerous test cases. The reader is referred for instance to work by Birch (58) who clearly demonstrates the need for improved turbulence models for reliable heat transfer predictions.

An interesting application of a three-dimensional Navier-Stokes computation is proposed by Davis, Ni and Carter (59). It concerns the prediction of leading edge pressure side separation induced by a velocity spike of the kind that was discussed in the previous sections. Figure 37 taken from (59) shows the predicted viscous blade pressure distribution on a turbine cascade versus the inviscid one; experimental data is also indicated. The predicted streamline pattern is presented in figure 38 where the separated flow region clearly appears on the pressure side of the blade. For this test case, the computation was run on the assumption of fully turbulent flow on the suction side and a transition on the pressure side determined from an empirical correlation for closed transitional separation bubbles. The turbulence model is the classical two-layer model of Baldwin-Lomax.

Good agreement between computed and experimental blade surface pressure distributions can also be obtained with three-dimensional viscous codes; see for instance Rhie (60), Nakahashi et al. (61), Subramanian and Bozzola (62). One of the main objectives of three-dimensional computations is naturally to calculate secondary effects. Figure 39 and 40 from (62) show the Mach number contours and the velocity vectors obtained at 1.2 percent span from the endwall of a low-speed linear turbine cascade. The saddle point near the leading edge of the blade is clearly visible.

Before closing this paragraph, attention is called over the problem of grid generation. Use of adequate grids is one of the main conditions for obtaining satisfactory computed results. This is particularly true for turbine applications where numerical viscosity can appear especially in the leading edge region of the rounded blade. The same problem was encountered in inviscid computations but takes on a new dimension in viscous flow calculations where real viscosity effects should not be perturbed by numerical ones.

4.5. Unsteady stator/rotor interaction

To conclude this long chapter on blade-to-blade computations and loss estimates, a few lines will be devoted to a point that turbine designers will have to confront in the future, i.e., unsteady stator/rotor interaction. Over the past few years, an increasing amount of research has been devoted to unsteady flows. Fourmaux (63), Giles (65) have calculated inviscid stator/rotor interactions in two dimensions and Lemeur (64) in three-dimensions. Rai has performed two-dimensional and three-dimensional Navier-Stokes computations of the stator-rotor interaction in a turbine stage (66), (67).

The main problem for the stator/rotor interaction is how to treat the interface condition when the stator/rotor pitch ratio is not a small integer ratio. Various techniques have been employed, such as changing the pitch of one blade row while changing the chordlength to retain the solidity (see Rai (67)), or applying a circumferential extension of the computed interface conditions (see Lemeur (64)). These procedures are used to bring the non-periodic problem back to a periodic one. The most satisfying approach is the one proposed by Giles (65) where a lagged periodic condition is applied which takes into account the fact that spatial periodicity does not necessarily mean temporal periodicity especially for viscous computations. Figure 41 taken from (65) shows an example of the two-dimensional stator-rotor interaction in a transonic turbine stage. The shock propagation and reflection are clearly visible. They induce a 40 percent variation of the lift on the rotor causing increased losses.

When computing three-dimensional inviscid interaction in choked transonic/supersonic turbines, simulation of losses through the blade rows becomes essential since it is the only way to obtain the correct stage reaction.

Introduction of these new codes into the design procedures involves two formidable problems :

- i) confidence in the computed results must be built up among the designers, i.e., validation must be achieved on a number of realistic configurations. This poses the problem of collecting the unsteady data that is needed to allow useful comparisons with computed results. Facilities like the MIT Blowdown Turbine Facility (68) have already begun to provide such data (69), but the effort will have to be sustained.
- ii) even if these codes could be fully validated today, their employment in a design procedure does not appear as straightforward. Many questions arise concerning the way of comparing two distinct designs. On what criteria can a given design be analyzed when unsteady flow is involved? Are steady state averages representative of the performance? The problem of defining relevant averaged values is also important. These various aspects will have to be confronted in the future if designers are to be able to take full advantage of what research will be offering soon.

5 - EXPERIMENTAL VALIDATIONS

The last chapter of this paper is devoted to experimental validations. Naturally, totally separating computations from experiments is not at all representative of the way development is actually carried out in the industry. Design of an engine is the result of closely integrated activities in the computational and experimental domains. It is true that actual design is carried out with computational methods. However, test rigs are as necessary as powerful computers to obtain a good product. It is mainly the way the experimental facilities are used that has changed in the past few years. Whereas before, large number of tests were required to design a component, the use of computational design methods has had the effect of reducing the amount of testing to obtain optimized performance. As a consequence, test rigs that were exclusively used to fine-tune performance became available for something else and testing took a new direction. Of course, tests are still required to fine-tune a turbine or a compressor or to validate overall component or engine performance. However, great emphasis is now given to the calibration of the design methods as well; this has led to a new philosophy concerning the complexity of new equipment and especially the amount and the quality of the instrumentation involved in testing.

Development of a cooled HP turbine is a very costly and difficult enterprise which requires a large number of component tests to check not only the blading aerodynamic and thermal performance but also disc cooling, mechanical design, bearings, etc... Optimization of this very high temperature component is typically something which takes many years of sustained effort. For the aero-thermal performance, these component tests take the form of two- and three-dimensional cascade tests, warm turbine tests, hot core tests and finally engine tests. The latter will not be considered here although they correspond to the ultimate application and the real conditions. However, engine instrumentation is often too limited to obtain an accurate picture of the HP turbine performance and the designers will prefer to use core tests where more freedom is offered to install probes and sensors.

5.1. Cascade tests

Two- and three-dimensional cascade tests are still a powerful tool to study new concepts of blading, to verify overall performance, to gather data in order to calibrate computational methods or simply to obtain empirical correlations.

A typical example for this latter application concerns tests that are run to obtain correlations on cooling effects on performance, film effectiveness and heat transfer coefficient in the presence of film. These experiments are often carried out in two-dimensional cascade wind-tunnels operating either in continuous or transient mode. SNECMA has been working in close collaboration with the Von Karman Institute to study these problems. Many tests have been run on the VKI CT2 two-dimensional cascade wind-tunnel which is quite representative of a state of the art transient facility. Figure 42 presents an overall view of this tunnel for which more information can be found in Richards (70). The heat transfer measurements are obtained via a transient technique using thin film gauges installed on glass ceramic blades. A typical blade model is shown in figure 43 where the thin film sensors are clearly visible. The technique used here is similar to the one pioneered at Oxford University and described in numerous publications; see, for instance, Schultz and Jones (71) for the principles and Jones (72) for a summary of Oxford studies.

Such facilities can not only yield information on the heat transfer characteristics but also on the loss which is then measured via a high response probe mounted on a high speed traversing mechanism. In addition, data about the detailed behaviour of the boundary layer can be obtained through in-depth analysis of the response of the thin film gauges; see for instance Arts and Graham (73).

Annular cascades of the same type exist, notably in England at the RAE at Pyestock (74), or are presently in development (like the CT3 Annular Cascade Transient Facility at VKI). Compared to two-dimensional facilities, they offer similar information in a more representative geometric and aerodynamic environment.

Partial or full annular cascade tests are also carried out to check thermal computational methods in a hot environment which is representative of actual engine conditions. Complete maps of the metal temperatures are determined both in steady and transient conditions and compared to compu-

ted results. In such tests, durability is also analyzed. Figure 44 shows an example of a rotor blade ready for a hot tests.

5.2. Warm turbine tests

Annular cascade tests should be restricted to nozzle guide vanes although some arguable approximations can be made for rotor blades and then only for special objectives (like in the previous paragraph, for durability testing, for instance). However, as soon as aerodynamic performance is involved, rotating blades have to be considered. Similarly, for aerodynamic studies on transonic HP turbines, instrumentation becomes a main concern because of the possible interaction between the probes and the high speed/high swirl flow in a confined flow-path. Minimizing the size of instrumentation is then of utmost importance and this means that temperature levels in the flow must be restricted to avoid using cooled probes that would certainly perturb the flow. One is thus led to carry out detailed turbine flow measurements in warm turbine facilities for which the inlet temperature level is high enough to allow simulation of the temperature ratio between primary air in the flowpath and ambient temperature coolant, yet low enough not to require cooled instrumentation.

These warm turbine facilities are usually very complex. Figure 45 and 46 give an example of the warm turbine facility used at SNECMA. In order to study the effects of cooling on the losses, a large number of independent cooling circuits must be available; cooling flows are adjustable. The primary flow is heated through a combustor before entering the turbine. Power is absorbed through a water brake. Special high speed yet steady flow measuring techniques have been implemented which allow gathering a very large body of data in a very short time. Extremely detailed flow field maps can be obtained to study phenomena like secondary flows, flowpath contouring or blade stacking. Many subjects of interest in turbine design can be thoroughly analyzed like tip clearance losses with shroud cooling (including the effects on the LP turbine first nozzle) or overlap geometry. Cooling problems are naturally one of the main topics of interest.

5.3. Hot core tests

Testing a turbine in a warm test rig is very well suited to obtain detailed pictures of the flow through the machine. However, it has the disadvantage of representing somewhat idealized conditions especially from the point of view of the actual geometry under real engine conditions. In addition, in a warm turbine test, real inlet pressure and temperature profiles to the turbine cannot be perfectly simulated, especially the circumferential temperature distortion induced by the combustor. In any case, for thermal analysis, including durability, hot tests must be carried out to complement the information gathered under cold or warm conditions. For high pressure turbines, these hot tests are executed on core engines.

Naturally, aerodynamic instrumentation cannot be as accurate in this aggressive engine environment as in warm turbine tests. Thus, from the point of view of aerodynamic performance, less should be expected from these core tests than from warm experiments. In addition, turbine power output is also subject to much more uncertainty when obtained from high pressure compressor measurements - including bleed mass flows and temperatures - than from torque measurements. Another source of uncertainty in the estimate for the turbine power output can also be found in the internal parasitic power dissipation which is more difficult to evaluate in core tests due to the added complexity on the core engine as compared to the more simple configuration of the warm test rig. For all these reasons, turbine designers are usually somewhat wary of the aerodynamic performance deduced from core tests or engine tests and will use them primarily for thermal development.

Figure 47 shows an overall view of a research core which is used at SNECMA and is dedicated to the calibration of turbine thermal methods and the development of new generation cooling systems. Close to 700 measurements are installed on the engine, most of them on the one stage transonic turbine.

Finally and to conclude this paper, the M88 core engine is presented on its test stand in figure 48. Even though the amount of instrumentation for the turbine is naturally smaller than in the above mentioned research core test due to the complexity of the actual engine environment and the extremely high temperature, several hundred measurements are still devoted to the analysis of the turbine aero and thermal performance.

With all this experimental data available, the difficult task of the design engineer is then to evaluate the actual performance of the turbine and to build correlations between test results and his computational design methods in order to improve the latter and pave the way for the design of even better machines.

REFERENCES

- (1) Wu, C.H. : "A General Theory of 3D Flow in Subsonic and Supersonic Turbomachines of Axial, Radial and Mixed Flow Types" Trans. ASME pages 1363-1380, Nov 1952.
- (2) Dejc, M.E. : "Method of Increasing the Efficiency of Turbine Stages with Short Blades" Translation n°2816, Associated Electrical Industries Ltd. (Manchester) 1960.
- (3) Morris A.W.H., Hoare R.G. : "Secondary Loss Measurements in a Cascade of Turbine Blades with Meridional Wall Profiling" ASME Paper n° 75-WA/GT - Nov 13, 1975.
- (4) Kopper F.C., Milano R., Vanco M. : "An Experimental Investigation of Endwalls Profiling in a Turbine Vane Cascade" AIAA Paper n°80-1089, June 1980.
- (5) Haas J.E. : "Analytical and Experimental Investigation of Stator Endwall Contouring in a Small Axial Flow Turbine. I-Stator Performance" NASA TP 2023-1982.
- (6) Haas J.E., Boyle R.J. : "Analytical and Experimental Investigation of Stator Endwall Contouring in a Small Axial Flow Turbine - II - Stage Results" - NASA TP 2309 - 1984.
- (7) Boletis E. : "Effect of Tip Endwall Contouring on the Three-Dimensional Flow Field in an Annular Turbine Nozzle Guide Vane : Part I - Experimental Investigation" ASME Paper n°85-GT-71.
- (8) Moustapha S.H. : "Investigation of the Effect of Two Endwall Contours on the Performance of an Annular Nozzle Cascade" AIAA/SAE/ASME/ASEE 21st Joint Propulsion Conference - Monterey 1985.
- (9) Arts T. : "Effects of Tip Endwall Contouring on The Three-Dimensional Flow Field in an Annular Turbine Nozzle Guide Vane : Part II - Numerical Investigation" ASME Paper 85-GT-108.
- (10) Tong S.S., Thompkins W.T. : "A Design Calculation Procedure for Shock-Free or Strong Passage Shock Turbomachinery Cascades" ASME Paper 82-GT-220, 1982.
- (11) Meauzé G. : "An Inverse Time Marching Method for the Definition of Cascade Geometry." ASME Paper 81-GT-167, 1981.
- (12) Cedar R.D., Stow P. : "A Compatible Mixed Design and Analysis Finite Element Method for the Design of Turbomachinery Blades" International Journal for Numerical Methods in Fluids Vol.5,331-345 (1985).
- (13) Zannetti L., Ayele T.T. : "Time Dependent Computation of the Euler Equations for Designing Fully 3D Turbomachinery Blade Rows Including the Case of Transonic Shock Free Design" AIAA 25th Aerospace Sciences Meeting, Jan. 12-15, 1987 RENO.
- (14) Lighthill M.J. : "A New Method of Two-Dimensional Aerodynamic Design" Aeronautical Research Council RnM 2104, 1945.
- (15) Stanitz J.D. : "Design of Two-Dimensional Channels with Prescribed Velocity Distributions along the Channel Walls" NACA Rep 1115, 1952.
- (16) Schmidt E. : "Computation of Supercritical Compressor and Turbine Cascades With a Design Method for Transonic Flows" Trans of the ASME Vol. 102, Jan. 1980.
- (17) Giles M.B., Drele M. : "Two-Dimensional Transonic Aerodynamic Design Method" AIAA Journal - Vol 25, Nr 9, Sept. 87.
- (18) Zhong-Chi Wang, Sheng-Kai Lai, Wen-Yuan Shu : "Aerodynamic Calculation of Turbine Stator Cascade With Curvilinear Leaned Blades and Some Experimental Results" 5th International Symposium on Air-Breathing Engines Feb. 16-21 1981 Bangalore India.
- (19) Hourmouziadis J., Hübner N. : "3D-Design of Turbine Airfoils" ASME-Paper 85-GT-188.
- (20) Han Wanjin, Wang Zhongqi, Xu Wenyuan : "An Experimental Investigation into the Influence of Blade Leaning on the Losses Downstream of Annular Cascades with a Small Diameter Height Ratio" ASME Paper 88-GT-19.
- (21) Dawes W.N. : "A Numerical Method for the Analysis of 3D Viscous Compressible Flow in Turbine Cascades; Application to Secondary Flow Development in a Cascade With and Without Dihedral" ASME Paper 86-GT-145.
- (22) Morgan S. : "Low Aspect Ratio Turbine Design at Rolls-Royce" in Secondary Flows and Endwall Boundary Layers in Axial Turbomachines. VKI LS 1984-05, 1984.
- (23) Katsanis T. : "Fortran Program for Calculating Transonic Velocities on a Blade-to-Blade Stream Surface of a Turbomachine" NASA TND-5427, 1969.
- (24) Luu T.S., Monfort G. : "Blade-to-Blade Transonic Flow Calculation in Axial Turbomachines" Sixth International Symposium on Air Breathing Engines (ISABE).
- (25) Viviani H., Veuillot J.P. : "Methodes Pseudo-Instationnaires pour le Calcul d'Ecoulements Transsoniques" ONERA Publication 1978-4.

- (26) Ni R.H. : "A Multiple Grid Scheme for Solving the Euler Equations" AIAA Paper 81-1025.
- (27) Sieverding C., Stanislas M., Snock J. : "The Base Pressure Problem in Transonic Turbine Cascades" ASME Paper 79-GT-120.
- (28) Denton J.D. : "Extension of the Finite Area Time Marching Method to Three Dimensions". in Transonic Flows in Axial Turbomachinery . VKI LS 84, 1976.
- (29) Denton J.D. : "An Improved Time-Marching Method for Turbomachinery Flow Calculation" ASME Paper 82-GS-239, 1982.
- (30) Van Hove W. : "Calculation of Three-Dimensional, Inviscid, Rotational Flow in Axial Turbine Blade Rows" ASME Paper 83-GT-119.
- (31) Brochet J. : "Calcul Numérique d'Ecoulements Internes Tridimensionnels Transsoniques" La Recherche Aéronautique, Vol.5, Sept. 1980 pp 301-315.
- (32) Arts T. : "Three-Dimensional Rotational Inviscid Flow Calculation in Axial Turbine Blade Rows", VKI Technical Note 154, 1985.
- (33) Krouthen B. : "Three-Dimensional Inviscid Turbomachinery Flow Simulations Obtained by Solving the Euler Equations on an O-H type Grid" The Aeronautical Research Institute of Sweden FFA TN-1986-77.
- (34) Povinelli L.A. : "Assessment of Three-Dimensional Inviscid Codes and Loss Calculations for Turbine Aerodynamic Computations" Transactions of the ASME, Journal of Engineering for Gas Turbines and Power vol 107, April 1985.
- (35) Denton J.D. : "The Use of a Distributed Body Force to Simulate Viscous Effects in 3D Flow Calculations" ASME Paper 86-GT-144.
- (36) Wittig S, Scherer V. : "Heat Transfer Measurements Downstream of a Two-Dimensional Jet Entering a Cross-Flow" ASME Paper 87-GT-119.
- (37) Pietrzyk J.R., Bogard D.G., Crawford M.E. : "Hydrodynamic Measurements of Jets in Cross-flow for Gas Turbine Film Cooling Application" ASME Paper 88-GT-174.
- (38) Dhawan S., Narasimha R. : "Some Properties of Boundary Layer Flows during Transition from Laminar to Turbulent Motion" Journal of Fluid Mechanics, Vol.3, pp 418-436, 1956.
- (39) Abu-Ghannam B.J., Shaw R. : "Natural Transition of Boundary Layers. The Effects of Turbulence, Pressure Gradient and Flow History" J. Fluid Mechanics, Vol 22, n°5, pp 213-228.
- (40) Eckert E.R.G., Goldstein R.J., Simon T.W. : "Studies of Gas Turbine Heat Transfer : Airfoil Surface and Endwall" Annual Progress Report 1985 - 1986 - AFOSR.
- (41) Adams E.W., Johnston J.P. : "A Mixing Length Model for the Prediction of Convex Curvature Effects on Turbulent Boundary Layers". ASME Paper 83-GT-80.
- (42) Gaugler R.E. : "Some Modifications to, and Operating Experiences with the Two-Dimensional Finite-Difference, Boundary-Layer Code STAN5" ASME Paper 81-GT-89.
- (43) Guyon B., Arts T. : "Boundary Layer Calculation Including the Prediction of Transition and Curvature Effects" to be published at the 34th ASME Meeting, Toronto, June 1989.
- (44) McDonald H, Fish B.W. : "Practical Calculation of Transitional Boundary Layers" International Journal of Heat and Mass Transfer, Vol.16, pp 1729-1744, 1973.
- (45) Keller H.B. : "Accurate Numerical Methods for Boundary Layer Flows.II : Two-Dimensional Turbulent Flows" AIAA Journal, Vol 10, PP 1193-1199, 1972.
- (46) Herring H.J. : "A Method of Predicting the Behavior of a Turbulent Boundary Layer with Discrete Transpiration Jets" ASME Paper 74-GT-48.
- (47) Miller K.L., Crawford M.E. : "Numerical Simulation of Single, Double and Multiple-Row Film Cooling Effectiveness and Heat Transfer" ASME Paper 84-GT-112.
- (48) Schönung B., Rodi W. : "Prediction of Film Cooling by a Row of Holes with a Two-Dimensional Boundary Layer Procedure" ASME Paper 87-GT-122.
- (49) Hartsel J.E. : "Prediction of Effects of Mass-Transfer Cooling on the Blade-Row Efficiency of Turbine Airfoils" AIAA Paper 72-11, January 1972.
- (50) Hauser C.H., Haas J.E., Reid L., Stepka F.S. : "Aeropropulsion 1979" NASA Conference Publication 2092, 1979.
- (51) Haller B.R., Camus J.J. : "Aerodynamic Loss Penalty Produced by Film Cooling Transonic Turbine Blades" ASME Paper 83-GT-77.
- (52) Camci C., Arts T. : "Experimental Heat Transfer Investigation Around the Film Cooled Leading Edge of a High Pressure Gas Turbine Rotor Blade" Transactions of the ASME, Journal of Engineering For Gas Turbines and Power, Vol 107, 1985, PP 1016, 1021.

- (53) Sieverding C.H. : "The Influence of Trailing Edge Ejection on the Base Pressure in Transonic Turbine Cascades" ASME Paper 82-GT-50.
- (54) Xu L., Denton J.D. : "The Base Pressure and Loss of a Family of Four Turbine Blades" ASME Paper 87-GT-202.
- (55) Sieverding C.H. : "Recent Progress in the Understanding of Basic Aspects of Secondary Flows in Turbine Blade Passages". Transactions of the ASME. Journal of Engineering for Gas Turbines and Power. Vol 107, 1985, pp 248,257.
- (56) Leboeuf F. : "Annulus End-Wall Boundary Layer Theory" VKI Lecture Series 1984-05.
- (57) Weinberg B.C., Yang R.J., McDonald H., Shamroth S.J. : "Calculations of Two and Three-Dimensional Transonic Cascade Flow Fields Using the Navier-Stokes Equations" ASME Paper 85-GT-66.
- (58) Birch N.T. : "Navier-Stokes Predictions of Transition, Loss and Heat Transfer in a Turbine Cascade" ASME Paper 87-GT-22.
- (59) Davis R.L., Ni R.H., Carter J.E. : "Cascade Viscous Flow Analysis Using the Navier-Stokes equations AIAA 24th Aerospace Sciences Meeting, January 8-9, 1986 Reno, Nevada.
- (60) Rhie C.M. : "A Pressure Based Navier-Stokes Solver Using the Multigrid Method" AIAA 86-0207, January 1986/Reno, Nevada.
- (61) Nakahashi K., Naito O., Kikuchi K., Tamura A. : "Navier-Stokes Computations of Two and Three-Dimensional Cascade Flow Fields" AIAA-87-1315, June 1987/Honolulu Hawaii.
- (62) Subramanian S.V., Bozzola R. : "Numerical Simulation of Three-Dimensional Flow-Fields in Turbomachinery Blade Rows Using the Compressible Navier-Stokes Equations" AIAA-87-1314 June 1987/Honolulu, Hawaii.
- (63) Fourmaux A. : "Unsteady Flow Calculation in Cascades" ASME Paper 86-GT-178, 1986.
- (64) Lemeur A. : "Three-Dimensional Unsteady Flow Computation in a Transonic Axial Turbine Stage" AIAA 26th Aerospace Sciences Meeting, Reno, 1988.
- (65) Giles M.B. : "Stator-Rotor Interaction in a Transonic Turbine" AIAA Paper 88-3093, 1988.
- (66) Rai M.M. : "Navier-Stokes Simulations of Rotor-Stator Interaction Using Patched and Overlaid Grids" AIAA Paper 85-1519, 1985.
- (67) Rai M.M. : "Unsteady Three-Dimensional Navier-Stokes Simulations of Turbine Rotor-Stator Interaction" AIAA Paper 87-2058, 1987.
- (68) Epstein A.H., Guenette G.R., Norton R.J.G. : "The Design of the MIT Blowdown Turbine Facility" MIT Gas Turbine Laboratory Report N°183, April 1985.
- (69) Guenette G.R., Epstein A.H., Giles M.B., Haines R., Norton R.J.G. : "Fully Scaled Transonic Rotor Heat Transfer Measurements" ASME Paper 88-GT-171.
- (70) Richards B.E. : "Heat Transfer Measurements Related to Hot Turbine Components in the Von Karman Institute Hot Cascade Tunnel" in Testing and Measurement Techniques in Heat Transfer and Combustion, AGARD CP 281, 1980.
- (71) Schultz D.L., Jones T.V. : "Heat Transfer Measurements in Short Duration Hypersonic Facilities" AGARD AG165, 1973.
- (72) Jones T.V. "Gas Turbine Studies at Oxford 1969-1987" ASME Paper 88-GT-112.
- (73) Arts T., Graham C.G. : "External Heat Transfer Study on a HP Turbine Rotor Blade" AGARD-CPP 390, Bergen, Norway, 1985.
- (74) Brooks A.J., Colbourne D.E., Wedlake E.T., Jones T.V., Oldfield M.L.G., Schultz D.L., Loftus P.J. : "The Isentropic Light Piston Annular Cascade Facility at RAE Pyestock" AGARD CP 390, Paper 31, 1985.

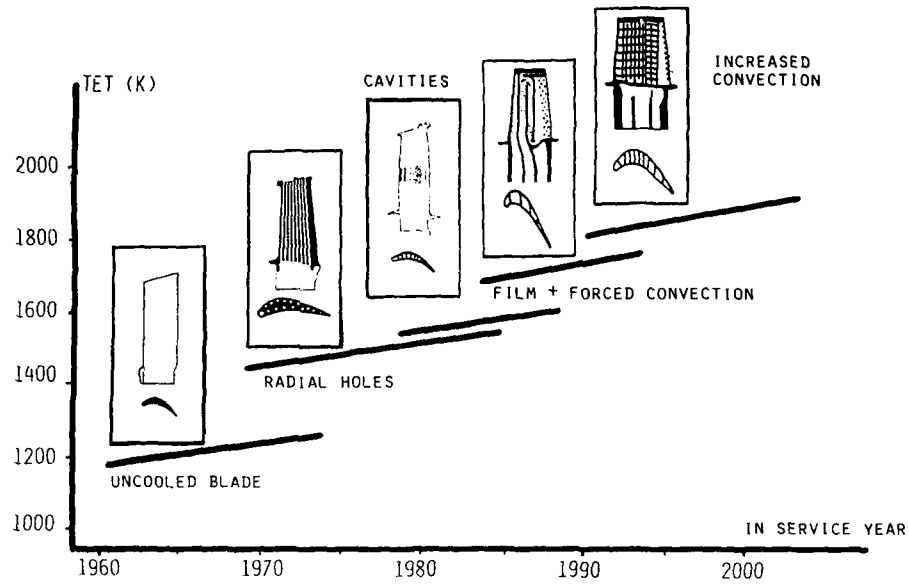


FIGURE 1 : TURBINE INLET TEMPERATURE INCREASE AND COOLED BLADES TECHNOLOGY IMPROVEMENT

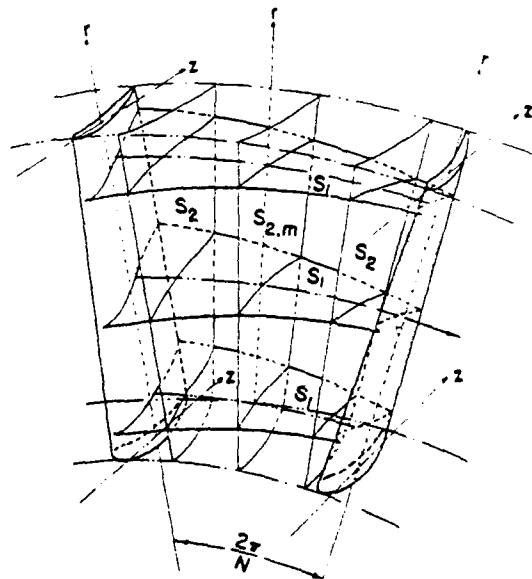


FIGURE 2 : RELATIVE STREAM SURFACES S_1 AND S_2

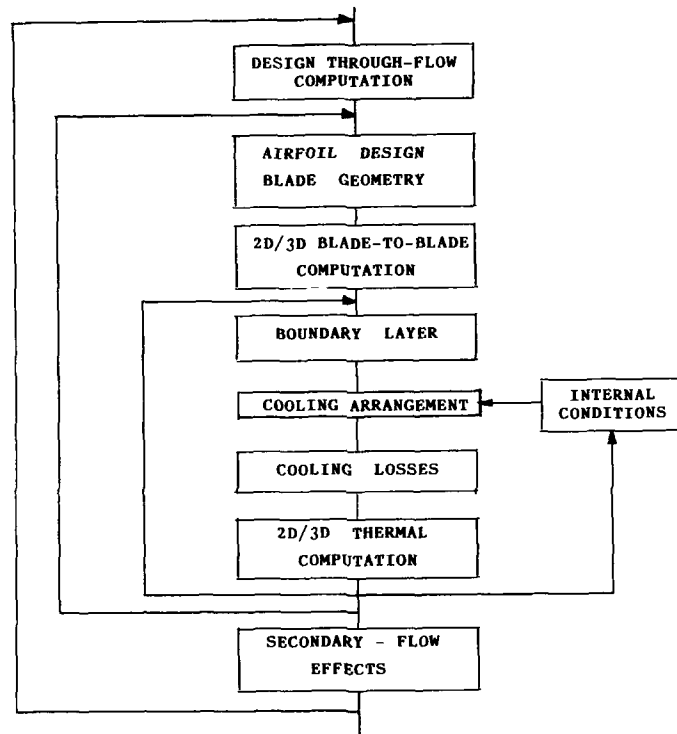


FIGURE 3 : COOLED TURBINE DESIGN PROCEDURE

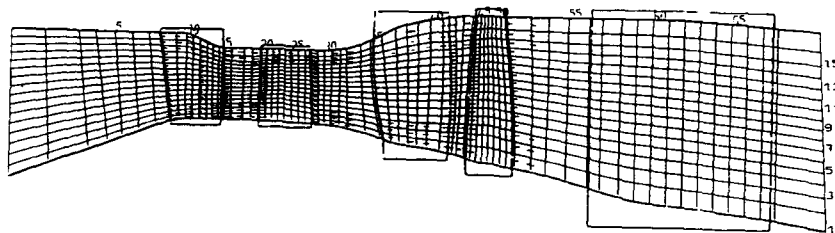


FIGURE 4 : EXAMPLE OF THROUGH-FLOW COMPUTATION IN
A STATE OF THE ART TURBINE CONFIGURATION

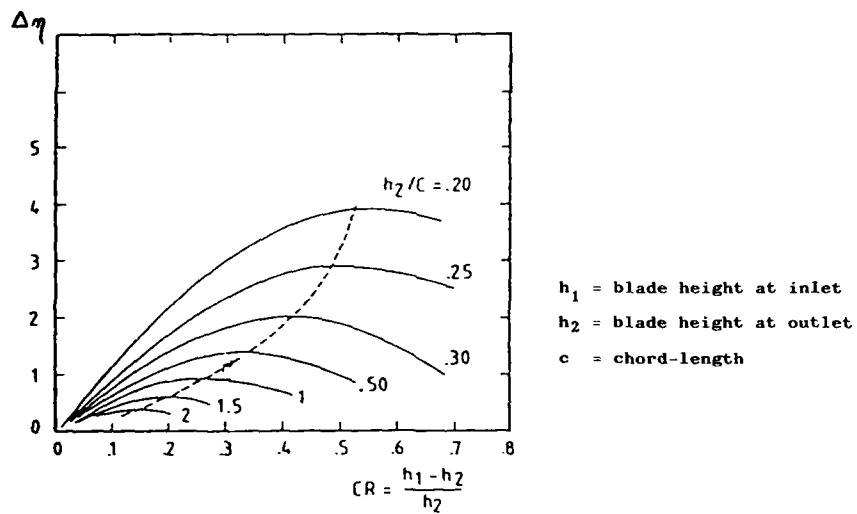


FIGURE 5 : IMPROVEMENT IN NOZZLE EFFICIENCY DUE TO
FLOW PATH CONTOURING, FROM DEJC (2)

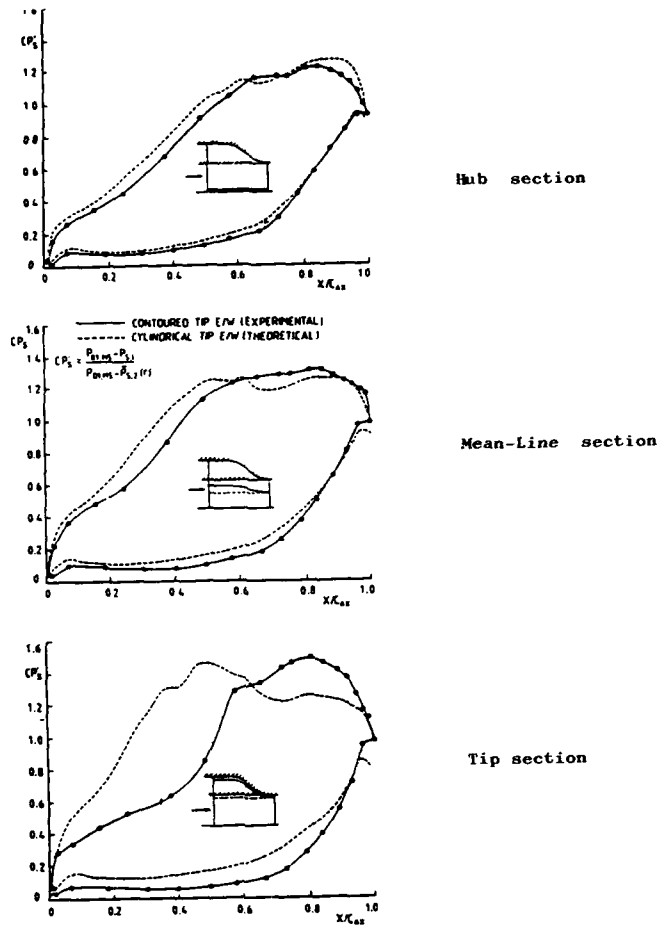


FIGURE 6 : EFFECT OF FLOW PATH CONTOURING ON VELOCITY DISTRIBUTIONS, FROM BOLETIS (7)

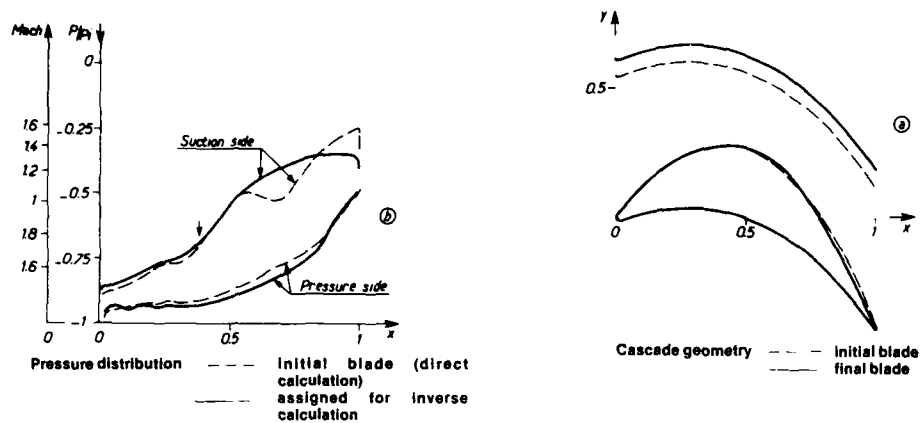


FIGURE 7 : EXAMPLE OF BLADE DESIGN WITH A MIXED-MODE METHOD, FROM MEAUZE (11)

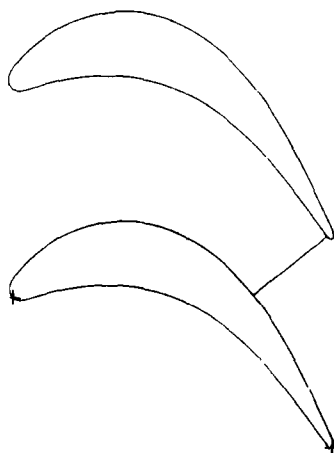


FIGURE 8 : EXAMPLE OF LP TURBINE NOZZLE PROFILE DESIGNED WITH THE METHOD OF STANITZ (15)

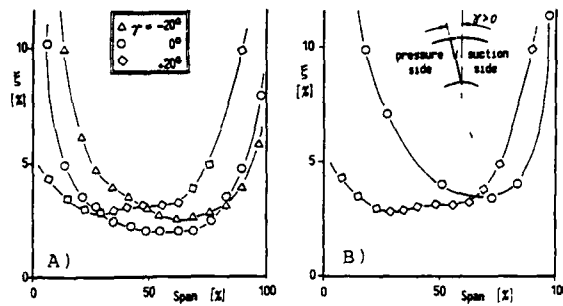


FIGURE 9 : LEAN EFFECTS ON THE LOSSES OF LINEAR CASCADES
 A) Axial end walls
 B) Diverging side walls
 FROM HOURMOUZIADIS AND HUBNER (19)

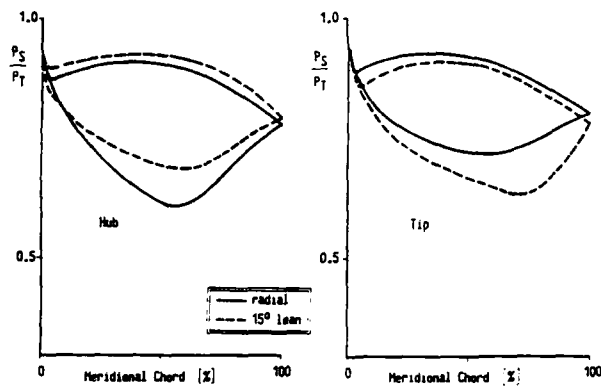


FIGURE 10 : COMPUTED EFFECT OF AIRFOIL LEAN ANGLE ON
 AERODYNAMIC LOADING, FROM HOURMOUZIADIS
 AND HUBNER (19)

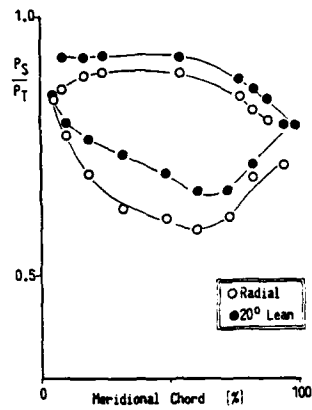


FIGURE 11 : EXPERIMENTAL RESULTS OF AIRFOIL LEAN EFFECT ON AERODYNAMIC LOADING AT THE HUB, FROM HOURMOUZIADIS AND HUBNER (19)

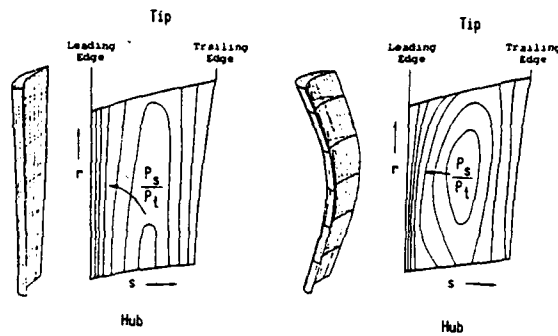


FIGURE 12 : AIRFOIL DESIGN BASED ON LEAN ANGLE OPTIMIZATION, FROM HOURMOUZIADIS AND HUBNER (19)

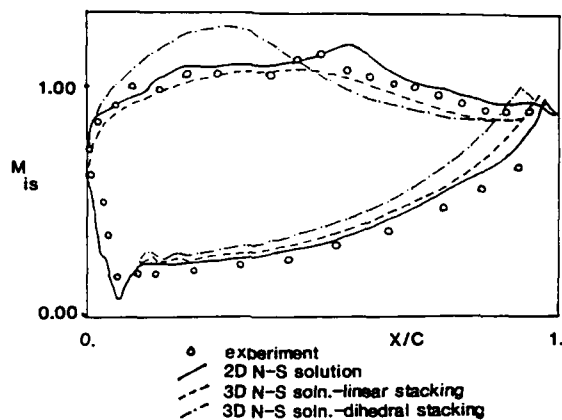


FIGURE 13 : BLADE SURFACE ISENTROPIC MACH NUMBERS IN THE CENTER-PLANE OF A LINEAR CASCADE, EFFECT OF STACKING, FROM DAWES (21)

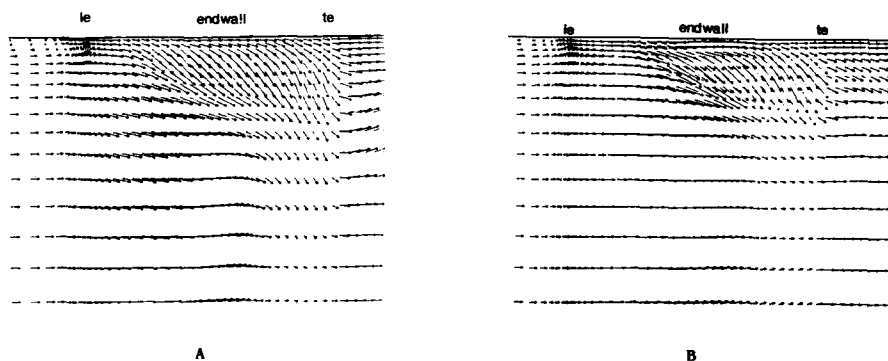


FIGURE 14 : PREDICTED VELOCITY VECTORS NEAR THE SUCTION SIDE OF A LINEAR CASCADE

A) With dihedral
B) Without dihedral
FROM DAWES (21)

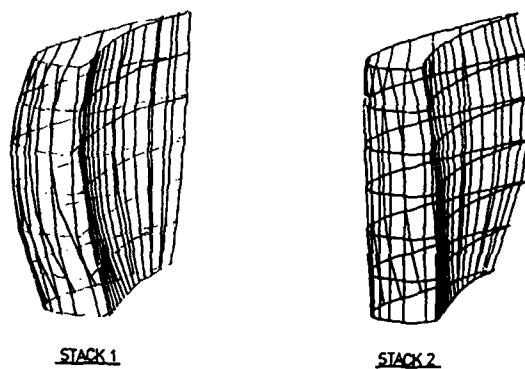


FIGURE 15 : COMPARISON OF 2 STACKS USED IN NOZZLE
GEOMETRY OPTIMIZATION, FROM MORGAN (22)

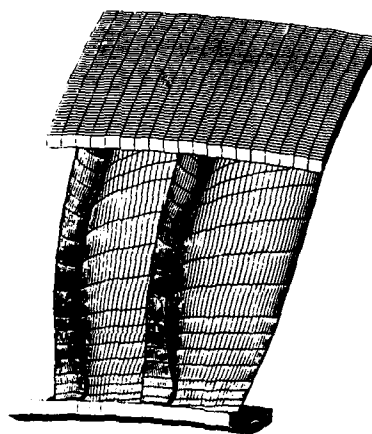


FIGURE 16 : EXAMPLE OF COMPLEX THREE DIMENSIONAL
COOLED LP TURBINE NOZZLE

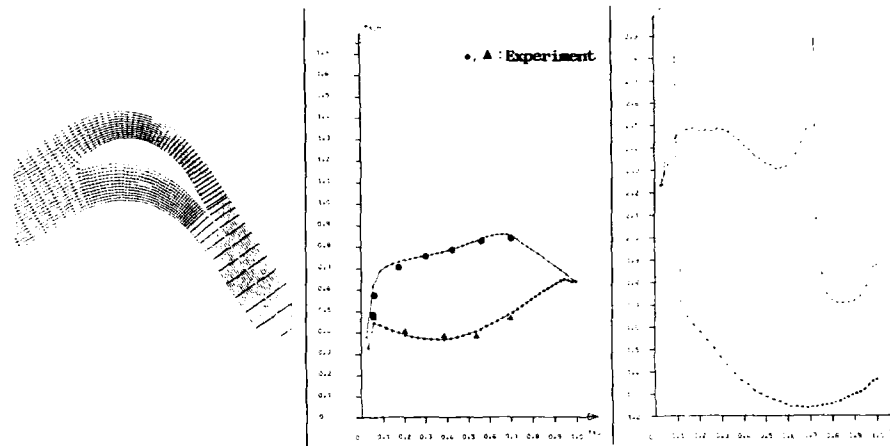


FIGURE 17 : EXAMPLE OF 2.5D BLADE-TO-BLADE COMPUTATION ON THE MEAN LINE OF A LP TURBINE NOZZLE

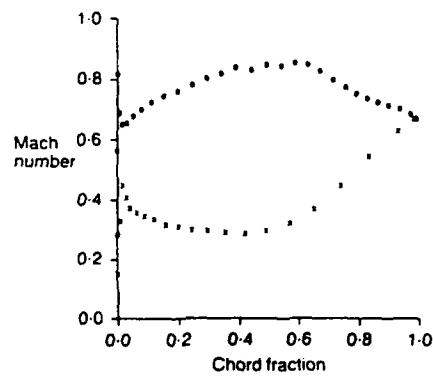


FIGURE 18 : ANALYSIS OF TURBINE BLADE WITH LEADING EDGE SPIKE, FROM CEDAR AND STOW (12)

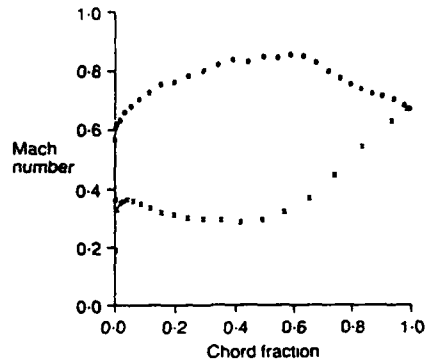


FIGURE 19 : REDESIGNED BLADE TO REMOVE LEADING EDGE SPIKE, FROM CEDAR AND STOW (12)

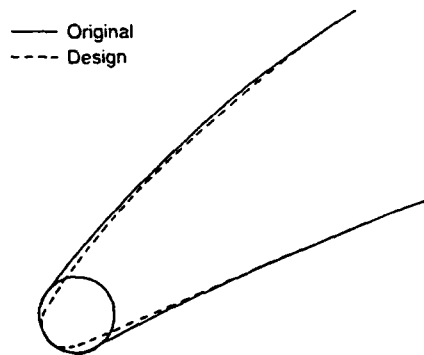


FIGURE 20 : CHANGE IN BLADE SHAPE TO REMOVE LEADING EDGE SPIKE, FROM CEDAR AND STOW (12)

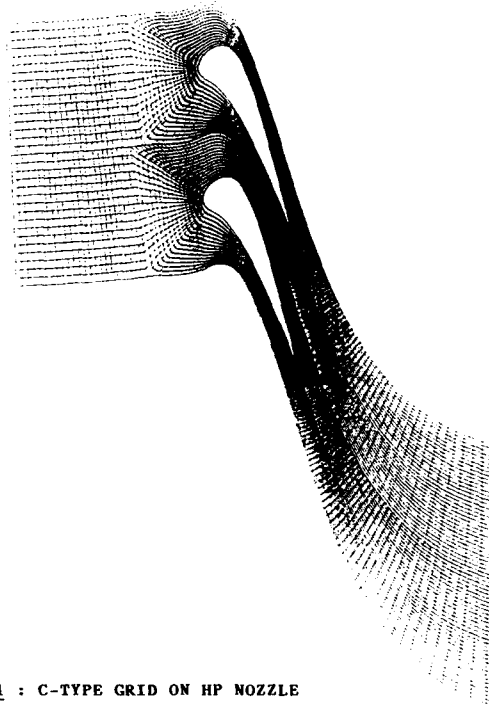


FIGURE 21 : C-TYPE GRID ON HP NOZZLE

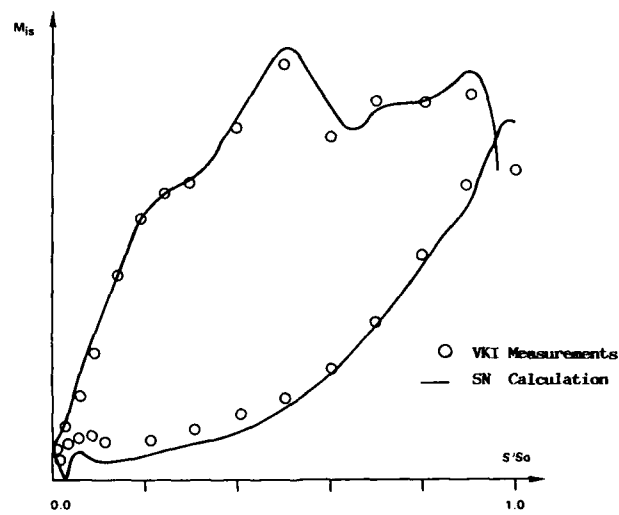
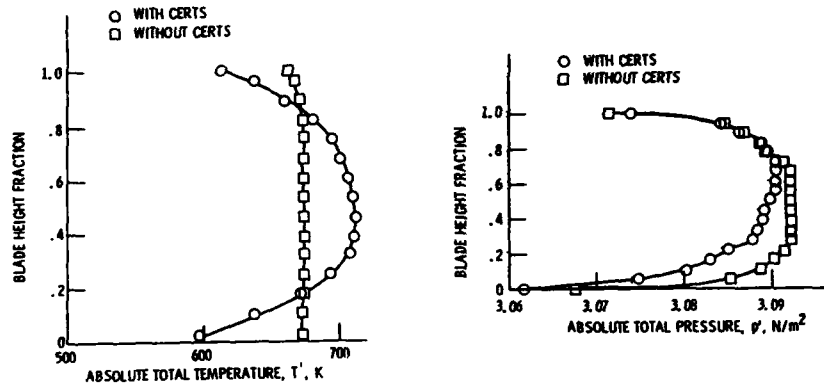


FIGURE 22 : 2.5D BLADE-TO-BLADE COMPUTATION
ON HP NOZZLE



CERTS = COMBUSTOR EXIT RADIAL TEMPERATURE SIMULATOR

FIGURE 23 : POVINELLI'S TEST CASE : STATOR INLET TEMPERATURE AND PRESSURE PROFILES, FROM POVINELLI (34)

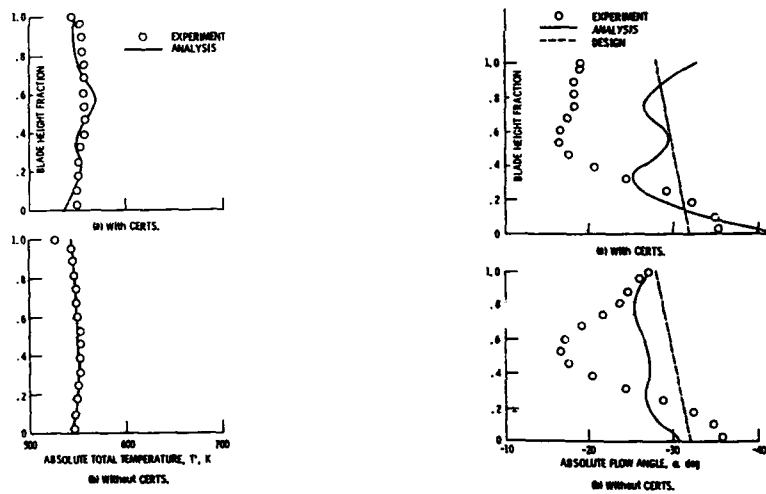


FIGURE 24 : POVINELLI'S TEST CASE : ROTOR EXIT TEMPERATURE AND FLOW ANGLE PROFILES, FROM POVINELLI (34)

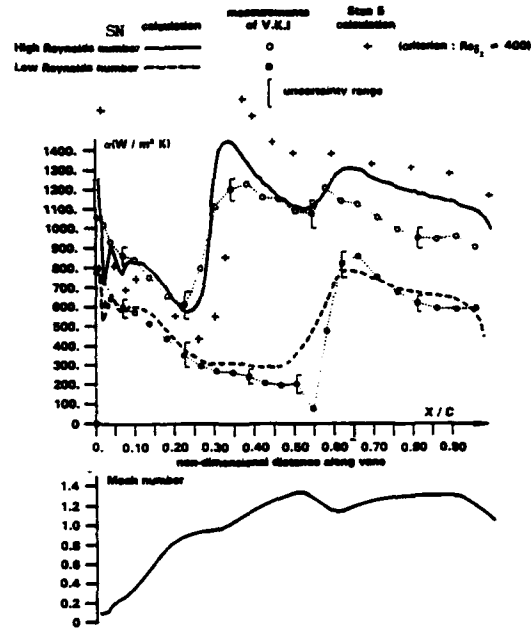


FIGURE 25 : EXAMPLE OF BOUNDARY LAYER COMPUTATION ON A HP VANE, FROM GUYON AND ARTS (43)

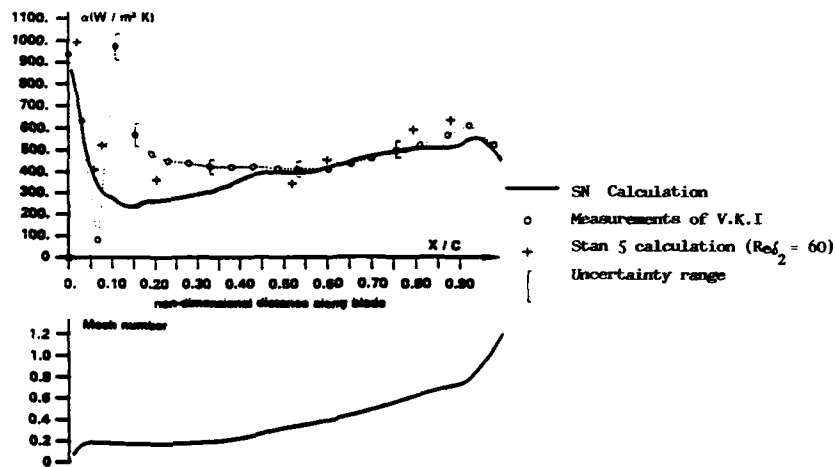


FIGURE 26 : EFFECT OF A SEPARATION BUBBLE ON THE HEAT TRANSFER COEFFICIENT ON A HP VANE, FROM GUYON AND ARTS (43)

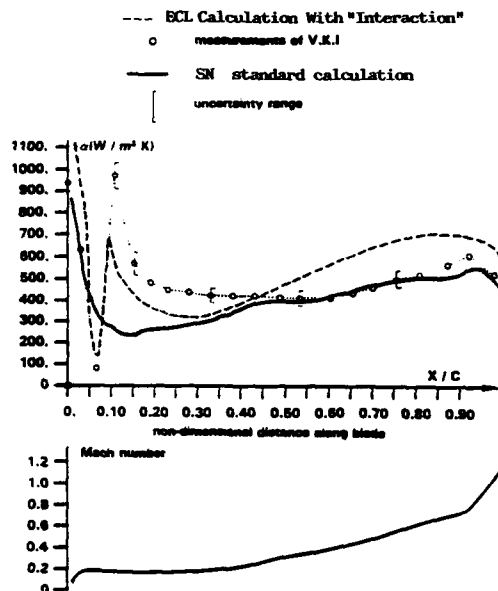


FIGURE 27 : COMPUTATION OF THE HEAT TRANSFER COEFFICIENT
 IN THE SEPARATED LEADING EDGE REGION OF A HP VANE

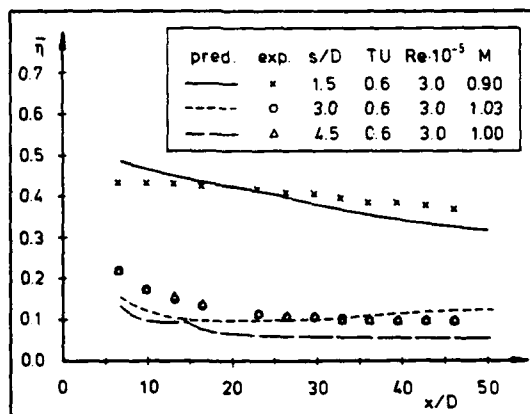


FIGURE 28 : COOLING EFFECTIVENESS AT DIFFERENT SPACINGS,
 FROM SCHÖNUNG AND RODI (48)

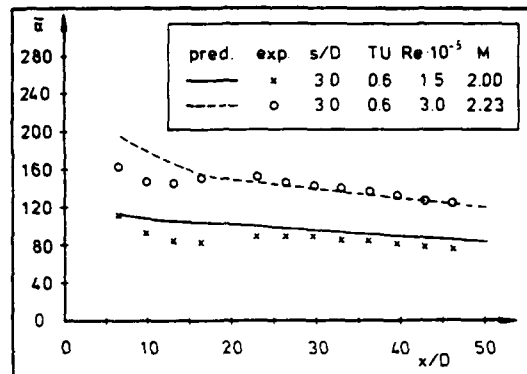


FIGURE 29 : INFLUENCE OF THE REYNOLDS NUMBER ON THE HEAT TRANSFER COEFFICIENT, FROM SCHONUNG AND RODI (48)

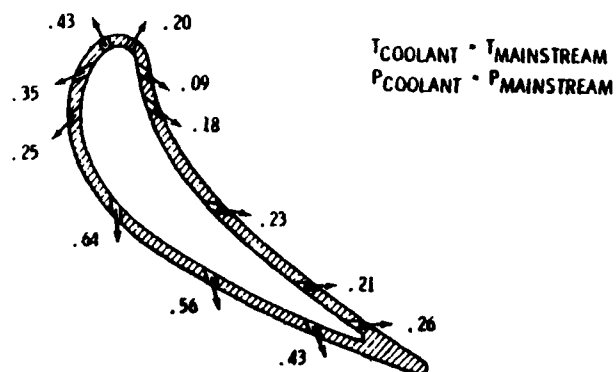


FIGURE 30 : PROFILE EFFICIENCY LOSS FOR 1% COOLING AIR EJECTION, FROM HAUSER ET AL. (50)

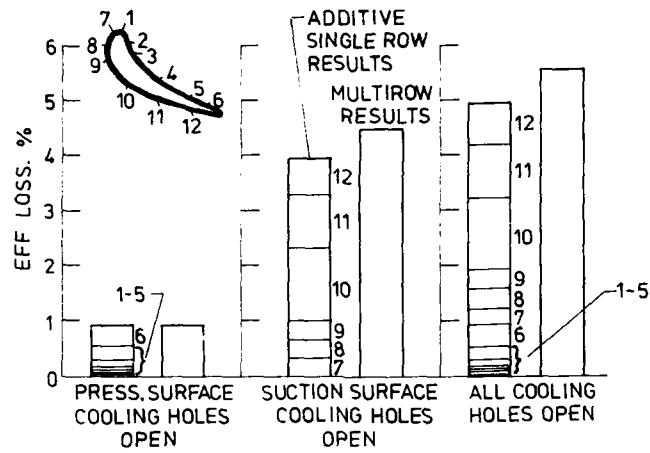


FIGURE 31 : PROFILE EFFICIENCY LOSS FOR SINGLE ROW AND MULTI-ROW BLADE FILM COOLING, FROM HAUSER ET AL. (50)

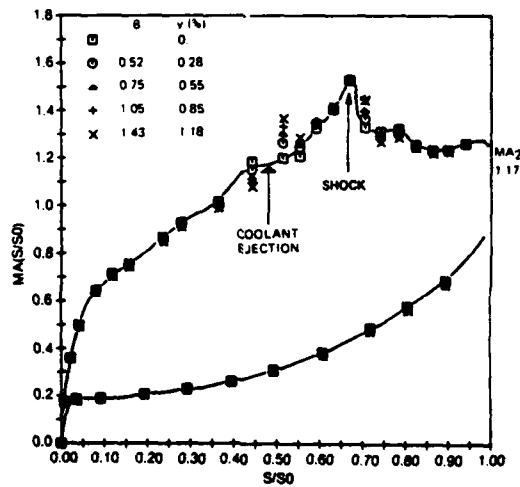
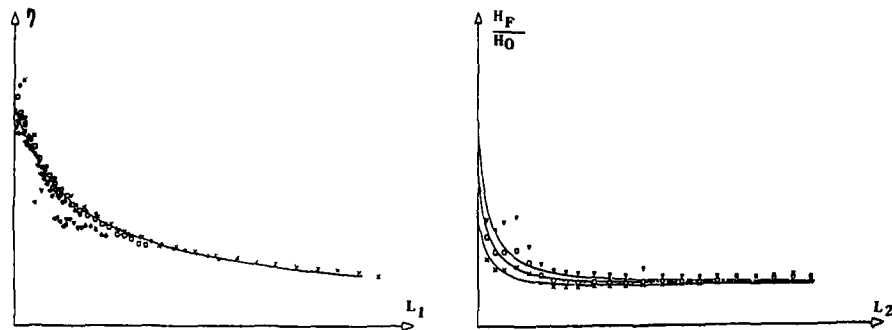


FIGURE 32 : MEASURED SURFACE MACH NUMBER DISTRIBUTION WITH AIR BLOWING NEAR THE THROAT, FROM HALLER AND CAMUS (51)



L_1, L_2 REDUCED LENGTH
 η FILM EFFECTIVENESS
 H_F, H_0 HEAT TRANSFER COEFF. W. AND W/O FILM

FIGURE 33 : TYPICAL CORRELATION FOR FILM COOLING EFFECTIVENESS AND HEAT TRANSFER COEFFICIENT

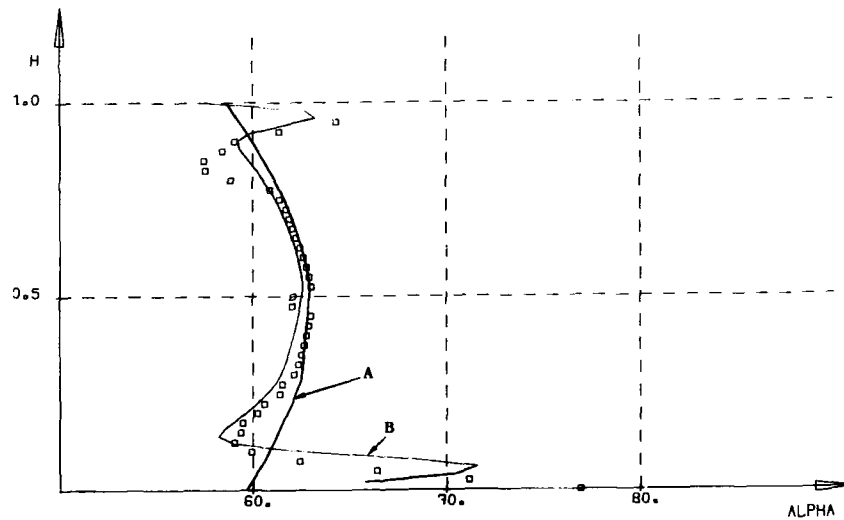


FIGURE 34 : EXIT ANGLE FROM A LP NOZZLE
 \square : Experiments
 A : Through-flow computation without correction
 B : Secondary flow method

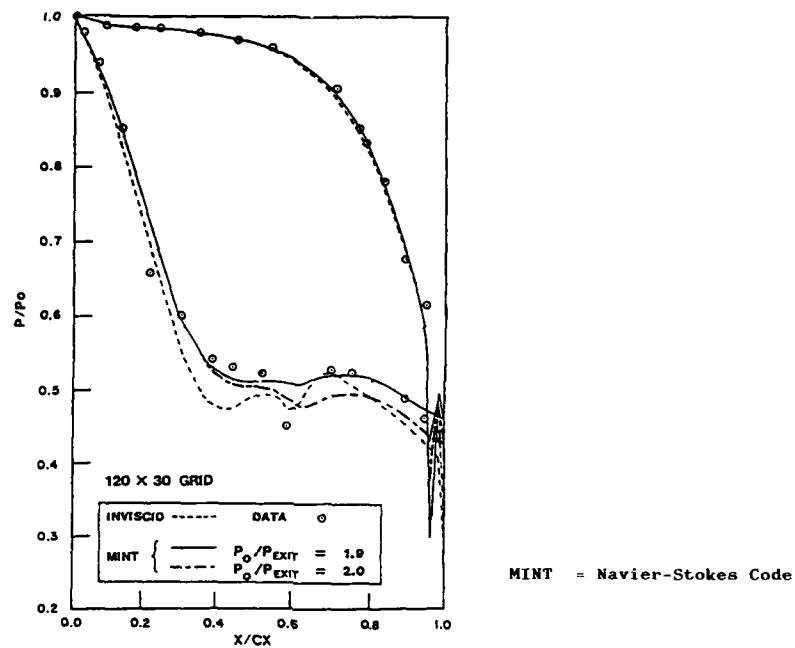


FIGURE 35 : COMPARISON BETWEEN MEASURED AND CALCULATED PRESSURE DISTRIBUTIONS ON THE C3X CASCADE, FROM WEINBERG ET AL. (57)

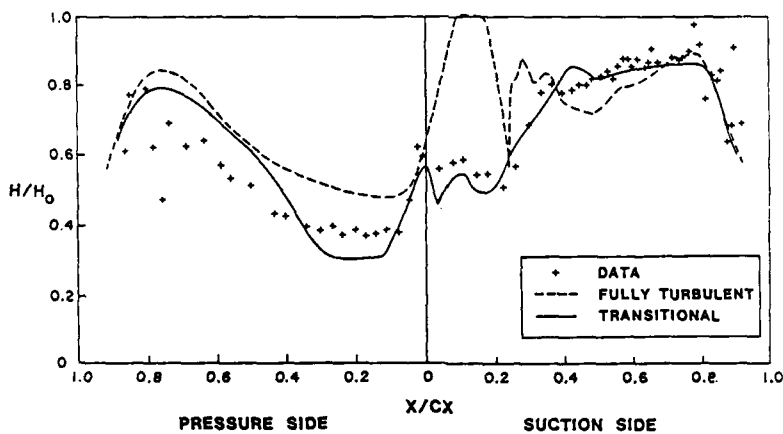


FIGURE 36 : COMPARISON BETWEEN MEASURED AND CALCULATED HEAT TRANSFER COEFFICIENT DISTRIBUTIONS, FROM WEINBERG ET AL. (57)

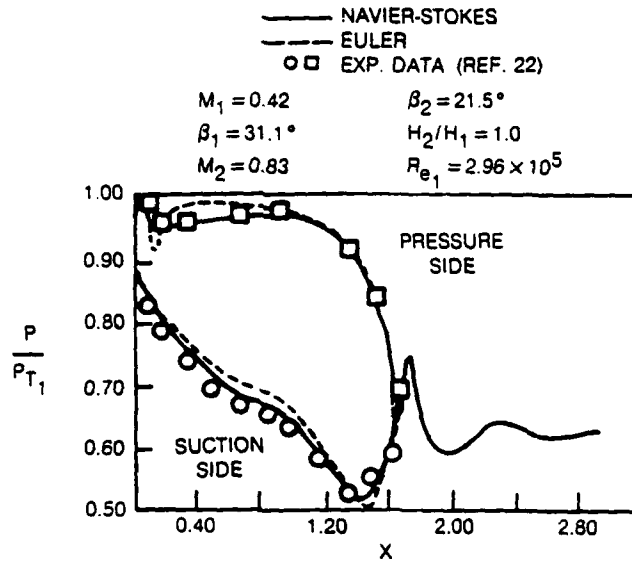


FIGURE 37 : COMPARISON BETWEEN PREDICTED PRESSURE DISTRIBUTIONS AND EXPERIMENTAL DATA FOR TURBINE CASCADE, FROM DAVIS ET AL. (59)

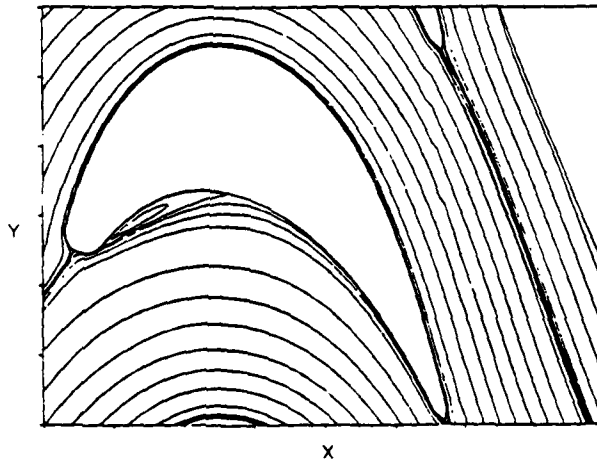


FIGURE 38 : PREDICTED STREAMLINE PATTERN FOR SEPARATED TURBINE CASCADE, FROM DAVIS ET AL. (59)

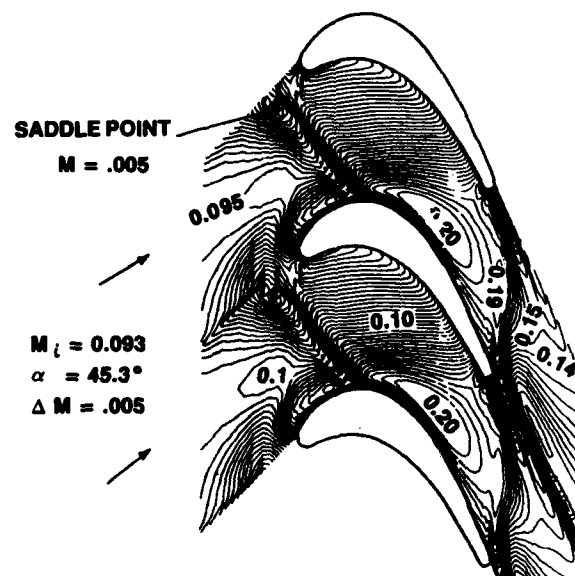


FIGURE 39 : MACH NUMBER CONTOURS AT 1.2 PERCENT SPAN FROM THE ENDWALL, FROM SUBRAMANIAN AND BOZZOLA (62)

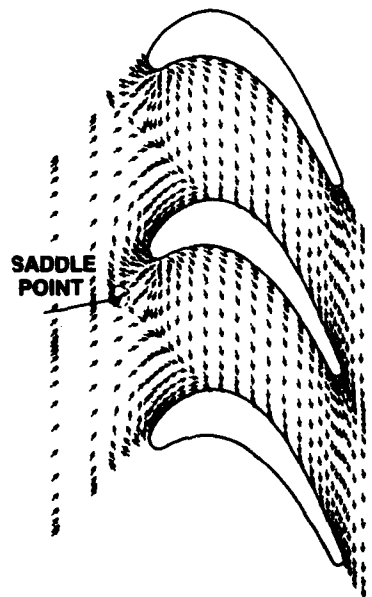


FIGURE 40 : UNIT VELOCITY VECTORS AT 1.2 PERCENT SPAN FROM THE ENDWALL, FROM SUBRAMANIAN AND BOZZOLA (62)

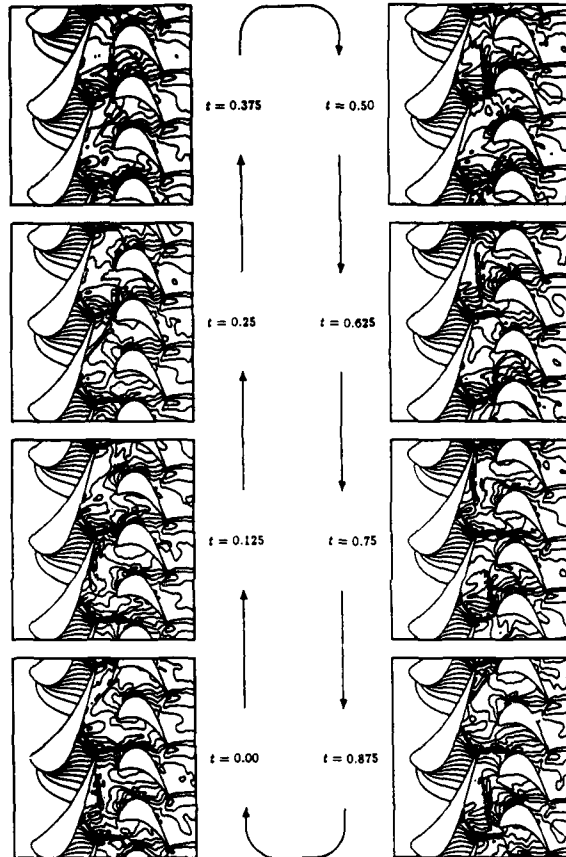


FIGURE 41 : PRESSURE CONTOURS IN UNSTEADY STATOR/ROTOR INTERACTION, FROM GILES (65)



FIGURE 42 : OVERALL VIEW OF THE VKI CT2 TRANSIENT
CASCADE WIND-TUNNEL

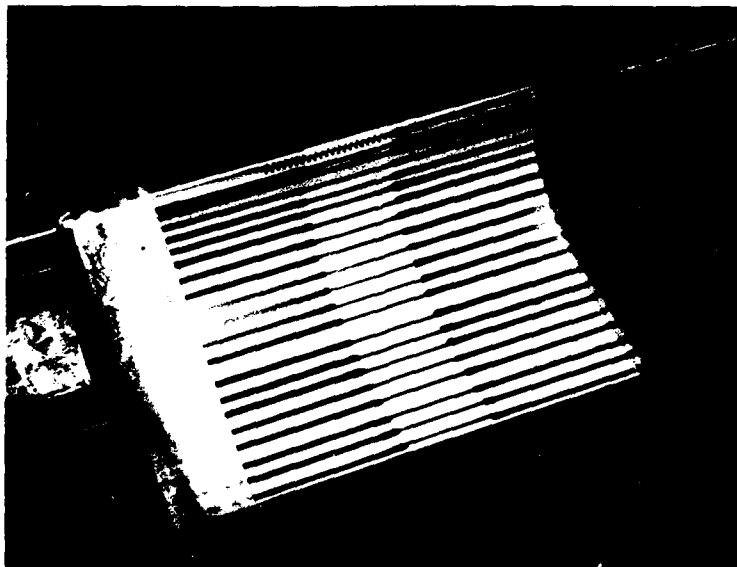


FIGURE 43 : CERAMIC BLADE WITH THIN FILM SENSORS

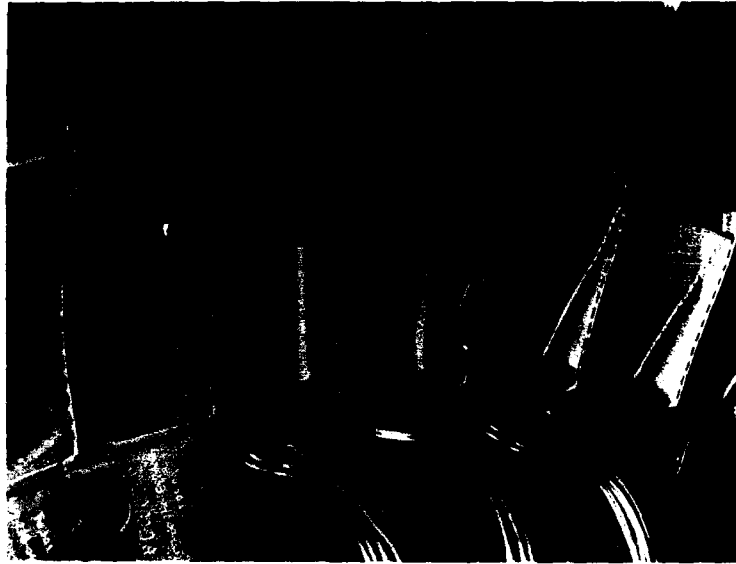


FIGURE 44 : INSTRUMENTED CASCADE FOR HOT TESTS

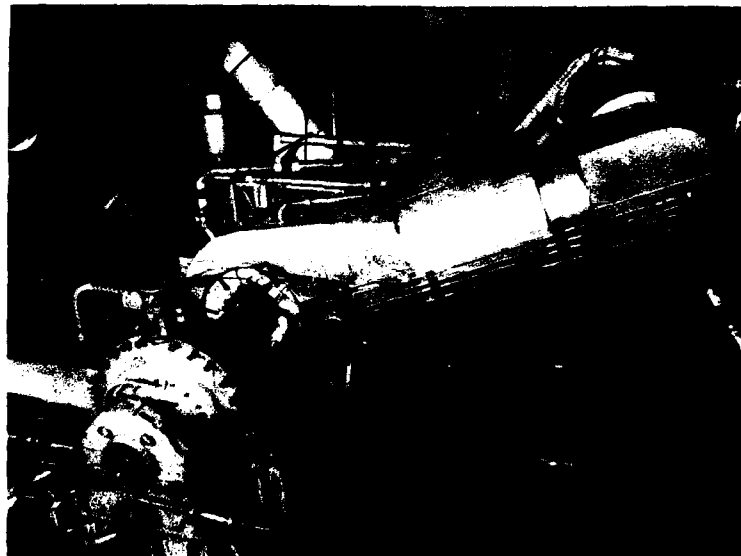


FIGURE 45 : OVERALL VIEW OF SNECMA WARM TURBINE TEST FACILITY

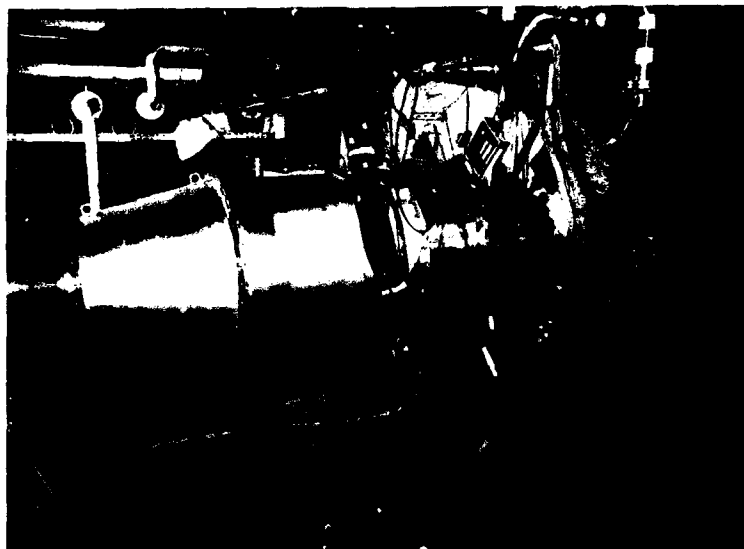


FIGURE 46 : VIEW OF THE TEST SECTION OF SNECMA
WARM TURBINE TEST FACILITY

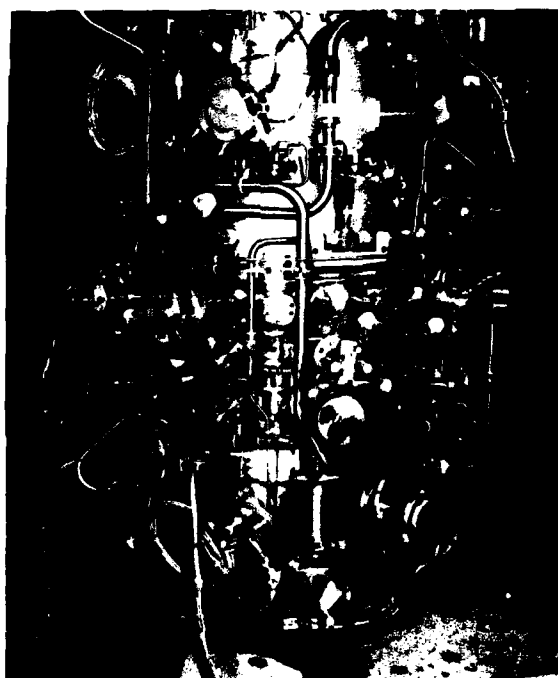


FIGURE 47 : OVERALL VIEW OF RESEARCH CORE ENGINE
USED AT SNECMA

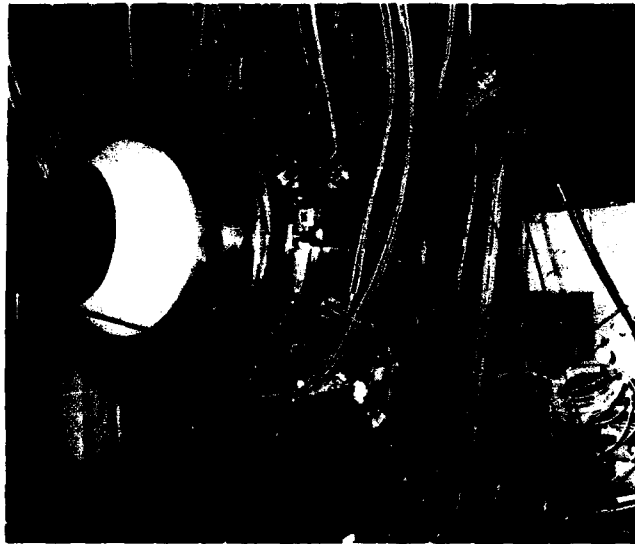


FIGURE 48 : M88 CORE ENGINE IN TEST CELL

AERODYNAMIC DESIGN OF LOW PRESSURE TURBINES

by

J. Hourmouziadis

MTU MOTOREN- UND TURBINEN-UNION MÜNCHEN GMBH
 Dachauer Straße 665
 8000 München 50
 GERMANY

SUMMARY

The aerodynamic requirements for LP turbines covering a wide range of Mach and Reynolds numbers are derived from the applications for turbofan, shaft and propfan engines. Designing turbines for high performance levels is based on extensive experience and modern prediction techniques. Methodology, experimental background, measurement techniques and design systems are reviewed. The merits and limitations of present computation procedures are commented upon. The close interaction between research and industrial development is discussed and the differences are pointed out.

Two dimensional pressure distributions can be predicted by a variety of very efficient inviscid methods. Boundary layer prediction is handicapped by the complexity including separation and transition. The characteristic of the Prandtl boundary layer is developed and the physical model leading to the concept of the CBL (Controlled Boundary Layer) design is presented. The effects of unsteadiness and turbulence in turbomachinery as well as the extension to transonic flow are considered. The understanding of inviscid 3D aerodynamics and their introduction in the design systems is presented. Secondary flows and their direct and indirect effects on losses are discussed.

The problems to be addressed in the intermediate and long term research and development work are listed and their significance commented upon.

SYMBOLS

a_t	m/s	Total velocity of sound (Eq. 2.5)	t	m	Cascade pitch
A	m^2	Area	T	K	Static temperature
AC	--	Acceleration parameter (Eq. 7.18)	T_t	K	Total temperature
Bu	--	Buri parameter (Eq. 7.24)	Tu	--	Degree of turbulence
c	m/s	Absolute velocity	u	m/s	Tangential velocity in the velocity vector diagram or Velocity component in x direction for the boundary layer equations
c_p	kJ/kgK	Specific heat capacity	U	m/s	Main stream velocity for the boundary layer equations
d	m	Trailing edge thickness	v	m/s	Velocity component in y direction for the boundary layer equations
F_r	N/kg	Radial blade force component	w	m/s	Relative velocity
h	m	Length	x	m	Cartesian coordinate
H	kJ/kg	Specific enthalpy drop	y	m	Cartesian coordinate
H_{12}	--	Form parameter of the boundary layer	α	°	Absolute flow angle
I	kg/s ²	Two dimensional momentum flux	β	--	Constant
m	m	Meridional coordinate	β'	°	Relative flow angle
M	--	Mach number	δ_1	m	Displacement thickness (Eq. 7.5 and 7.11)
M_c	--	Mach number of the absolute velocity	δ_2	m	Momentum loss thickness (Eq. 7.5 and 7.11)
M_t	--	Mach number referred to the total velocity of sound	Δ_2	m	Total momentum loss thickness
M_s	--	Main stream Mach number	ϵ	°	Meridional flow angle
N	rpm	Rotational speed	ζ	--	Loss coefficient
p, P	N/m ²	Static Pressure	η	m	Variable
P_t	N/m ²	Total Pressure	θ	--	Displacement parameter (Eq. 9.2)
P_o	--	Pohlhausen parameter (Eq. 7.17)	θ^*	--	Momentum loss parameter (Eq. 9.2)
r	--	Radius, radial coordinate	x^*	--	Isentropic exponent
r_k	--	Kinematic degree of reaction	μ	kg/ms	Viscosity
R	m	Radius of curvature	ν	m ² /s	Kinematic viscosity
R	kJ/kgK	Gas constant	ρ	kg/m ³	Density
Re	--	Reynolds number	τ_w	N/m ²	Wall shear stress
Re_2	--	Momentum loss thickness Reynolds number			
Re^*	--	Transition Reynolds number			
s	m	Surface length coordinate			
s	kJ/kgK	Entropy			

Subscripts

m	Meridional	1	Entry, inlet
PS	Pressure side	2	Exit, outlet
r	Radial		
SS	Suction side	δ	Main stream quantity at the edge of boundary layer
u	Tangential		

1. INTRODUCTION

Low pressure turbines are favoured by the engine environment, compared with high pressure turbines. The aerodynamic design is not plagued to the same extent by stressing constraints imposed by the high speeds or by geometrical limitations resulting from cooling system requirements. Accordingly efficiency levels are usually higher, which is quite significant for engine performance. Exchange rates for percentage efficiency to specific fuel consumption range from 1:0.7 for modern high bypass ratio jet engines to 1:1 for turboshaft engines.

The turbine designs that can be found in aircraft engines are illustrated in Fig. 1. Two fundamentally different groups can be identified. Direct drive turbines with relatively low speed, set by the fan, such as in the PW 2037. Geared turbines where high speeds are utilized to minimize the number of stages, such as in the MTR390 helicopter engine or in the MTU CRISP concept. The size of the blading varies from about 25 mm height for small 1000 kW class turboshafts to over 300 mm for the 60000 lb turbofans.

It is obvious that this wide range of designs will lead to different but nevertheless quite demanding aerodynamic requirements. The present lecture will give a short review of overall design criteria and will derive these requirements from general considerations and statistics. High performance levels are based on extensive experience and modern prediction techniques. Methodology, experimental background and design systems will be discussed and the close interaction between research and development demonstrated.

Blade to blade flow can be predicted by a variety of very efficient inviscid methods. Boundary layer prediction is handicapped by the complexity of separation and transition phenomena. The characteristic of the Prandtl boundary layer will be developed in some more detail and the physical model leading to the concept of the CBL (Controlled Boundary Layer) design will be presented. The effects of unsteadiness and turbulence in turbomachinery as well as the extension to transonic flow are considered.

The understanding of inviscid 3D aerodynamics and their introduction in the design systems as well as secondary flows and their direct and indirect effects on losses will be discussed. The problems to be addressed in the intermediate and long term research and development work will be summarized and their importance commented upon.

2. OVERALL PERFORMANCE CONSIDERATIONS

The best known correlation among overall stage parameters and turbine performance was developed by Smith (1965). He used the tangential velocity of the rotor to normalize the velocity vector diagrams and to introduce kinematic similarity for the incompressible flow in a cylindrical annulus. With the meridional velocity component c_m and the Euler work H , a flow factor c_m/u and a loading factor H/u^2 were defined. Using available experimental data he found that stage efficiency correlates quite well with these two parameters. The original Smith diagramm is shown in Fig. 2. It can be seen that for a given loading, there is an optimum flow factor which gives the maximum efficiency. The parameters that bring about this effect can be found, when the loading factor is developed appropriately

$$\frac{H}{u^2} = \frac{u(c_{u1} - c_{u2})}{u^2} = \frac{c_{u1} - c_{u2}}{u} = \frac{c_m}{u} (\tan \alpha_1 - \tan \alpha_2) \quad (2.1)$$

or using the velocity vector relations

$$\frac{H}{u^2} = \frac{u + w_{u1} - u - w_{u2}}{u} = 2 \left(\frac{1}{2} \frac{w_{u1} + w_{u2}}{u} - \frac{w_{u2}}{u} \right) = 2 \left(r_k - \frac{c_m}{u} \tan \beta_2 \right) \quad (2.2)$$

with the kinematic degree of reaction r_k

$$r_k = \frac{1}{2} \frac{w_{u1} + w_{u2}}{u} \quad (2.3)$$

Eq. 2.1 indicates the effects of turning and Eq. 2.2 the effects of reaction. In fact to the left of the efficiency maxima in the Smith diagramm turning becomes too high and to the right, reaction is too large.

In compressible flow with a conical annulus the formulas are modified, but still show the same characteristics, for example

$$\frac{H}{u^2} = \frac{c_{m1}}{u_1} (\tan \alpha_1 - \frac{u_2}{u_1} \frac{c_{m2}}{c_{m1}} \tan \alpha_2) \quad (2.4)$$

where u_2/u_1 represents the Coriolis effect along a varying mean radius and c_{m2}/c_{m1} the compressibility plus radial divergence effect.

The conclusions of S.F. Smith have been verified for a variety of parameters in the design diagramm study of David, Hourmouziadis and Marx (1969) and present the accepted state of the art today. Designers always try to put their turbines close to the maximum performance curve. Fig. 3 shows published data and MTU experience for individual stages. In spite of the rather high scatter, caused by limited numbers of stages and other design constraints, they cluster around the optimum line. Nevertheless three distinct groups can be distinguished. High pressure turbines are located on the low flow factor c_m/u side of the diagramm, fan drive low pressure turbines on the high side and geared turbines in between with a trend to the lower c_m/u values. Kinematic loading levels are quite similar, indicating that Euler work per stage has been reduced in direct drive low pressure turbines to adapt to the lower circumferential velocity u . Obviously this cannot be done with the flow factor, because the kinematic similarity does not include compressibility effects. The meridional velocity c_m is limited by Mach number in high pressure turbines and is kept high in low pressure turbines to reduce annulus cross section and engine size.

Compressibility can be accounted for with the introduction of Mach number similarity. The convenient parameter usually applied is the speed of sound, defined with the total temperature upstream of the rotor blading.

$$a_1 = \sqrt{\gamma R T_1} \quad (2.5)$$

Normalizing the Euler work H gives

$$\frac{H}{a_{11}^2} = \frac{u_1}{a_{11}} \left(\frac{c_{u1}}{a_{11}} - \frac{u_2}{u_1} \frac{c_{u2}}{a_{11}} \right) = \frac{u_1}{a_{11}} (M_{11} \sin \alpha_1 - \frac{u_2}{u_1} \sqrt{\frac{T_{12}}{T_{11}}} M_{12} \sin \alpha_2) \quad (2.6)$$

The new parameters that have been introduced are the referred work H/a_{11}^2 and the referred rotational velocity u/a_{11} . If the rotational velocity u is expressed by the speed N and for a given turbine all constants like isentropic exponent, radius etc. are eliminated, then the well known functions H/T_{11} and $N/\sqrt{T_{11}}$ emerge. The relation to the kinematic loading factor is given by

$$\frac{H}{u^2} = \frac{H/a_{11}^2}{(u/a_{11})^2} \quad (2.7)$$

The statistics of turbine designs with these parameters are shown in Fig. 4. They all lie in a narrow band given by the kinematic loading range from 1 to 2. Here again high pressure turbines are located in the higher levels of referred work and rotational velocity and have to cope with high Mach numbers and transonic flow. Direct drive low pressure turbines are situated in the range of lower values with generally subsonic Mach numbers. Geared turbines lie in between. Both power turbines in the turboshaft and CRISP engines shown in Fig. 1 have to be designed for transonic aerodynamics.

The high temperatures in the rear part of the engine give low viscosity values. Combined with the low pressure, this results in the lowest Reynolds numbers in the engine as shown in Fig. 5. Typical values for high altitude cruise operation based on true chord and exit conditions range from 250000 for large turbines, like that of the General Electric CF6, down to about 50000 for the small Pratt & Whitney/MTU PW 300 engine. Decreasing Reynolds numbers require particularly careful design to avoid laminar separation and they limit the aerodynamic loading capability of the profiles. It is a very narrow balance between reducing the number of aerofoils and avoiding the collapse of efficiency.

Stressing and mechanical integrity requirements finally present a further constraint for the optimization. The high aspect ratio blading of the rear stages in low pressure turbines is rather sensitive to a large number of vibration modes as well as to aerodynamic instability. The need to design stiff blades does not just have detrimental effects on performance but also increases the rim loading of the discs leading to greater weight. An overall parameter giving some indication of this effect is the annulus cross section multiplied by the rotor speed $A_r N^2$. Fig. 6 shows typical values versus speed. Direct drive turbines have low speeds, which are set by the large diameter fans. They have low rim loadings resulting in light disc designs. Geared turbines lie in the range of high pressure turbines and require similarly thick and heavy discs.

This statistical review of the operational environment gives some indication of the problems that have to be resolved in the design of low pressure turbines. They cover

- High kinematic loadings and flow factors
- Subsonic to transonic Mach number range
- Medium to very low Reynolds number range
- Geometrical constraints from mechanical requirements

It should be noted that if combustor exit temperatures continue rising at the present pace, cooling of the front rows of low pressure turbine blading will have to be generally introduced by the end of this century. Such blading is already being incorporated in advanced military engines.

3. DESIGN METHODOLOGY AND BACKGROUND

The achievement and continuous improvement of aerodynamic performance calls for steady evolution of methodology. For the designer this includes two equally important aspects.

- The provision of design criteria. The physics of the flow have to be well enough understood, so that optimization conditions for the flow in the blading can be defined; and
- The provision of prediction techniques, that permit a cascade geometry to be defined, which produces the optimum flow in a real turbine with sufficient accuracy.

The process has been very successful. For example, it has completed the transition from the profile family to the controlled pressure distribution blading. As indicated in the schematic of Fig. 7, two partners are involved. Both the scientific as well as the industrial researcher and designer have offered major contributions. The different tasks they have to perform complement each other.

The industrial application usually reveals the fluid dynamics problems that need to be solved. Scientific research tries to generalize the questions and to provide answers with universal validity. This is normally done either with sophisticated experimental and numerical analysis of the fullscale problem or with simplified models which simulate a particular aspect of the flow. The direct design application of the results is not necessarily considered during the exercise.

The industrial engineer takes these results and eliminates whatever he cannot incorporate into available design methods. The remainder is combined with his own development and research experience to improve the turbine methodology. The resulting design system must be

- Simple enough to permit integration into the overall design of the machine, and

- Fast, reliable, robust, and within certain limits sufficiently precise to permit optimization with the necessary iterative processes within the very short time scales of an industrial application.

It is this latter constraint, the time scales, that imposes very strong limitations on the acceptance of advanced techniques. There is generally a time lag of about a decade between what scientific research produces and its introduction into industrial routine work. This situation requires from the participants different orientations.

- The scientific researcher should conduct long term investigations trying to define new advanced aspects of optimization and the means by which it can be achieved.
- The industrial engineer should support the development of advanced techniques. His main task is to use these techniques to continuously develop and improve his own design tools, so that he can successfully complete the short term work of making the presently best possible blading.

If these factors are considered, then the interaction between the partners will be most effective.

Turbine design systems are made up of two different levels of work, as illustrated in Fig. 8. The lower level consists of the already mentioned prediction techniques and design criteria and represents the design application phase. The first level is of a more general and fundamental nature. It forms the background of the scientific and design work accumulated over the years. It consists of five items of equal importance.

- Physics and flow analysis

Analytical studies are the basis of all numerical work leading to modern prediction techniques. They are also of great significance for the development of simplified models or semiempirical correlations. They help identify the predominant parameters of the problem, thus giving such models and correlations the desirable universality. A typical example are the boundary layer equations of L. Prandtl.

- Numerical methods

Numerical computer programmes are an accepted industrial design tool today. In fact the high performance levels and future improvements for advanced turbomachinery can only be achieved with such techniques. Two-dimensional inviscid flow and boundary layer codes are state of the art for routine design. Three-dimensional inviscid methods have reached a high level of maturity, their general use however is inhibited by the relatively low speed of the computers. This applies even more to Navier-Stokes and unsteady flow solutions. Dramatic advances are required and should be expected both for software and computer hardware by the end of the century. Meanwhile such codes should be used to improve the understanding of the details of fluid flow.

- Data processing, reduction and presentation

Data processing and presentation of results is emerging as a new challenging task. Three-dimensional and unsteady flows pose extreme difficulties to human comprehension. Sophisticated computer graphics and videofilm animation will be necessary to help understand numerical and experimental results and draw the right conclusions.

- Measurement techniques

Instrumentation for turbomachinery experiments has undergone just as dramatic an evolution as computational methods. Both classical pneumatic probes as well as modern laser and hot wire anemometry give the aerodynamicist an extensive insight into the details of the flow. Interpretation of the results often demands criminological talents from the engineer. Most techniques are indirect, measuring the interaction of a physical quantity of the probe with the flow parameter to be evaluated. Therefore an understanding of both the flow phenomena and the response of the probe are required.

- Experimental facilities, rigs and models

Experimental facilities have grown in size and operating range. Low pressure turbine rigs for example can be tested from take off conditions to the extremely low Reynolds number environment of high altitude flight. The most important development however has probably been the introduction of electronic computerized data acquisition systems. Reasonable handling of very large amounts of experimental results and the exploitation of the potential of advanced measurement techniques can only be achieved with their help.

This background forms the basis from which reliable and accurate prediction methods are developed and design criteria are derived. They are the ingredients of turbine design systems.

4. FLOW PREDICTION

Computational fluid dynamics is an integral part of industrial design systems and presents the basis for future turbomachinery development and improvement. The algorithms for computer programmes have been widely publicized in the recent years and are well known. In this lecture attention shall be drawn to some aspects of the maturity and application of current prediction techniques.

The codes available in a typical turbine prediction system as shown in Fig. 9. They comprise a basic quasi 3D design system and a variety of more complex inviscid and viscous, steady and unsteady, two and three dimensional methods.

The quasi 3D system always starts with an axisymmetric streamline curvature programme based on the original work of Chung-Hua Wu (1951). The model used might look rather simple, however one should bear in mind the fact that any turbomachinery design starts with nothing more than a rotor speed, some inlet conditions, a pressure ratio and a desirable efficiency level, so there is no alternative. These methods are the most versatile tool for the aerodynamicist.

They are used to define the annulus, the number of stages, work split and the radial distribution of the flow parameters. The optimization carried out by the engineer in this phase sets the performance potential of the turbine.

This exercise is the first step in the turbine design system described by Hourmouziadis and Kübner (1985), and shown in Fig. 10. The blading itself is defined after some interaction with structural requirements using two-dimensional inviscid blade to blade methods on curved stream surfaces with variable stream tube thickness and boundary layer analysis. After stacking the individual profiles into an aerofoil the process is repeated in a second cycle introducing some of the effects of the three-dimensionality of the blade geometry into the streamline curvature prediction. These are usually blockage and radial blade forces, but more precise methods using circumferential averaging of the flow have also been developed, as described for example by Jennion and Stow (1984). If the geometry looks too complicated and one does not feel very comfortable with the quasi 3D calculations, then three-dimensional inviscid computations are added. Such codes are available for individual rows, see Happel and Stubert (1988), single stages, see J. Denton (1985), or complete multistage turbines.

The experience accumulated with such systems forms the basis for some particular considerations, which will be discussed at greater length below.

4.1 TWO-DIMENSIONAL COMPUTATION OF A THREE-DIMENSIONAL PROBLEM

Quasi 3D systems are very efficient, can predict quite accurately the main characteristics of the flow, and can help design high performance turbomachinery. Nevertheless the methods used are essentially two-dimensional. Following the original idea of Chung-Hua Wu, the flow is separated into an axisymmetric (hub to tip) and a two-dimensional (blade to blade) part. On the one hand this principle has some advantages which cannot be done without today. On the other hand important phenomena, such as secondary flows, are lost by the tangential averaging and can only be accounted for in some mean way.

Advanced models could be of some help here. Even the inviscid Euler codes can predict the qualitative characteristics of secondary flows, if vorticity is introduced with the boundary conditions. Unfortunately the problem is that although prediction methods may be good enough, presently it is not possible to estimate boundary conditions with sufficient accuracy to permit computation of quantitatively reliable results.

The evolution of the end wall boundary layer moving from one row to another across a gap with leakage flow and changing from the stationary to the rotating frame is effectively terra incognita on the aerodynamics map of the engineer. This aspect of the problem is common to all turbomachinery and has to be considered together with the development of prediction techniques. It could be argued that the complete engine could be calculated. Computer time and storage however are prohibitive.

4.2 TWO-DIMENSIONAL OPTIMIZATION IN THREE-DIMENSIONAL FLOW

The design of turbine blading involves the optimization of a three-dimensional machine. One of the advantages of the quasi 3D system is the separation of this optimization into two different steps, the hub to tip and the blade to blade design. The latter is carried out on 5 to 9 spanwise sections and an average of 20 to 40 passes for the profile of each section are required until the engineer is satisfied with the result. Although the computer programmes are very efficient and the overall turnaround time for the calculation is not more than 15 min, it takes about 2 to 4 weeks to define an optimized aerofoil for a given axisymmetric solution. Feeding the result back into the hub to tip prediction and reoptimizing stacking and wall contouring takes another 20 to 40 passes and requires about 2 weeks. The two cycles shown in Fig. 10 would therefore last about 10 weeks, which are the accepted time scales today. This optimization procedure, illustrated in Fig. 11 is "twice two-dimensional". If a true three-dimensional optimization were required, then for every pass, say in the hub to tip calculation, a complete optimization of the blade profiles would be necessary to check the effect and decide if there is an improvement. It would probably take one or more years to define the turbine. This is not surprising when the degrees of freedom for the geometry variation in a turbine are considered. Presently no true 3D optimization can be carried out. It is covered primarily by the criteria used for the axisymmetric design. The situation does not change when advanced three-dimensional prediction methods are applied. Obviously automated optimization techniques will be necessary to take advantage of the full potential. Aerodynamic optimization is a trial and error procedure, with the engineer controlling the process. Expert systems and artificial intelligence will probably have to take over the role of the engineer if automated methods with acceptable time consumption are to be developed.

4.3 THREE-DIMENSIONAL EFFECTS VERSUS RESOLUTION OF FLOW DETAILS

One of the main limitations to the application of computational fluid dynamics is the computer memory size required. Given a certain storage capacity, mesh density has to be reduced with increasing space of the flow domain. In other words going from a two-dimensional to a three-dimensional prediction method, the resolution of the flow has to be decreased. Fig. 12 compares a high mesh density blade to blade solution with the results of a three-dimensional prediction of a transonic turbine blade. Capturing the details of the flow around the trailing edge is virtually impossible for the latter method. However it is exactly this part of the flow that defines the strength of the shock originating on the pressure side of the trailing edge. After crossing the passage it interacts with the suction side boundary layer and may cause total separation. Along large portions of the span these phenomena dominate over 3D effects and present the main design concern.

This example demonstrates that the selection of the prediction method should not be based on the universality of the computational model alone, but primarily on its ability to resolve the important characteristics of the flow.

4.4 THE RIGHT CODE FOR THE RIGHT PROBLEM

A similar situation arises whenever the question is posed, which is the appropriate technique to handle a specific problem. An example is given in Fig. 13. It shows a typical low pressure turbine annulus with a first guide vane of a multistage machine and the calculated pressure distributions at the mean section. They were predicted with

- a quasi 3D system on a stream surface of revolution,

- a 3D Euler code and taken along a stream surface of revolution, and
- with the same code, along the individual suction and pressure side stream lines (twisted stream surface).

The differences are rather small and except for the suction side diffusion, well within the necessary accuracy for a safe design. Obviously for this type of blading with an aspect ratio of about 3, the inviscid three-dimensional effects are only of secondary importance. Therefore for the computation of the profile pressure distribution the simpler two-dimensional code would be sufficient.

As already mentioned, the main difference can be observed on the rear half of the suction side. The level of the static to total pressure ratio is lower, or the Mach number higher, for the quasi 3D prediction. This can be easily explained when the radial distribution of the Mach number upstream and downstream of the guide vane row is compared in Fig. 14. The quasi 3D and the full 3D methods predict the same inlet conditions, but the former gives the higher exit Mach number at the mean section. The reason for this is that the quasi 3D system uses the complete turbine for the hub to tip solution, whereas the guide vane is isolated for the full 3D code. This procedure has no influence on the inlet flow, because in both cases a diffusing annulus without blading is used. In the exit flow however the interaction with the closely spaced downstream rotor blade has been eliminated for the full 3D case. When the effects on streamline curvature are considered, then the resulting differences in radial flow distribution shown in Fig. 14 are as expected.

This example shows that for the investigated problem the inviscid three dimensional effects are far less important than the interaction between rows. If the aerofoil has to be isolated from the multistage turbine to do the prediction, then the application of a full 3D model gives less accurate results and is not justified. However this should not be misunderstood as a recommendation to abandon advanced techniques in favour of simpler ones. The point that should be made is that the different methods have to be applied selectively. There are other examples, where the contrary is true. Quasi 3D systems are absolutely inadequate for calculations of large pitch, long chord cascades, or of the heavily twisted, bend and bowed blading for secondary flow control. The minimum required in these cases are 3D Euler codes.

5. EXPERIMENTAL TECHNIQUES

Experimental facilities and measurement techniques constitute the second main contributor to turbine design methodology and have also undergone a revolutionary development in the past two decades. Research and development work is undertaken today with models, plane cascades, annular cascades and rotating rigs in test facilities which permit simulation of the most extreme aerodynamic operating conditions. Appropriately instrumented rigs, modern measurement techniques and computerized data acquisition systems offer the possibility to gain a tremendous insight into the details of the flow.

A general survey of the available methods is shown in Fig. 15. The classical techniques for power, mass flow, temperature and pressure measurement ranging from wall pressure taps to five hole probes for three-dimensional flow have been complemented by a variety of more sophisticated ones. Some of them are applicable to the stationary frame only, others can be used to carry out an experimental analysis of the flow in the rotating frame. A review has been presented by Hourmouziadis and Lichtfuß (1985). Difficulties with experimental studies and diagnostics arise primarily with the access to the flow in the rotor blading. The techniques that have been used to deal with this particular problem and some recent developments will be discussed in more detail.

5.1 TELEMETRY

The original methods to transfer electric signals from the rotating to the stationary frame were slip rings or mercury drums for higher rotating speeds. Pressure measurements which are more interesting from an aerodynamic point of view required much more complicated equipment. Fig. 16 shows one of the early rigs used by Dettmering (1957) to measure blade profile statics and to traverse the rotor exit total pressure. A special gear was necessary to position the probe, which was mounted on the turbine wheel. A switching system mounted in the shaft fed the individual pressures into a semirotating drum, from where they were picked up for indication. The facility was very successful, but it required much space which is only available in rigs for laboratory research.

In the meantime there has been strong pressure on the industry to develop telemetry systems for the verification of the structural reliability of rotating parts. Using strain gages, overstressing, vibration and flutter risks can be identified and improvements can be introduced early in the engine programme. These telemetry systems have reached a high level of maturity and are already being used for aerodynamic investigations. Fig. 17 from Hourmouziadis and Lichtfuß (1985) shows the components of such a system mounted on the shaft axis. It consists of pressure transducers, pressure and temperature signal transmitters, antenna and power receiver.

The rotor blade Mach number distributions derived from static pressures on the aerofoil surface are shown in Fig. 18. One of the main problems encountered with this technique is the correction of the indicated value for the difference between the location of the pressure tap and the transducer. The pressure lines are rotating with the relative frame and considerable gradients build up between different radii. One way of resolving this problem is to measure reference static pressures on both the stationary and the rotating system. These results can then be used for calibration purposes.

5.2 SURFACE HOT FILMS

With surface hot films the principle of hot wire anemometry is applied to the flow on the wall. The probes are mounted on thermally and electrically insulated surfaces and the heat transfer to the flow is measured. If the wall is adiabatic, then the signal is only a function of the mean wall shear stress. Accordingly, this technique has been applied widely for boundary layer research. In turbomachinery the adiabatic conditions can only be realized in a laboratory environment, such as cascade tunnels (Bräunling, Quast and Dietrichs, 1988) and low speed rotating blading (Hodson, 1983; Hodson and Addison, 1988).

For industrial applications telemetry offers the full potential for investigations in the rotating frame, although it has not been applied extensively yet. The main problem here is that the adiabatic wall condition can hardly be fulfilled in high speed fullscale turbomachinery. Nevertheless qualitative analysis of the signal can give a very detailed

understanding of the boundary layer flow. Fig. 19 gives an example of measurements on the guide vane of a two-stage turbine reported by Hourmouziadis, Buckl and Bergmann (1986). The wakes of the upstream blading make it difficult to isolate flow disturbances from the overall signal. In the lower part of the oscilloscope pictures the passing frequency has been filtered out revealing the local structure of the boundary layer.

- Stable laminar flow to relative surface length 55.8%
- Increasing instability until laminar separation occurs between 68.8% and 75.3%
- Bursts appearing at 75.3% indicating transition in the separated shear layer
- Strong turbulent reattachment fluctuations at 81.8%
- Low disturbance level in the fully developed attached turbulent boundary layer at 94.8%.

5.3 HOT WIRE ANEMOMETRY

Pressure taps and surface hot films on rotor blading require a device to transfer the signals from the rotating to the stationary frame. This also applies to hot wire anemometry when it is used on the rotor, as reported by Hodson (1984) for his investigations in a large scale turbine. The latter technique however can also be used with the probe located on the stationary frame and still permits an evaluation of the rotor flow. The hot wire is traversed radially downstream of the rotor. Computerized ensemble averaging of the data gives detailed information of the wake flow of the individual aerofoils in one circumferential position. The potential of this technique for three dimensional analysis of the flow has been demonstrated by Sharma, Butler, Joslyn and Dring (1985) with the data obtained with the UTRC Large Scale Rotating Rig (LSRR) research turbine. Further evaluation of the data and application of the reduction and presentation techniques discussed earlier resulted in the very impressive animation of the unsteady secondary flow presented by Sharma, Butler, Renaud, Millsaps, Dring and Joslyn (1988).

The potential for industrial applications has been shown by Binder, Schröder and Hourmouziadis (1988). Hot wire measurements and the ensemble averaging technique were applied to a multistage low pressure turbine with subsonic flow (Fig. 20). A beat frequency was observed both in the velocity wakes as well as in the turbulence wakes of the blading. The analysis of the experimental data identified a strong interaction between two successive rotor blade rows. The downstream blade separated when the wakes of the upstream rotor hit the leading edge and had attached flow when they were convected through the middle of the passage. The phenomenon was steady in the rotating frame. This means that aerofoils with separated flow always remained separated because they were always hit by the wakes of the corresponding upstream rotor blade.

5.4 LASER ANEMOMETRY

Laser anemometry is even more suitable for the investigation of the relative flow. Provided the test volume is accessible to the light beam, the flow field can be measured even within the blade passage. Laser beams are focused through a window in a very small volume (measuring point) within the flow. The laser light scattered by very small particles is the signal that is used for further evaluation. Assuming that the momentum of the particles is very small so that they move with the local and instantaneous velocity of the flow, then the measured signal is some function of that velocity.

Two methods have evolved from this principle. Doppler laser anemometry works with one beam and the Doppler effect is used to evaluate the signal. Laser 2 focus anemometry works with two beams focused very close together and the particle passage through the individual foci is statistically analysed to evaluate the flow velocity. The former technique is primarily applied in America the latter in Europe. Both have their merits and have been very successful. They have provided some excellent results. Application in compressor tests has been published by Williams (1987) and Epstein, Gertz, Owen and Giles (1988). Binder (1985) and Binder, Förster, Kruse and Rogge (1985) used the laser 2 focus method for an experimental study of secondary flows in turbine rotors.

The problem with laser anemometry is the presence of a sufficient amount of light scattering particles in the flow. The technique requires a large number of events (particle passages through the focus) for the statistical evaluation. In dead water regions with low velocities and poor mass exchange rates with the main stream this condition is not satisfied. The method does not give quantitative results. But even in this case it can be very well used to diagnose the presence of the separation. Such a situation is illustrated in Fig. 21 taken from Hourmouziadis and Lichtfuß (1985). The velocity vectors were measured in five radial and five axial stations within the blade passage. Only the velocities at the hub mean and tip sections are plotted in the figure. Separation at the tip could be clearly identified from these tests. The results initiated a redesign of that section improving the efficiency of the turbine by 2%.

Both laser and hot wire anemometry can evaluate velocity as well as turbulence. The former has the advantage that no probe disturbs the flow. The latter however provides the complete time history in a continuous signal. This last characteristic can prove to be very useful when unique events, for example turbulent bursts have to be identified. Recording the analog signal on tape permits repeated evaluation without having to run the experiment again. This can be a great advantage when new questions arise during the analysis of the results.

6. SOME ASPECTS OF TWO DIMENSIONAL OPTIMIZATION

The designer of turbines for aircraft engines is required to achieve two targets simultaneously

1. High efficiency
2. Low weight

High efficiency should be available under different operating conditions. Typical conditions are shown in the flight envelope of Fig. 22. They range from take off rating at low altitude to high altitude high Mach number cruise and very high altitude low mach number flight at the upper left hand corner of the envelope. Lines of constant Reynolds number

for the low pressure turbine blading are also included. They indicate the wide range that has to be covered by the design.

The characteristics of such blading are shown in Fig. 23 (Hourmouziadis and Lichtfuß, 1985), which shows the evolution of losses with Reynolds number. At high values (a) transition occurs far upstream and turbulent separation near the trailing edge produces mixing losses (3), which are added to the shear layer losses (2). With decreasing Reynolds number the turbulent separation disappears (b), transition moves downstream beyond the laminar separation point and a separation bubble (c) appears on the suction surface. In this region loss generation takes place in the wall shear layers and the wake of the trailing edge only.

Further down the Reynolds scale, losses increase dramatically (d). Transition has now moved so far downstream that the turbulent free shear layer cannot reattach before the trailing edge. The largest part of the losses now is produced by the mixing out of the separation in the wake (1). The extension of this separation away from the profile wall increases rapidly with decreasing Reynolds number, because transition is shifted downstream. It has a maximum when the transition point in the free shear layer reaches the plane of the trailing edge. Beyond that point (e) rising losses are caused by the growing free shear layer thickness with falling Reynolds number. Not reattaching laminar separation is the case of the so called strong viscous/inviscid interaction or separation bubble bursting.

There appears to be a wide Reynolds number range with low losses. The second optimization criterion however, low weight, demands small size aerofoils, which means the lowest possible Reynolds number. The designer has to work very carefully to avoid the risk of an efficiency collapse.

The loss characteristic of Fig. 23 is repeated in Fig. 24 as curve A. Of course there are alternative profile designs which can reduce the risks just described. Curve B is such an alternative. The efficiency loss at low Reynolds numbers has been reduced substantially. Unfortunately this is accompanied by a significant increase in the minimum loss levels. The first optimization criterion, high efficiency, has been penalized.

These considerations demonstrate again that two dimensional optimization needs precise and reliable design tools. One of the main physical phenomena of the flow that has to be included is the viscous regions of the flow. The engineer must be able to ensure close boundary layer control for his design.

7. THE CHARACTERISTIC OF THE PRANDTL BOUNDARY LAYER

7.1 BOUNDARY LAYER EQUATIONS

The development of the approximation of the wall shear layer can be found in every text book on fluid flow, and the theory has been applied widely in the design of turbomachinery. The fundamental equations will only be reviewed briefly here, because they form the basis for the development of the boundary layer characteristic. Ludwig Prandtl used the two dimensional, incompressible Navier-Stokes and continuity equations for his analysis.

$$\begin{aligned} u \frac{\partial u}{\partial x} + v \frac{\partial u}{\partial y} &= -\frac{1}{\rho} \frac{\partial p}{\partial x} + \nu \left\{ \frac{\partial^2 u}{\partial x^2} + \frac{\partial^2 u}{\partial y^2} \right\} \\ u \frac{\partial v}{\partial x} + v \frac{\partial v}{\partial y} &= -\frac{1}{\rho} \frac{\partial p}{\partial y} + \nu \left\{ \frac{\partial^2 v}{\partial x^2} + \frac{\partial^2 v}{\partial y^2} \right\} \\ \frac{\partial u}{\partial x} + \frac{\partial v}{\partial y} &= 0 \end{aligned} \quad (7.1)$$

Starting from the observation that strong viscous effects are only present within a thin layer close to the wall, he developed a set of equations for high Reynolds numbers neglecting all second order terms in Eq. 7.1

$$\begin{aligned} u \frac{\partial u}{\partial x} + v \frac{\partial u}{\partial y} &= -\frac{1}{\rho} \frac{\partial p}{\partial x} + \nu \frac{\partial^2 u}{\partial y^2} \\ \frac{\partial p}{\partial y} &= 0 \\ \frac{\partial u}{\partial x} + \frac{\partial v}{\partial y} &= 0 \end{aligned} \quad (7.2)$$

The momentum equation in the y direction in Eq. 7.2 contains the most significant law of wall shear layers, namely the fact that the static pressure normal to the wall is constant. The boundary layer is isobaric. This permits the Bernoulli equation of the inviscid main flow to be used to calculate the pressure gradient in the x direction from the velocity gradient dU/dx of the main stream.

$$U \frac{dU}{dx} = -\frac{1}{\rho} \frac{\partial p}{\partial x} \quad (7.3)$$

The flow field within the boundary layer can be calculated from this system of equations with the boundary conditions:

$$\begin{aligned} x = x_0 &: & u &= u(x_0, y) \\ y = 0 &: & u &= v = 0 \\ y \rightarrow \infty &: & u &= U(x) \end{aligned}$$

Further reduction of Eq. 7.2 was developed by von Karman. He introduced Eq. 7.3 into the momentum equation in the x direction and integrated along the y coordinate.

$$\int_0^{\infty} \left\{ u \frac{\partial u}{\partial x} - \frac{\partial u}{\partial y} \int_0^y \frac{\partial u}{\partial x} d\eta - U \frac{dU}{dx} \right\} dy = \nu \int_0^{\infty} \frac{\partial}{\partial y} \left(\frac{\partial u}{\partial y} \right) dy = \frac{\tau_w}{\rho} \quad (7.4)$$

with the

$$\text{Displacement thickness} \quad \delta_1 = \int_0^{h \rightarrow \infty} \left(1 - \frac{u}{U}\right) dy \quad (7.5)$$

$$\text{Momentum loss thickness} \quad \delta_2 = \int_0^{h \rightarrow \infty} \frac{u}{U} \left(1 - \frac{u}{U}\right) dy$$

he arrived at the integral form of the Prandtl boundary layer equation.

$$\frac{d}{dx} (U^2 \delta_2) + \delta_1 U \frac{dU}{dx} = \frac{\tau_w}{\rho} \quad (7.6)$$

The quotient δ_1/δ_2 is called the form parameter of the boundary layer H_{12} and is generally used to describe the state of the shear layer in terms of sensitivity to separation.

7.2 COMMENTS ON THE BOUNDARY LAYER EQUATIONS AND THEIR PARAMETERS

The displacement and momentum loss thicknesses are really only abbreviations substituting the integrals in Eq. 7.4. Nevertheless they are important quantities of the flow. The displacement thickness indicates the surplus area required in the viscous case to convect the same mass of fluid as the inviscid flow with the constant velocity U . In the case of the momentum loss thickness the nomenclature used is somewhat misleading. Actually it does not include momentum loss connected with the mass flow defect. The total momentum loss is

$$I_{\text{inviscid}} - I_{\text{viscous}} = \int_0^{h \rightarrow \infty} U \rho U dy - \int_0^{h \rightarrow \infty} u \rho u dy \quad (7.7)$$

Defining a total momentum loss thickness

$$\Delta_2 = \frac{I_{\text{inviscid}} - I_{\text{viscous}}}{\rho U^2} = \int_0^{h \rightarrow \infty} \left\{1 - \left(\frac{u}{U}\right)^2\right\} dy \quad (7.8)$$

it can be easily seen that

$$\Delta_2 = \int_0^{h \rightarrow \infty} \left\{1 - \frac{u}{U} + \frac{u}{U} \left(1 - \frac{u}{U}\right)\right\} dy = \delta_1 + \delta_2 \quad (7.9)$$

Both δ_1 and δ_2 have proved to be the appropriate parameters to describe the state of the attached wall boundary layer. In the case of separated flow however the displacement thickness fails. Separations can be handled approximately by the boundary layer concept if the velocity in the dead water zone is very low. From the definitions in Eq. 7.5 it can be readily seen that the dead water contributes directly to the displacement thickness, the height of the separation zone being added to the displacement of the free shear layer. Contrary to this, the momentum loss thickness gives only the momentum defect of the free shear layer, because the momentum loss associated with the mass defect in the dead water zone is not included and the remaining is very small within the separation. It has been observed that as long as the low velocity assumption is valid, the free shear layer is not significantly affected by the shape of the wall or by the height of the separation perpendicular to the wall. This can result in a large variation of values for the displacement thickness for the same viscous phenomenon, which is concentrated in the free shear layer, whereas momentum loss thickness remains practically constant. Accordingly it should also be kept in mind that in separated boundary layer flow the form parameter H_{12} does not necessarily make any physical sense.

The Prandtl boundary layer theory has been developed for true two dimensional incompressible flow. When it is used along curved surfaces, the stream line curvature superimposes a pressure gradient normal to the wall. This in general requires some correction. The original theory however has been applied successfully to turbomachinery profiles. In these cases the approximation appears to be acceptably good for radii of curvature larger than 20 to 50 times the boundary layer thickness.

Compressibility effects are less dominating in subsonic boundary layers than in the isentropic main flow. In the latter case it is generally accepted that they become significant for Mach numbers above about 0.3 to 0.5. The von Karman equation derived from the compressible Navier-Stokes equations is

$$\frac{d}{dx} (U^2 \delta_2) + (\delta_1 + M_\infty^2 \delta_2) U \frac{dU}{dx} = \frac{\tau_w}{\rho} \quad (7.10)$$

where M_∞ is the main stream Mach number and δ_1 , δ_2 are now defined as

$$\text{Displacement thickness} \quad \delta_1 = \int_0^{h \rightarrow \infty} \left(1 - \frac{\rho u}{\rho_\infty U}\right) dy \quad (7.11)$$

$$\text{Momentum loss thickness} \quad \delta_2 = \int_0^{h \rightarrow \infty} \frac{\rho u}{\rho_\infty U} \left(1 - \frac{u}{U}\right) dy$$

Eq. 7.10 is identical with Eq. 7.6 except for the Mach number term on the left side. It has a noticeable effect on the evolution of the shear layer for Mach numbers higher than 0.5 to 0.7. This can be understood when changes in the state

of an isentropic inviscid fluid are compared to those in an isobaric shear layer (Fig. 25). From the equations of state, where the index r indicates referenced parameters

$$\begin{aligned}\Delta s &= c_p \ln H_r - R \ln P_r \\ P_r &= \rho_r T_r = \rho_r H_r\end{aligned}\quad (7.12)$$

The density gradients with enthalpy can be derived to be

$$\begin{aligned}\text{isentropic} \quad \left. \frac{\partial \rho_r}{\partial H_r} \right|_s &= - \frac{P_r}{H_r^2} \\ \text{isobaric} \quad \left. \frac{\partial \rho_r}{\partial H_r} \right|_s &= \frac{c_p - R}{R} \frac{c_p}{H_r} \frac{1}{P_r}\end{aligned}\quad (7.13)$$

The absolute value of their ratio is

$$\left| \frac{\partial \rho_r / \partial H_r|_s}{\partial \rho_r / \partial H_r|_p} \right| = \frac{c_p - R}{R} \frac{H_r}{P_r} \frac{c_p}{P_r} \quad (7.14)$$

In cold air this gives 2.5 times higher gradients for the isentropic flow. For low pressure turbines for commercial turbofan engines, with relatively low Mach number levels, the incompressible boundary layer concept gives very reasonable results.

7.3 THE CHARACTERISTIC OF THE LAMINAR BOUNDARY LAYER

For the development of the main characteristics of the boundary layer the simple incompressible model is sufficient and will be used here. The x coordinate will be substituted by the more general streamwise coordinate s . Eq. 7.6 can be transformed into the more convenient form

$$\frac{d}{ds} \left(\frac{U \delta_2^2}{\nu} \right) + (3 + 2H_{12}) \left(\frac{U \delta_2^2}{\nu} \right) \frac{1}{U} \frac{dU}{ds} = 2 \frac{\tau_w \delta_2}{\mu U} \quad (7.15)$$

The fundamental work to arrive at an approximate solution of this equation was performed by Pohlhausen (1921) using the concept of the single parameter boundary layer. Walz (1941) developed a linearized approximation eliminating the form parameter H_{12} and the wall shear stress τ_w .

$$\frac{d}{ds} \left(\frac{U \delta_2^2}{\nu} \right) + 5 \left(\frac{U \delta_2^2}{\nu} \right) \frac{1}{U} \frac{dU}{ds} = 0.47 \quad (7.16)$$

Thwaites (1949) gives 0.45 for the constant on the right.

The important part of Eq. 7.16 is the second term on the left, known as the Pohlhausen parameter Po . It can be rewritten as

$$Po = \frac{\delta_2^2}{\nu} \frac{dU}{ds} = Re_2^2 \frac{\nu}{U^2} \frac{dU}{ds} = Re_2^2 AC \quad (7.17)$$

The Pohlhausen parameter is a function of the momentum loss thickness Reynolds number Re_2 and the acceleration parameter AC .

$$AC = \frac{\nu}{U^2} \frac{dU}{ds} \quad (7.18)$$

These two variables actually define the state of the boundary layer. In a double logarithmic diagram, with Re_2 for the ordinate and AC for the abscissa, $Po = \text{const}$ are straight lines. They are plotted in Fig. 26. The accelerating flow is shown on the right side and the absolute value of the acceleration parameter has been used for the decelerating flow and is presented mirrored about a zero AC axis on the left of the diagram.

For a zero momentum loss thickness gradient, $d\delta_2/ds = 0$, Eq. 7.16 gives $Po = 0.08$. This is the thick full line on the right hand side of the boundary layer map (Fig. 26). On this line, the boundary layer thickness remains constant along the wall. For a given Re_2 , increasing acceleration parameters beyond this curve reduce boundary layer thickness. On the left of the curve thickness increases. There is now an interesting effect that can be read out of the characteristic. In order to grow thinner, a high Reynolds number boundary layer requires a smaller AC . The acceleration parameter from Eq. 7.18 can be rewritten to read

$$AC = \frac{\mu}{2} \frac{dU/ds}{U^2} \quad (7.19)$$

This means that a high kinetic energy main flow needs very high velocity gradients to achieve high acceleration parameters. In other words, it is much easier to obtain a low velocity boundary layer thinner than a high velocity one.

Laminar separation would appear on the decelerating part of the diagram. Pohlhausen introduced fourth degree polynomial velocity profiles and tried to define separation at zero wall shear stress. He was not very successful. Thwaites (1949) used experimental results to assess a quite reliable empirical value of $Po = -0.082$ at separation. The laminar separation line is the thick dashed line on the decelerating side of the map in Fig. 26.

The map could be further completed considering the lines of constant gradients of momentum loss thickness derived from Eq. 7.16

$$\frac{d\delta_2}{ds} = \frac{1}{Re_2} (0.23 - 3Po) \quad (7.20)$$

Finally another characteristic curve can be introduced, the line of constant momentum loss thickness Reynolds number. This is important because most transition criteria are based on this parameter. For this case Eq. 7.14 gives $Po = 0.12$ also shown on Fig. 26 completing the characteristic of the laminar boundary layer.

7.4 THE CHARACTERISTIC OF THE TURBULENT BOUNDARY LAYER

A similar approach to that of Pohlhausen, regarding the turbulent boundary layer was performed by Buri (1931). However, the method was never developed to the maturity of the laminar case. One of the reasons is the higher complexity of the nature of turbulent flow. Another is the fact that with the potential of modern computers, the development of simple integral models has been largely abandoned in favour of a full numerical analysis of the two-dimensional flow.

Assuming turbulent wall shear stress to be

$$\frac{\tau_w}{\rho U^2} = \frac{\beta}{Re_2^{1/4}} \quad (7.21)$$

where β is a constant, Eq. 7.6 can be transformed into

$$\frac{d\delta_2}{ds} + (2 + H_{12}) \frac{\delta_2}{U} \frac{dU}{ds} = \frac{\beta}{Re_2^{1/4}} \quad (7.22)$$

or

$$\frac{d}{ds} (\delta_2 Re_2^{1/4}) + \frac{9 + 5H_{12}}{4} (\delta_2 Re_2^{1/4}) \frac{1}{U} \frac{dU}{ds} = \frac{5}{4} \beta \quad (7.23)$$

which looks similar to Eq. 7.16. The important parameter here is the Buri parameter Bu

$$Bu = Re_2^{1/4} \frac{\delta_2}{U} \frac{dU}{ds} = Re_2^{5/4} AC \quad (7.24)$$

It is structured very similar to the Pohlhausen parameter, the difference lying in the exponent of the momentum loss thickness Reynolds number. In a double logarithmic diagram $Bu = \text{const}$ are again straight lines (Fig. 27). Obviously a similar behaviour can be expected in terms of boundary layer growth. Using $\beta = 0.0128$ after Schlichting and Truckenbrodt (1967) and assuming a constant value $H_{12} = 1.4$ Eq. 7.22 and Eq. 7.24 give

$$\frac{Bu}{ds} = \frac{1}{Re_2^{1/4}} (0.013 - 3.4 Bu) \quad (7.25)$$

In the characteristic map of the turbulent boundary layer the line with zero thickness growth is given by $Bu = 0.0038$. The curve for constant Reynolds number follows from Eq. 7.23 with $Bu = 0.0050$. These lines are plotted on the acceleration side of the characteristic in Fig. 27. The considerations for the laminar flow still hold. A high Reynolds number turbulent boundary layer needs a smaller acceleration parameter to grow thinner. A high kinetic energy main flow requires high velocity gradients to achieve high acceleration parameters.

As already stated, Buri's work has not attracted much attention from boundary layer investigators. The more recent experimental data from the 1968 Stanford conference (Coles and Hirst, 1968) were used here to check the validity of the analysis. They are plotted in the characteristic diagram in Fig. 28. The accelerated flow reported by Herring and Norbury was driven into the region of negative thickness gradients. It can be seen very clearly that this is followed immediately by a drop in Reynolds number.

On the left of the diagram the experimental data are limited by turbulent separation. For a given Reynolds number the boundary layer cannot be decelerated beyond a certain AC value. Buri's parameter has not been used yet to define the separation condition, the limit however can be closely approximated by $Bu = -0.050$ again confirming the validity of his analysis.

7.5 LAMINAR / TURBULENT TRANSITION

Transition from the laminar to the turbulent microstructure of the flow is probably the most important phenomenon in shear layers. This is particularly true for the turbomachinery application with high levels of free stream turbulence and unsteady periodic disturbances. Nevertheless the investment in transition research compared to that for turbulence is rather limited.

The fundamental work based on laminar flow stability theory is being done in low turbulence research facilities. Taylor (1936) showed that significant effects are to be expected from free stream turbulence. These effects should correlate a characteristic size parameter of the boundary layer to the length scales of turbulence. This actually means that both amplitude as well as frequency structure of turbulence are of importance, indicating the complexity of the problem.

Experimental investigation of these phenomena using turbulence grids has been carried out mostly in low speed boundary layer tunnels and has concentrated on the effects of overall amplitude in terms of the degree of turbulence Tu . Fig. 29 shows transition Reynolds number over the degree of turbulence from the experimental results reported by McDonald and Fish (1972), Dunham (1972), Abu-Ghanam and Shaw (1980) and Blair (1982). Researchers have tried to correlate the results to the streamwise pressure gradient following the stability theory. Van Driest and Blumer (1963) give

$$Re_2^* (1 - 3.71 \cdot AC \cdot Re_2^{*2} + 29.4 \cdot Re_2^* \cdot Tu^2) = 1127 \quad (7.26)$$

Hall and Gibbings (1972) give

$$Re_2^* = 190 + e^{6.88 - 1.03 \cdot Tu} \quad (7.27)$$

Finally, Dunham (1972) gives

$$Re_2^* = (0.27 + 0.73 \cdot e^{-0.8 \cdot Tu}) \left\{ 550 + \frac{680}{1 + Tu - 21 \cdot Re_2^{*2} \cdot AC} \right\} \quad (7.28)$$

The formulas evaluated for the range of Fig. 29 yield results quite close to the experiment. However the scatter in trend with the pressure gradient (represented by the acceleration parameter) is of the same order of magnitude as the scatter of the test results. This also holds for the experiments. No general trend can be identified among the results of different investigations. The identification of different pressure gradients has therefore been omitted in the diagram. With the uncertainty of the data presently available, a straight line appears to be good enough an approximation

$$\frac{Re_2^*}{1000} = \left(\frac{TU [s]}{0.3} \right)^{-0.65} \quad (7.29)$$

Unfortunately the situation in turbomachinery is even worse. Fig. 30 shows a comparison with turbine cascade results which have been confirmed in real turbine tests. The difference is rather discouraging. One of the reasons is probably the fact that in turbomachinery flow pressure gradients are very strong, transition very often occurs in the free shear layer of separation bubbles and the mechanisms might very well differ. Another reason is that uniform and isotropic turbulence can only be established in closely controlled boundary layer experiments. Particularly in turbomachinery neither assumption holds. From the general comments about stability it is evident that the structure of turbulence should have a significant effect as suggested by Hourmouziadis, Buckl and Bergmann (1986).

This is the state of the art today. Industrial designers either develop their own transition criteria from a limited amount of turbine data and take the risk that the next design might be just beyond the edge of the cliff, or they reduce the risk at some penalty on performance as discussed earlier.

Returning to the characteristic of the Prandtl boundary layer, a range of transition Reynolds numbers between 100 and 1000 has to be assumed depending on the individual flow environment. The Reynolds number may be correlated to the level of turbulence with Eq. 7.29 and can be given in the map as a second scale on the ordinate. This completes the characteristic. It can be assembled from Fig. 26 and 27. Fig. 31 shows the laminar domain in the lower part, the transition range in the middle and the turbulent flow in the upper part.

Finally, another set of useful curves can be introduced in the characteristic. Lines of constant boundary layer growth rate are plotted in Fig. 32 using Eq. 7.20 and Eq. 7.25.

7.6 RELAMINARIZATION

While transition of the flow from the laminar to the turbulent microstructure is a well known phenomenon, the reverse is usually difficult to observe. The characteristic (Fig. 31 and 32) gives some indication as to where relaminarization could take place. The turbulent boundary layer would have to be accelerated beyond the limit of zero Reynolds number gradients into the upper right side of the diagram. Increasing the velocity gradients, the momentum loss thickness would then have to be reduced well into the transition region, probably down to Reynolds number levels of 100 to 1000 and acceleration parameters of $1.E-5$ to $1.E-6$. These high acceleration rates make it particularly difficult to carry out experiments.

Test evidence indicates that these considerations present a good approximation of the real phenomenon. Some published data have been collected in Fig. 33. Misu, Okamoto, and Kai (1985) have reported on such an investigation. Relaminarization was observed at about $Re_2 = 400$ and $AC = 4.0E-6$. Murphy, Chambers and McEligot (1983) give a range of $AC = 2.5E-6$ to $3.7E-6$ from their literature survey (Blackwelder and Kovaszny; Kline, Reynolds, Schraub and Runstadler) and $4.0E-6$ for their own experiments. Launder (1964) observed relaminarization at $Re_2 > 500$.

In turbine flow a relaminarization situation can only occur on the pressure side close to the trailing edge of the profile. However no experimental confirmation of such a phenomenon is known to the author.

8. APPLICATION TO TURBINE FLOW

Flow in axial turbines is usually quite a complex, three-dimensional phenomenon, nevertheless practically two-dimensional flow prevails over large portions of high aspect ratio aerofoils in low pressure turbines. Prediction and experimental results at the mean section of a subsonic guide vane will be used here to demonstrate the application of the Prandtl boundary layer characteristic. The investigation was carried out in a full scale turbine rig. The quasi 3D prediction system shown in Fig. 10 was used to calculate the flow. Fig. 34 shows the predicted Mach number distribution on the suction and on the pressure side of the profile. The solid line indicates the inviscid flow prediction, the dashed line shows the calculated effects of local separation for the viscous flow. Agreement with test results is satisfactory. The predicted development of momentum loss thickness around the profile is also shown.

8.1 SUCTION SIDE OF THE PROFILE

Starting at the stagnation point with a very small boundary layer thickness, zero Reynolds number and an infinit acceleration parameter, the flow accelerates very fast and the boundary layer thickens rapidly. Close behind the leading edge Re_2 and AC have reached the values shown in the boundary layer map (Fig. 35), near the line of zero boundary layer growth. Downstream of this location the velocity gradient (Fig. 34) remains almost constant for a large part of the suction surface. Because of the increasing kinetic energy in the main flow, the acceleration parameter Eq. 7.19 decreases continuously. The boundary layer stays close to the zero growth line up to about mid chord. Accordingly the increase of momentum loss thickness is very slow.

At the velocity peak the flow changes in the map across the zero AC axis into the deceleration region. Boundary layer thickness increases rapidly reaching maximum rates at the laminar separation point (see Fig. 32). The free shear layer develops downstream along the separation line of the characteristic. The viscous pressure rise in the separated region is significantly weaker than the inviscid prediction. The relatively thick laminar free shear layer becomes increasingly unstable with eventual transition into turbulence.

For the prediction, momentum loss thickness is set constant during transition. Extensive cascade and turbine rig experimental observations indicate that this is a reasonable assumption. For the very thin boundary layers encountered on turbine aerofoils transition length is practically zero and cannot be resolved with the available measurement techniques. With this assumption the free shear layer jumps in the characteristic from the laminar to the turbulent separation line at a constant Reynolds number. The acceleration parameter now has a significantly higher absolute value, which indicates that the turbulent shear layer can follow stronger deceleration rates (Fig. 34), a well known phenomenon.

In the case of the vane tested here, the shear layer reattaches. Fig. 32 again shows that the highest growth rates can be expected on the turbulent separation line. The growth rate decreases after reattachment because the acceleration parameter moves away from the separation line in the map. Beyond the reattachment point the main flow velocity decreases and the boundary layer again grows toward the separation line. In the case studied here turbulent separation before the trailing edge was just missed.

The behaviour described above, based on the predicted flow, is confirmed by the pressure measurements shown in Fig. 34. The separation bubble can be identified clearly on the flow visualization in Fig. 36. The extensive hot film measurements reported by Pucher and Göhl (1986) and Hourmouziadis, Buckl and Bergmann (1986) also prove the validity of these considerations.

8.2 PRESSURE SIDE OF THE PROFILE

Starting at the stagnation point again the inviscid prediction shows a sharp velocity peak at the leading edge (Fig. 34) caused by negative incidence. In the characteristic diagram (Fig. 37) the boundary layer upstream of the peak lies on the lower right of the acceleration side, practically on the zero growth line. Immediately after the peak it moves over to the deceleration on the separation line. Because of the low Re_2 levels -AC is particularly high, indicating that the thin laminar free shear layer can follow strong deceleration rates. This is shown in the enlarged detail in Fig. 34. The shear layer reattaches before it can transition. The downstream boundary layer is still laminar. The size of this separation bubble on true scale turbines is less than 1 mm and cannot be identified by statics or hot films. Flow visualization however (Fig. 38) shows that it is really there. The whole process takes place very close to the leading edge and at very small momentum loss thickness, therefore it has been omitted in Fig. 34.

After reattachment the flow accelerates again. In the map (Fig. 37) the boundary layer moves back across the zero AC ordinate into the acceleration part. The short acceleration is followed by a deceleration over one third of the pressure side. Rates are quite low but at low velocity giving high AC levels. This results in a fast boundary layer growth, leading to a maximum laminar thickness.

At the velocity minimum the boundary layer crosses over again into the acceleration side of the characteristic. It is now thick, at high Re_2 . As mentioned above, only moderate acceleration parameters are required to reduce the thickness. In fact the AC on the rear half of the profile lies even beyond the zero growth line. Boundary layer thickness decreases down to the levels of the leading edge. No transition was predicted on the pressure side for the aerofoil Reynolds number investigated here.

Similar results for the boundary layer development around turbine aerofoils have been reported by Hashimoto and Kimura (1984).

9. DESIGN OPTIMIZATION

The selection of the blade profiles is generally based on the requirement to minimize losses. An optimization has to be carried out for every individual application. This can be done with the help of profile families. A set of parameters is used to define a systematic variation of profile geometry. Systematic cascade tests are then carried out to determine the performance characteristics. The results are used to select the best performer for the application. Best known are the NACA family series which have been widely used for the design of aeroplane wings and compressor blading. An example for turbines has been given by Hausenblas (1961).

As already mentioned, this method was abandoned in favour of the prescribed pressure distribution design, which has become possible with the emerging of efficient computational techniques. The profiles of such blading never look the same. They are adapted individually to the aerodynamic situation in every row and spanwise location. This methodology has been given a variety of names like "Custom Tailored" or "Inverse Design", which are only other words for "Prescribed Pressure Distribution". In all cases criteria are required to decide which pressure distribution is the optimum. Usually such criteria are based on the empirical background of the designer. With the characteristic of the Prandtl boundary layer just developed however, a step further into the details of the flow is possible. This has led to the "Controlled Boundary Layer" (CBL) concept, which bases the optimization process on the evolution of the boundary layer around the profile.

Optimizing losses with this concept requires some correlation between the boundary layer parameters and the loss coefficient. The theory has been presented by Scholz (1965). The following approximate equation was derived for the losses as a function of momentum loss and displacement thickness at the trailing edge (Fig. 39)

$$\zeta = \frac{\theta_2}{1 - 2.7 \theta_1} \quad (9.1)$$

with

$$\theta_1 = \frac{\delta_{1SS} + \delta_{1PS} + d}{t \cos \alpha_2} ; \quad \theta_2 = \frac{\delta_{2SS} + \delta_{2PS}}{t \cos \alpha_2} \quad (9.2)$$

They are directly proportional to the sum of suction and pressure side momentum loss thickness of the profile. The displacement thickness in the denominator plays some kind of an amplification role and is equivalent to the effect of the trailing edge thickness d . As it was mentioned earlier, a "small" separation does not significantly affect δ_2 but contributes directly to δ_1 through the displacement of the dead water. This means that separated flow upstream of the trailing edge adds up to the amplifying effect of the trailing edge thickness. These considerations give the first three rules for the CBL concept

1. Minimize boundary layer thickness at the trailing edge
2. Minimize trailing edge thickness
3. Avoid separation upstream of the trailing edge

Eq. 9.1 and 9.2 show that it is not these parameters themselves that define losses, but the values referred to the exit flow area $t \cos \alpha_2$ shown in Fig. 39. For a given exit flow angle α_2 a high pitch t appears to be favourable. However this would tend to increase the loading and thus the boundary layer thickness at the trailing edge of the profile, which would be contrary to the first rule mentioned above. In fact there is an optimum for the pitch t which gives the minimum losses shown in Fig. 23. The curve however is very flat. In accordance with the second optimization criterion, low weight, pitch can be increased while avoiding the dramatic effects described in Par. 6. So the fourth rule would be

4. Select the highest pitch possible avoiding separation upstream of the trailing edge

These four rules are well known to the designer. The question is how to fulfill them best. Returning to the first item, Fig. 34 gives some indication of the potential for decreasing boundary layer thicknesses at the trailing edge. The pressure side has a thick boundary layer at the middle of the profile which is reduced significantly by the very strong acceleration towards the cascade exit. This is typical for the pressure side flow. Comparison of its thickness at the trailing edge with that of the suction side shows that it contributes less than one fourth of the total loss. A numerical study shows that neither the maximum thickness nor separation bubbles have a significant effect on the parameters at the trailing edge as long as the acceleration parameter is high enough. This can be also seen from the characteristic of Fig. 37. The higher the momentum loss thickness Reynolds number at the trailing edge for a given AC is, the stronger will be the reduction rate of boundary layer thickness. This holds true both for the laminar and the turbulent flow. So the fifth rule would be

5. High acceleration on the pressure side upstream of the trailing edge

On the suction side Fig. 34 shows very clearly the differences in growth rate between the laminar and the turbulent flow. The highest rate of the former, observed at the separation point (see also Fig. 32), is several times less than that of the latter. This corresponds to the well known relation for the flat plate, where laminar thickness is inverse proportional to the square root of the Reynolds number, and turbulent to the fifth root. For the example shown in Fig. 34 the last 20% of the suction surface length with turbulent flow is responsible for about one half of the total loss of the cascade. Reasonably the sixth rule would be

6. Delay transition on the suction surface as long as possible

Since transition correlates with thickness Reynolds number, Fig. 31 and 32 would suggest a design on the zero Reynolds number growth line. This requires a high positive acceleration parameter, as has been indicated by Eckardt and Weiss (1984). This in turn means that with the increasing velocity, the acceleration rate has to rise too (see Eq. 7.19). In fact the suction side Mach number distribution of Fig. 34 should be curved the other way around on the first half of the profile to meet this requirement. The seventh rule reads

7. Use suction side acceleration to control transition

In the rear part of the suction side the flow diffuses. If the boundary layer stays laminar up to the suction peak than it separates. The free shear layer transitions and reattaches forming a separation bubble (Fig. 34 and 36). This however can only happen if there is sufficient length upstream of the trailing edge for the turbulent free shear layer to reattach, requiring

8. Force suction side transition early enough to ensure reattachment

Reattachment as well as turbulent separation depend on Reynolds number and acceleration parameter too (fig. 31 and 35). Since separation at the trailing edge should be avoided and high momentum loss thickness Reynolds number boundary layers can follow lower deceleration rates only, the last rule is

9. Limit trailing edge diffusion to keep the flow attached

The controlled boundary layer concept sounds reasonable. Prediction techniques today are good enough to permit its successful application. Unfortunately it includes a fundamental problem which has not been solved yet. Items 6 and 8 require precise prediction of transition. As discussed in Par. 7.5 the theoretical and experimental basis today is not sufficient. Neither boundary layer nor Navier-Stokes solutions appear to have the capability to give an answer. Presently the application of the nine CBL design rules will have to rely in this point on the experience of the designer.

10. TRANSSONIC TURBINES

Geared low pressure turbines work with transsonic flow because of the high tangential velocities of the rotors. Direct drive turbines can also have transsonic Mach numbers to increase power output per stage and reduce the number of stages. Brief comments will be made here on the two main problems encountered in such designs:

- Shock structures and related losses
- Shock boundary layer interactions

Transonic aerodynamics are inevitably connected with compression shocks which cause an entropy rise without viscous effects being involved. These losses grow exponentially with the intensity of the shocks and local shock Mach numbers should be limited to less than 1.5 to avoid strong performance deterioration. The shock structures that can appear in a turbine cascade are shown in Fig. 40. A supersonic bubble (f) can develop on the suction side close to the leading edge usually returning to subsonic velocities via a compression shock (e). This phenomenon depends on the inlet conditions and the profile geometry and can occur at entry Mach numbers as low as 0.5 to 0.6 limiting significantly the design flexibility. At subsonic exit Mach numbers higher than about 0.9 a similar supersonic bubble develops upstream of the trailing edge (g) and closes with a straight shock (h). With increasing Mach number this shock moves downstream and forms the suction side trailing edge shock. For supersonic exit conditions a shock structure with two oblique shocks is formed at the trailing edge. This configuration is shown in the schlieren photograph of Fig. 40 from Dietrichs, Hourmouziadis, Malzacher and Bräunling (1987). The pressure side leg of this shock structure (a) crosses the passage and is reflected on the suction surface of the profile (c). Shock losses can be kept low if Mach numbers are limited. The designer has to take care that in transonic regions, where the flow is particularly sensitive to minor geometry changes, unnecessarily strong accelerations increasing the shock intensity are avoided. Isentropic diffusion can also be applied, as has been widely introduced for the supercritical compressor aerofoils. It can be used to decelerate the flow from the supersonic bubble into the subsonic regime. Unfortunately this principle does not work for the most intensive trailing edge shocks. The schlieren of Fig. 40 show that these shocks originate essentially from the wake region of the profile and are not affected directly by geometry variations. No tools are available today to control the flow in this region.

The second problem of transonic flow, the shock boundary interaction, has attracted much experimental and analytical attention. Comprehensive reviews have been presented by Stanewsky (1973) and Delery and Marvin (1986). Two characteristics of the phenomenon make it much more difficult to model than the subsonic boundary layer.

- The Prandtl theory does not apply to the shock impingement point
- Even in weak interactions there is a distinct upstream effect on the boundary layer.

Fig. 41 from Dietrichs, Hourmouziadis, Malzacher and Bräunling (1987) will be used to describe the interaction and comment on the problems for the designer. Laminar flow is assumed upstream of point (a) and the wall curvature is such, that together with the displacement effects of the wall boundary layer the incoming flow is parallel. An oblique shock impinges on the shear layer. The viscous flow cannot follow the discontinuity and tends to spread the pressure rise over a finite length. Starting at (a) the boundary layer can follow an adverse pressure gradient until laminar separation occurs at (b). In this region the pressure rise leads to a faster boundary layer growth. This creates in combination with the wall contour a stream line curvature which initiates in the supersonic flow a compression wave at (a). The streamwise pressure distribution on the wall is produced by the main flow. The interaction of the stream line curvature resulting from the growth of displacement thickness and the camber of the wall give the pressure rise law in the so called "free interaction" region from (a) to (b).

Pressure gradients in laminar flow are usually very weak and the effects on the flow cannot be separated with the schlieren optics. The typical pressure rise cannot be clearly identified from wall statics either, suggesting that the free interaction in laminar turbine flow is negligibly short.

At the separation point (b) the flow has the strongest adverse gradients the laminar shear layer can follow. Since it thickens downstream, these gradients must decrease continuously resulting in a slowing down of the pressure rise. Here again the pressure will be imposed by the main flow. The streamline curvature must be such that the induced compression wave gives the pressure distribution required by the shear layer. This is achieved in the flow with the adaption of the dead water zone. The shear layer is lifted so far away from the wall that the total displacement effect gives the necessary curvature. The pressure gradient tends asymptotically to zero, the compression wave becomes weaker and the flow tends to become parallel. The compression waves usually combine within the cascade passage to form a first reflected shock which can be recognized in the schlieren of Fig. 40. The behaviour of the viscous flow up to the shock impingement point (c) is very similar to the subsonic case and at least for moderate supersonic Mach number levels the Prandtl theory appears to be applicable.

At (c) the oblique shock arrives at the fringe of the free shear layer. By now it has interacted with the compression waves and the discontinuity has weakened considerably. Outside of the interaction zone the oblique shock turns the flow. At the shear layer this turning has to be realized by an expansion wave at (c) which can be identified very clearly in the schlieren photograph. It can be observed that this expansion takes place over a very short length, indicating effectively the presence of a Prandtl Meyer corner expansion. It is at this point that the most dramatic change in the properties of the shear layer occur. The diffusion capability increases suddenly. The gradients downstream of (c) are significantly stronger than upstream. This phenomenon cannot be explained with the Prandtl boundary layer theory which obviously does not apply because of the extremely small radii of curvature. In fact the impingement point of the shock seems to be the only situation in the interaction where the assumptions required for the Prandtl approximation are not valid. The mechanism introducing momentum into the shear layer is not understood yet. Downstream of the expansion wave the pressure distribution is again defined by the free shear layer leading to a second continuously weakening compression which forms a second reflected shock. Downstream of the reattachment point (d) the compression wave is weaker because the pressure gradients for the attached flow are lower than those for the separated boundary layer. Parallel flow is assumed downstream of point (e).

These characteristics apply both to the fully laminar as well as to the fully turbulent flow. The main difference is the considerably higher pressure gradients in the latter case. The presence of laminar/turbulent transition within the interaction tends to severely complicate the problem. Although the behaviour of the flow is of extreme importance for transonic turbine performance and some excellent predictions of the fundamental phenomenon exist, no model appropriate for design is available today, including transition initiated by the shock impingement.

11. 3D BLADING DESIGN

The final step in the aerodynamic turbine design process is the stacking of the two-dimensionally defined profiles into a three-dimensional aerofoil. Of course turbine blading has always been three-dimensional. The modern name for "3D designed blades" simply indicates that the stacking is done purposefully to achieve some clearly defined aerodynamic target.

There are two different effects that can be achieved by the selection of the stacking law:

- Change in the radial distribution of flow parameters through radial blading forces
- Reduction of secondary flows and losses

The former can be derived directly from the well known radial equilibrium equation for axisymmetric turbomachinery flow:

$$\frac{1}{\rho} \frac{\partial p}{\partial r} = \frac{c_u^2}{r} - \frac{c_m^2}{R} \cos \epsilon - c_m \frac{\partial c_m}{\partial m} \sin \epsilon + F_r \quad (11.1)$$

The first term on the right side is the swirl component which is used in forced vortexing to change the radial pressure gradient. The second is the streamline curvature and the third the conical flow term. Both can be influenced by end wall contouring. The last is the blading force term. If the aerofoil force has a component in radial direction than Eq. 11.1 shows that it can influence the radial pressure gradients the same way the swirl of the flow or the streamline curvature do.

One school of thought interpreting these effects evolved in the Soviet Union from the first experiments reported by Fillipov and Wang (1964) and is now regularly represented by more recent publications from China. The explanation offered suggests that leaning the aerofoils moves high loss fluid from one end wall to the other, increasing losses there. This argument is not very convincing. Since entropy is a mass specific property, a very strong radial mass transport all across the span would have to be involved. Radial transport occurs in axial turbomachinery only in the dead water of separation zones. However the radial velocities are so small that no significant amount of mass is moved along the span.

The explanation given by Dejc and Trojanovskij (1973) appears to be more reasonable. They suggest that the observed redistribution of losses is caused indirectly by the radial redistribution of reaction. This has been confirmed by more recent measurements. The results reported by Hourmouziadis and Hübner (1985) show that the selection of radial stacking can substantially change the spanwise distribution of loading, as it is shown in Fig. 43 for the straight, tangentially leaned and bowed vanes of Fig. 42. This effect gives the designer another degree of freedom besides forced vortexing to optimize the blading. The individual rows can be designed for maximum loading at best performance. Such low pressure turbines are already in production today.

The other phenomena that can be influenced by 3D design are secondary flows and associated end wall losses. Although the general characteristics of secondary flow development have been investigated experimentally and analytically for some time now, there is no detailed understanding of loss production and how it is affected by the aerodynamic design parameters today. However the database is building up so that the industry should be in a position to design turbines with reduced secondary losses in the next few years.

Presently the philosophy applied essentially tries to compensate the indirect effects of over and underturning caused by the secondary vortices. The resulting incidence changes give rise to higher losses in the downstream row. In compressor aerodynamics this has led to the "end bend" blading. Fortunately turbines are not so sensitive to incidence changes, so no end bend bladings have been offered yet. There is one component in low pressure turbines however that can profit from such a compensation and can improve directly the engine performance. It is the exit guide vane, which eliminates the swirl of the flow, to avoid separation losses at the hub cone and thrust reduction at the nozzle. Such solutions have also already been developed for production engines.

12. CONCLUDING REMARKS

This lecture has given a short review of the state of the art in the optimization of low pressure turbine design from the industrial point of view. Of course it cannot possibly be complete because it is based on the experience of the author alone. Nevertheless it has demonstrated the transition from the profile family to the more sophisticated design philosophies and has given some indication of the background that is necessary today to build up a modern high performance level methodology. The following list of unresolved fundamental problems and comments will conclude the presentation.

- A turbine design methodology requires both accurate prediction as well as optimization criteria. Both items are of equal importance.
- Transition control is of paramount importance for the exploitation of the aerodynamic performance potential. Present understanding of transition phenomena in turbomachinery is not sufficient to ensure low risk high performance design.
- Turbulence and periodic unsteadiness are different phenomena. They have to be clearly separated to be able to develop simplified models with universal validity.
- Transonic turbines will contribute significantly to the overall performance of gas turbine engines in the future. Efficient design tools as well as optimization criteria still have to be developed.
- End wall losses present several percent of efficiency potential. The understanding of their production, their interaction with secondary flows and criteria for minimization still have to be developed.
- Presentation techniques to improve comprehension of three dimensional and unsteady flow will play an important role in future aerodynamic research.

ACKNOWLEDGEMENT

The author would like to dedicate this lecture to his father Dr. Anastasios Hourmouziadis on his 90th birthday. His deep understanding and respect for nature and physical phenomena, his knowledge of human nature and his considerate but demanding guidance have enabled this report.

REFERENCES

- Abu-Ghanam B.J., R.Shaw (1980)
Natural Transition of Boundary Layers - The effects of Turbulence, Pressure Gradient and Flow History
Journal of Mechanical Engineering Science, No 5, 1980, pp 213-228
- Binder A. (1985)
Instationary Flow Effects in the Rotor of a Turbine
PhD thesis, RWTH Aachen, FRG, 1985, ESA-TT-1001
- Binder A., W.Förster, H.Kruse, H.Rogge (1985)
An Experimental Investigation into the Effect of Wakes on the Unsteady Turbine Rotor Flow
Journal of Engineering for Gas Turbines and Power, April 1985, pp 458-465
- Binder A., T.Schröder, J.Hourmouziadis (1988)
Turbulence Measurements in a Multistage Low-Pressure Turbine
33rd ASME Gas Turbine and Aeroengine Congress, Amsterdam, The Netherlands, 6-9 June 1988, Paper 88-GT-79
- Blair M.F. (1982)
Influence of Free Stream Turbulence on Boundary Layer Transition in Favourable Pressure Gradients
Journal of Engineering for Power, October 1982, pp 743-750
- Bräunling W., A.Quast, H.-J.Dietrichs (1988)
Detection of Separation Bubbles by Infrared Images in Transonic Turbine Cascades
33rd ASME Gas Turbine and Aeroengine Congress, Amsterdam, The Netherlands, 6-9 June 1988, Paper 88-GT-33
- Buri A. (1931)
Eine Berechnungsgrundlage für die turbulente Grenzschicht bei beschleunigter und verzögerter Grundströmung
Dissertation, ETH Zürich, 1931
- Coles D.E., E.A.Hirst (1968)
Computation of turbulent Boundary Layers
AFOSR-IFP-Stanford Conference, Volume II, 1968
- David O., J.Hourmouziadis, N.Marx, (1969)
Auslegungsdiagramme für Axialturbinenstufen
Mitteilungen aus dem Institut für Luftfahrttriebwerke der Technischen Universität Berlin, Nr. 3, März 1969
- Dejc M.E., B.M. Trojanovskij (1973)
Untersuchung und Berechnung axialer Turbinenstufen
VEB Verlag Technik, Berlin, 1973
- Delery J., J.G.Marvin (1986)
Shock-Wave Boundary Layer Interactions
AGARDograph No 280, Agard-AG-280, February 1986
- Denton J.D. (1985)
The calculation of Fully Three Dimensional Flow through Any Type of Turbomachine Blade Row
AGARD lecture Series on Three Dimensional Computation Techniques Applied to Internal Flows in Propulsion Systems
Rome, Italy, 6-7 June 1985
- Detterming W. (1957)
Strömungsuntersuchungen an rotierenden Schaufelgittern
Jahrbuch 1957 der WGL
- Dietrichs H.-J., J.Hourmouziadis, F.Malzacher, W.Bräunling (1987)
Flow Phenomena in Transonic Turbine Cascades - Detailed Experimental and Numerical Investigation
8th ISABE, International Symposium on Air Breathing Engines, Cincinnati, Ohio, 15-19 June 1987
- Dunham J. (1972)
Predictions of Boundary Layer Transition on Turbomachinery Blades
NATO AGARDograph No 164, 1972, pp. 55-71
- Eckardt D., H.Weiss (1984)
Entwicklung der Niederdruckturbinen für das Triebwerk PW 2037
DGLR Jahrestagung, Hamburg 1-3 Oktober 1984
- Epstein A.H., J.B.Certz, P.R.Owen, M.B.Giles (1988)
Vortex Shedding in High-Speed Compressor Blade Wakes
Journal of Propulsion and Power, May 1988, pp 236-244

- Filippov G.A., Zhong-Chi Wang (1964)
The Effect of Flow Twisting on the Characteristic of Guide Rows
Teploenergetika, May 1964, pp 54-57
- Hall D.J., J.C.Gibbins (1972)
Influence of Free Stream Turbulence and Pressure Gradient upon Boundary Layer Transition
Journal of Mechanical Engineering Science, No 2, 1972, pp 134-146
- Hapel H.-W., B.Stubert, (1988)
Computation of Transonic 3D Cascade Flow and Comparison with Experiment
AGARD 62nd Fluid Dynamics Panel, Symposium on Validation of Computational Fluid Dynamics
Lisbon, Portugal, 2-5 May 1988
- Hausenblas H. (1961)
Profilmfamilien für Turbinenteile von Gasturbinen
Motortechnische Zeitschrift, 1.1961, pp 26-29
- Hodson H.P. (1983)
Boundary Layer and Loss Measurements on the Rotor of an Axial-Flow Turbine
28th ASME Gas turbine Conference, Phoenix, Arizona, USA, 27-31 March 1983, Paper 83-GT-4
- Hodson H.P. (1984)
Measurements of Wake-Generated Unsteadiness in the Rotor Passages of Axial Flow Turbines
29th ASME Gas turbine Conference, Amsterdam, The Netherlands, 4-7 June 1984, Paper 84-GT-189
- Hodson H.P., J.S.Addison (1988)
Wake Boundary Layer Interactions in an Axial Flow Turbine Rotor at Off-Design Conditions
33rd ASME Gas Turbine and Aeroengine Congress, Amsterdam, The Netherlands, 6-9 June 1988, Paper 88-GT-233
- Hourmouziadis J., F.Buckl, P.Bergmann (1986)
The Development of the Profile Boundary Layer in a Turbine Environment
31st ASME Gas Turbine Conference, Düsseldorf, Germany, June 1986, Paper 86-GT-244
- Hourmouziadis J., N. Hübner (1985)
3-D Design of Turbine Airfoils
ASME 30th International Gas Turbine Conference, Houston, Texas, USA, 18-21 March 1985, Paper 85-GT-188
- Hourmouziadis J., H.-J.Lichtfuß (1985)
Modern Technology Application to Compressor and Turbine Aerodynamics
7th ISABE, International Symposium on Airbreathing Engines, Beijing, People's Republic of China, 2-6 September 1985
- Jennion I.K., P.Stow (1984)
A Quasi-Three-Dimensional Turbomachinery Blade Design System
Part 1 - Throughflow Analysis
Part 2 - Computerized System
ASME 29th International Gas Turbine Conference, Amsterdam, The Netherlands, 4-7 June 1984, Papers 84-GT-26 and 84-GT-27
- Launder B.E. (1964)
Laminarization of the Turbulent Boundary Layer in a Severe Acceleration
Journal of Applied Mechanics, December 1964, pp 707-708
- McDonald H., R.W.Fisch (1972)
Practical Calculations of Transitional Boundary Layer
NATO AGARDograph No. 164, 1972, pp 33-45
- Misu I., T.Okamoto, Y.Kai (1985)
Reverse Transition of Turbulent Corner Flow in Contraction of Rectangular Section
Journal of the Japanese Society of Aeronautical and space Sciences, March 1985, pp 38-44
- Murphy H.D., F.W.Chambers, D.M.McEligot (1983)
Laterally Converging Flow. Part I Mean Flow
Journal of Fluid Mechanics, 1983, pp 379-401
- Pohlhausen K. (1921)
Zur näherungsweise Integration der Differentialgleichung der laminaren Reibungsschicht
Zeitschrift für Angewandte Mathematik und Mechanik 1, 1921, S. 252-268
- Pucher P., R.Göhl (1986)
Experimental Investigation of Boundary Layer Separation with Heater Thin-Film Sensors
31st ASME Gas Turbine Conference, Düsseldorf, Germany, June 1986, Paper 86-GT-254
- Schlichting H., E.Truckenbrodt (1967)
Aerodynamik des Flugzeuges
Vol. 1, 2nd Ed., Springer Verlag, 1967
- Scholz N. (1965)
Aerodynamik der Schaufelgitter, Band 1
G.Braun, Karlsruhe, 1965

Sharma O.P., T.L.Butler, H.D.Joslyn, R.P.Dring (1985)
Three-Dimensional Unsteady Flow in an Axial Flow Turbine
Journal of Propulsion and Power, January 1985, pp 29-38

Sharma O.P., E.Renaud, T.L.Butler, K.Milsaps Jr., R.P.Dring, H.D.Joslyn (1988)
Rotor-Stator Interaction in Multi-Stage Axial-Flow Turbines
24th AIAA/SAE/ASME/ASCE Joint Propulsion Conference, Boston, Massachusetts, 11-13 Juli 1988, Paper AIAA 88-3013

Smith S.F., (1965)
A Simple Correlation of Turbine Efficiency
Journal of the Royal Aeronautical Society, July 1965, pp 467-470

Stanewsky E. (1973)
Shock-Boundary Layer Interaction in Transonic and Supersonic Flow
VKI Lecture Series 59, Transonic Flows in Turbomachinery, 21-23 May 1973

Taylor G.I. (1936)
Some Recent Developments in the Study of Turbulence
Proceedings of the Royal Aeronautical Society, 56, 1936

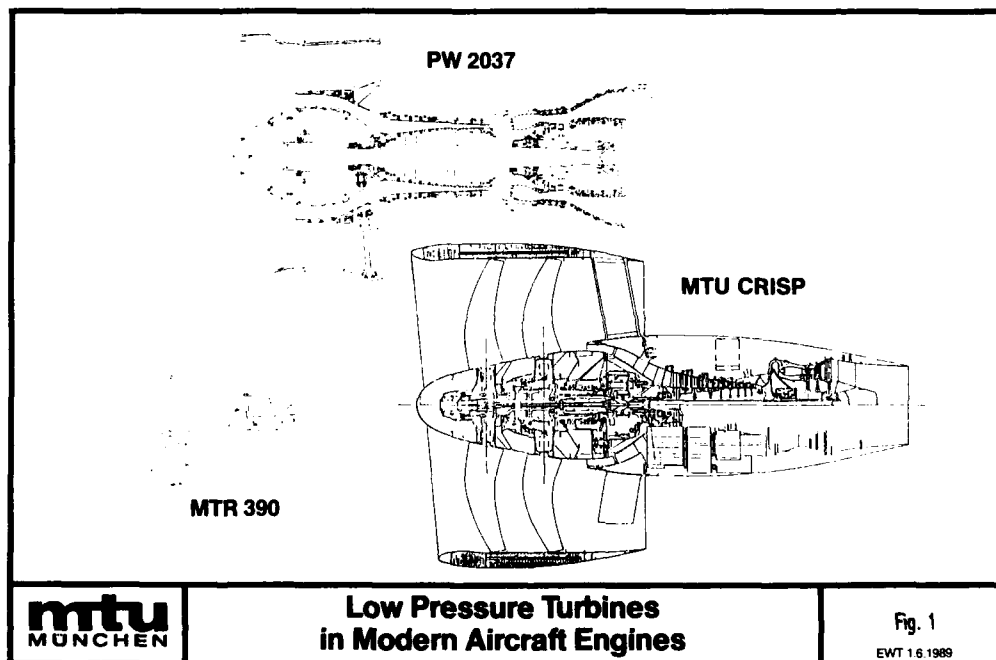
Thwaites B. (1949)
Approximate Calculation of the Laminar Boundary Layer
Aeronautical Quarterly, 1949, pp 245-280

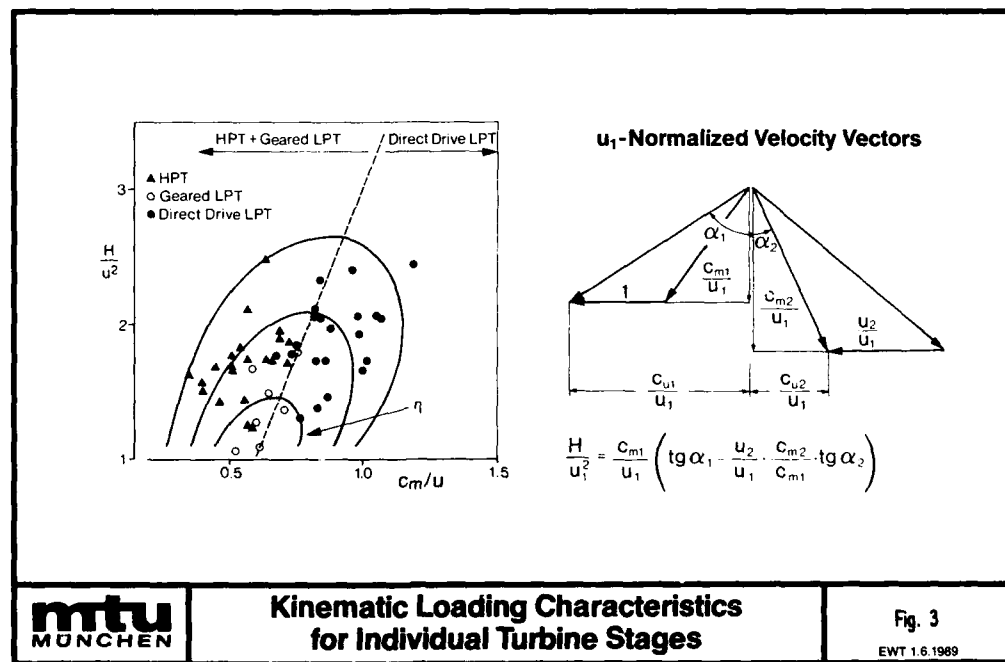
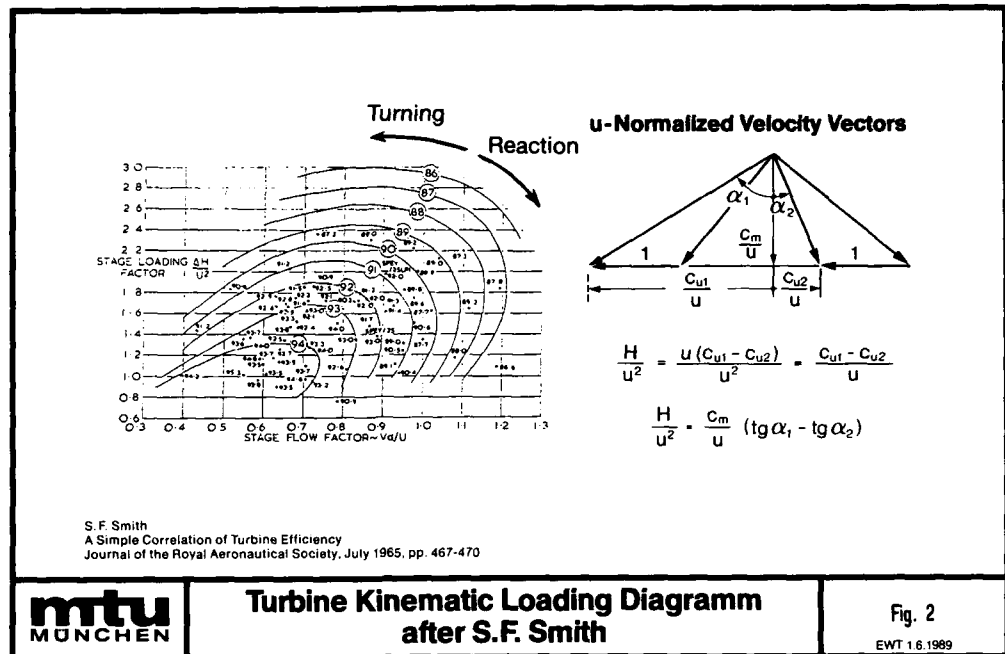
Van Driest E.R., C.B.Blumer (1963)
Boundary Layer Transition: Free Stream Turbulence and Pressure Gradient Effects
AIAA Journal, June 1963, pp 1303-1306

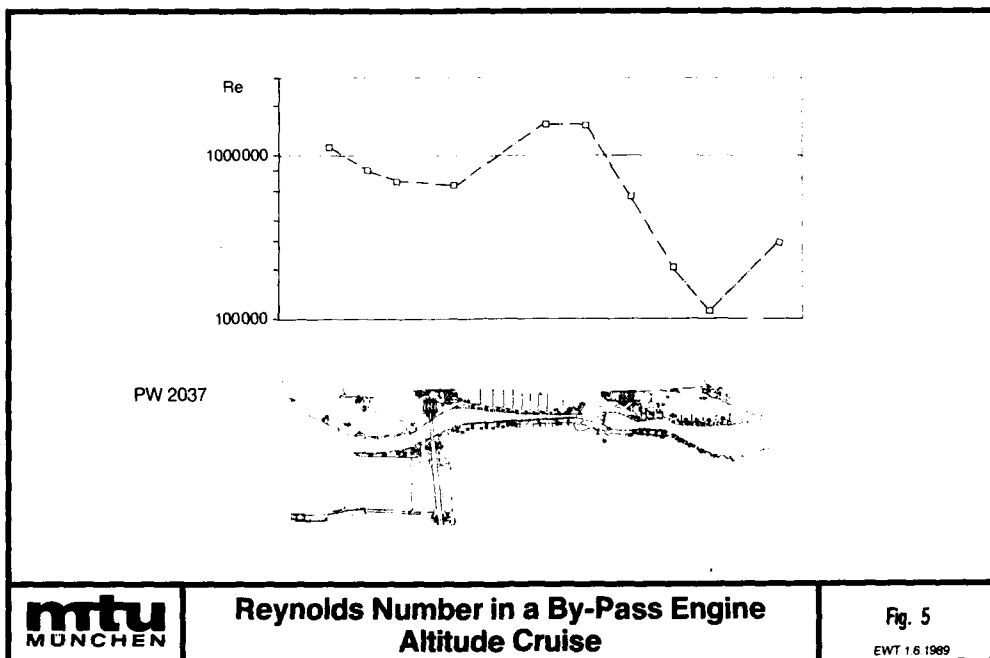
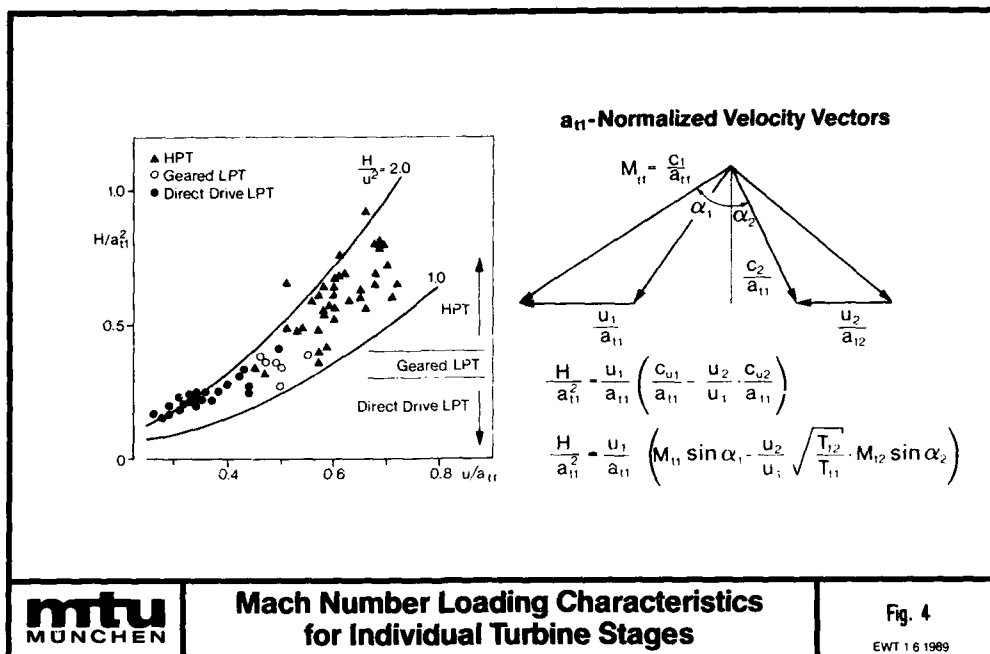
Walz A. (1941)
Ein neuer Ansatz für das Geschwindigkeitsprofil der laminaren Reibungsschicht
Lilienthal-Bericht 141, 1941, S. 8-12

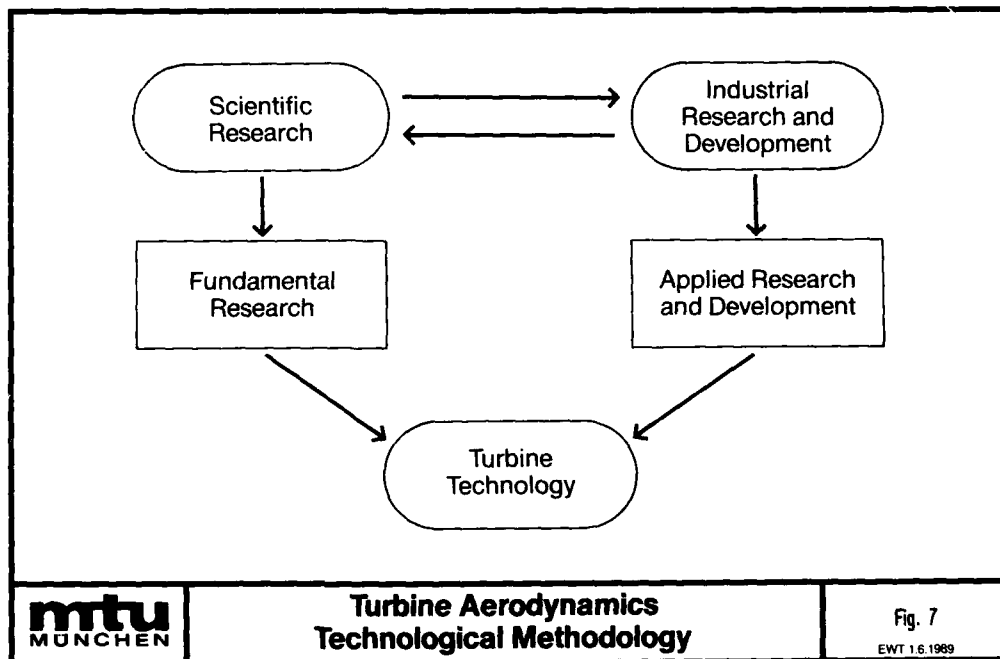
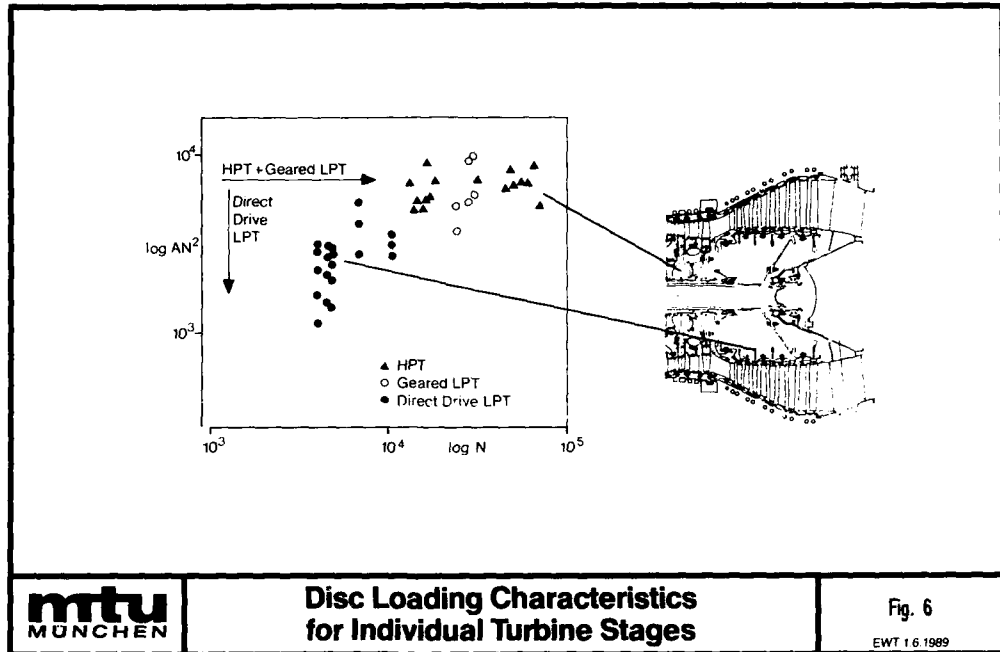
Williams M.C. (1987) Inter & Intra Blade Row Laser Velocimetry Studies of Gas Turbine Compressor Flows
32nd ASME Gas Turbine Conference, Anaheim, California, 31 May - 4 June 1987, Paper 87-GT-235

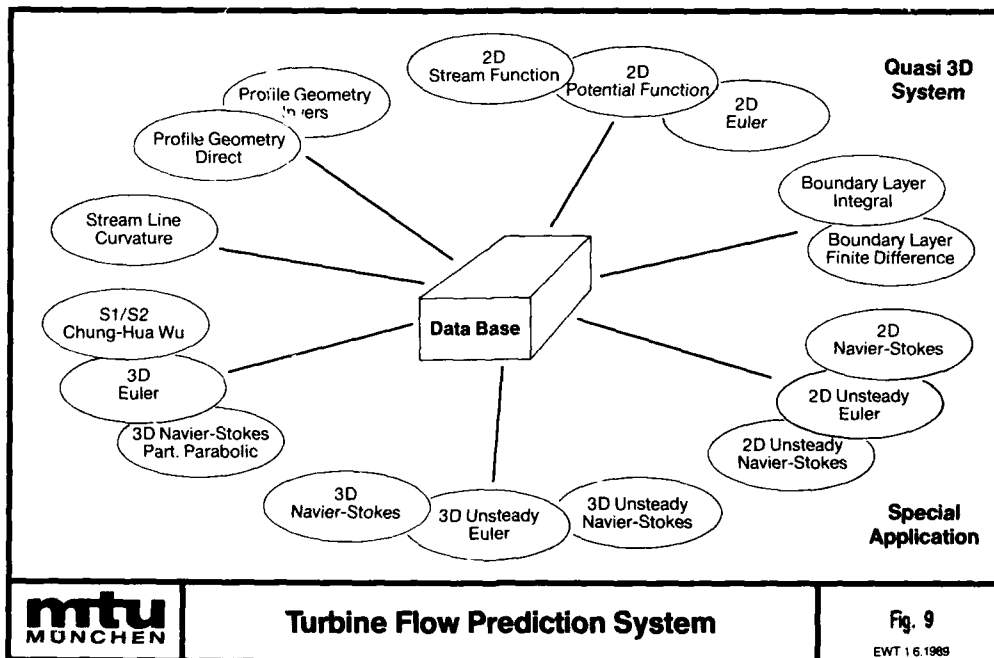
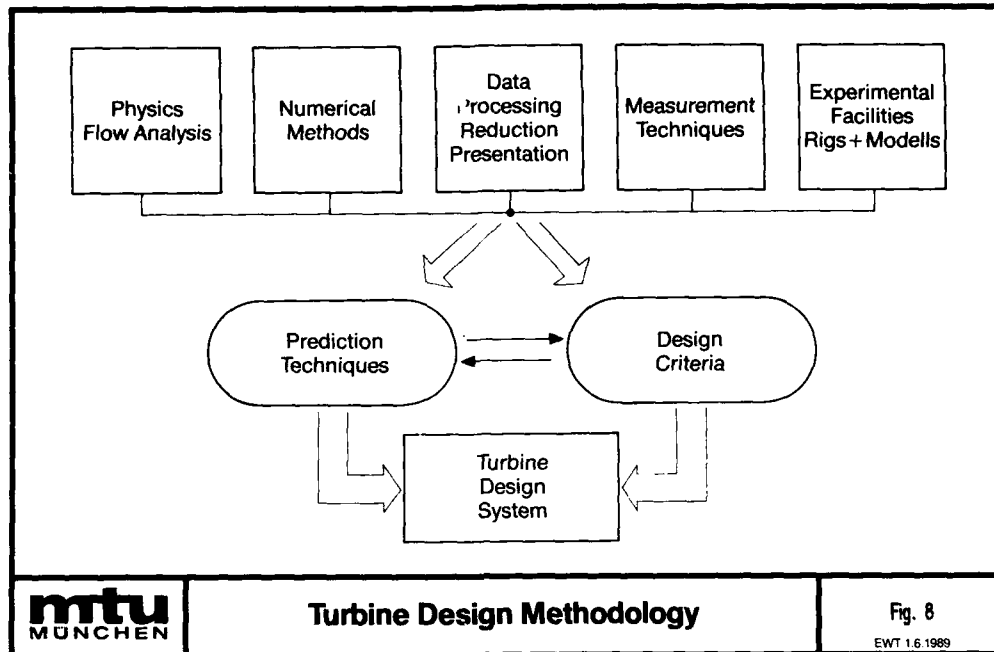
Wu Chung-Hua, (1951)
A General Through-Flow Theory of Fluid Flow with Subsonic or Supersonic Velocity in Turbomachines
NACA TN 2302, March 1951

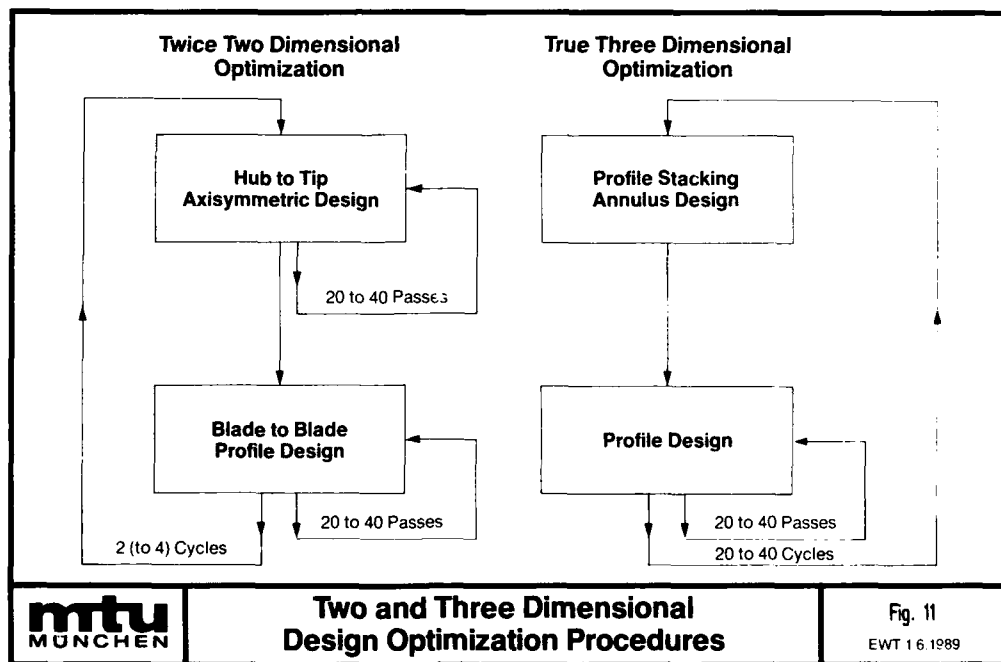
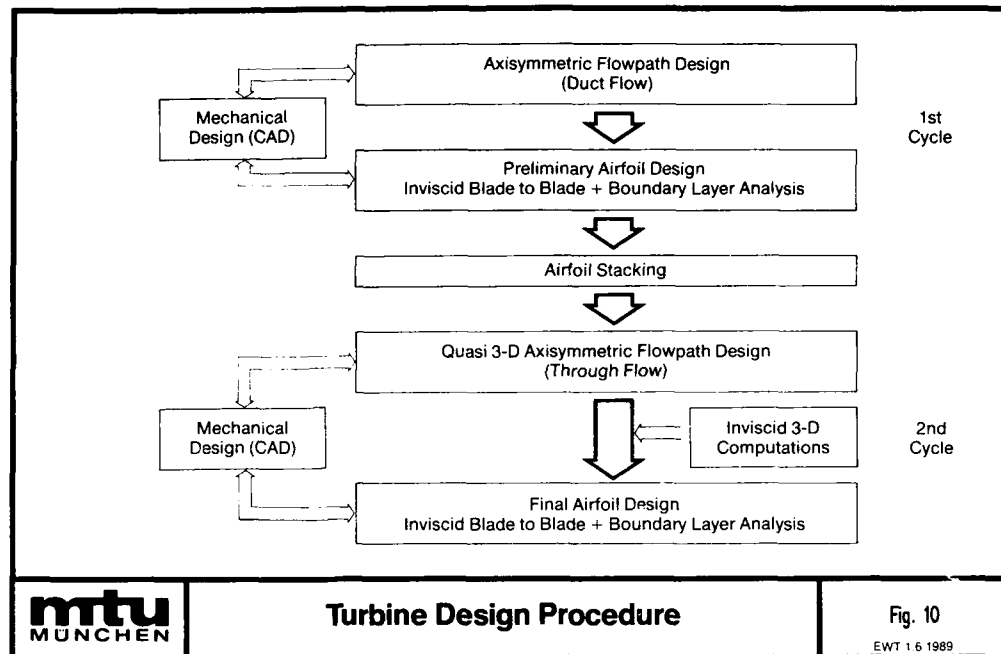


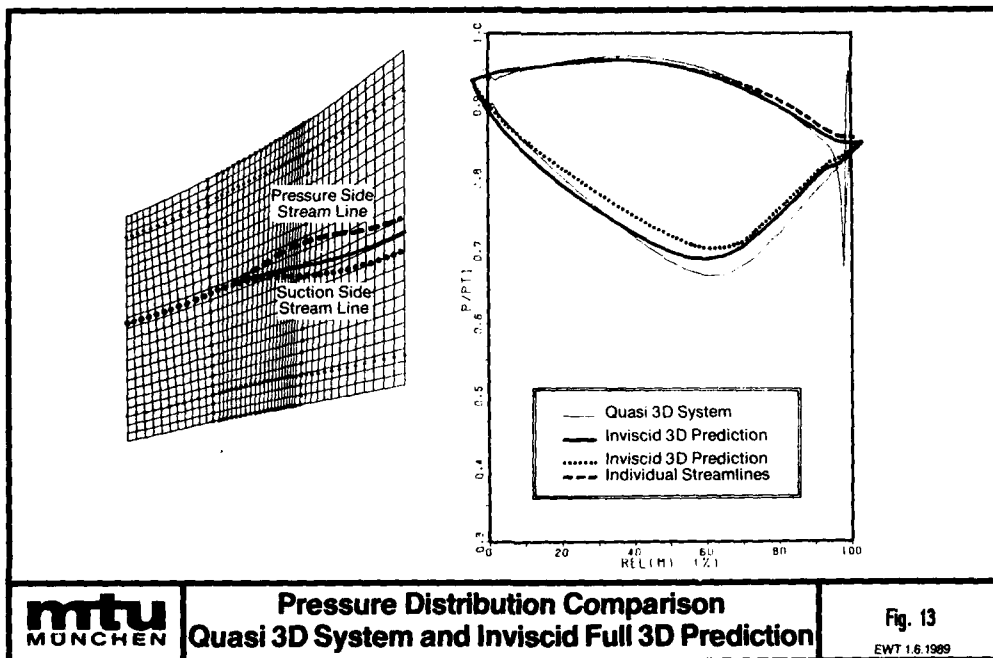
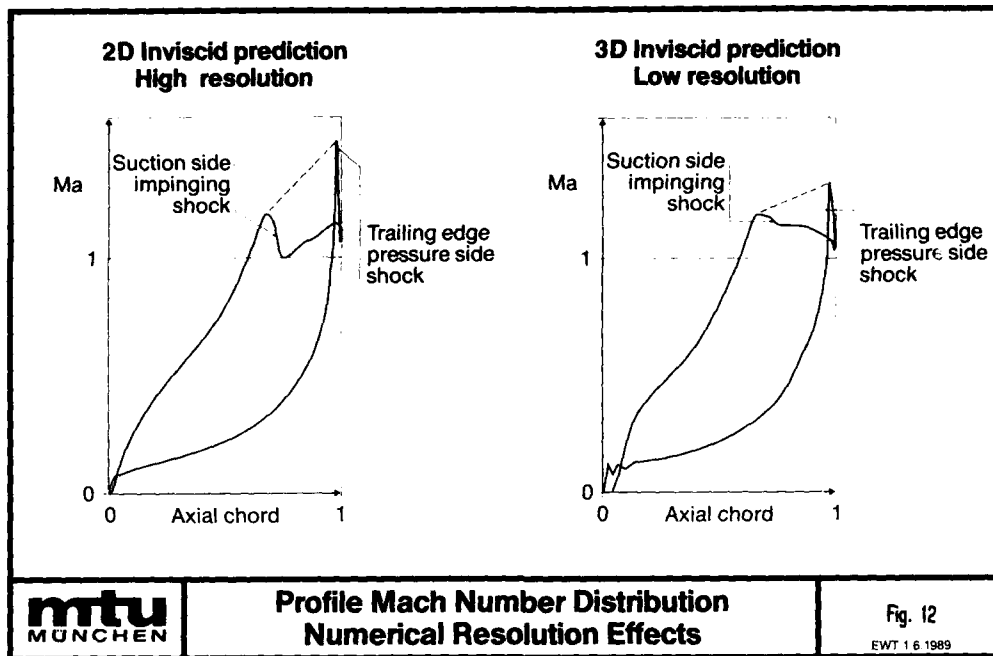


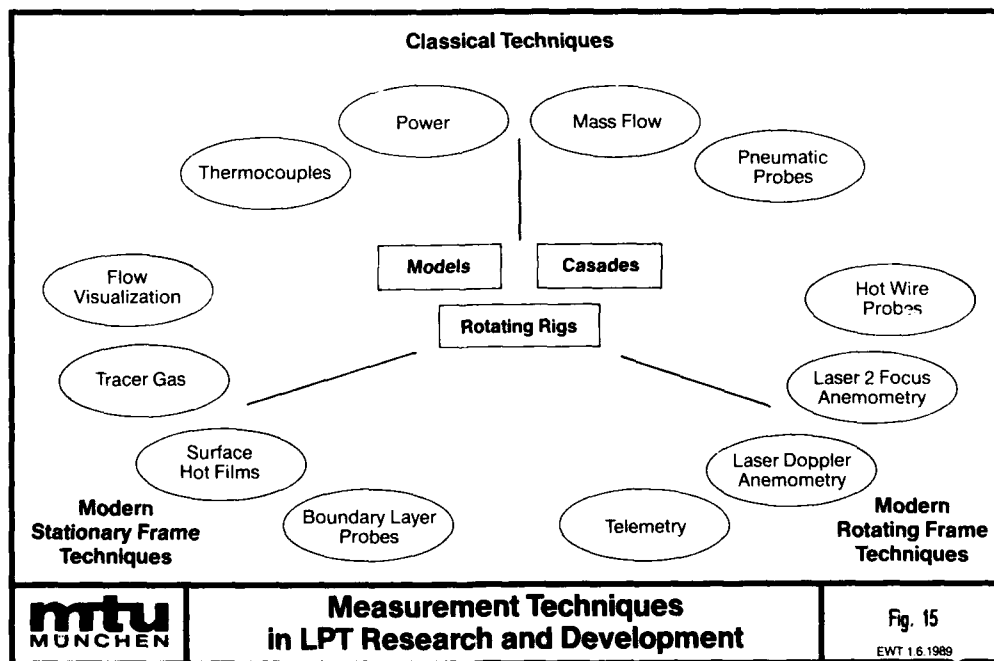
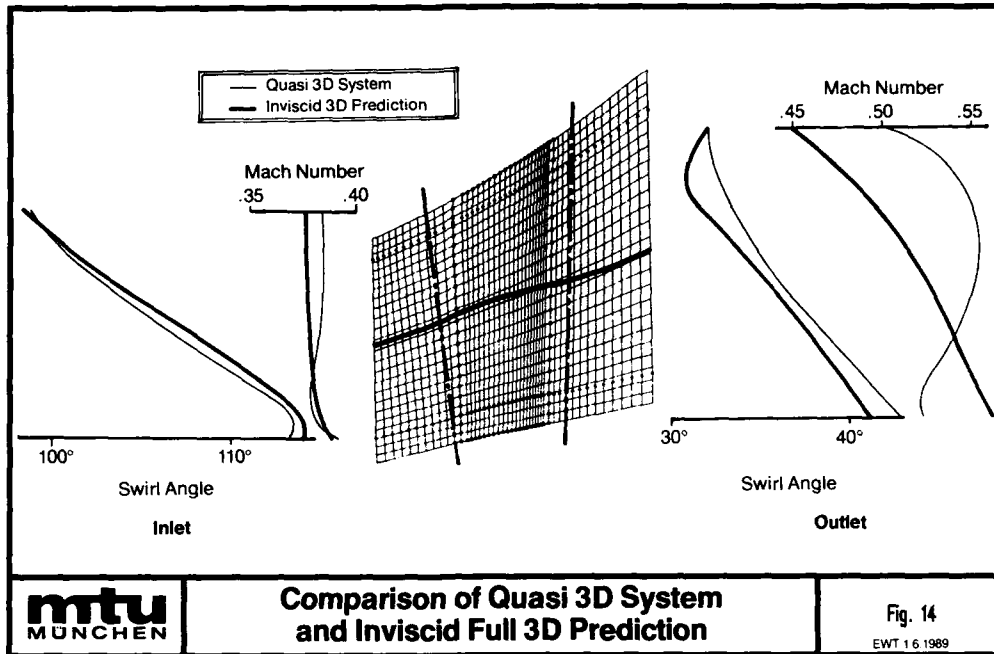


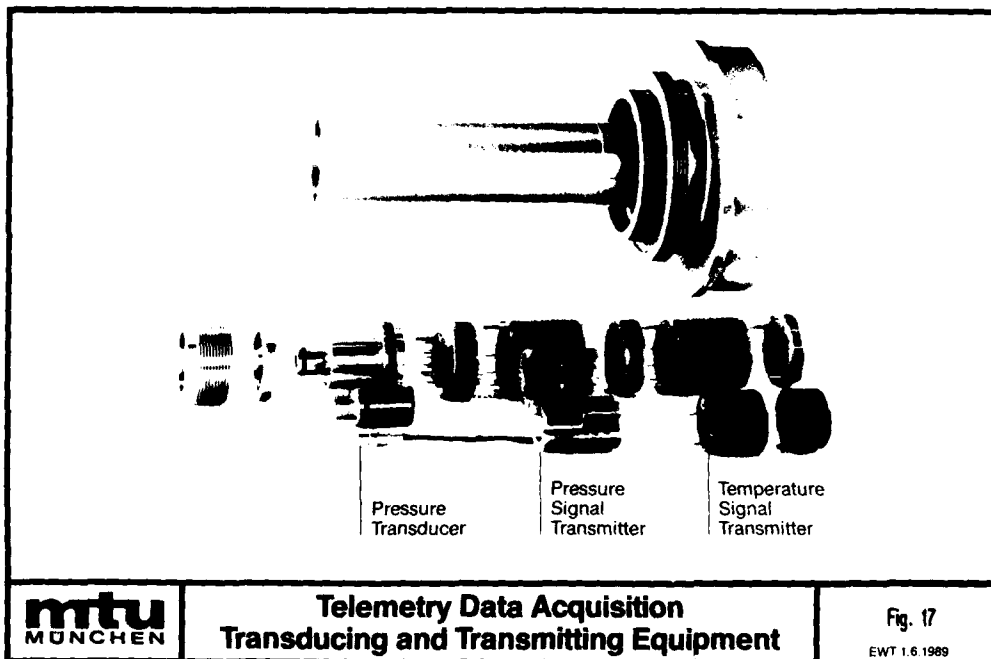
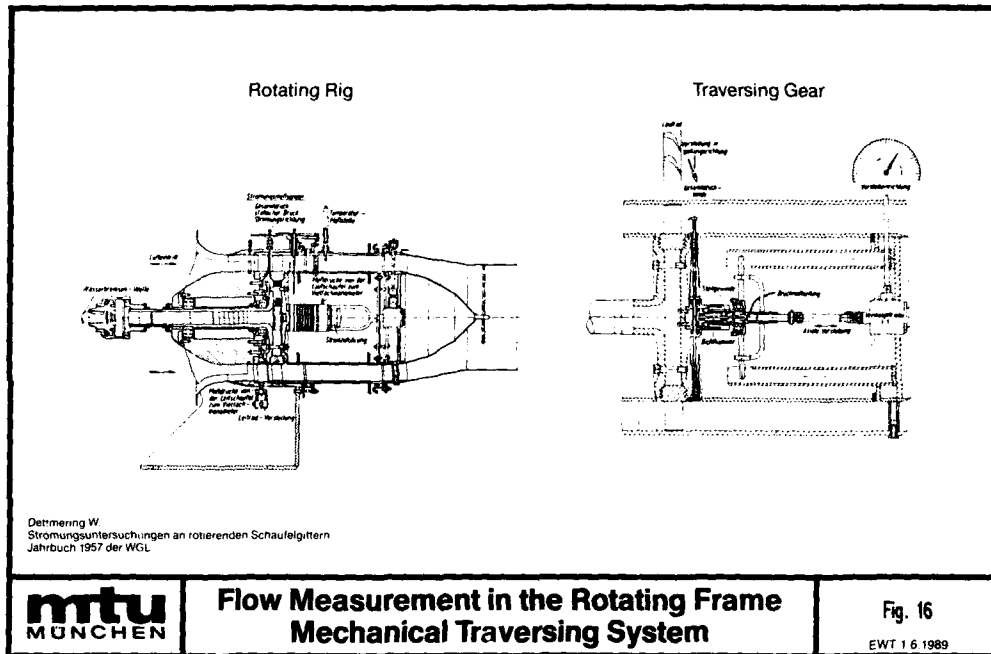


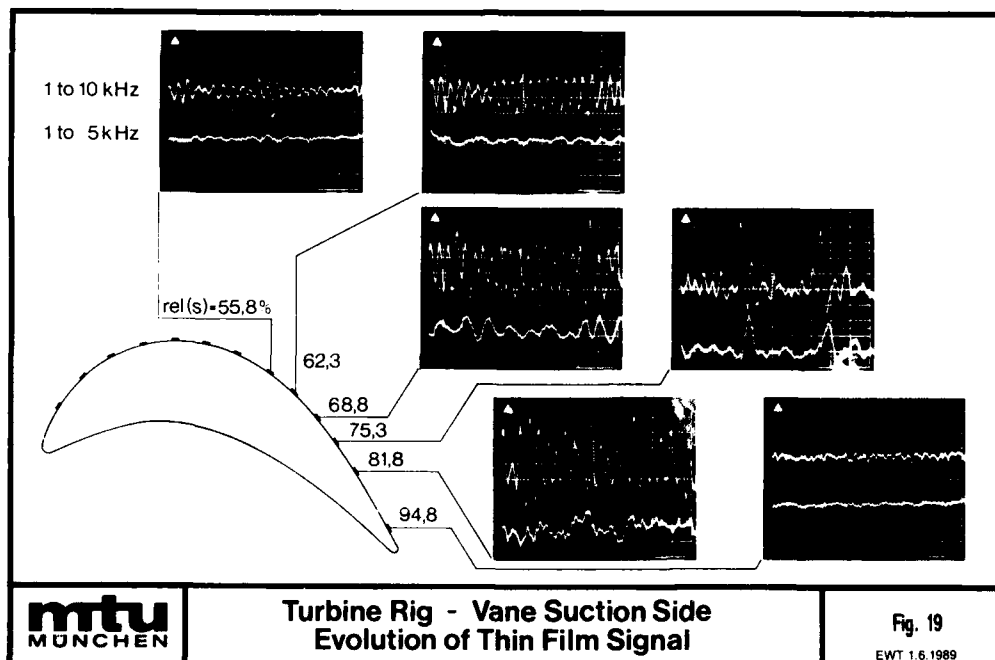
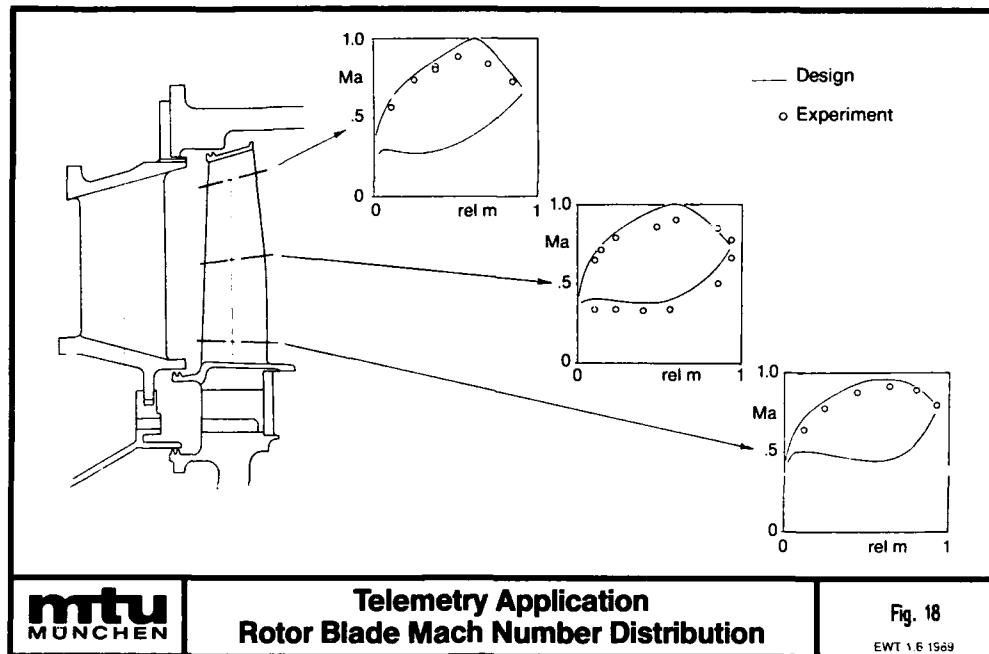


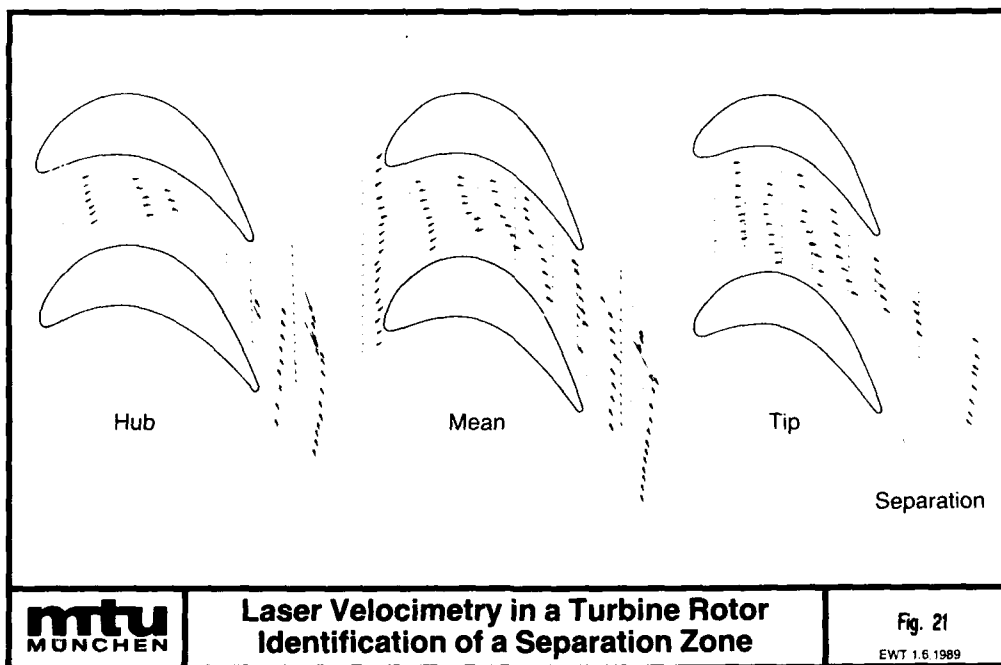
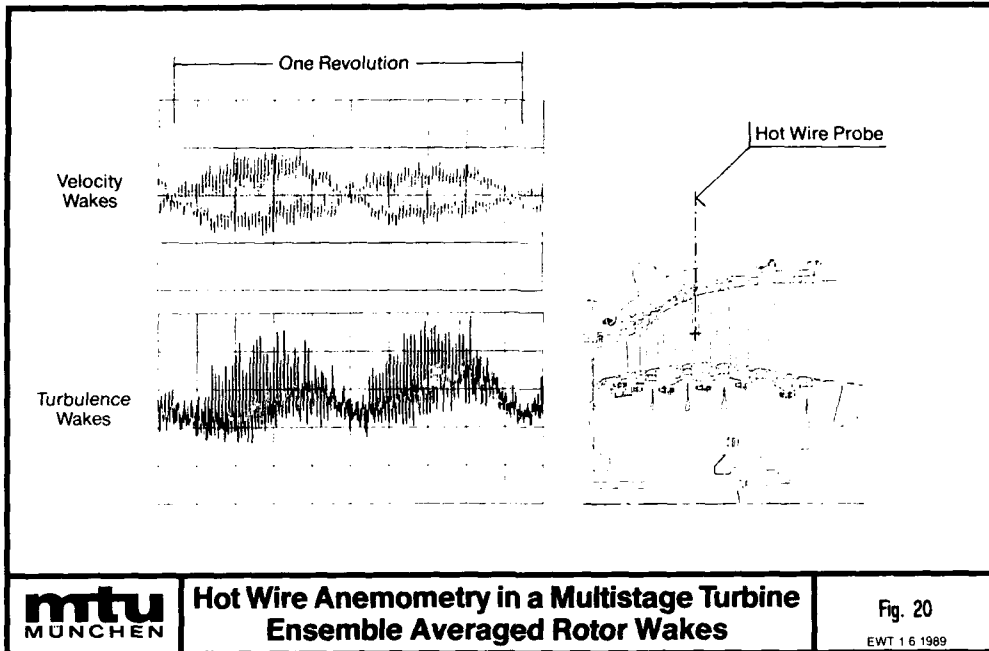


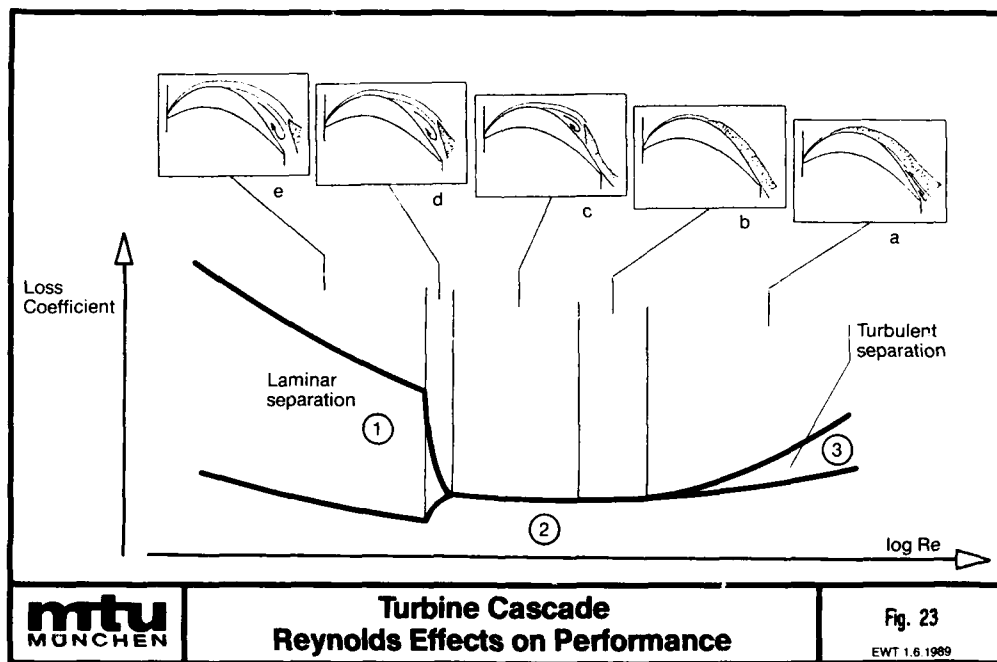
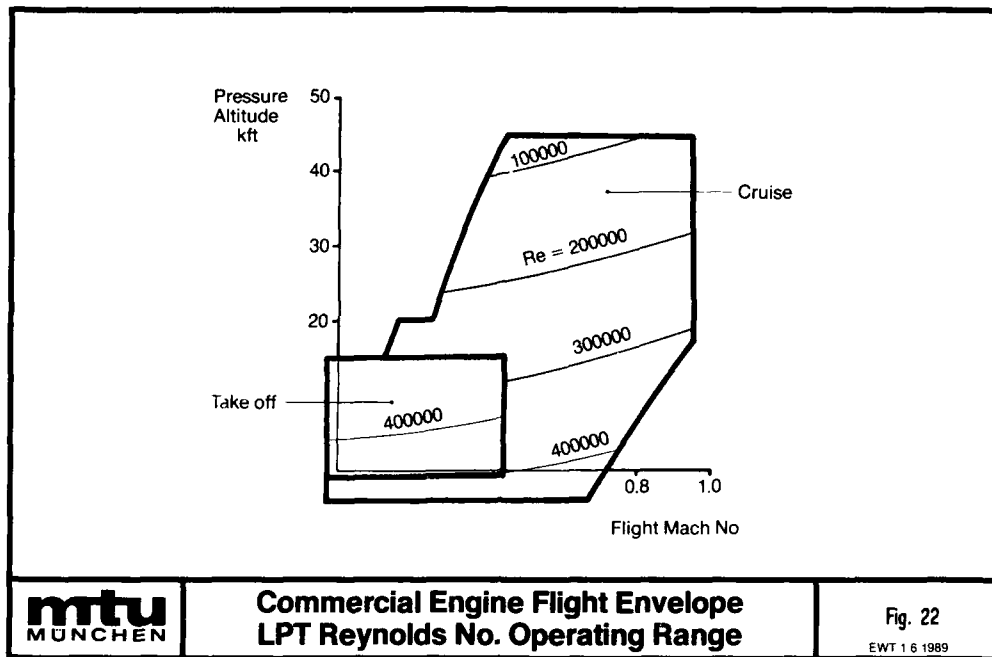


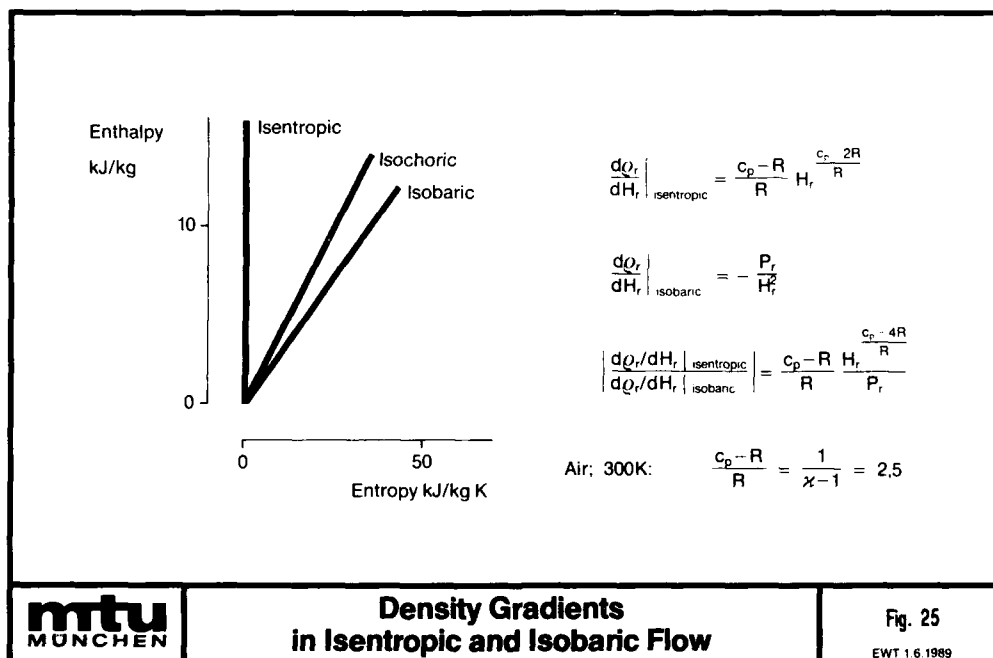
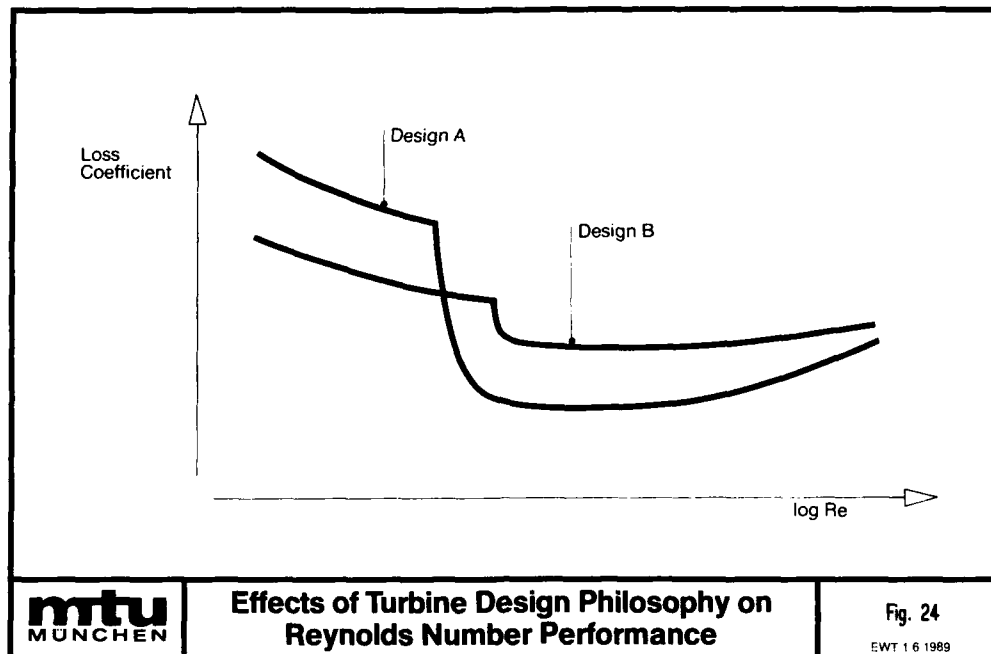


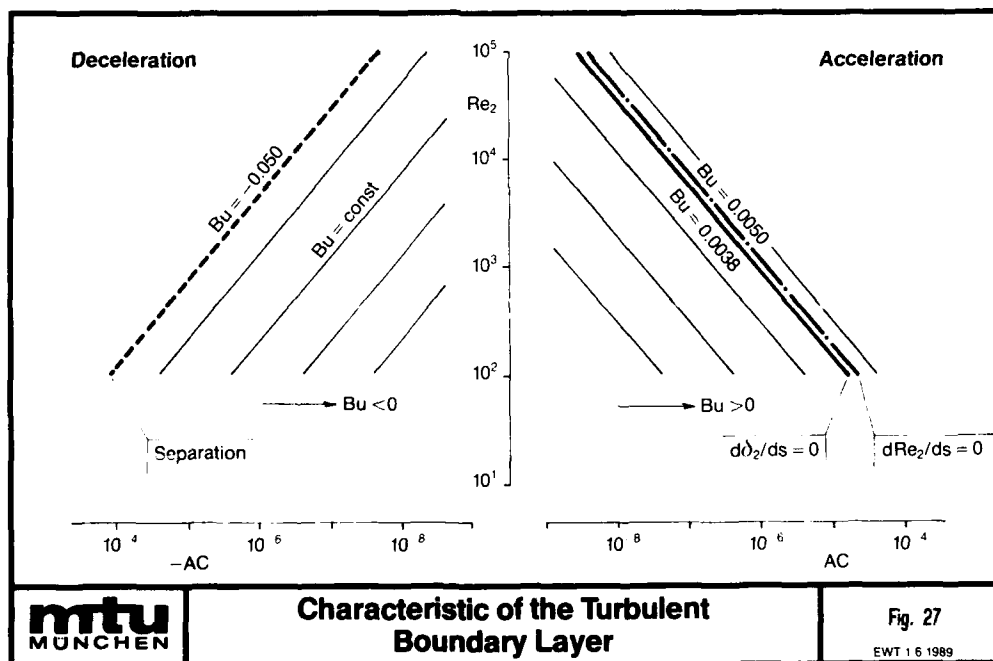
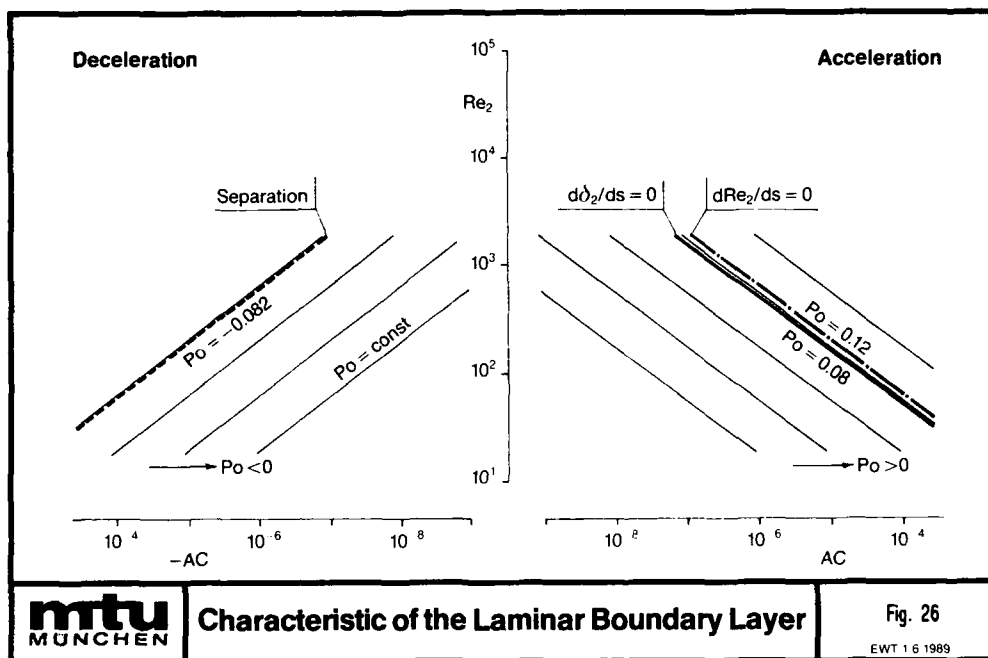


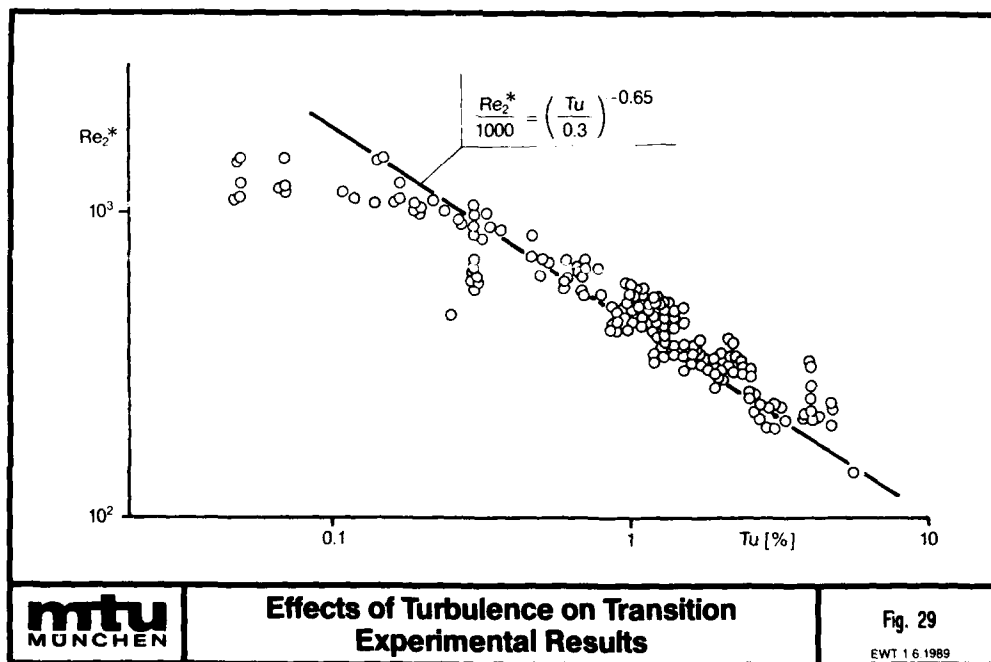
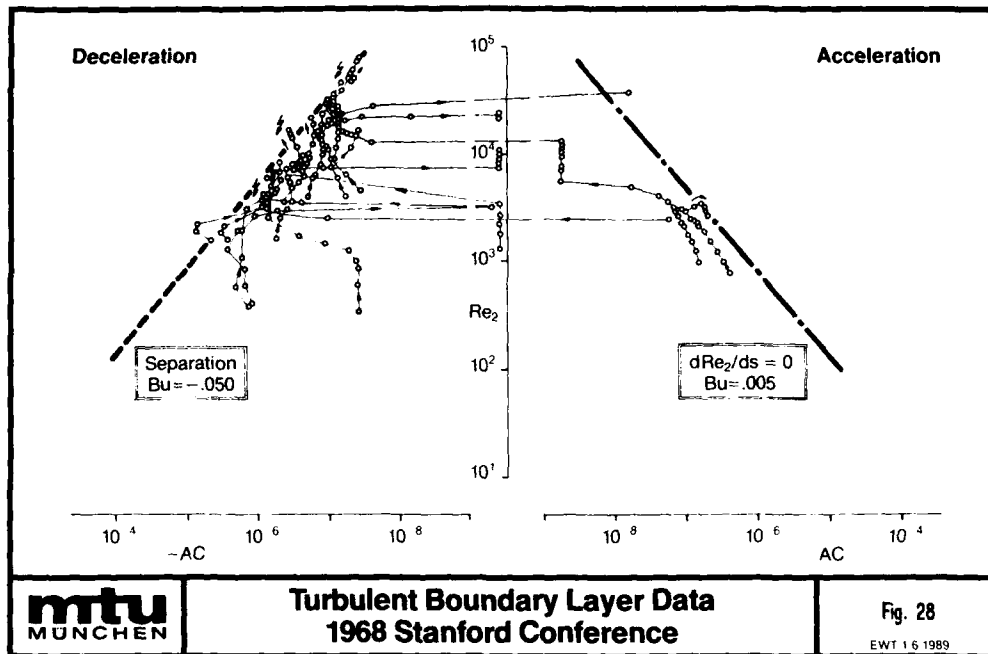


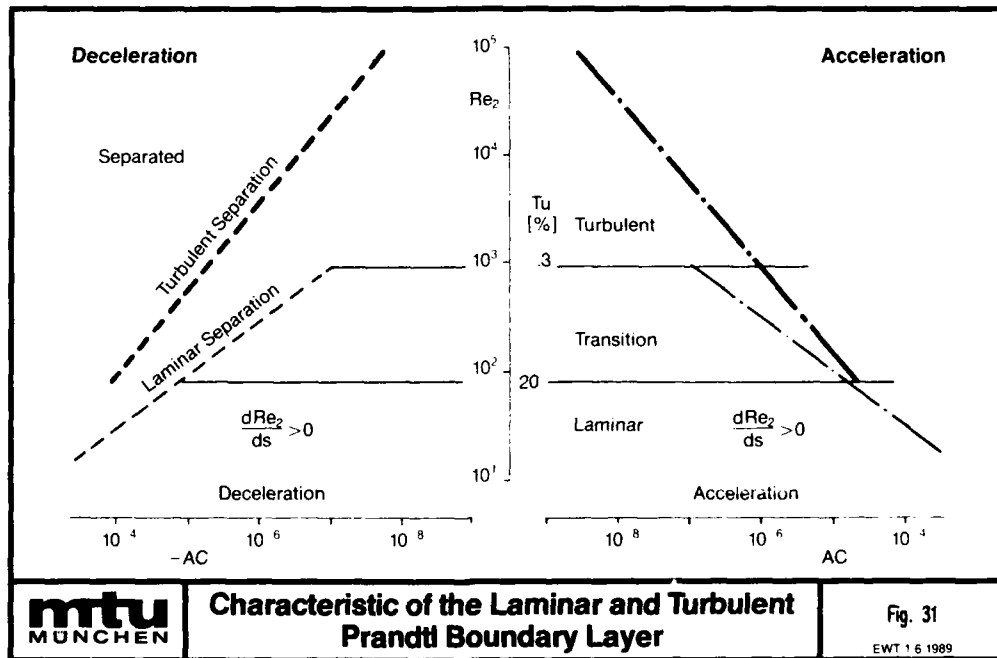
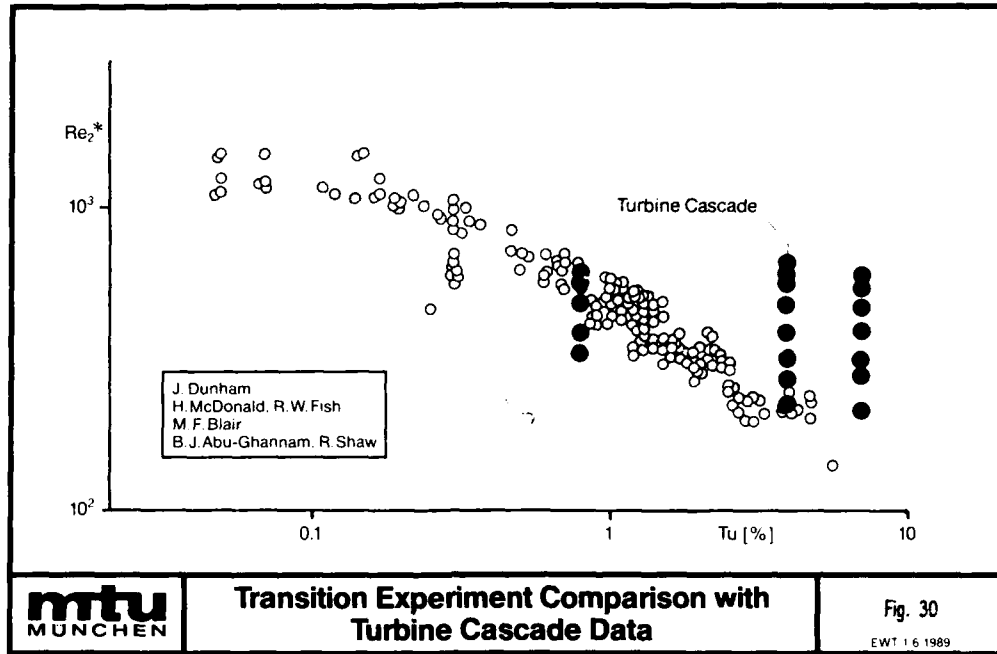


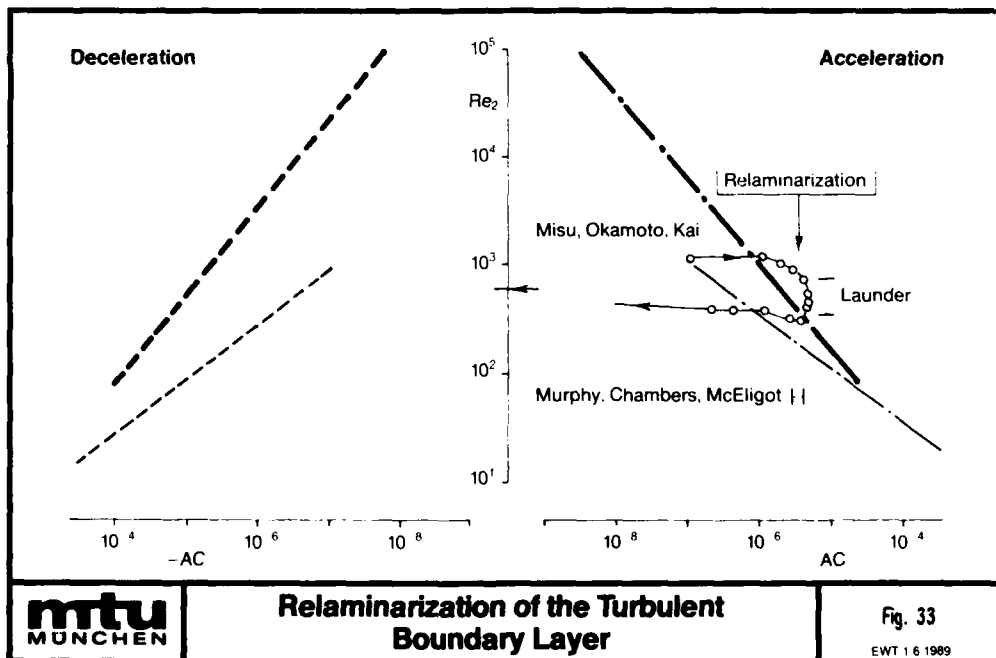
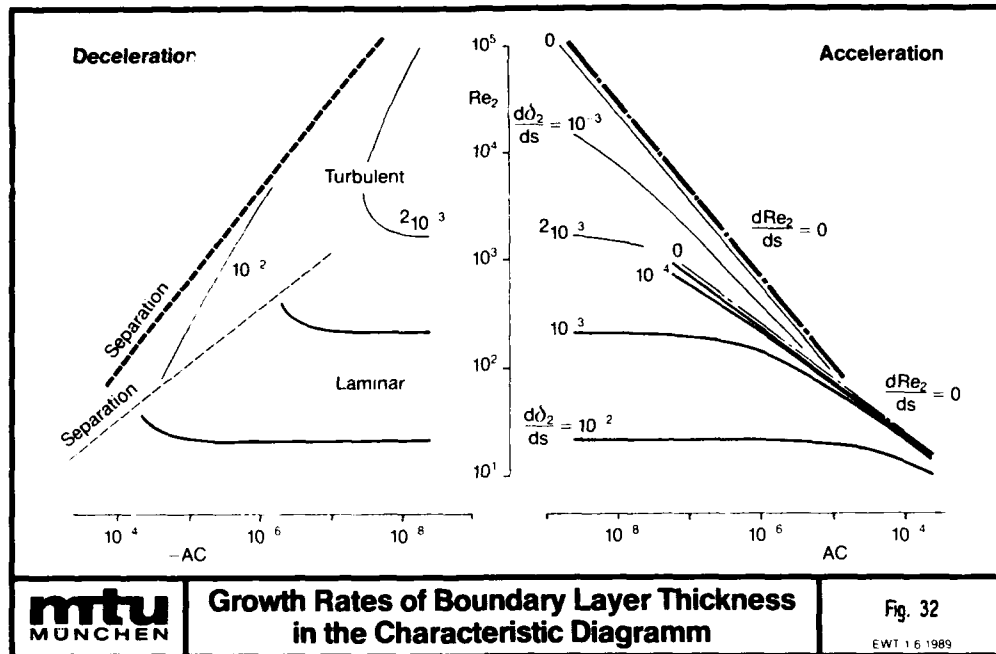


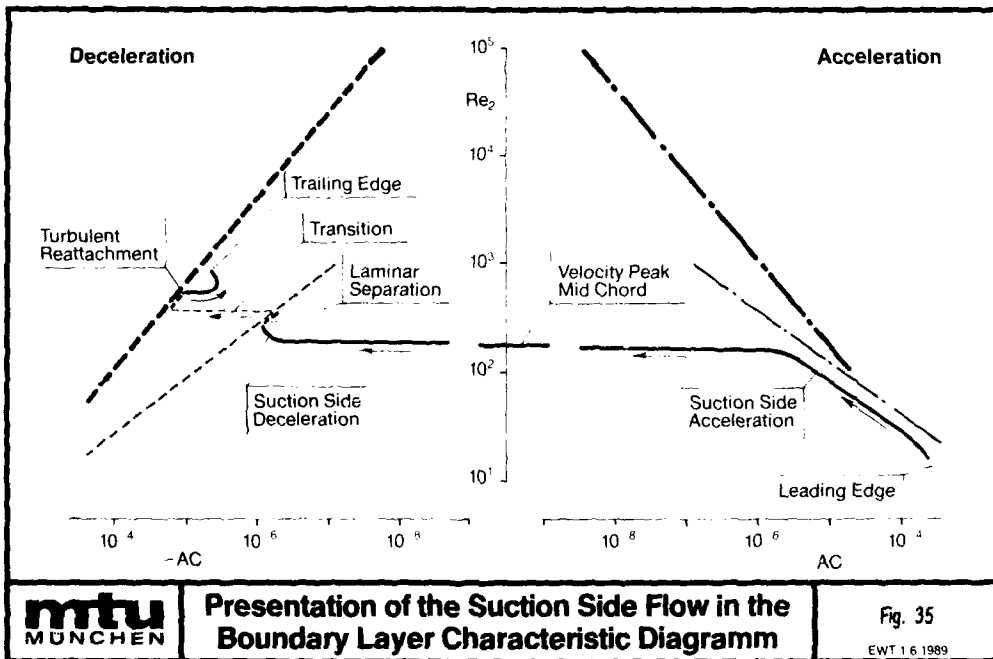
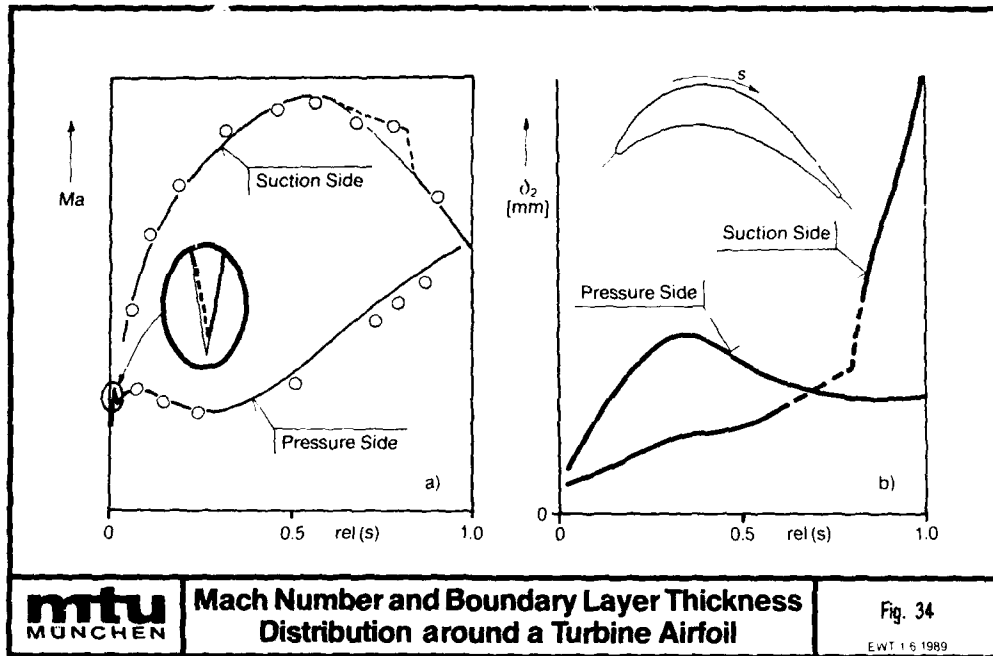


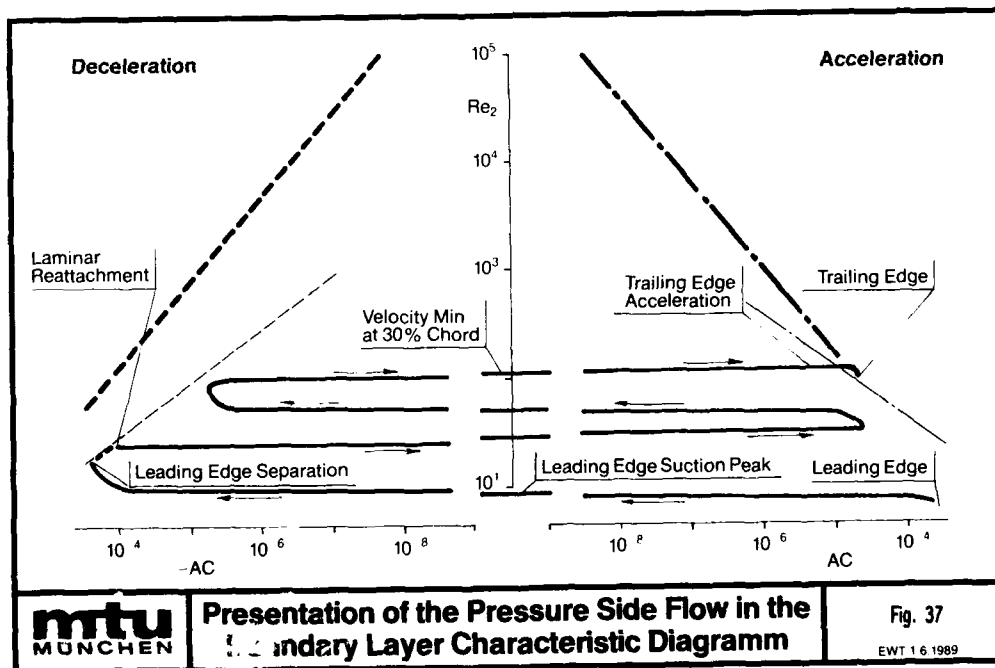
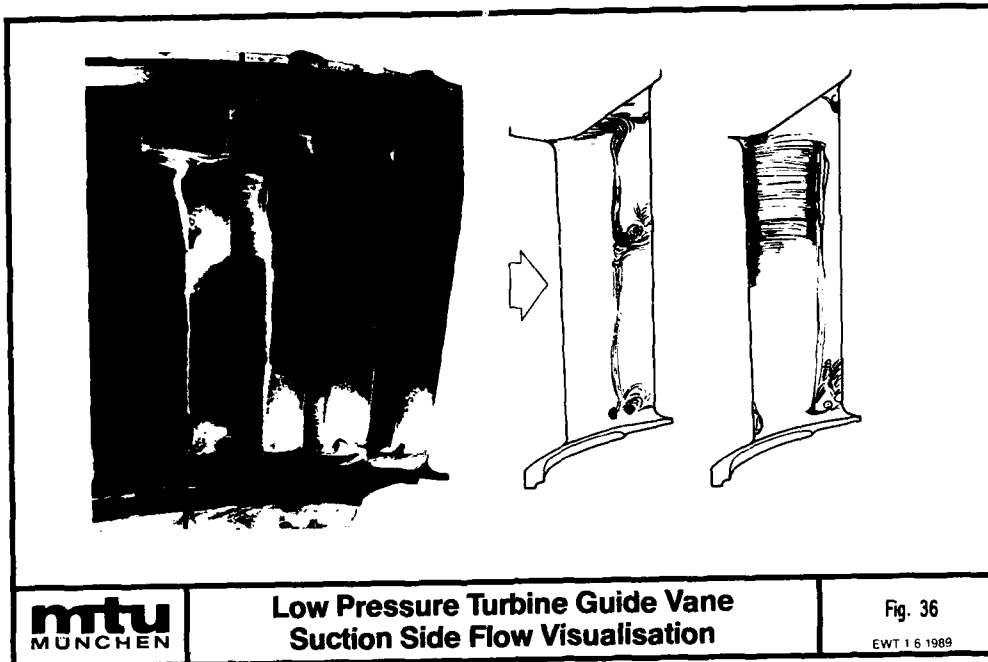


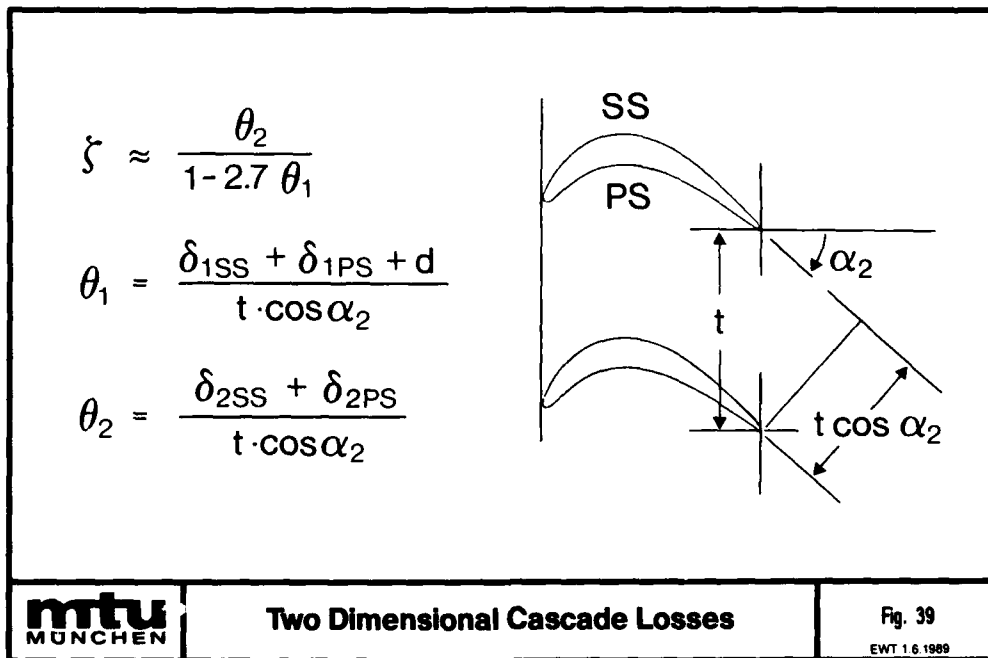
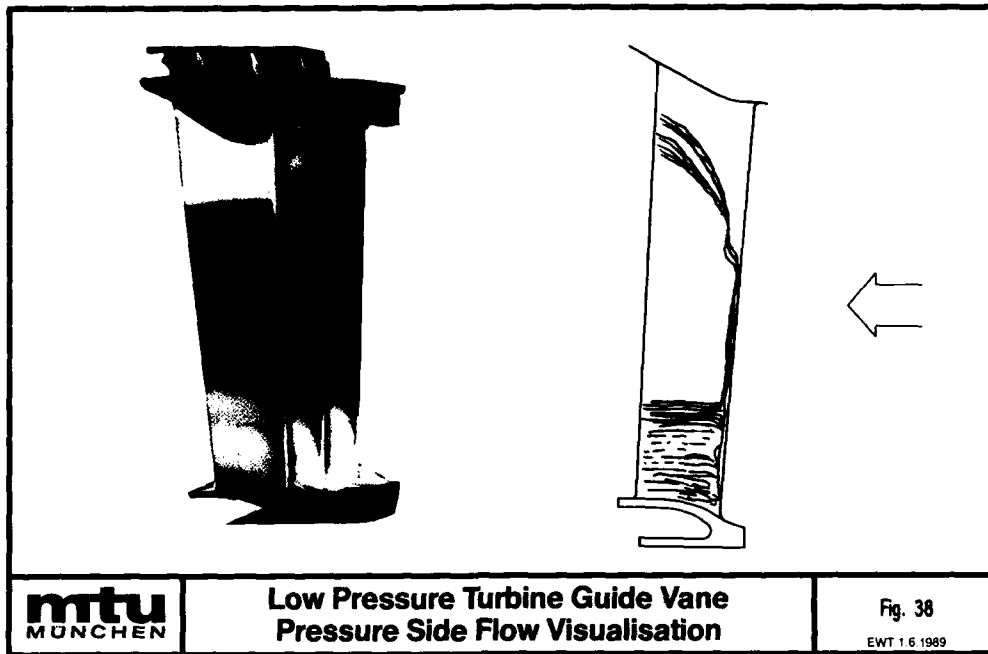


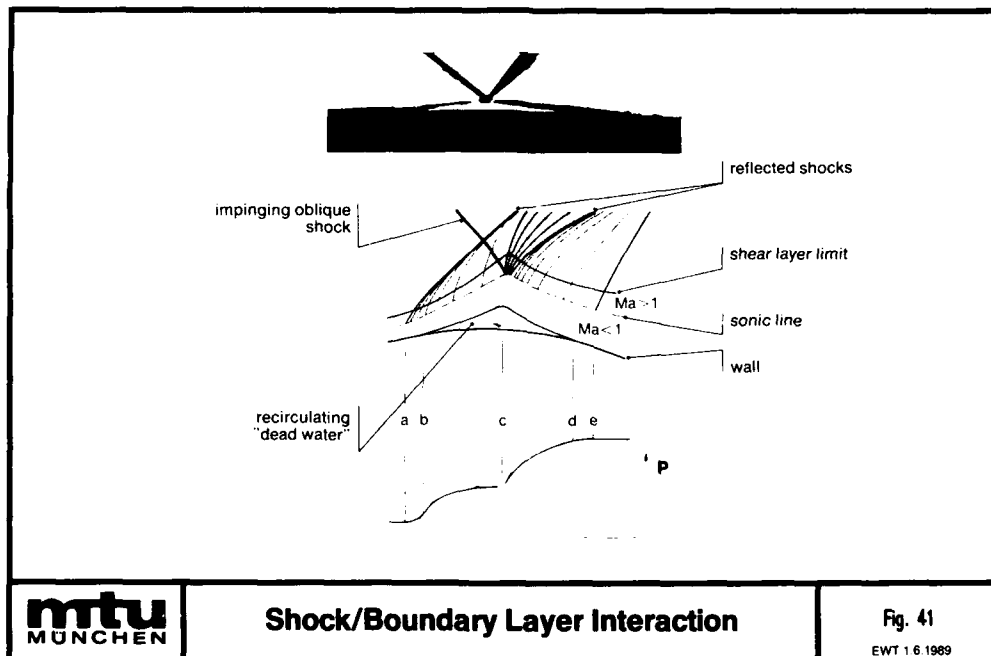
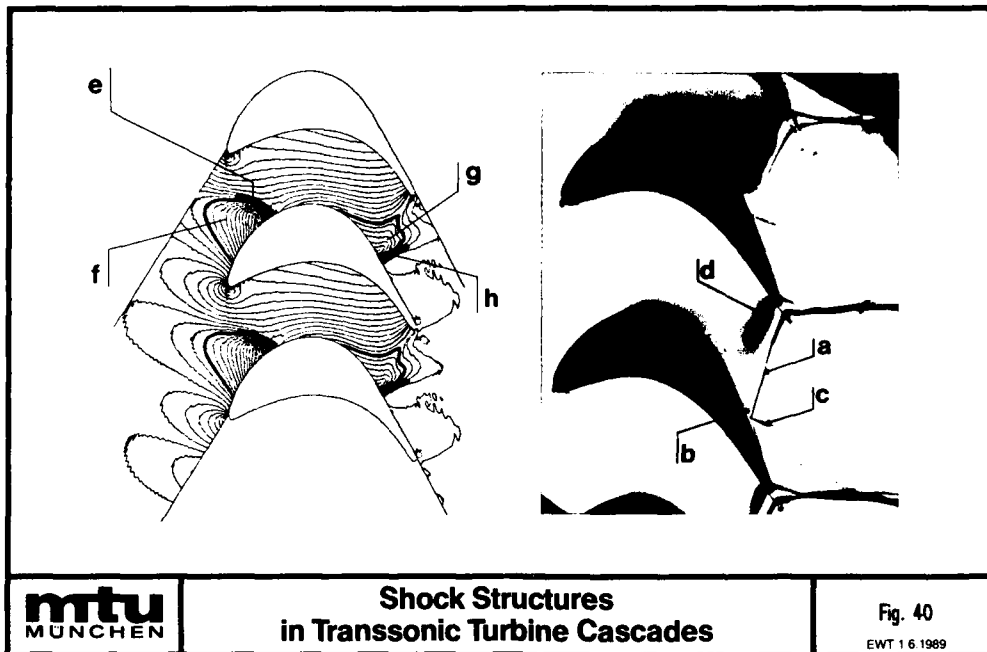


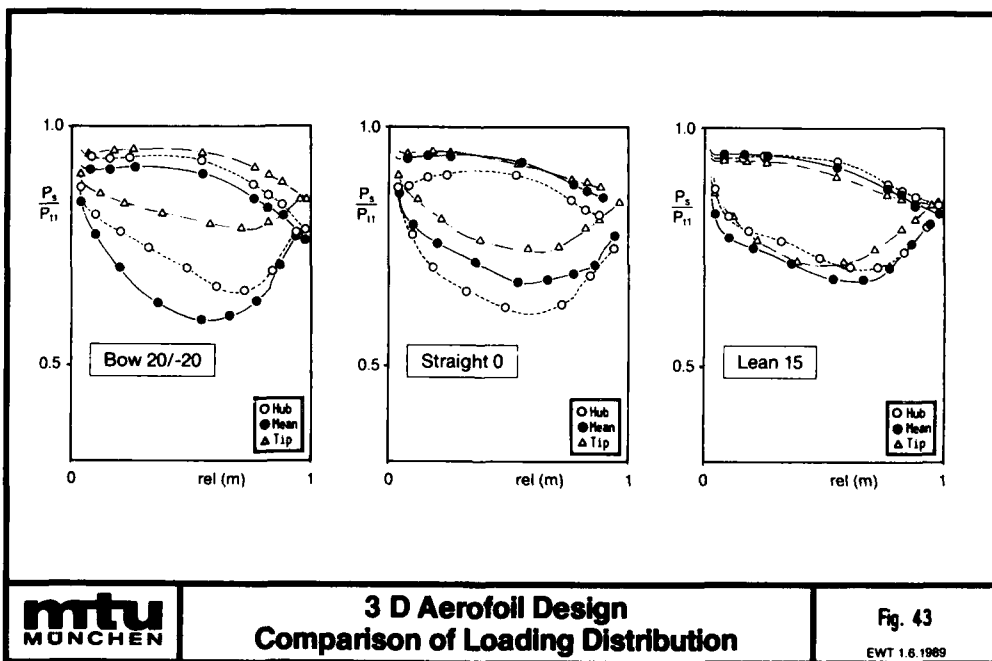
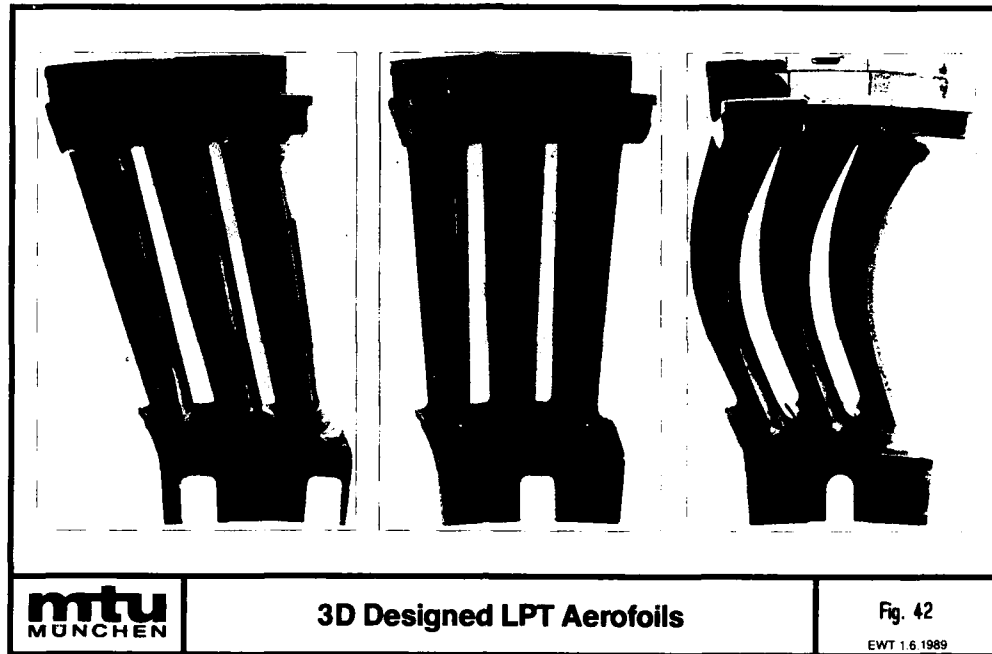












REPORT DOCUMENTATION PAGE			
1. Recipient's Reference	2. Originator's Reference	3. Further Reference	4. Security Classification of Document
	AGARD-LS-167	ISBN 92-835-0512-3	UNCLASSIFIED
5. Originator	Advisory Group for Aerospace Research and Development North Atlantic Treaty Organization 7 rue Ancelle, 92200 Neuilly sur Seine, France		
6. Title	BLADING DESIGN FOR AXIAL TURBOMACHINES		
7. Presented at			
8. Author(s)/Editor(s)	Various		9. Date May 1989
10. Author's/Editor's Address	Various		11. Pages 214
12. Distribution Statement	This document is distributed in accordance with AGARD policies and regulations, which are outlined on the Outside Back Covers of all AGARD publications.		
13. Keywords/Descriptors	<div style="display: flex; justify-content: space-between;"> <div> Aircraft engines Axial flow compressors Axial flow turbines </div> <div> Gas turbine blades Design </div> </div>		
14. Abstract	<p>The efficiency and performance of the turbomachinery components of future aero engines can considerably be improved by applying recent advances in understanding the flow behaviour of axial compressor and turbine bladings. Thus, the optimal profile pressure distribution as input for new blading design methods has an important effect on losses and flow deflection. The boundary-layer behaviour has to be carefully taken into account with respect to laminar/turbulent transition, shock/boundary-layer interaction and separation effects. In addition to these aerodynamical questions, unsteady effects and the limitations from structural and vibrational conditions also have to be taken into account.</p> <p>The Lecture Series deals with two main topics:</p> <ul style="list-style-type: none"> —design methods and their principles, limitations —application to axial compressors and turbines, experience <p>This Lecture Series, sponsored by the Propulsion and Energetics Panel of AGARD, has been implemented by the Consultant and Exchange Programme.</p> <p>This material in this publication was assembled to support a Lecture Series under the sponsorship of the Propulsion and Energetics Panel of AGARD and the Consultant and Exchange Programme of AGARD presented on 1-2 June 1989 in Toronto, Canada, on 15-16 June 1989 in Cologne, Germany and on 19-20 June 1989 in Ecully (near Lyon), France.</p>		

<p>AGARD Lecture Series 167 Advisory Group for Aerospace Research and Development, NATO BLADING DESIGN FOR AXIAL TURBO-MACHINES Published May 1989 214 pages</p> <p>The efficiency and performance of the turbomachinery components of future aero engines can considerably be improved by applying recent advances in understanding the flow behaviour of axial compressor and turbine bladings. Thus, the optimal profile pressure distribution as input for new blading design methods has an important effect on losses and flow deflection. The boundary-layer behaviour has to be carefully taken into account with</p> <p>P.T.O</p>	<p>AGARD-LS-167</p> <p>Aircraft engines Axial flow compressors Axial flow turbines Gas turbine blades Design</p>	<p>AGARD Lecture Series 167 Advisory Group for Aerospace Research and Development, NATO BLADING DESIGN FOR AXIAL TURBO-MACHINES Published May 1989 214 pages</p> <p>The efficiency and performance of the turbomachinery components of future aero engines can considerably be improved by applying recent advances in understanding the flow behaviour of axial compressor and turbine bladings. Thus, the optimal profile pressure distribution as input for new blading design methods has an important effect on losses and flow deflection. The boundary-layer behaviour has to be carefully taken into account with</p> <p>P.T.O</p>	<p>AGARD-LS-167</p> <p>Aircraft engines Axial flow compressors Axial flow turbines Gas turbine blades Design</p>
<p>AGARD Lecture Series 167 Advisory Group for Aerospace Research and Development, NATO BLADING DESIGN FOR AXIAL TURBO-MACHINES Published May 1989 214 pages</p> <p>The efficiency and performance of the turbomachinery components of future aero engines can considerably be improved by applying recent advances in understanding the flow behaviour of axial compressor and turbine bladings. Thus, the optimal profile pressure distribution as input for new blading design methods has an important effect on losses and flow deflection. The boundary-layer behaviour has to be carefully taken into account with</p> <p>P.T.O</p>	<p>AGARD-LS-167</p> <p>Aircraft engines Axial flow compressors Axial flow turbines Gas turbine blades Design</p>	<p>AGARD Lecture Series 167 Advisory Group for Aerospace Research and Development, NATO BLADING DESIGN FOR AXIAL TURBO-MACHINES Published May 1989 214 pages</p> <p>The efficiency and performance of the turbomachinery components of future aero engines can considerably be improved by applying recent advances in understanding the flow behaviour of axial compressor and turbine bladings. Thus, the optimal profile pressure distribution as input for new blading design methods has an important effect on losses and flow deflection. The boundary-layer behaviour has to be carefully taken into account with</p> <p>P.T.O</p>	<p>AGARD-LS-167</p> <p>Aircraft engines Axial flow compressors Axial flow turbines Gas turbine blades Design</p>

<p>respect to laminar/turbulent transition, shock/boundary-layer interaction and separation effects. In addition to these aerodynamical questions, unsteady effects and the limitations from structural and vibrational conditions also have to be taken into account.</p> <p>The Lecture Series deals with two main topics:</p> <ul style="list-style-type: none"> — design methods and their principles, limitations — application to axial compressors and turbines, experience. <p>This Lecture Series, sponsored by the Propulsion and Energetics Panel of AGARD, has been implemented by the Consultant and Exchange Programme.</p> <p>This material in this publication was assembled to support a Lecture Series under the sponsorship of the Propulsion and Energetics Panel of AGARD and the Consultant and Exchange Programme of AGARD presented on 1-2 June 1989 in Toronto, Canada, on 15-16 June 1989 in Cologne, Germany and on 19-20 June 1989 in Ecullly (near Lyon), France.</p> <p>ISBN 92-835-0512-3</p>	<p>respect to laminar/turbulent transition, shock/boundary-layer interaction and separation effects. In addition to these aerodynamical questions, unsteady effects and the limitations from structural and vibrational conditions also have to be taken into account.</p> <p>The Lecture Series deals with two main topics:</p> <ul style="list-style-type: none"> — design methods and their principles, limitations — application to axial compressors and turbines, experience. <p>This Lecture Series, sponsored by the Propulsion and Energetics Panel of AGARD, has been implemented by the Consultant and Exchange Programme.</p> <p>This material in this publication was assembled to support a Lecture Series under the sponsorship of the Propulsion and Energetics Panel of AGARD and the Consultant and Exchange Programme of AGARD presented on 1-2 June 1989 in Toronto, Canada, on 15-16 June 1989 in Cologne, Germany and on 19-20 June 1989 in Ecullly (near Lyon), France.</p> <p>ISBN 92-835-0512-3</p>
<p>respect to laminar/turbulent transition, shock/boundary-layer interaction and separation effects. In addition to these aerodynamical questions, unsteady effects and the limitations from structural and vibrational conditions also have to be taken into account.</p> <p>The Lecture Series deals with two main topics:</p> <ul style="list-style-type: none"> — design methods and their principles, limitations — application to axial compressors and turbines, experience. <p>This Lecture Series, sponsored by the Propulsion and Energetics Panel of AGARD, has been implemented by the Consultant and Exchange Programme.</p> <p>This material in this publication was assembled to support a Lecture Series under the sponsorship of the Propulsion and Energetics Panel of AGARD and the Consultant and Exchange Programme of AGARD presented on 1-2 June 1989 in Toronto, Canada, on 15-16 June 1989 in Cologne, Germany and on 19-20 June 1989 in Ecullly (near Lyon), France.</p> <p>ISBN 92-835-0512-3</p>	<p>respect to laminar/turbulent transition, shock/boundary-layer interaction and separation effects. In addition to these aerodynamical questions, unsteady effects and the limitations from structural and vibrational conditions also have to be taken into account.</p> <p>The Lecture Series deals with two main topics:</p> <ul style="list-style-type: none"> — design methods and their principles, limitations — application to axial compressors and turbines, experience. <p>This Lecture Series, sponsored by the Propulsion and Energetics Panel of AGARD, has been implemented by the Consultant and Exchange Programme.</p> <p>This material in this publication was assembled to support a Lecture Series under the sponsorship of the Propulsion and Energetics Panel of AGARD and the Consultant and Exchange Programme of AGARD presented on 1-2 June 1989 in Toronto, Canada, on 15-16 June 1989 in Cologne, Germany and on 19-20 June 1989 in Ecullly (near Lyon), France.</p> <p>ISBN 92-835-0512-3</p>

AGARD

NATO  OTAN

7 rue Ancelle • 92200 NEUILLY-SUR-SEINE
FRANCE

Telephone (1)47.38.57.00 • Telex 610 176

**DISTRIBUTION OF UNCLASSIFIED
AGARD PUBLICATIONS**

AGARD does NOT hold stocks of AGARD publications at the above address for general distribution. Initial distribution of AGARD publications is made to AGARD Member Nations through the following National Distribution Centres. Further copies are sometimes available from these Centres, but if not may be purchased in Microfiche or Photocopy form from the Purchase Agencies listed below.

NATIONAL DISTRIBUTION CENTRES

BELGIUM

Coordonnateur AGARD — VSL
Etat-Major de la Force Aérienne
Quartier Reine Elisabeth
Rue d'Evere, 1140 Bruxelles

LUXEMBOURG

See Belgium

NETHERLANDS

Netherlands Delegation to AGARD
National Aerospace Laboratory, NLR

CANADA

Director Scientific In
Dept of National Def
Ottawa, Ontario K1/



National Aeronautics and
Space Administration

Washington, D.C.
20546

**SPECIAL FOURTH CLASS MAIL
BOOK**

Postage and Fees Paid
National Aeronautics and
Space Administration
NASA-461

Official Business
Penalty for Private Use \$300



DENMARK

Danish Defence Res
Ved Idrætsparken 4
2100 Copenhagen C

FRANCE

O.N.E.R.A. (Directi
29 Avenue de la Di
92320 Châtillon

GERMANY

Fachinformationsz
Physik, Mathematil
Karlsruhe
D-7514 Eggensteir

L1 001 AGARDLS167890725S002672D
DEPT OF DEFENSE
DEFENSE TECHNICAL INFORMATION CENTER
DTIC-FDAC
CAMERON STATION BLDG 5
ALEXANDRIA VA 223046145

GREECE

Hellenic Air Force
Aircraft Support Equ
Department of Research and Development
Holargos, Athens, TGA 1010

ICELAND

Director of Aviation
c/o Flugrad
Reykjavik

ITALY

Aeronautica Militare
Ufficio del Delegato Nazionale all'AGARD
3 Piazzale Adenauer
00144 Roma/EUR

UNITED KINGDOM

Defence Research Information Centre
Kentigern House
65 Brown Street
Glasgow G2 8EX

UNITED STATES

National Aeronautics and Space Administration (NASA)
Langley Research Center
M/S 180
Hampton, Virginia 23665

THE UNITED STATES NATIONAL DISTRIBUTION CENTRE (NASA) DOES NOT HOLD
STOCKS OF AGARD PUBLICATIONS, AND APPLICATIONS FOR COPIES SHOULD BE MADE
DIRECT TO THE NATIONAL TECHNICAL INFORMATION SERVICE (NTIS) AT THE ADDRESS BELOW.

PURCHASE AGENCIES

National Technical
Information Service (NTIS)
5285 Port Royal Road
Springfield
Virginia 22161, USA

ESA/Information Retrieval Service
European Space Agency
10, rue Mario Nikis
75015 Paris, France

The British Library
Document Supply Centre
Boston Spa, Wetherby
West Yorkshire LS23 7BQ
England

Requests for microfiche or photocopies of AGARD documents should include the AGARD serial number, title, author or editor, and publication date. Requests to NTIS should include the NASA accession report number. Full bibliographical references and abstracts of AGARD publications are given in the following journals:

Scientific and Technical Aerospace Reports (STAR)
published by NASA Scientific and Technical
Information Branch
NASA Headquarters (NTI-40)
Washington D.C. 20546, USA

Government Reports Announcements (GRA)
published by the National Technical
Information Services, Springfield
Virginia 22161, USA

Printed by Specialised Printing Services Limited
40 Chigwell Lane, Loughton, Essex IG10 3TZ

ISBN 92-835-0512-3

END

DATE

FILMED

10-89